2005

Speciation, Equilibrium Distribution and Kinetics of Rainfall-Runoff Phosphorus in Adsorptive-Filtration Unit Operations and Processes

Jia Ma
Louisiana State University and Agricultural and Mechanical College, jiamawood@gmail.com

SPECIATION, EQUILIBRIUM DISTRIBUTION AND KINETICS OF RAINFALL-RUNOFF PHOSPHORUS IN ADSORPTIVE-FILTRATION UNIT OPERATIONS AND PROCESSES

A Dissertation

Submitted to the Graduate Faculty of the
Louisiana State University and
Agricultural and Mechanical College
in partial fulfillment of the
requirements for the degree of
Doctor of Philosophy

in

The Department of Civil and Environmental Engineering

By
Jia Ma
B.S., Tianjin University, 1995
M.S., Beijing University of Chemical Technology, 2000
M.S., Louisiana State University, 2003
December 2005

ACKNOWLEDGMENTS

No word is enough to express my greatest appreciation and gratitude to my advisor, Dr. John J. Sansalone, who has shed light in my life when it was grey. Without his encouragement, counsel and support, it would be nearly impossible for me to finish this doctorate journey. On top of that, my confidence and capability on a professional level have been greatly strengthened

I would like to particularly thank Dr. Amitava Roy for his cooperation and work on characterization of AOCM.

I am also very grateful to my committee members for their helpful advice on the dissertation work: Dr. Donald Dean Adrian, Dr. John H. Pardue, Dr. Dandina N. Rao and Dr. Frank T-C. Tsai.

I would like to thank Ms. R. Stich for her consistent participation in data collection and analysis. My thanks also go to those folks in our group, who have shown interest in my work and shared me with their knowledge and helpful discussion.

I appreciate my parents and sisters and they are always behind me in spite of the great distance separating us.

Finally, I would like to express my deepest gratitude to my wife, Ms Rong Jin. She keeps supporting me with love and patience. I could hardly imagine accomplishing anything without her.

TABLE OF CONTENTS

LIST OF TABLES

LIST OF FIGURES

ABSTRACT

This study examined the influence of hydrology on rainfall runoff phosphorus partitioning between aqueous and particulate-bound phase, and dissolved phosphorus speciation at the upper end of a Cementitious Porous Pavement (CPP) small urban watershed. This study also investigated particulate bound phosphorus temporal distribution during storm event and phosphorus equilibrium distribution on a wide gradation of solids captured by hydrodynamic separator after the storm completed. Results indicate that EMC of urban rainfall runoff phosphorus exceeds EPA water quality criteria, with majority of particulate-bound phosphorus while rainfall by itself contains non-comparable low concentration of phosphorus. Dissolved phosphorus was mainly $H_2PO_4^-$ and HPO_4^{-2} by Minteq modeling. Equilibrium granulometric distribution indicated that particulate-bound phosphorus sorption capacity ranging from 0.82 to 3.4 mg/g, increases with deceasing solids size.

This study also investigated pollutant transport modeling of particulate-bound phosphorus in urban rainfall-runoff and in-situ removal mechanism and efficiency by hydrodynamic separator on the basis of representative sampling and appropriate P measurement. Treatment of P by hydrodynamic separator is a combination of dynamic screening and quiescent settling. In the range of 10 ~ 50%, overall P removal efficiencies depend pronouncedly on size and distribution of particulate matter. P pollutant power law model could be successfully applied for intra-event P transport in urban rainfall-runoff.

Isotherm, kinetics and breakthrough of adsorption of phosphorus from synthetic rainfall-runoff onto highly porous aluminum oxide coated media (AOCM) were investigated. Under the typical simulated runoff conditions, AOCM showed high adsorption capacity for P. Freundlich isotherm could successfully represent isotherm data. The kinetics of P adsorption on AOCM was

fast, with the reactions completed within the first few hours, sometimes even within minutes. Pseudo second order reaction model fitted the kinetics data best under all experimental conditions and intraparticle diffusion model could be successfully applied for the first hour P adsorption kinetics. Bed volumes at breakthrough are in terms of hundreds and at exhaustion of double or triple value. Empirical and mechanistic models were found good applicability. Cost effective AOCM are capable of efficient treatment for urban rainfall runoff P.

CHAPTER 1 GLOBAL INTRODUCTION

Characterized as oxygen depletion, reduced light transparency, loss of biodiversity, and problematic algal blooms, eutrophication is one of the most common problems of surface waters contamination (Berner and Berner 1996). Algal blooms, a striking outcome of eutrophication, are aesthetically unpleasant and can emit disagreeable odors. Moreover, they can have devastating effects on fish and bottom fauna by reducing the levels of dissolved oxygen or producing toxins. A large number of freshwater lakes suffer from the deleterious affects of eutrophication (Sutcliffe and Jones 1992). Nutrient contamination of surface and ground waters is of major worldwide concern, with many lakes and rivers becoming eutrophic and some exceeding public health concentration limits for dissolved nitrate and phosphorus (Bowes et al. 2005). Continuing to impose a high environmental, ecological and health cost on many sectors of economy around world, eutrophication are caused by excessive nutrient inputs, especially of phosphorus (P), from point source or non-point source in particular urban rainfall-runoff (Vollenweider 1989). Abundant supply of nutrients from non-point sources such as leaves, fertilizers, detergents, animal wastes and traffic, point sources such as domestic and industrial sewage waters can lead to high biological production. In Europe and USA, much work has been done in reducing point-source inputs of nutrients from industrial and municipal wastewater, but the problems associated with non-point sources such as urban rainfall-runoff are still of major concern and more difficult to manage (Duda, 1993).

Eutrophic states in lakes, common urban rainfall-runoff receiving waters, range from 0.016 to 0.386 mg/L with a mean of 0.084 mg/L for total phosphorus (TP) (Vollenweider and Kerekes 1980). To prevent the development of biological nuisances and control the accelerated eutrophication, total phosphates as phosphorus should not exceed 0.05 mg/L in any stream at the

point where it enters any lake or reservoir, nor 0.025 mg/L within the lake reservoir. A desired goal for the prevention of plant nuisances in streams or other flowing waters not discharging directly to lakes or impoundments is 0.1 mg/L of TP (EPA quality criteria for water 1986).

Phosphorus nominally partitions in urban rainfall-runoff between dissolved and particulate-bound phases. Partitioning, particulate-bound distribution and speciation of phosphorus in urban rainfall-runoff is of interest not only for understanding P fate and transport, but also for selection of suitable unit operations and processes (UOP). The environmental parameters that affect the rate and extent of partitioning of phosphorus are pH, oxidation-reduction, mixing, particulate composition and particulate-bound concentration gradient (Premazzi and Provoni 1985). Besides a simple partitioning concept between dissolved and particulate phases, phosphorus also distributes across the particulate size gradation in rainfall-runoff. Physical and chemical characteristics of particulate matter combined with variable residence time, unsteady loadings and water chemistry dictate the partitioning, distribution and speciation of phosphorus in urban rainfall-runoff. Many structural and non-structural rainfall-runoff UOPs (commonly known as Best Management Practices, BMPs) target on the particulate-bound fraction of phosphorus (Barrett et al. 1998; Bartone et al. 1999; Comings et al. 2000; Dechesne et al. 2005).

Numerous P treatment methods with varying removal mechanism and efficiency have been investigated: infiltration and detention basin (Bartone and Uchrin 1999; Dechesne et al. 2005); constructed wetland system (Gervin and Brix 2001; Seo et al. 2005); vegetative controls (Barrett et al. 1998); stormtreat system (sedimentation tank) (Stenstrom et al. 2002); filtration with floating media filter (Visvanathan et al. 1996); urban wet detention ponds (Wu et al. 1996; Comings et al. 2000; Wang et al. 2004). Total P removal efficiencies are typically smaller than

50% and show a large variability. P treatability in urban rainfall-runoff is strongly influenced by sorption at surface of particulate matter and partition between the dissolved and particulate bound phase. Common particulate P removal mechanisms are sedimentation and filtration. Sedimentation generally needs large operational space which is limited in populated urban area. Possible contamination of underlying soil and groundwater is another problem which can not be neglected for application of sedimentation. If not managed filtration process commonly encounters clogging which is characterized by the elevated hydraulic resistance. Moreover, sand as a typical filter media can not achieve good P removal efficiency (Bubba et al. 2003; Forbes et al. 2004). To meet current and expected water quality requirement, advanced in-situ urban rainfall-runoff P treatment technologies and processes have to be investigated. Hydrodynamic separator attracted more and more attention due to its favorable characteristics: flexibility to unsteady flow; easiness to install, operate and maintain; work singly or in concert with other facilities; small footprint; satisfactory particle removal efficiency in potential, especially coarse particle fractions.

A variety of physical, biological and chemical operations and processes have been investigated for the treatment of phosphorus from water. It is not surprising to see discrepant P removal results by different researchers using different sampling and measurement methods because: a) Phosphorus occurs in urban rainfall-runoff in the form of both dissolved and particulate-bound phase, while dissolved P is available for immediate uptake by algae, particulate bound P provides a variable but long term source in water bodies; b) P always dynamically partitions between the two phases and distributes among the wide size range of particulate matter (from 1^{-} μm to $4{,}750^{+}$ μm) (Sansalone and Buchberger 1997). Nevertheless, each of the operations and processes has its own advantage and disadvantage. Conventional

physical methods targeting on removal of predominant particulate-bound fraction of phosphorus, such as hydrodynamic separation and quiescent settling, have proved to be in most cases barely satisfactory if operated singly considering the demanding phosphorus discharge level - TP removing efficiency varying from 10% to 50% (Clark et al. 1997). Advanced physical methods such as reverse osmosis and electrodialysis are effective, but costly, which may hinder their widespread use (Omoike and Vanloon 1999). Enhanced biological treatment can remove higher percentage of TP, but this process often encounters operational difficulties when dealing with urban rainfall runoff. Alternatively, chemical adsorption processes by metal (Al and Fe) oxides, have become favorable and reliable due to their strong affinity for sorbing phosphorus even at low P concentration. Ca and Mg are less commonly employed because of handling difficulties and production of large amount of sludge. Besides, its optimum dosing pH of 11 is undesirable for discharge to surface water directly (Clark et al. 1997; Sawada et al. 2003).

Studying for economical and easily accessible sorption materials for effective removing phosphorus form aqueous solution such as urban rainfall-runoff, has attracted great attention lately. A range of adsorbents has been investigated for phosphate adsorption, including: aluminas, aluminum hydroxide, aluminum oxide, synthetic boehmite, gibbsite, goethite, amorphous calcium silicate, polymeric hydrogels, fly ash and blast furnace slag (Gangoli and Thodos 1973; Huang 1977; Deborah and Marcia 1979; Hisashi et al. 1986; Shin et al. 2004; Kim et al. 2003; Kostura et al. 2005). In these studies, various minerals, commercial materials and some industrial wastes were evaluated for phosphate adsorption. It was found that low concentrations of phosphorus (1 mg/L) can be removed by activated alumina (Donnert and Salecker, 1999a; Donnert and Salecker, 1999b). Therefore aluminum oxides has stood out

among the many alternatives and turned out to be very efficient for the removal of dissolved phosphorus.

Aluminum oxide coated media (AOCM) with high porosity and large specific surface area were developed to selectively bind the phosphorus anions into the media matrix, permitting their subsequent removal from the urban rainfall-runoff. The engineered media need be readily available and have both high hydraulic conductivity and high P adsorption capacity. The treated urban rainfall-runoff can then be safely discharged into natural surface waters. Sorptive filter system with AOCM could have apparent unique benefits over sedimentation ponds and wetlands in that they can operate in-situ or 'pump and treat', their footprint is small and they can even be placed subsurface if needed. All these advantages are especially favorable in urban area use.

Adsorption on aluminum oxide includes physical and chemical processes. Both can be rapid, occurring within minutes or hours of contacting. After initial stage, slower reactions continue to remove phosphate from solution for periods of from several days to months. Continued removal of phosphate from solution has been contributed to physically adsorbed P forms shifting to chemically adsorbed forms, the diffusion of phosphate adsorbed on the surface of structurally porous oxides of Al to positions inside the matrix, and the precipitation of crystalline Al phosphates (Nichols 1983).

Numerous research studies have been carried out in an attempt to develop and assess new adsorbent for P removal. The major problem is that only scattered fixed-bed data available and most of the data were based on batch equilibrium system. The direct application of batch isotherm data on designing the adsorption column often encounters problems may lead to false direction. The primary reason is that flow through adsorption column is not at equilibrium. The extent of adsorption in flow through adsorption is dependent of diffusion, flow regimes and

contacting patterns. Consequently, carrying out lab-scale flow through adsorption test becomes particularly appropriate prior to the full-scale design. In addition to essentially minimize operating and maintenance costs and to maximize treatment effectiveness, modeling the P adsorption on AOCM would provide valuable insights on the mechanism and necessary guidance on scale up and operation strategy.

P adsorption column with AOCM could operate singly or in conjunction with other pretreatment technologies such as hydrodynamic separator. It is generally designed to operate under natural hydraulic gradients to treat and/or remove P in urban rainfall-runoff. Furthermore, it only takes a limited space which is appreciable especially in highly developed urban area.

In this study, we investigated the simulated urban rainfall-runoff P subsequent removal from hydrodynamic separator effluent by means of upflow adsorption column by AOCM in order to guarantee ultimate P effluent concentration below 0.1 mg/L prior to discharging to receiving waters. Though hydrodynamic separator could remove considerable amount of particulates and P associated (Jia and Sansalone), dissolved fraction of P is still of great concern. Since effluent of hydrodynamic separator contains low concentration of particulate matter and P associated, therefore adsorptive filtration by AOCM would be a very good candidate in terms of further P removal and control. In addition, the fluctuated runoff flow could also be damped and stabilized more or less because hydrodynamic separator would function as a temporary volume buffer. The quasi-stabilized flow condition is apparently favorable for consistent adsorption and filtration on AOCM column.

REFERENCES

Barrett, M.E., Walsh, P.M., Malina, J.F. Jr. and Charbeneau, R.J., 1998. Performance of Vegetative Controls for Treating Highway Runoff. Journal of Environmental Engineering, 124(11), 1121-1128.

Bartone, D.M. and Uchrin, C.G., 1999. Comparison of Pollutant Removal Efficiency for Two Residential Storm Water Basins. Journal of Environmental Engineering, 125(7), 674-677.

Berner, E.K. and Berner, R.K. 1996. Global Environment-Water, Air, and Geochemical Cycles, Prentice Hall, Englewood Cliffs, New Jersey.

Bowes, M.J., House, W.A., Hadgkinson, R.A. and Leach, D.V., 2005. Phosphorus-Discharge Hysteresis During Storm Events Along a Rivers Catchment: the River Swale, UK. Water Research, 29, 751-762.

Bubba, M.D., Arias, C.A. and Brix, H., 2003. Phosphorus Adsorption Maximum of Sands for Use as Media in Subsurface Flow Constructed Reed Beds as Measured by the Langmuir Isotherm. Water Research, 37, 3390-3400.

Clark, T., Stephenson, T. and Pearce, P.A., 1997. Water Research. 31(10) 2557-2563.

Comings, K.J., Booth, D.B. and Horner, R.R., 2000. Storm Water Removal by Two Wet Ponds in Bellevue, Washington. Journal of Environmental Engineering, 126(4), 321-330.

Deborah, L.V. and Marcia, H.B. (1979). High-calcium flyash for tertiary phosphorus removal. Wat. Swge Wks., 6, 62-104.

Dechesne, M., Barraud, S., and Bardin, J.P., 2005. Experimental assessment of stormwater infiltration basin evolution. Journal of Environmental Engineering, 131, 1090-1098.

Donnert, D. and Salecker, M., 1999a. Elimination of phosphorus from waste water by crystallization. Environ. Technol. 20, 735-742.

Donnert, D. and Salecker, M., 1999b. Elimination of phosphorus from municipal and industrial waste water. Water Sci. Technol. 40, 195-202.

Duda, A.M., 1993. Addressing nonpoint sources of water pollution must become an international priority. Water Sci. Technol. 28, 1-11.

Forbes, M.G., Dickson, K.R., Golden, T.D., Hudak, P. and Doyle, R.D., 2004. Dissolved Phosphorus Retention of Light-Weight Expanded Shale and Masonry Sand Used in Subsurface Flow Treatment Wetlands. Environmental Science & Technology, 38(3), 892-898.

Gangoli, N. and Thodos, G. (1973). Phosphorus adsorption studies. J. Wat. Pollut. Control Fed., 45(4).

Gervin, L. and Brix, H., 2001. Removal of Nutrients from Combined Sewer Overflows and Lake Water in a Vertical-Flow Constructed Wetland System. Water Science and Technology, 44(11-12), 171-176.

Hisashi, Y., Mitsu, K., Kazuo, S. and Masakazu, H.A. (1986). A fundamental research on phosphate removal by using slag. Wat. Res. 20(5), 547-557.

Huang, C.P., 1977. Removal of phosphate by powdered alumina oxide adsorption. J. Wat. Pollut. Control Fed. 49(8), 1811-1817.

Kim, J.G., Kim, J.H., Moon, H.S., Chon, C.M. and Ahn, J.S., 2003. Removal Capacity of Water Plant Alum Sludge for Phosphorus in Aqueous Solutions. Chemical Speciation and Bioavailability, 14, 67-73.

Kostura, B. Kulveitova, H. and Lesko J. 2005. Blast furnace slags as sorbents of phosphate from water solutions. Water Research. 39, 1795-1802.

Nichols, D.S. J. Water Pollut. Control Fed. 1983, 55(5), 495-505.

Omoike, A.I. and Vanloon, G.W., 1999. Water Research. 33(17), 3617-3627.

Premazzi, G., and Provoni, A. 1985. Internal P loading in lakes: A different approach to its evaluation. Hydrobiologia, Vol. 120, pp 23–33.

Sansalone, J.J. and Buchberger, S.G., 1997. Partitioning and First Flush of Metals in Urban Roadway Storm Water. Journal of Environmental Engineering, American Society of Civil Engineers, Vol. 123. No. 2, February, pp 134-143.

Sawada, K., Abdel-Aal, N., Sekino, H. and Satoh, K., 2003. Adsorption of Inorganic Phosphates and Organic Polyphosphonate on Calcite. The Royal Society of Chemistry, 342-347.

Seo, D.C., Cho, J.S., Lee, H.J., and Heo, J.S., 2005. Phosphorus Retention Capacity of Filter Media for Estimating the Longevity of Constructed Wetland. Water Research, 39, 2445-2457.

Shin, E.W., Han, J.S., Jang, M., Min, S.H., Park, J.K. and Rowell, R.M., 2004. Phosphate Adsorption on Aluminum-Impregnated Mesoporous Silicates: Surface Structure and Behavior of Adsorbents. Environmental Science & Technology, 38(3), 912-917.

Sonstrom, R.S., Clausen, J.C. and Askew, D.R., 2002. Treatment of Parking Lot Stormwater Using a StormTreat System. Environmental Science & Technology, 36(20), 4441-4446.

Sutcliffe, D.W. and Jones, J.G. Eds, 1992. Eutrophication: research and application to water supply; Freshwater Biological Association: Ambleside.

U.S. EPA, 1986. Quality Criteria for Water. Office of Water Regulation and Standards, US Government Printing Office (PB81-226759), Washington, DC 20460. EPA 440/5-86-001.

Visvanathan, C., Werellagama, D.R.I.B., and Aim, R.B., 1996. Surface water pretreatment using floating media filter. Journal of Environmental Engineering, 122,25-33.

Vollenweider, R.A., 1989. Global problems of eutrophication and its control. In conservation and management of lakes, Salanki, J., Herodek, S., Eds.; Symposium Biologica Hungarica Vol. 38; Akademiai Kiado: Budapest, pp 19-41.

Vollenweider, R.A. and Kerekes, J., 1980. The Loading Concept as Basis for Controlling Eutrophication Philosophy and Preliminary Results of the Oecd Programme on Eutrophication. Prog. Wat. Tech., 12, 5-38.

Wang, G.T., Chen, S., Barber, M.E. and Yonge, D.R., 2004. Modeling Flow and Pollutant Removal of Wet Detention Pond Treating Stormwater Runoff. Journal of Environmental Engineering, 130(11), 1315-1321.

Wu, J.S., Holman, R.E. and Dorney, J.R., 1996. Systematic Evaluation of Pollution Removal by Urban Wet Detention Ponds. Journal of Environmental Engineering, 122(11), 983-988.

CHAPTER 2 PARTITIONING AND PARTICULATE-BOUND DISTRIBUTION OF PHOSPHORUS IN URBAN RAINFALL-RUNOFF

SUMMARY

This study examined the influence of hydrology on rainfall runoff phosphorus element partitioning between aqueous and particulate-bound phase, and dissolved phosphorus speciation at the upper end of a Cementitious Porous Pavement (CPP) small urban watershed. This study also investigated particulate bound phosphorus temporal distribution during storm event and phosphorus equilibrium distribution on a wide gradation of solids captured by hydrodynamic separation (HS) after the storm completed. Results indicate that EMC of urban rainfall runoff phosphorus exceeds EPA quality criteria for water, with majority of particulate-bound phosphorus from antecedent dry deposition while rainfall by itself contains non-comparable low concentration of phosphorus. Dissolved phosphorus was mainly $H_2PO_4^-$ and HPO_4^{-2} utilizing water quality analyses, measured ion balances and Minteq modeling. Particulate phosphorus intra-event distribution among various sizes of solids, i.e. sediment, settleable and suspended, was strongly dependent of hydrology. Equilibrium granulometric distribution indicated that particulate-bound phosphorus association/sorption capacity ranging from 0.82 to 3.4 mg/g, increases with deceasing solids size. Results from this study indicate that effective control of rainfall runoff phosphorus at the upper end of the urban watershed requires unit operations and processes that account for particulate-bound species, hydrology of event specific and the dissolved species.

INTRODUCTION

As a limiting nutrient for eutrophication in fresh waters, elevated concentrations of phosphorus (P) have been identified in many types of non-point rainfall-runoff discharges from

urban areas (EPA 1993). Eutrophication is generally defined as deterioration of water quality by excess input of dissolved and particulate nutrients into the receiving water body (Correll 1998, Helen Bennion et al. 1996). Having many adverse consequences, eutrophication imposes a high environmental, ecological and health cost on many sectors of economy around world. For example, it is estimated that the costs of freshwater eutrophication in England and Wales to be 105-160 million USD per year (Pretty et al. 2003) and a major bloom in the Gippsland Lakes (1987-1988) caused a reduction in expenditure and loss in recreational value assessed to be between 8 and 25 million Australian dollars (Anon 1998).

Phosphorus nominally partitions in urban rainfall-runoff between dissolved and particulate-bound phases. Partitioning, particulate-bound distribution and speciation of phosphorus in urban rainfall-runoff is of interest not only for understanding of phosphorus fate and transport, but also for facilitating selection of unit operations and processes (UOP). Many structural and non-structural rainfall-runoff Best Management Practices (BMPs) target on the particulate-bound fraction of phosphorus (Barret et al. 1998; Bartone et al. 1999; Comings et al. 2000; Dechesne et al. 2005).

Particulate-bound phosphorus has received significant attention due to the partitioning and accumulation of phosphorus to sediments in receiving water bodies (Seo and Canale 1999). For example, after the reduction of external loading for more than 20 years, the partitioning from sediment-bound phosphorus still has a significant influence on the dynamics of total phosphorus in the lake (Dong-il and Raymond 1999). The environmental parameters that affect the rate and extent of partitioning of phosphorus are pH, oxidation-reduction, mixing, particulate composition and particulate-bound concentration gradient (Premazzi and Provoni 1985; House and Denison 2002; Barlow et al. 2004; Zhou et al. 2005).

Besides a simple partitioning concept between dissolved and particulate phases, phosphorus also distributes across the particulate size gradation in rainfall-runoff. Ranging from less than 1 μm to greater than 4,750 μm, particulate and solid matter in rainfall-runoff can be operationally classified as sediment (> 75 μm), settleable (75 ~ 25 μm) and suspended (< 25 μm) based on the Imhoff settling test convention (Lin and Sansalone 2004). Material or debris larger than 4750 μm is generally classified as gross solids or debris. Physical and chemical characteristics of particulate matter combined with variable residence time, unsteady loadings and water chemistry dictate the partitioning, distribution and speciation of phosphorus in urban rainfall-runoff (Detenbeck and Brezonik 1991).

Phosphorus in urban rainfall-runoff comes from multiple sources: a) atmospheric depositions from leaves, pollens, seeds of flowers and animal wastes. Cowen and Lee (1973) investigated and measured a yield of 0.054 ~ 0.23 mg/g of soluble phosphate per dry weight of leaves, therefore vegetation is a primary source of dissolved nutrients in urban rainfall-runoff if vegetation is abundant and adjacent to transportation land; b) fertilizers leached from lawn use or litters containing phosphorus by anthropogenic activities; c) phosphorus associated with sediments leaching from construction sites; d) site specific rainfall dependant on atmospheric conditions; e) phosphorus-rich matters existed in nature, i.e. apatite; f) construction or infrastructure materials; g) traffic (Marklund et al. 2005; Culbert and France 1995; Sharma et al. 1996; Wong et al. 1998; Huanxin et al. 1997).

Eutrophic states in lakes, common urban rainfall-runoff receiving waters, range from 0.016 to 0.386 mg/L with a mean of 0.084 mg/L for total phosphorus (TP) (Vollenweider and Kerekes 1980). To prevent the development of biological nuisances and control the accelerated eutrophication, total phosphates as phosphorus should not exceed 0.05 mg/L in any stream at the

point where it enters any lake or reservoir, nor 0.025 mg/L within the lake reservoir. A desired goal for the prevention of plant nuisances in streams or other flowing waters not discharging directly to lakes or impoundments is 0.1 mg/L of TP (EPA quality criteria for water 1986).

Development of UOPs to control the significant loads of phosphorus in urban rainfall-runoff may be ineffective without a more thorough understanding of the partitioning, speciation and distribution of phosphorus. Therefore, quantification of constitutive relationships between phosphorus and anthropogenic matter is needed. The physico-chemical processes that control the fate and transport of P in rainfall-runoff need to be examined in order to develop effective measures to prevent negative impacts on the receiving waters.

OBJECTIVES

There were five major objectives of this study. Rainfall-runoff hydrologic and water quality data was collected from an instrumented 1,088-m^2 paved catchment site located in urban Baton Rouge, Louisiana. The first objective was to examine the temporal partitioning of phosphorus between dissolved and particulate-bound phases as a function of hydrology. Partitioning has implications for transport and fate of phosphorus as well as suggesting what physicochemical mechanisms will be most effective for treating these partitions. Utilizing water chemistry data from the catchment, the second objective examined equilibrium speciation of phosphorus. The third objective examined event mean concentration (EMC) values for dissolved and particulate total phosphorus and these results were compared to discharge criteria and data from other research sources. Fourth, the phenomenon of a first flush was evaluated for dissolved and particulate-bound total phosphorus and solids transported directly from the catchment. To date, the studies that have investigated particulate P distributions by particle size are very rare (Jai and Francis 2004). Finally, TP distribution across the gradation of particles was examined.

BACKGROUND

Total phosphorus (TP) refers to the summation of all the different forms of phosphorus (P) in urban rainfall-runoff: orthophosphates, polyphosphates and pyrophosphates (Standard methods 1998; Spivakov et al. 1999). The only immediately bio-available and reactive form of P is orthophosphate, of which there are two types in many aquatic systems: HPO_4^{2-}, which predominates in alkaline conditions; and $H_2PO_4^-$ in acidic conditions (Huang 1975; Karthikeyan et al 2004). Analysis of P in water usually categorizes TP into two fractions: dissolved TP (TDP) and particulate TP (PTP). The separation between operationally dissolved and particulate-bound phases is based on filtration through 0.45 μm filter (Standard methods 1998).

As an indicator of bio-availability, measurement of dissolved P is crucial and has implications for transport and immobilization. Equilibrium P partitioning is a continuous dynamic process where equilibrium is reached when partition and repartition rates are equal under a given set of aqueous conditions (Bowes et al. 2005; Gächter et al. 2004). The degree of P partitioning between dissolved and particulate-bound phase depends on particulate physico-chemical properties and urban rainfall-runoff hydrodynamics. Important physico-chemical particle indices are surface area, specific, fractal structure composition, surface charge, pH, dissolved oxygen value, redox status, and concentration gradient between P phases (Mason et al. 1999; Okus et al. 2002; Sauve et al. 2000). Hydrodynamics influence partitioning through residence time, flow regime and rate, mixing and dilution (Gao et al. 2004; Gächter et al. 1998).

The speciation of P in solution, instead of its total concentration, is often much more important in terms of its bioavailability (Bricker 1999). P speciation is dependent on water chemistry (Langmuir 1997), with implications for the mobility and transport of phosphorus. Particulate-bound phosphorus may partition to the dissolved phase, into a more reactive form and

become available to interact with biota or other components of the surrounding system, when chemical conditions vary during transport or after deposition. This partitioning can be inducted by changes in pH and conductivity along the rainfall-runoff pathway or changes in dissolved oxygen level and oxidation-reduction level.

METHODOLOGY

EXPERIMENTAL SITE

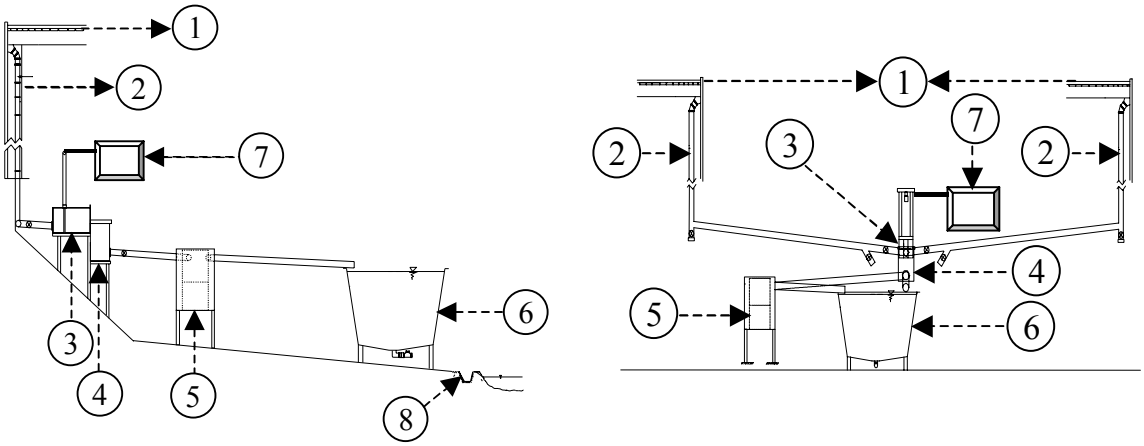

1: Free way bridge deck
2. Runoff drain collection pipe & gutter
3. Parshall flume
4. Sampling drop box
5. Hydrodynamic separation (HS)
6. Storage tank
7. Ultrasonic level sensor & data logger
8. Drainage

Figure 2-1. Profile and Plan view of Experimental Setup at I-10 interstate.

An instrumented catchment site was selected in urban Baton Rouge, Louisiana for sampling rainfall-runoff to examine phosphorus partitioning, speciation and distribution as influenced by hydrology. The site is representative of urban source area catchments and site hydrologic and water quality loadings have been compared to other similar urban land use catchments for constituents other than phosphorus including metals and particles (Teng and Sansalone 2004, Sansalone and Teng 2004). The concrete-paved catchment is comprised of two

44.6-m long, 12.2-m wide, with a total area of 1,088-m^2 (11,706-ft^2). The paved (Portland cement concrete) catchment slope is 2.0%. Runoff generated from the catchment was in a form of lateral pavement sheet flow and manually sampled and measured at a closely-spaced time intervals throughout the duration of each event. Flow was routed through a clarification unit to a series of 4000-L settling basins for storage and eventual characterization of particulate matter. All particulate matter was recovered from basins and the intermediate clarification unit for later analyses. The average annual daily traffic volume (AADT) for the paved catchment was 70,400 vehicles. Mean annual precipitation at the site is 1460 mm/year. Details of site configuration are shown in Figure 2-1.

SAMPLING AND HYDROLOGIC DATA COLLECTION

Rainfall-runoff was sampled from the drop box, immediately downstream of the Parshall flume. At each sampling time across the entire duration of the event, replicate 12-L 1-L and 0.5-L samples were manually taken of the entire cross-section of flow using wide-mouth polypropylene containers. 12-L samples were used to recover sediment/settleable solids and 1-L samples were utilized for water quality parameters of: pH, redox, conductivity, total dissolved solids (TDS) and 0.5-L samples utilized for suspended sediment concentration (SSC). At least fifteen samples were taken from each event with the exception of short event so that the results provided a reasonable estimate of temporal constituent concentrations (McBean et al. 1997).

Rainfall was recorded with a tipping bucket gauge in increments of 0.254 mm (0.01 inch). A 70 kHz ultrasonic level sensor was mounted 26 cm above the top of Parshall flume to measure flow depths. Flow levels were transmitted to the datalogger of American Sigma (1994) every second and averaged over one minute to provide a single average flow level for each minute. The one minute flow level average value was calibrated to the flow rate using the

upstream head-discharge calibration curve for the 2-inch (50.8 mm) Parshall flume. The upper limit of flow height of the flume is 13 inches (330.2 mm), which corresponds to 25.54 L/s flow capacity when compared to calibration curve. The lower limit of the flume and ultrasonic sensor is 0.03 (0.762 mm) inches, which corresponds to 0.02 L/s flow capacity.

Hydrologic and water quality data were collected during a number of rainfall runoff events from 2004 to 2005 at the experimental site. The rainfall events varied in duration, intensity, mode of peak, inter-arrival times and generated flows from the low-flow to high-flow capacity of the Parshall flume. Samples were analyzed sediment TP, settleable TP, suspended TP and dissolved TP in addition to particulate indices, pH, redox and conductivity.

PARTICULATES TP ANALYSIS

There are numerous analytical procedures for TP reported in the literature. Currently employed methods are adapted from methods used for soil, solid waste, and wastewater quality analyses (Standard Methods 1998). The ascorbic acid method was used to detect orthophosphate as recommended by other researchers (Harwood and Hattingh, 1973, Murphy and Riley, 1962). The persulfate digestion was used to measure TP by converting all forms of phosphorus to orthophosphate.

Measurement of particle-bound phosphorus in rainfall-runoff involves three steps: 1) Particulate/solution separation; 2) Acid digestion and conversion particulate bound phosphorus to dissolved phosphate; 3) Analytical measurement of the dissolved phosphate using colorimetric reagent. The details were followed:

Particulate/Solution Separation

Wet and dry sieving are commonly used methods of separating and fractionating particles from a solution (Allen 1981). Wet sieving was utilized to separate sediment (> 75 μm) from the

1-L and 12-L containers for each discrete rainfall runoff sample. After sediment was removed from the 1-L samples, settleable (75 μm ~ 25 μm) and suspended (< 25 μm) was fractionated by the Imhoff Cone protocol. Particles settled in the Imhoff cone were designated as settleable, and supernatant was a mixture of suspended and aqueous phases. After settleable particles were recovered from the Imhoff cone, the suspended fraction was separated using a 0.45 μm membrane filter. The sediment, settleable and suspended fractions were then analyzed for TP.

In addition, dry sieving was also used to quantify TP distribution across the particle size gradation for the entire gradation of recovered particles to generate subsequent particle and particulate phosphorus analysis. Particulate matter was dried at 40 ^{0}C. Dried particulate matter was carefully disaggregated before mechanical sieving. Mass-based particle size distributions were generated from serial mechanical sieving that ranged in size from 9500 μm to 25 μm (17 sieves). A mass balance was conducted to ensure that the mass balance error was less than 2%.

Acid Digestion and Conversion of Particulate P to Phosphate

Replicate samples of a precisely-measured dry particulate mass (approximately 0.5 g) were obtained from each of the 17 particle gradations. Particles were mixed with up to 80-mL of de-ionized water. Each of these replicate solutions were separately digested to convert all particulate-bound phosphorus (primarily polyphosphates and organic P) to dissolved phosphate using the Persulfate Digestion Method (Standard Methods 1998).

Analytical Measurement of the Dissolved Phosphate

Phosphorus was measured by HACH DR/2000 Spectrophotometer using PhosVer 3 Ascorbic Acid Method (Standard Method 1998). The ascorbic acid method was used to detect orthophosphate and a persulfate digestion was used to convert any other forms of phosphorus to orthophosphate (Siyuan et al. 2003).

CHARACTERIZATION INDICES FOR PHOSPHORUS

The total concentration of P (C_t) is the sum of dissolved concentration (C_d) and particulate-bound concentration (C_t).

$$C_t = C_d + C_p \qquad \text{Equation 2-1}$$

Therefore, the dissolved fraction, f_d, and particulate bound fraction, f_p, are defined, respectively, as follows.

$$f_d = \frac{C_d}{C_d + C_p} = \frac{m_d}{m_d + m_p} \qquad \text{Equation 2-2}$$

$$f_p = \frac{C_p}{C_d + C_p} = \frac{m_p}{m_d + m_p} \qquad \text{Equation 2-3}$$

In these expressions, m_d represents dissolved mass of phosphorus (mg); and m_p denotes particulate-bound mass of phosphorus (mg). If $f_d > 0.5$, P is mainly in dissolved form, otherwise P is predominantly in particulate-bound form (Sansalone and Buchberger 1997).

The equilibrium partitioning coefficient, K_d, for dilute solutions expresses the ratio of phosphorus mass normalized to the dry mass of particles to the phosphorus concentration in solution. K_d is defined as follows.

$$K_d = \frac{C_s}{C_d} \qquad \text{Equation 2-4}$$

In this expression K_d is the equilibrium partitioning coefficient between particulate bound mass and dissolved mass (L/g); C_s is the particulate bound phosphorus mass (mg/g of dry particulate mass). The partitioning coefficient can be used to evaluate the distribution between dissolved and particulate bound phosphorus. There is an inverse relationship between the dissolved fraction, f_d, and the partition coefficient, K_d, as shown by the following equation.

$$f_d = \frac{1}{1 + K_d m}$$ Equation 2-5

In this expression m is the particulate mass concentration (g/L^3).

ADDITIONAL WATER QUALITY ANALYSES

Immediately following each event, samples were transported to the laboratory within one hour for water quality analysis. Alkalinity was measured by titration in duplicate (Method 2320 B) (Standard methods 1998). Alkalinity plays a role in pH control and acts as a source of anions in the charge balance when determining phosphorus speciation. Conductivity and TDS were measured in duplicate using a YSI-85 Orion variable function conductivity meter. A three-point standard curve for TDS was developed for calibration prior to each event analysis. TDS was used to approximate a mass balance on the dissolved constituents of storm water. Conductivity data were utilized to determine the ionic strength of the runoff (Snoeyink and Jenkins 1980).

$$I \approx 1.6 * 10^{-5} * EC$$ Equation 2-6

In this expression *I* is ionic strength [mol/L] and EC is the measured electrical conductivity (μS/cm). Redox potential, pH, and temperature were measured in duplicate using an Orion 290A combination electrode. Redox potential was determined using a potentiometer that records the potential difference between a platinum electrode and reference electrode immersed in a solution. Redox potential was calibrated using a one-point calibration curve developed from an oxidation-reduction potential (ORP) standard solution of +435 mV at 25°C (Method 2580A) (APHA 1995). The pH meter (Orion 290A combination electrode) was calibrated using a three-point calibration curve with reference units at a pH of 4, 7, and 10.

SSC and VSSC (volatile suspended sediment concentrations) were analyzed for each sample following the protocol developed by the USGS (Gray et al. 2000). Samples were

vigorously mixed and the entire sample volume immediately passed through a pre-weighed 1.2 μm glass fiber filter (Gray et al. 2000).

After sampling at the experimental site, samples were rapidly fractionated into dissolved and particulate phases (sediment, settleable and suspended) to minimize time dependant changes in partitioning (Sansalone et al 1997). All analyses were analyzed in duplicate. Quality controls, blanks, and mass balance checks were maintained throughout each analysis.

PHOSPHORUS SPECIATION MODELING

Equilibrium phosphorus speciation was modeled using MINTEQ. MINTEQ utilizes aqueous ionic constituents, water pH, redox potential and ionic strength to determine the concentration of each aqueous species formed under specified conditions. For a complete charge balance, all major dissolved ionic measurements were required. Each sample was fractionated prior to analysis. Nitrates, sulfates, phosphates, bicarbonate, carbonate and chlorides were determined by colorimetric analyses. Respective reagents were combined with 25-mL of sample to determine concentrations of NO^{-}_{3}-N, SO_4^{-2}, PO_4^{-3}-P, HCO^{3-} or CO_3^{-2}, and Cl^{-}.

DOC was measured using a Shimadzu TOC-5050A analyzer. Prior to analysis, DOC samples were fractionated into their dissolved phases and acidified to a pH of 2 using trace metal sulfuric acid. The TOC concentrations measured by this procedure were actually DOC concentrations. All particulate organic carbon was removed during fractionation. Any inorganic carbon was removed during the purging step. Samples were purged at room temperature to remove inorganic carbon such as carbonates and hydrogen carbonates. Once purged, 40 μL of sample was injected into a combustion tube containing an oxidation catalyst and heated to 680^{o}C. Analyses were conducted in triplicate. Statistical analyses carried out on the results revealed no significant error (< 10%). A four-point standard curve was developed for calibration.

To model the behavior of DOC in the rainfall-runoff, the DOM sub model of MINTEQ was utilized. DOC acts as a negatively charged ligand that has a high affinity for positively charged ions such as ionic metals. MINTEQ utilizes a Gaussian model to statistically determine the extent of proton binding in solution. The Gaussian DOM model derives complexation at a multi-dentate site and applies this behavior to the entire ligand, assuming site heterogeneity. The Gaussian model requires the assumption that ligands of the DOM mixture are normally distributed with respect to their log K value (Allison et al. 1991). All reactions assume a 1:1 stoichiometry between complexing anions and ligands. MINTEQ offers up to three types of surface binding entities for a complex representation of the DOM surface chemistry. However, this research will use a monodentate model that utilizes a carboxylic binding site subset (Allison et al. 1991). The two dominant parameters influencing complexation reactions are pH and ligand concentrations (Hoin et al. 1993). The major ligand components include DOC, $Cl^{-,}$ SO_4^{-2}, NO_3^- and $PO_4^{-3}$and HCO_3^-. The concentrations of these complexes will be plotted as a function of time for the duration of the storm event. By determining speciation as a function of time, the formation of phosphorus complexes as a function of hydrology was examined.

EQUILIBRIUM AND PARTITIONING KINETICS

The model used to predict phosphorus speciation assumes that the aqueous system is in equilibrium. However, rainfall-runoff events are dynamic processes that exhibit changes in constituent concentrations that can vary by an order of magnitude throughout the duration of an event. From the instant that a raindrop impacts the impervious surface to the time it is discharged into the environment, the various phases of constituents are subjected to processes that can alter their partitioning and speciation. While partitioning and speciation changes throughout the event, samples were taken, rapidly fractionated, stabilized and preserved.

Therefore partitioning was measured at discrete points in time during the event and speciation modeled given the measured water quality analyses at these discrete points in time.

EXPERIMENTAL CONTROL – RAINFALL ANALYSIS

Rainfall was sampled and tested to indicate whether it was a contributing factor to the final TP concentration of the runoff leaving the pavement. During each event, rainfall sampling was conducted at approximately 100-m from the experimental site using a set of three 304.8×457.2 mm^2 glass tray units. A second assemblage was placed at a residential location 3-km away from the experimental site. Such a replicate rainfall collection at separate locations aims to reduce sampling error. Preceding each event, each rainfall sampling units was washed in 30% Nitric Acid and rinsed with de-ionized water to prevent sample contamination. After each event, Samples were immediately transferred back to the laboratory facility and analyzed for the water quality parameters and ionic constituents in the runoff. Rainfall analyses were utilized in MINTEQ for the modeling of P speciation and also used as the baseline to distinguish between atmospheric and urban surface sources of phosphorus.

RESULTS

RAINFALL-RUNOFF INDICES

Partitioning was studied on a number of rainfall runoff events. Table 2-1 presents hydrologic indices for each event, and indices related to the major anthropogenic loading for the catchment. Table 2-2 summarizes concentrations of TP measured from composite rainfall and event mean concentrations of TP measured from runoff. For all of the events studied results indicate that TP mean concentrations in rainfall over the catchment were relatively low (at least an order of magnitude or larger) compared to the mean concentrations measured in the runoff generated from the catchment surface.

Table 2-1. Summary of hydrologic, traffic and sampling based indices for 4 events analyzed for the I-10 experimental catchment site (1088-m2 of pavement) over East Lakeshore Drive.

Rainfall Runoff Event	Hydrologic, Rainfall TDP and Sampling based indices								
	PDH[1] (hrs)	Rainfall[2] Duration (min)	Runoff[3] Duration (min)	Total Precip.[4] (mm)	Total Flow[5] (L)	Q_p[6] (L/s)	t_p[7] (min)	Rainfall TP[8] [mg/L]	IPRT[9] (min)
14-Mar-04	204	413	408	26.2	24076	6.38	295	0.023	8
24-Apr-04	313	184	215	7.2	7288	1.78	116	0.027	16
20-Aug-04	26	29	59	17.3	12307	17.5	23	0.025	12
14-Oct-04	86	179	197	2.6	1672	0.58	60	0.022	48
05-Jun-05	117	53	51	7.1	5856	9.35	13	0.021	6
30-Jun-05	143	72	71	19.1	15117	13.75	21	0.026	8
21-Aug-05	94	112	106	51.1	50002	17.32	36	0.024	7
3-Oct-05	217	9	14	3.81	2615	12.1	5	N/A	2

Notes:
1: PDH: Previous dry hours: Time between current and last event that accumulated at least 0.02 inches of rainfall.
2: Rainfall Duration: The time span between the start and stop of effective rainfall.
3: Runoff Duration: The time spanning between the start and stop of runoff for each event.
4: Total Precipitation: The total amount of precipitation recorded on site for each event.
5: Total Flow: The total amount of runoff generated for each event.
6: Q_p: The measured peak flow of runoff for each event.
7: t_p: The time spanning between start of effective runoff and the peak flow for each event.
8: Rainfall TP: Rainfall total phosphorus concentration.
9: IPRT: Initial pavement residence time = time between start of effective rainfall and observable runoff.

Table 2-2. Summary of TP event mean concentrations and concentration ranges on an event basis for Baton Rouge catchment site (1088-m2 of pavement).

	Concentration of TP [mg/L]							
	10/14/04	8/20/04	4/24/04	3/14/04	6/5/05	6/30/05	8/21/05	10/3/05
Rainfall EMC	0.022	0.025	0.027	0.023	0.021	0.026	0.024	N/A
Runoff EMC	1.735	1.629	2.53	0.706	1.355	1.376	0.818	1.526
Runoff Low bound	1.009	0.368	0.389	0.445	0.416	0.726	0.403	1.2
Runoff High bound	4.838	8.918	64.206	0.656	8.298	14.096	7.267	1.868

Note: Up to 90% of all P dissolved species are: HPO_4^{2-}, $H_2PO_4^-$, $MgHPO_4$ (aq) and $CaHPO_4$ (aq).

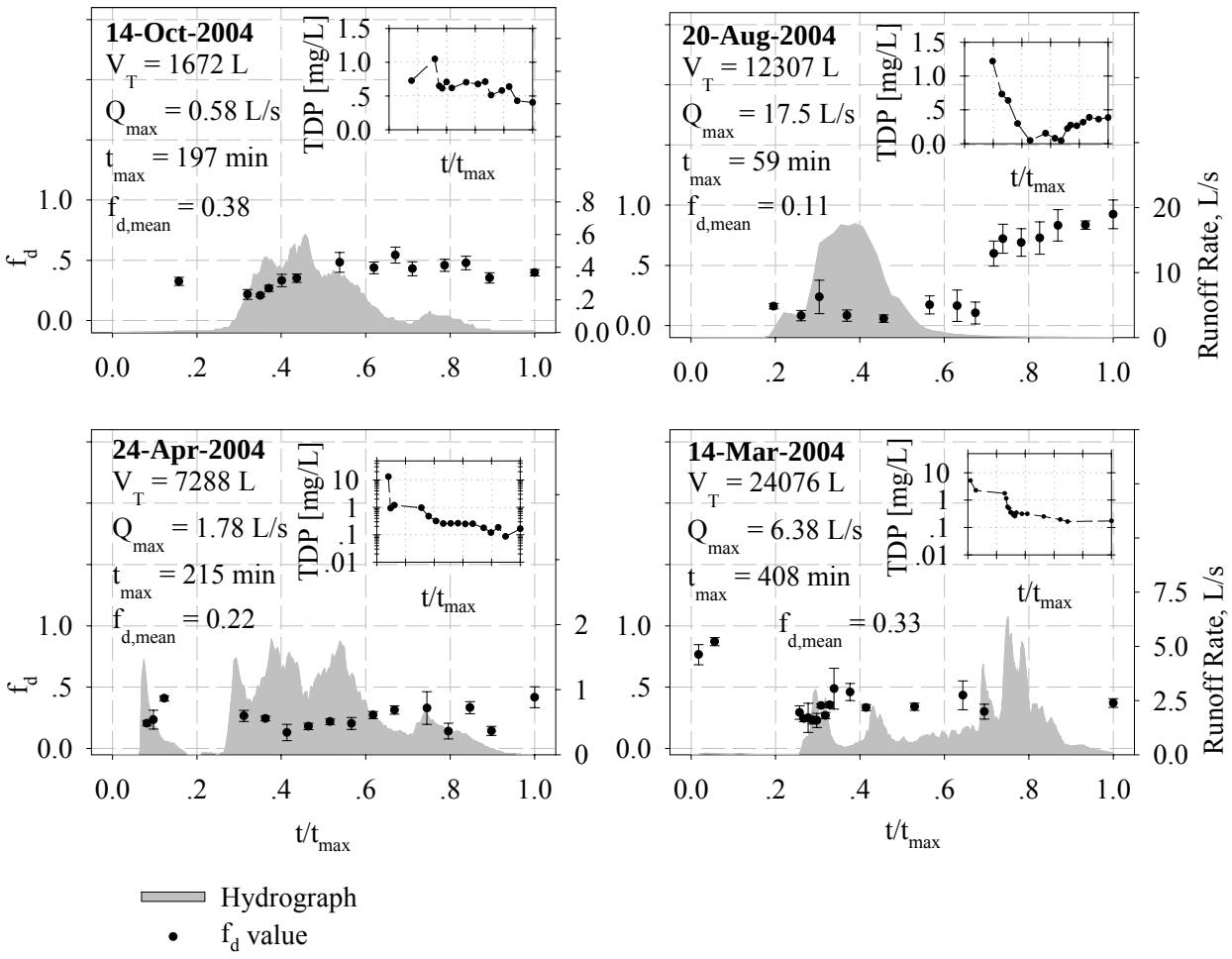

Figure 2-2. Phosphorus dissolved and particulate-bound phases temporal partitioning as a function of hydrograph for each of the four storm events. Values of f_d indicate the dissolved fraction of the total phosphorus mass.

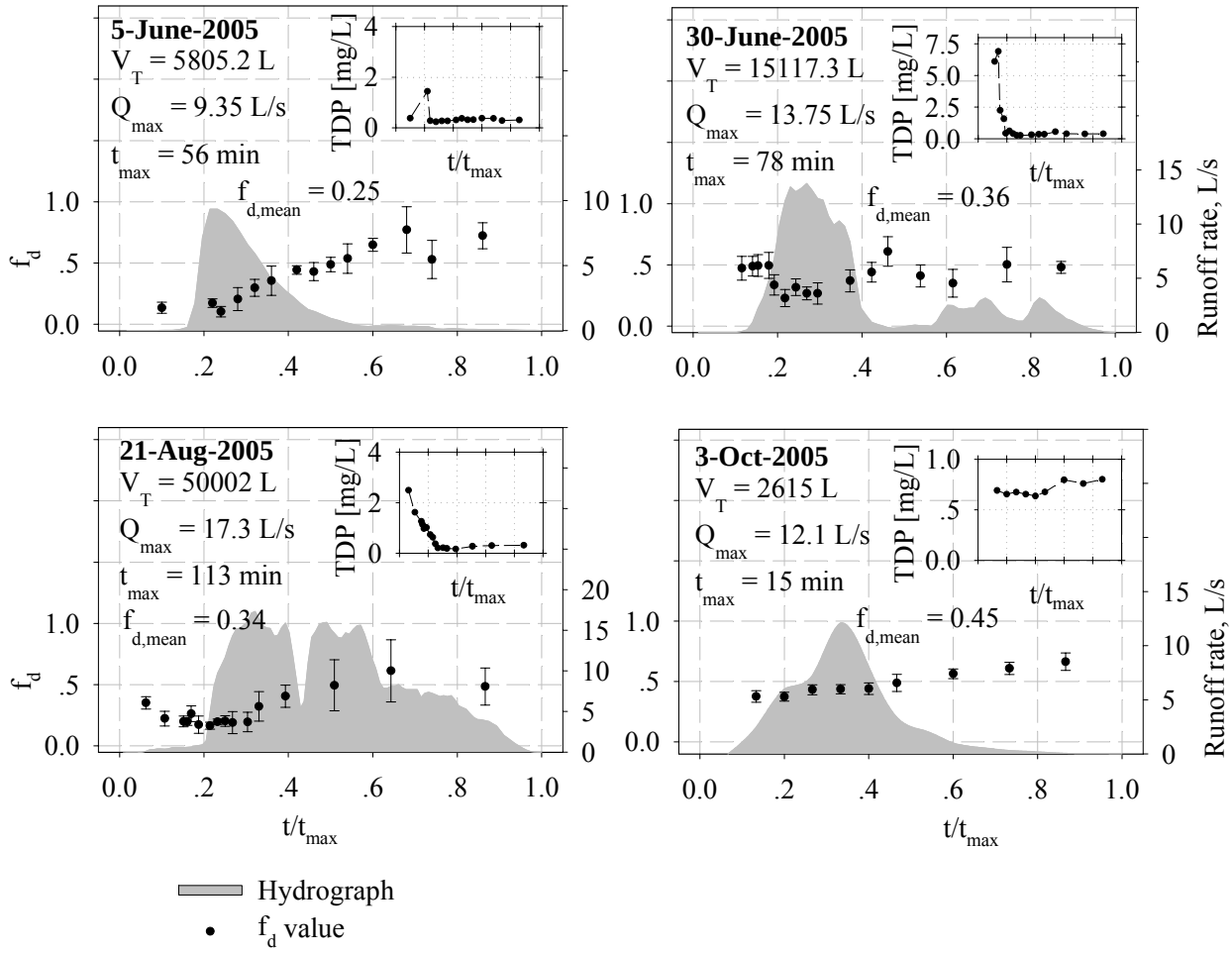

Figure 2-3. Phosphorus dissolved and particulate-bound phases temporal partitioning as a function of hydrograph for each of the four storm events. Values of f_d indicate the dissolved fraction of the total phosphorus mass.

DISSOLVED FRACTION (f_d)

Figure 2-2 and Figure 2-3 summarized the trends in the dissolved fraction (f_d) of TP and the absolute magnitude of total dissolved phosphorus (TDP) concentration as a function of hydrology for all the events. The trend of variation of f_d does not follow the changing of flow rate exactly, partly because of the hydrologic complexity and response variability for a small paved catchment subject to traffic loadings for all events. But the variations of f_d of 20 August 2004 event illustrates that values of f_d trends towards lower values at higher flow rates and higher values at the beginning and towards the tail of the runoff hydrograph on an event-base. Event mean f_d values ranged from 0.11 to 0.38 indicating that the predominance of TP was associated with the particulate gradation. With respect to TDP, there was not a unique transport gradient for the catchment other than exhibiting a lower TDP at the end of the event as compared to the beginning of the event. Additionally, initial TDP varied by over an order of magnitude between events, with this variation potentially related to previous dry hours. For all events initial TDP exceeded 1 mg/L, at least 40 times greater than TP (entirely as TDP) in rainfall itself.

In addition to hydrologic transport there are also many physico-chemical indices affecting the partitioning of phosphorus in the urban rainfall-runoff. These include the loading and composition of particulate phosphorus from dry deposition prior to the rainfall and pH during the hydrograph development. Recognizing that dry deposited particulate-bound phosphorus is the donor and rainfall contacting this dry deposition is the recipient of the phosphorus dissolution, the hydrologic/mass transport and chemistry become the primary driving forces. These include physical and chemical phenomena that occur sequentially and/or in parallel: a) solubility and partitioning of particulate P into the aqueous phase due to the phosphorus concentration gradient between phases; b) aqueous phase phosphorus mixing and

transport due to advection and diffusion at the relative low runoff rate; c) entrainment and transport of particulate P with relatively high runoff rate and ease of particle mobility increasing with decreasing particle size and specific gravity; d) dilution of dissolved phosphorus also due to the high rainfall intensity changing the concentration gradient between phases and promoting phosphorus partition from particulate-bound to dissolved phase; and e) on the falling limb of the hydrograph, the particulate phosphorus mobility decreased due to the loss of driving force from runoff with dissolution playing a more predominant role. From the above hypotheses the dissolved fraction of phosphorus would be high at the two ends of hydrograph, while low at the peak of hydrograph. Results agree with these hypotheses.

DISSOLVED PHOSPHORUS SPECIATION

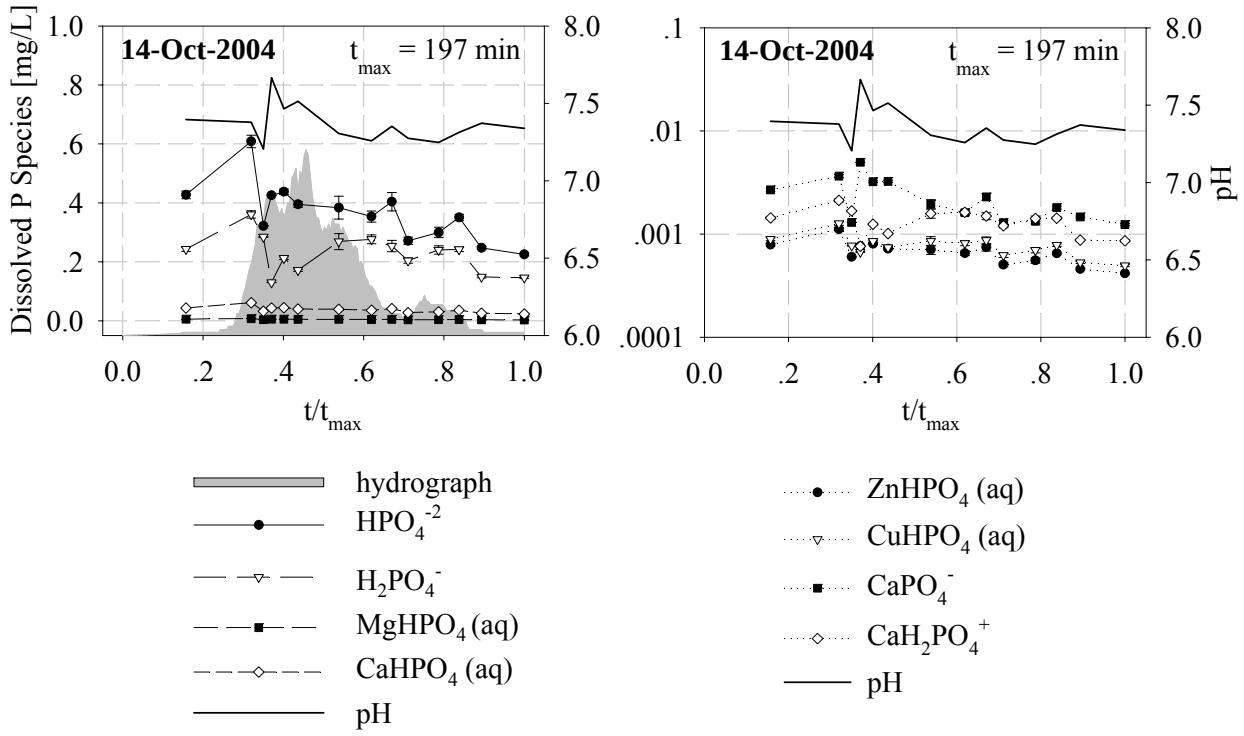

Figure 2-4. MINTEQ-calculated dissolved phosphorus species as a function of the hydrograph for the 14 October 2004 flow-limited rainfall-runoff event. The indicated species were determined to be the dominant 8 species. Samples were taken from the I-10 East Lakeshore Dr. experimental site throughout the duration of the event.

Speciation of dissolved phosphorus at the Baton Rouge site was examined for the 14 October 2004 event. Results are illustrated in Figure 2-4. Orthophosphates, HPO_4^{2-} and $H_2PO_4^{1-}$, dominated the speciation and accounted for more than 80% of total dissolved phosphate mass. Due to the competition and interaction between ions and changing water chemistry during the passage of the hydrograph these species also vary over time although their relative order do not significantly change.

TEMPORAL TRANSPORT AND DISTRIBUTION OF PARTICULATE P FRACTIONS

The temporal transport of phosphorus associated with the sediment, settleable and suspended fractions was examined for all the events. Results are summarized in Figure 2-5 through Figure 2-11 for each fraction. Runoff phosphorus EMCs, low bound and high bound concentrations for each event are summarized in Table 2-2. The 14 October 2004 event was a low intensity, long duration event, with a peak flow of 0.58 L/s and runoff volume of 1672 L. This event transported 1111.8 mg of suspended TP, 205.3 mg of settleable TP, and 86.4 mg of sediment TP. In contrast, the 20 August 2004 event was a high intensity and short duration event with a peak flow of 17.5 L/s and runoff volume of 12,307 L. This event transported 4364.3 mg of suspended TP, 5224.9 mg of settleable TP, and 8144.1 mg of sediment TP. These events represent flow and mass transport limiting conditions, respectively (Sansalone et al 1998, Cristina and Sansalone 2003). The 24 April 2004 event was intermediate to these limiting conditions with a peak flow of 1.78 L/s and runoff volume of 7288 L. This event transported 4022.2 mg of suspended TP, 4180.7 mg of settleable TP, and 5974.7 mg of sediment TP. The 14 March 2004 event was not analyzed for TP associated with the suspended, settleable and sediment fractions. Instead, only total dissolved P and total P were examined for the 14 March 2004 event.

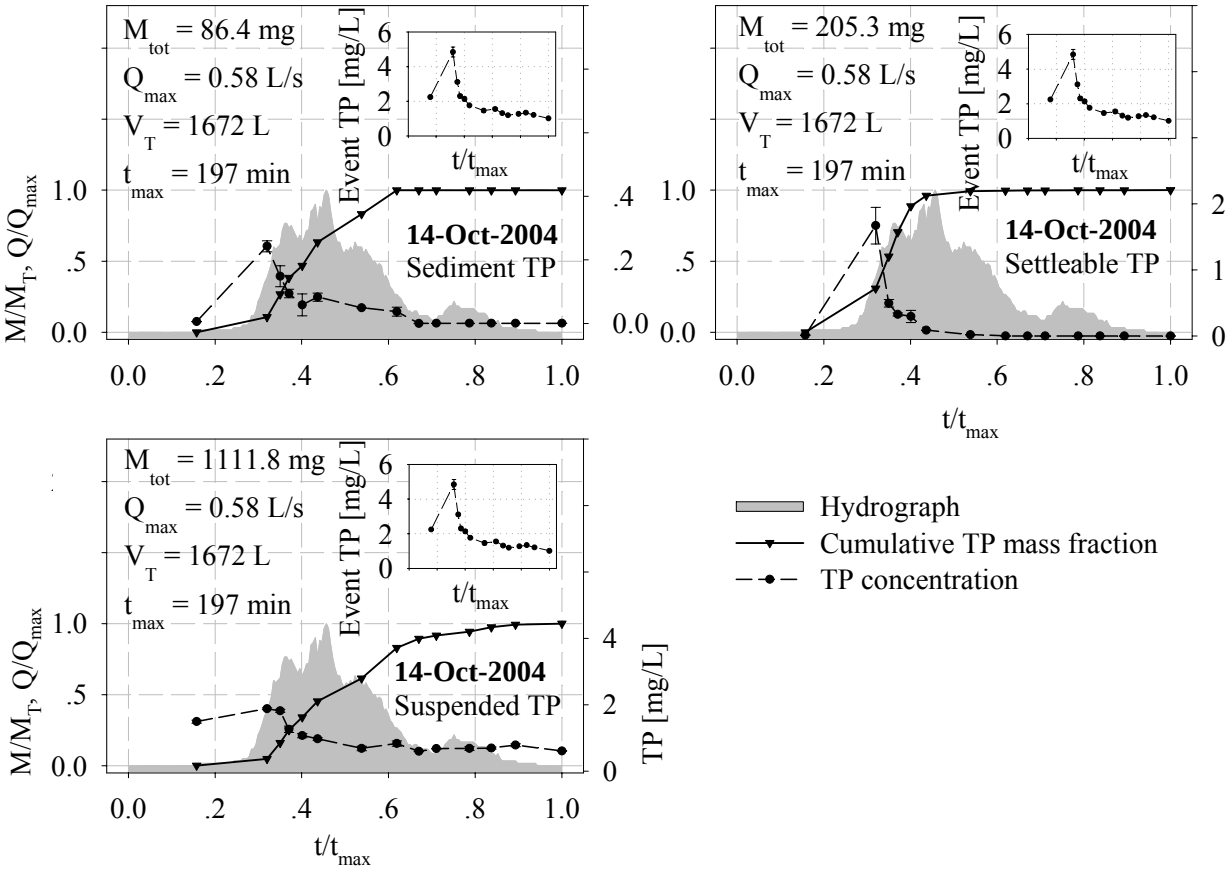

Figure 2-5. Temporal transport of sediment, settleable and suspended total phosphorus as a function of the hydrograph for the 14 October 2004 flow-limited rainfall-runoff event. Samples were taken from the I-10 East Lakeshore Dr. experimental site throughout the duration of the event.

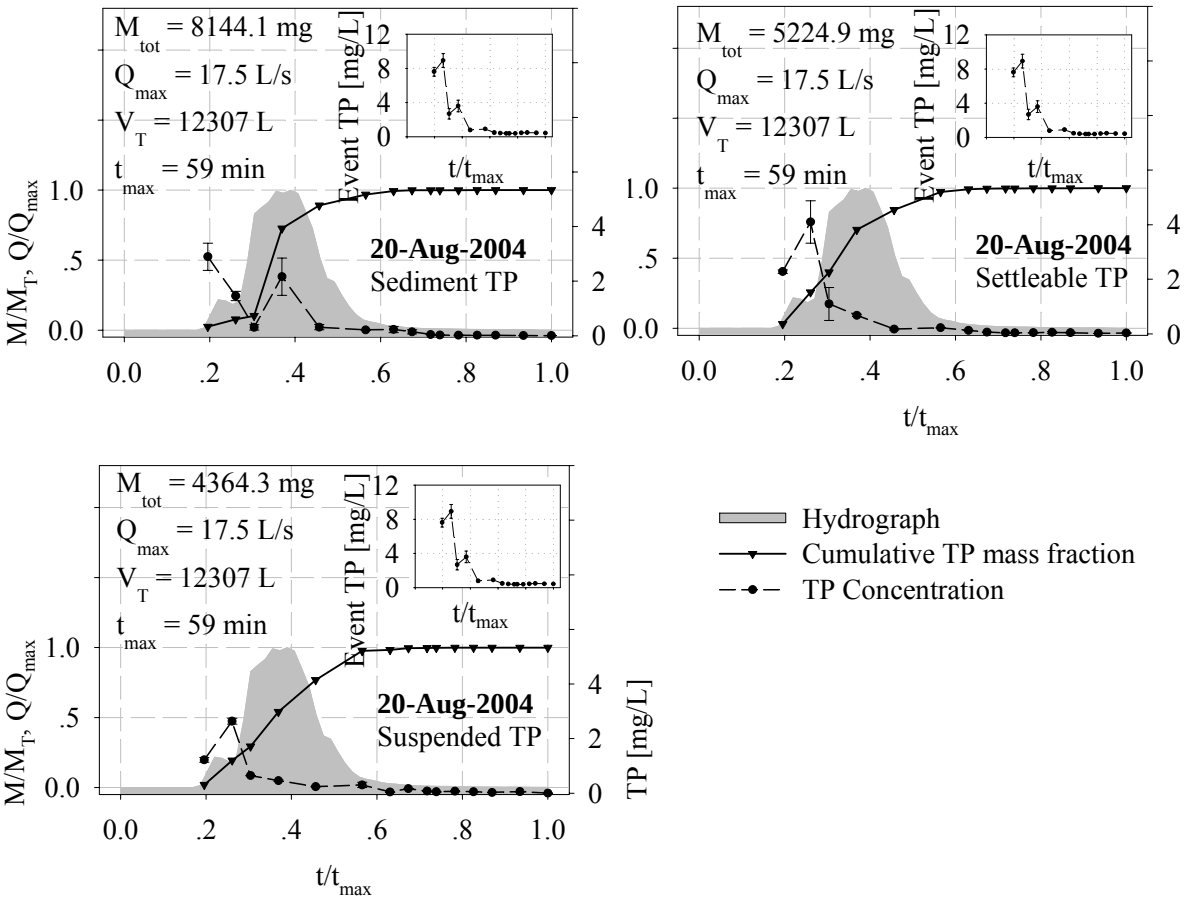

Figure 2-6. Temporal transport of sediment, settleable and suspended total phosphorus as a function of the hydrograph for the 20 August 2004 mass-limited rainfall-runoff event. Samples were taken from the I-10 East Lakeshore Dr. experimental site throughout the duration of the event.

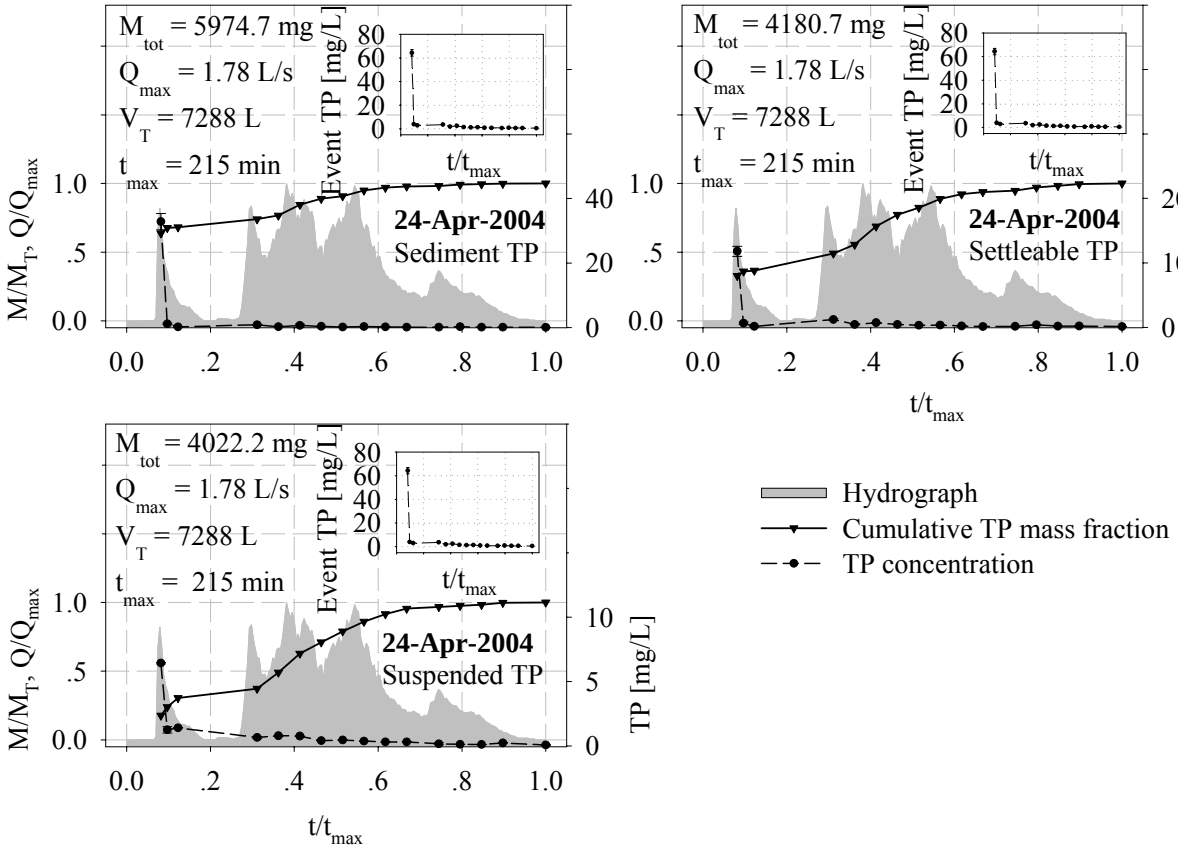

Figure 2-7. Temporal transport of sediment, settleable and suspended total phosphorus as a function of the hydrograph for the 24 April 2004 mass-limited rainfall-runoff event. Samples were taken from the I-10 East Lakeshore Dr. experimental site throughout the duration of the event.

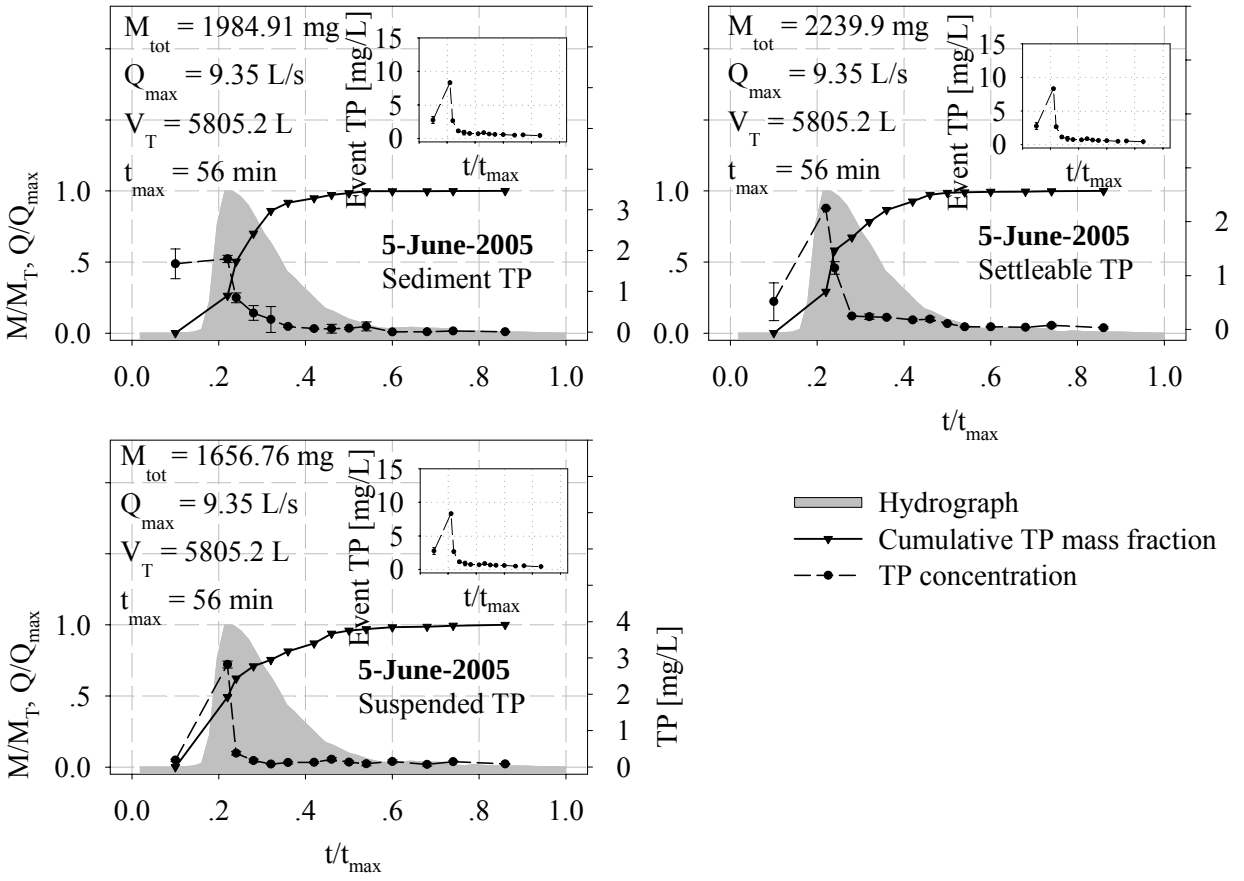

Figure 2-8. Temporal transport of sediment, settleable and suspended total phosphorus as a function of the hydrograph for the 5 June 2005 mass-limited rainfall-runoff event. Samples were taken from the I-10 East Lakeshore Dr. experimental site throughout the duration of the event.

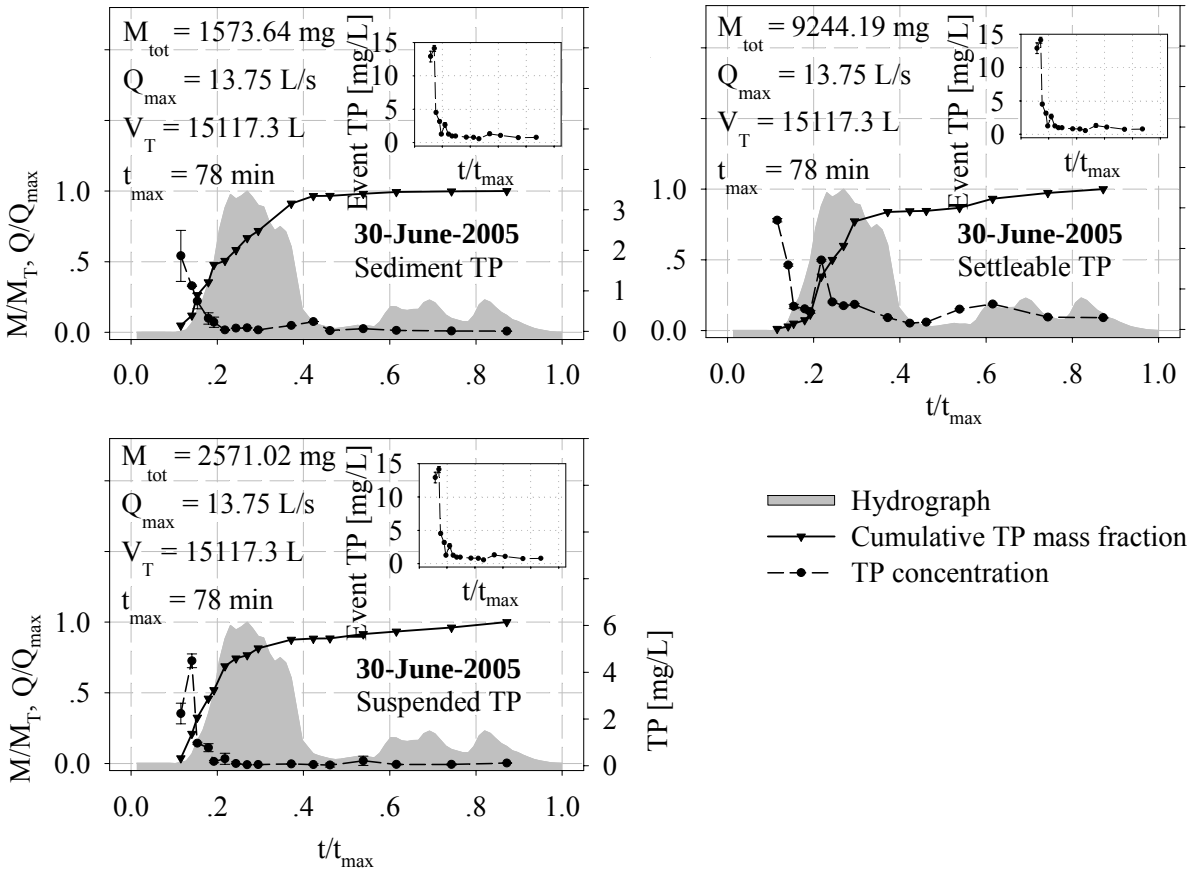

Figure 2-9. Temporal transport of sediment, settleable and suspended total phosphorus as a function of the hydrograph for the 30 June 2005 mass-limited rainfall-runoff event. Samples were taken from the I-10 East Lakeshore Dr. experimental site throughout the duration of the event.

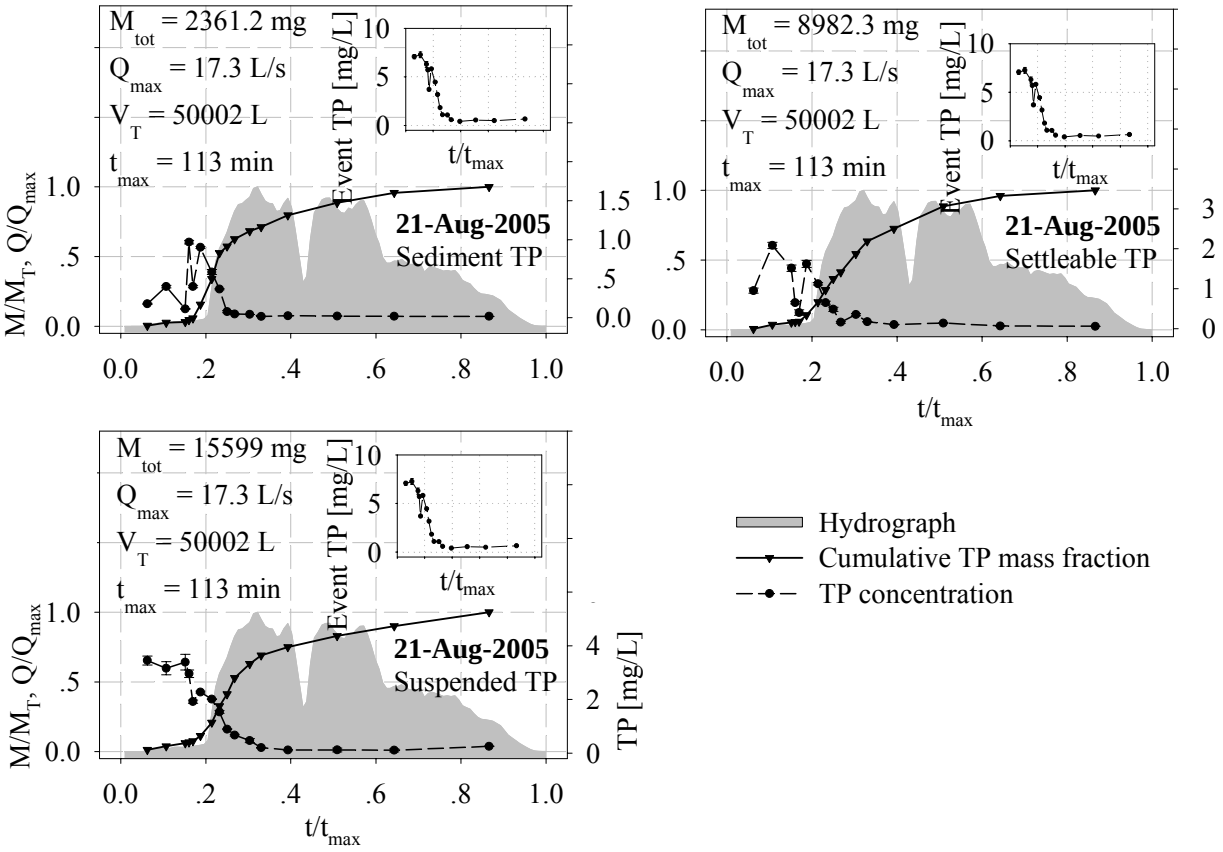

Figure 2-10. Temporal transport of sediment, settleable and suspended total phosphorus as a function of the hydrograph for the 21 August, 2005 mass-limited rainfall-runoff event. Samples were taken from the I-10 East Lakeshore Dr. experimental site throughout the duration of the event.

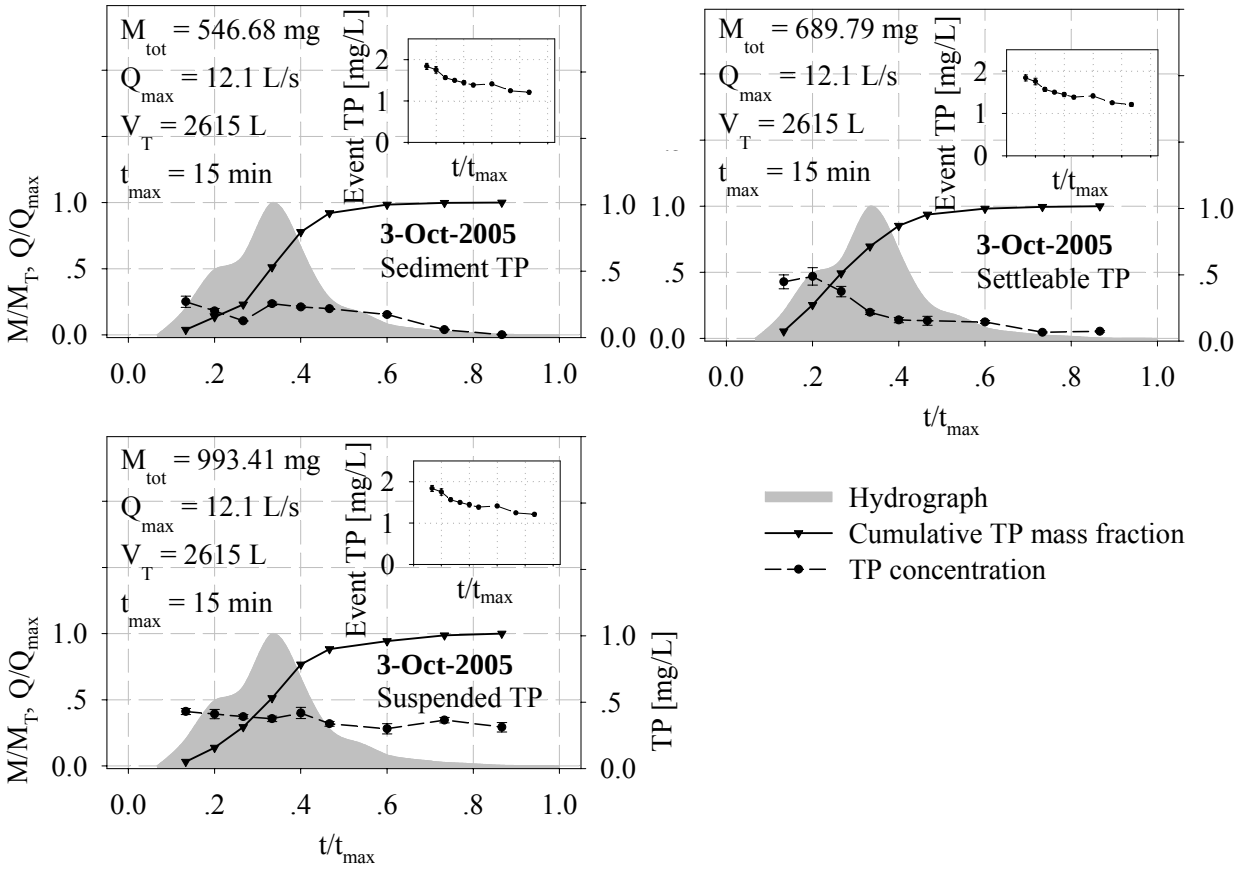

Figure 2-11. Temporal transport of sediment, settleable and suspended total phosphorus as a function of the hydrograph for the 3 October, 2005 flow-limited rainfall-runoff event. Samples were taken from the I-10 East Lakeshore Dr. experimental site throughout the duration of the event.

The 5 June 2005 was a short duration high intensity and mass limited event. The amounts of TP associated with suspended solids, settleable solids and sediment solids were comparable. The 30 June 2005 lasted 78 minutes and generated about 15,000 L of runoff. Interestingly, mass of TP associated with settleable was the highest among the three categories. The 21 August, 2005 event generated about 50,000 L of runoff within 2 hours because of high rainfall intensity. Note that mass of TP associated with suspended solids became the largest for this event. The results indicate that temporary transport and distribution of particulate bound fractions of TP during the rainfall runoff is a complicated phenomena. It could be predicated by a few effecting factors. Nevertheless, events with high flow rate and short duration tends to transport more sediment bound TP while events with low flow rate and long duration inclines to introduce more suspended bound TP.

FIRST FLUSH PHENOMENON

In general the term "first flush" has been utilized to indicate a disproportionately high delivery of either concentration or mass of a constituent during the initial portions of a rainfall-runoff event (Sansalone and Cristina 2004). The idea of a first flush is based on the premise that much of the material that accumulates on the surfaces of urban environment during dry weather period is swept up in the first wave of runoff from a new rainfall (Characklis and Wiesner 1997). Equation (8) defines the quantitative criterion used for defining the occurrence of a first flush (Sansalone and Buchberger 1997).

$$\frac{m'(t)}{v'(t)} \geq 1 \qquad \text{Equation 2-7}$$

In this expression m'(t) and v'(t) represent normalized cumulative mass and flow volumes transported from the urban surface.

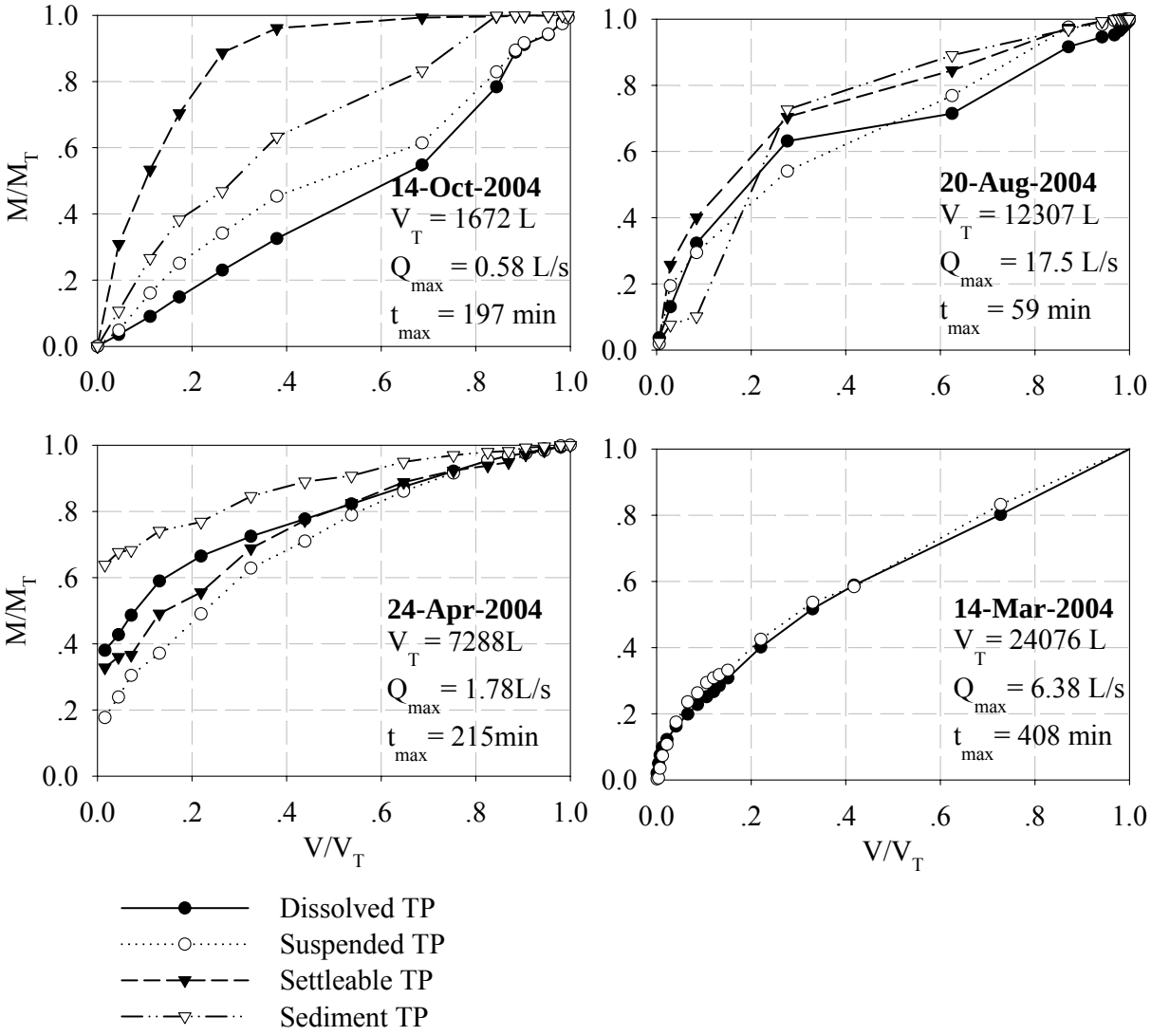

Figure 2-12. First flush phenomena for temporal transport of sediment, settleable, suspended and dissolved total phosphorus as a function of the hydrograph for the four events. Samples were taken from the I-10 East Lakeshore Dr. experimental site throughout the duration of the event.

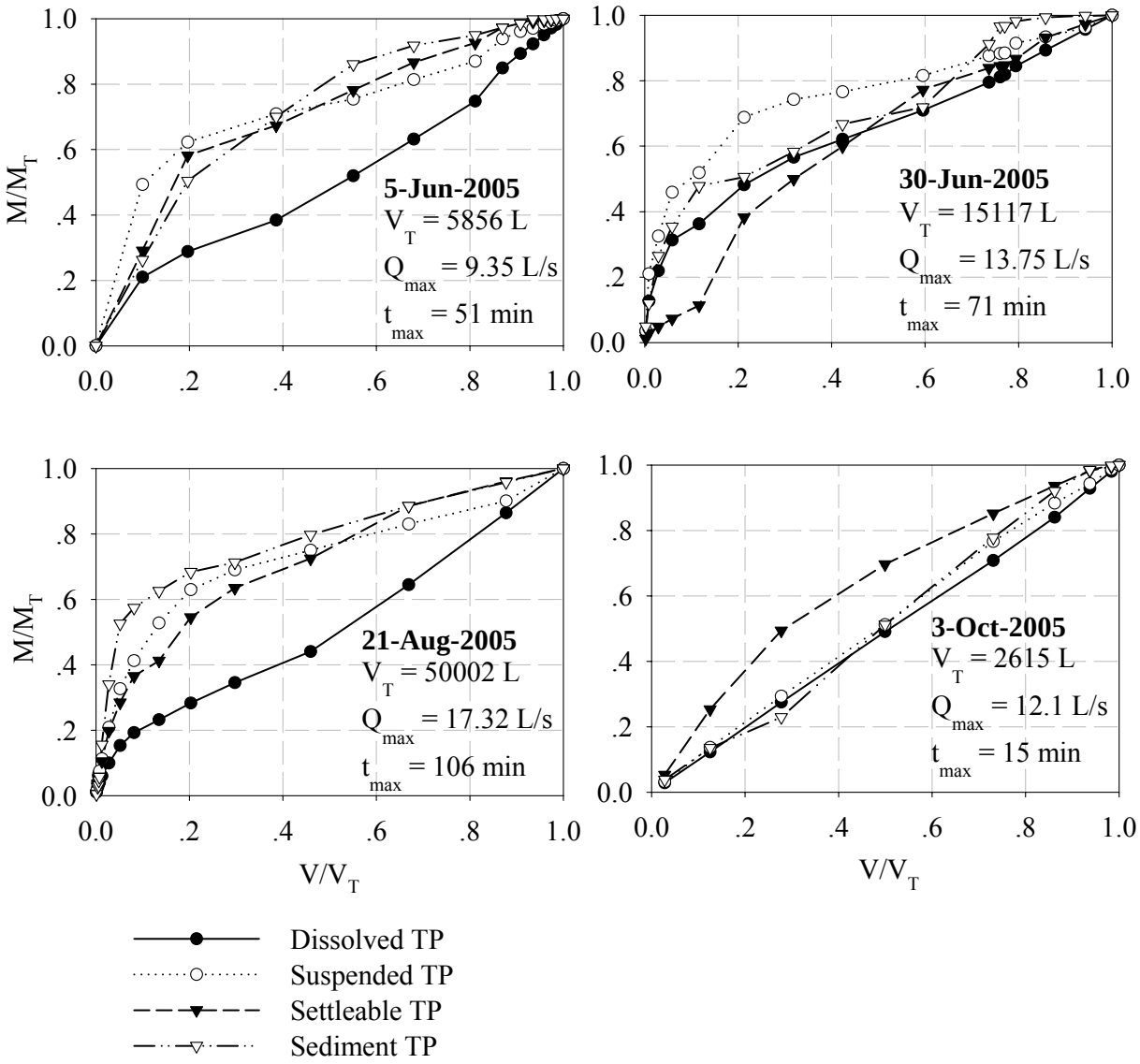

Figure 2-13. First flush phenomena for temporal transport of sediment, settleable, suspended and dissolved total phosphorus as a function of the hydrograph for the three events. Samples were taken from the I-10 East Lakeshore Dr. experimental site throughout the duration of the event.

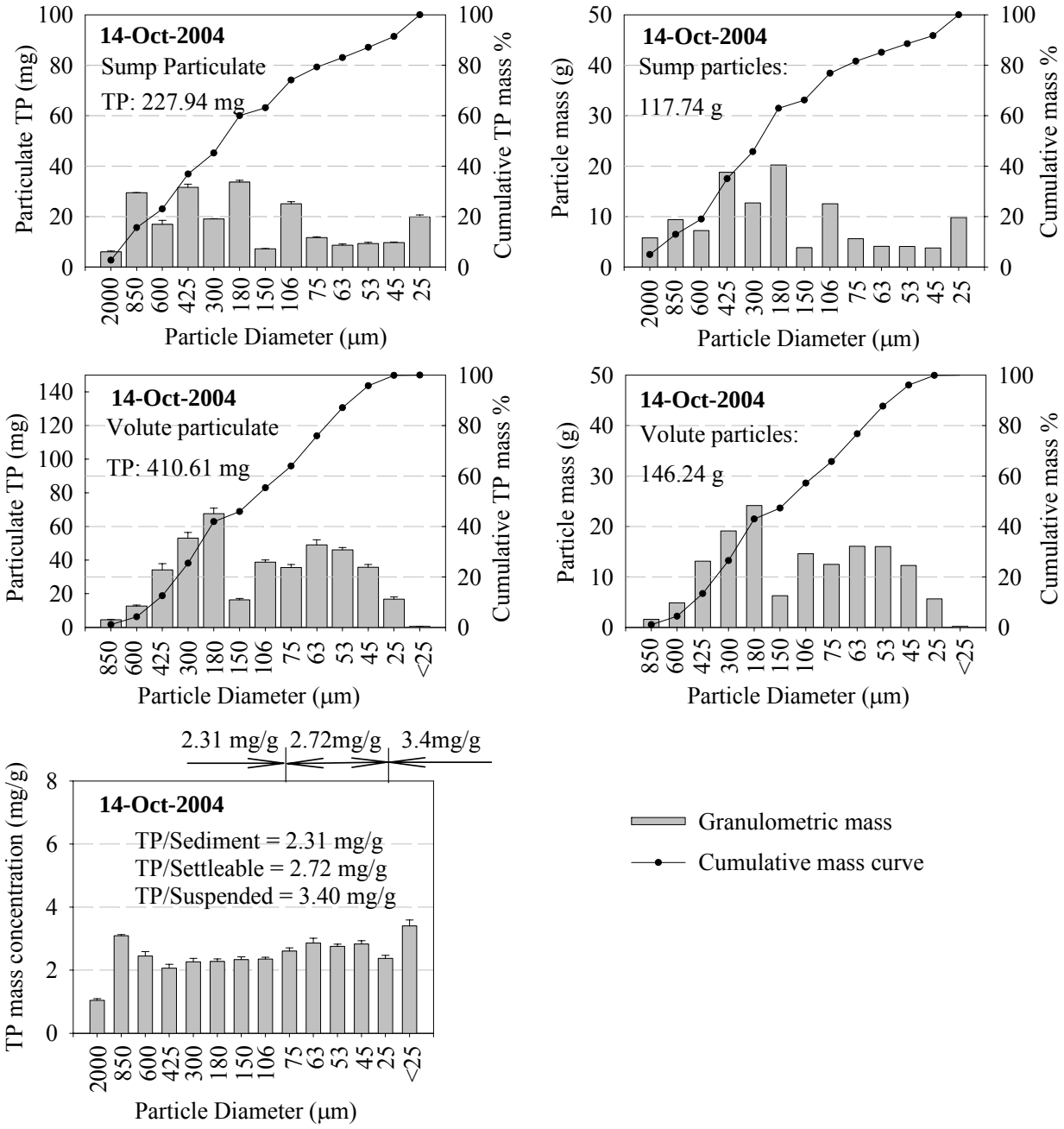

Figure 2-14. Granulometric equilibrium distribution of total phosphorus and particles on the basis of 14-October-2004. Samples were taken from HS sump and volute area respectively in the I-10 East Lakeshore Dr. experimental site. After 24 hour quiescent settling, particle concentrated runoff collected in HS unit from each event was siphoned to remove supernatant and solids deposited in HS sump and volute chamber were recovered for the subsequent particles and particulate phosphorus analysis.

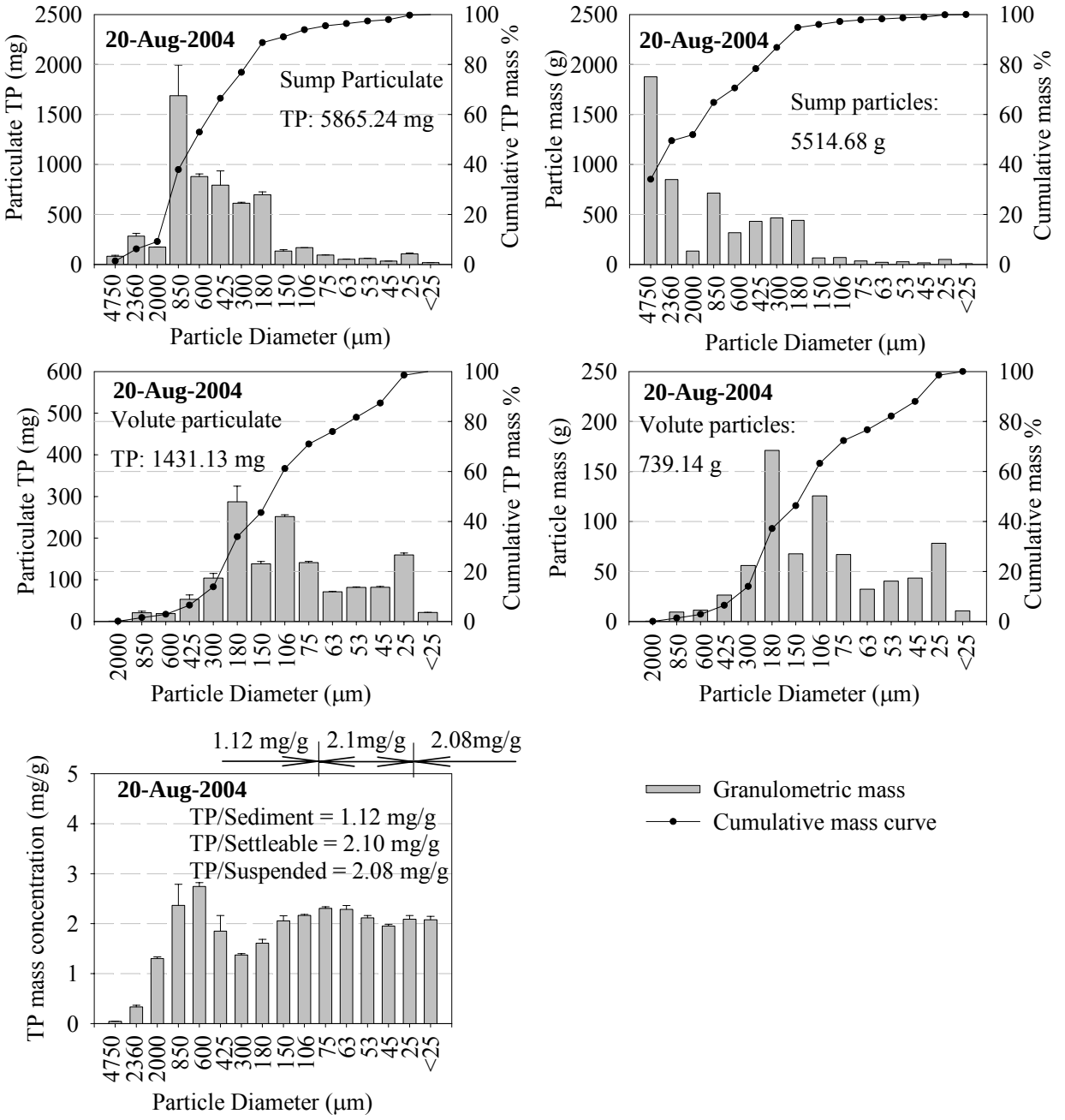

Figure 2-15. Granulometric equilibrium distribution of total phosphorus and particles on the basis of 20-August-2004. Samples were taken from HS sump and volute area respectively in the I-10 East Lakeshore Dr. experimental site. After 24 hour quiescent settling, particle concentrated runoff collected in HS unit from each event was siphoned to remove supernatant and solids deposited in HS sump and volute chamber were recovered for the subsequent particles and particulate phosphorus analysis.

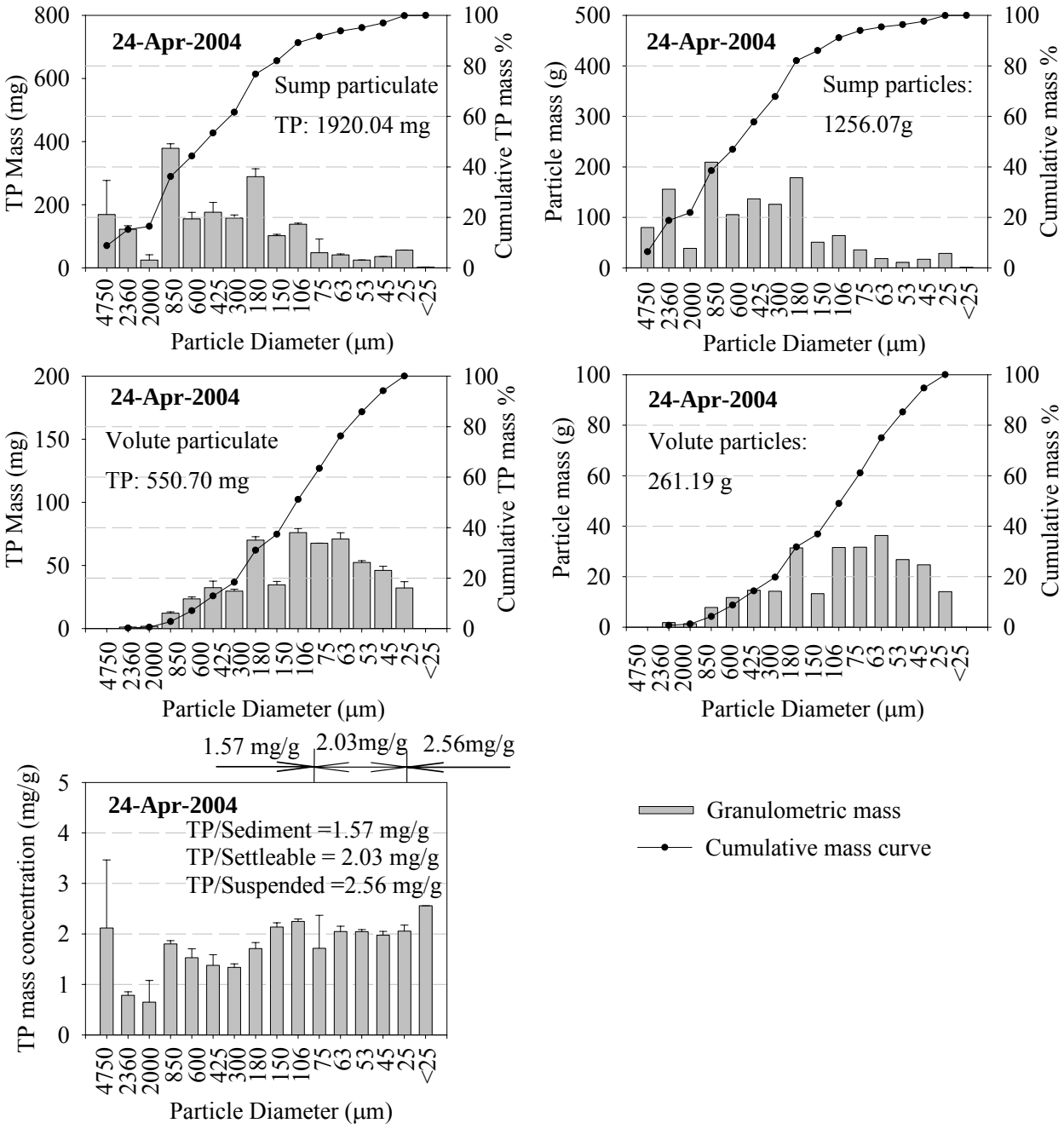

Figure 2-16. Granulometric equilibrium distribution of total phosphorus and particles on the basis of 24-April-2004. Samples were taken from HS sump and volute area respectively in the I-10 East Lakeshore Dr. experimental site. After 24 hour quiescent settling, particle concentrated runoff collected in HS unit from each event was siphoned to remove supernatant and solids deposited in HS sump and volute chamber were recovered for the subsequent particles and particulate phosphorus analysis.

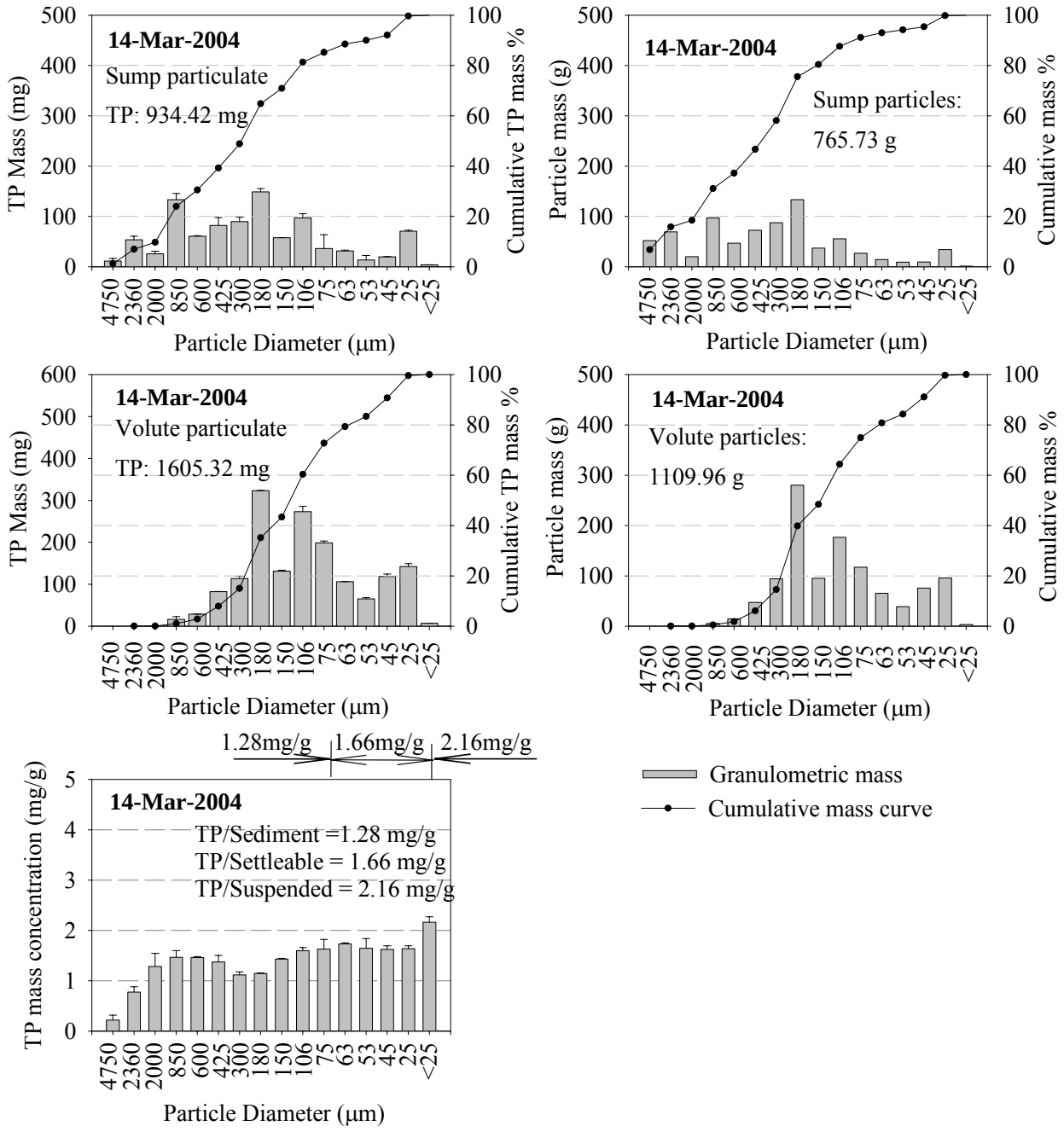

Figure 2-17. Granulometric equilibrium distribution of total phosphorus and particles on the basis of 14-March-2004. Samples were taken from HS sump and volute area respectively in the I-10 East Lakeshore Dr. experimental site. After 24 hour quiescent settling, particle concentrated runoff collected in HS unit from each event was siphoned to remove supernatant and solids deposited in HS sump and volute chamber were recovered for the subsequent particles and particulate phosphorus analysis.

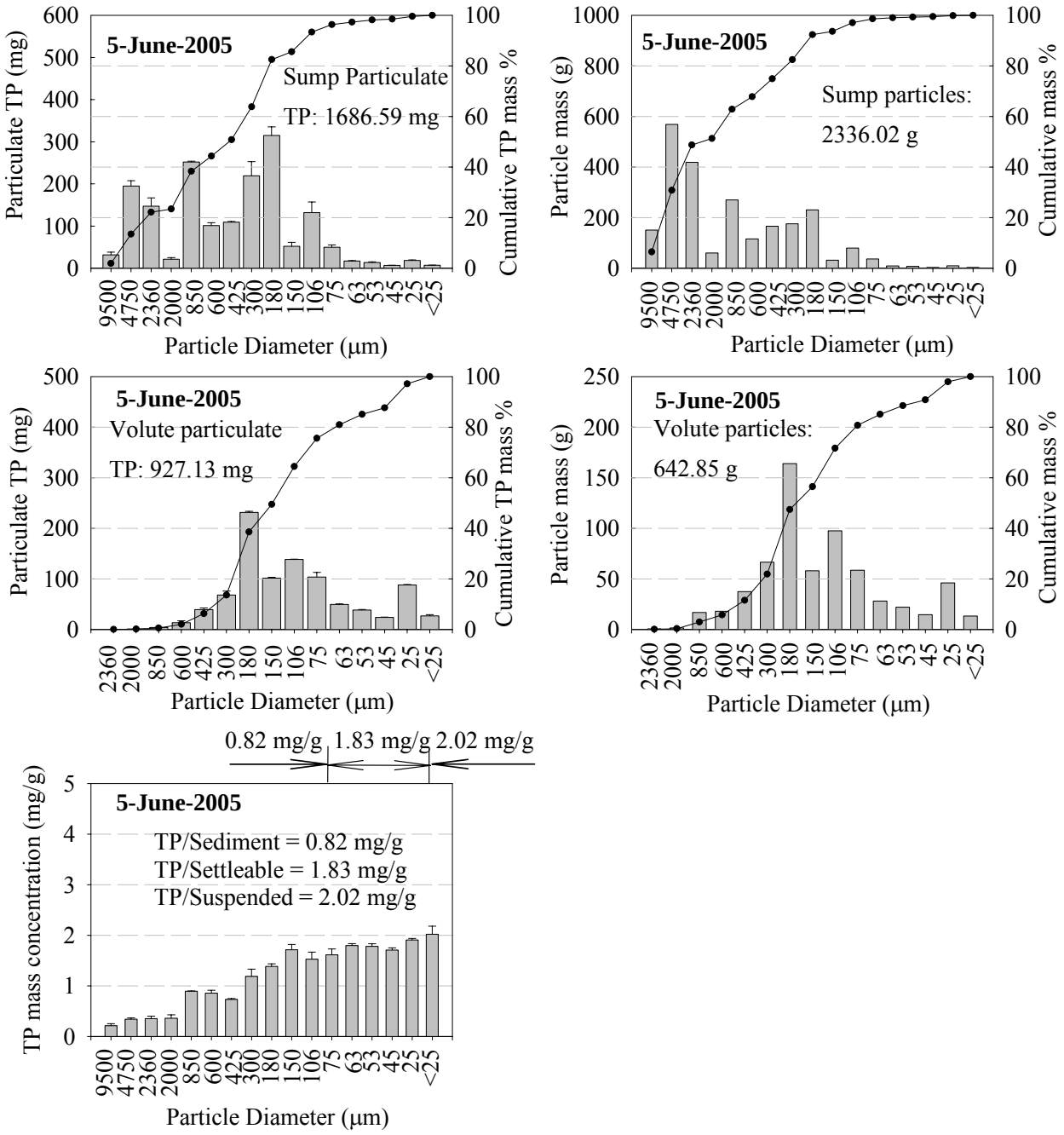

Figure 2-18. Granulometric equilibrium distribution of total phosphorus and particles on the basis of 5-June-2005. Samples were taken from HS sump and volute area respectively in the I-10 East Lakeshore Dr. experimental site. After 24 hour quiescent settling, particle concentrated runoff collected in HS unit from each event was siphoned to remove supernatant and solids deposited in HS sump and volute chamber were recovered for the subsequent particles and particulate phosphorus analysis.

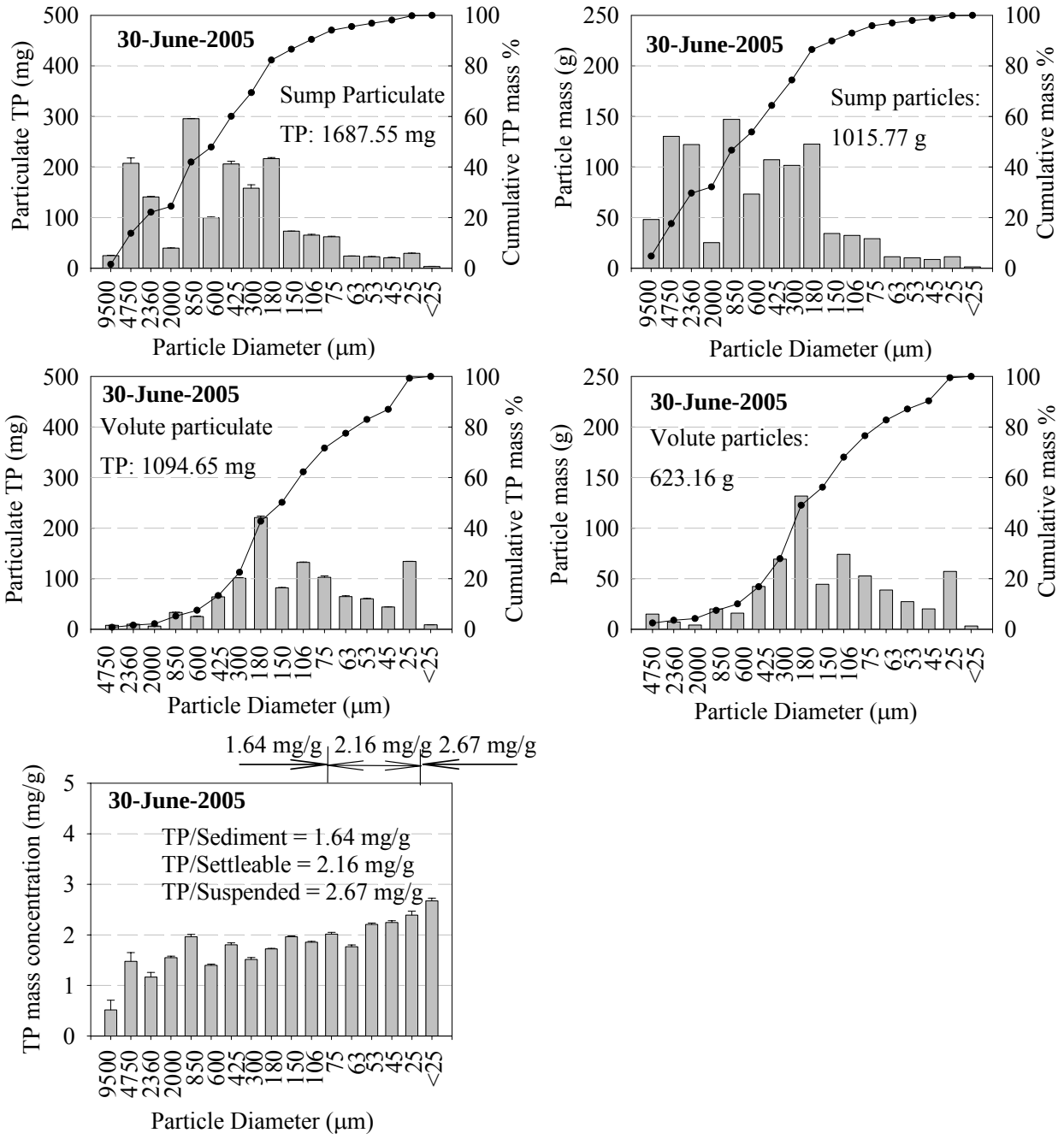

Figure 2-19. Granulometric equilibrium distribution of total phosphorus and particles on the basis of 30-June-2005. Samples were taken from HS sump and volute area respectively in the I-10 East Lakeshore Dr. experimental site. After 24 hour quiescent settling, particle concentrated runoff collected in HS unit from each event was siphoned to remove supernatant and solids deposited in HS sump and volute chamber were recovered for the subsequent particles and particulate phosphorus analysis.

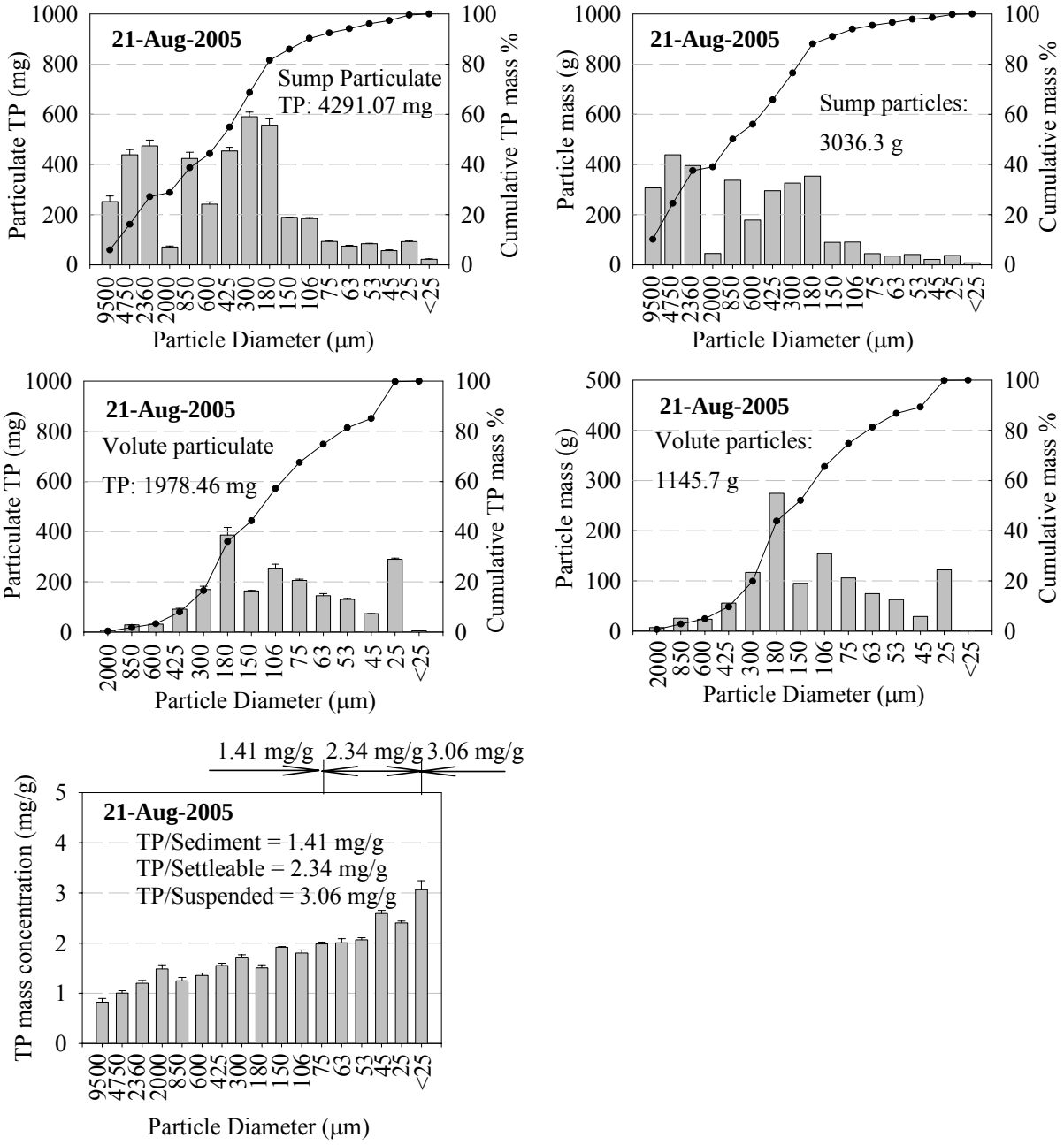

Figure 2-20. Granulometric equilibrium distribution of total phosphorus and particles on the basis of 21-Aug-2005. Samples were taken from HS sump and volute area respectively in the I-10 East Lakeshore Dr. experimental site. After 24 hour quiescent settling, particle concentrated runoff collected in HS unit from each event was siphoned to remove supernatant and solids deposited in HS sump and volute chamber were recovered for the subsequent particles and particulate phosphorus analysis.

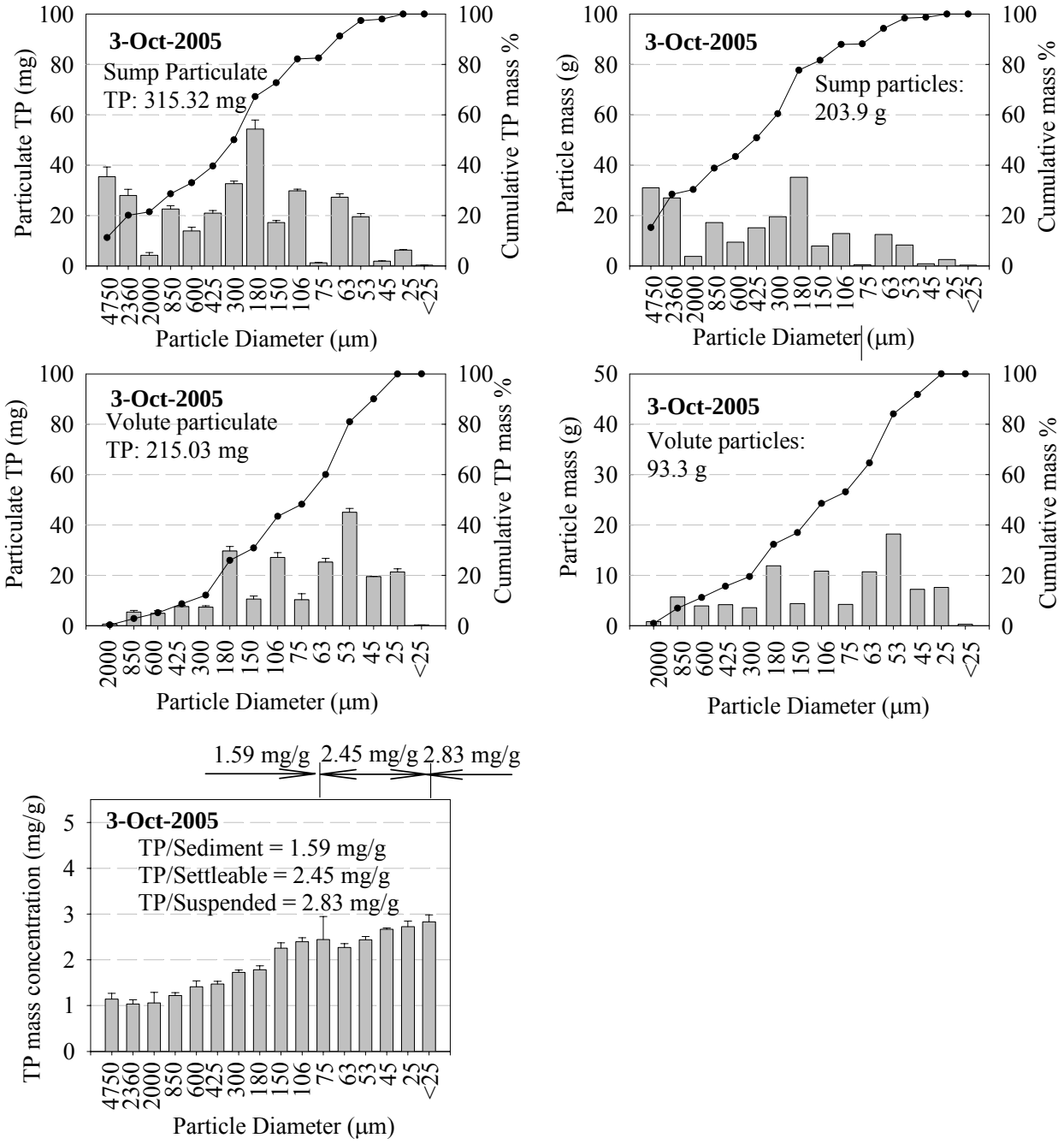

Figure-2-21. Granulometric equilibrium distribution of total phosphorus and particles on the basis of 3-Oct-2005. Samples were taken from HS sump and volute area respectively in the I-10 East Lakeshore Dr. experimental site. After 24 hour quiescent settling, particle concentrated runoff collected in HS unit from each event was siphoned to remove supernatant and solids deposited in HS sump and volute chamber were recovered for the subsequent particles and particulate phosphorus analysis.

The results of first flush phenomenon of phosphorus in urban rainfall runoff are summarized in Figure 2-12 and Figure 2-13. In general, TP associated with sediment and settleable fractions, and to a lesser extent the suspended fraction, demonstrated a mass-based first flush based on equation 8 for all the events studied. Except for the flow-limited 14 October 2004 event, TDP also exhibited a first flush. For higher intensity flow events the sediment and settleable fractions illustrated the strongest first flush.

EQUILIBRIUM PHOSPHORUS GRANULOMETRIC DISTRIBUTION

After a rainfall-runoff event particulate matter was recovered from an experimental stainless steel hydrodynamic separator unit operation within 24 hour of the event. Particulate matter in the hydrodynamic separator was separated by hydrodynamic separation within the deflective screen area into an inner sump area, and by sedimentation in an outer concentric volute area outside of the deflective screen. All particulate matter was recovered, dried and sieved so that total phosphorus equilibrium content could be quantified as a function of particle size. Results are summarized in Figure 2-14 through Figure 2-21 for each rainfall-runoff event.

For the distribution of TP across the particulate matter there are a number of common trends that can be illustrated from these results. First, while the distribution of particulate matter mass gradations are different between sump and volute areas as would be expected due to different predominant unit operations in each area, when comparing particulate mass and particulate TP within each of these areas, the distribution of particulate mass and particulate TP within each event is similar. When comparing incremental particulate matter distribution mass and TP mass for a specific area and specific event, incremental distributions are similar and cumulative distributions are similar. Secondly, the sump area of the hydrodynamic separator removes a coarser gradation of particles as compared to the volute area, for each event. These

mass gradation differences illustrate the two differing mechanisms of particle separation, and that these differing mechanisms result in differing distributions and amounts of TP mass. Finally, the particulate phosphorus association capacity/sorption, i.e. phosphorus content per particle mass in each gradation, [mg/g], ranged from 1.0 ~ 3.5 regardless of hydrograph. In general, this indice increases with decreasing particle size for all events.

IMPLICATIONS

Table 2-3. Summary of TP from other source.

Constituents	Rainfall*	Urban storm water[1]		Urban Highway[2]	Road runoff[3]	Highway[4]
		Median EMC	Mean EMC	Runoff Sites	Median 1st flush	runoff
TSS, mg/L	-----	100	141 ~ 224	127.8 ~ 360.0	60 ~ 1350	45 ~ 798
TP, mg/L	0.02~0.15	0.33	0.37 ~ 0.47	0.21 ~ 0.34	0.19 ~ 1.8	0.11 ~ 0.998
DP, mg/L		0.12	0.13 ~ 0.17	0.1 ~ 0.12	-----	-----

Note:
1: Nationwide Urban Runoff Program (NURP) values from U.S. EPA. 1983; Metcalf & Eddy, Inc., 1991; Novotny, 1992
2: Kayhanian et al., 2003
3: Drapper et al., 2000, Brisbane, in southeast Queensland, Australia
4: Barrett et al., 1993

As indicated in the results, partitioning and the particulate-bound distribution of phosphorus in rainfall-runoff are phenomena that influence the transport and fate of phosphorus. Two factors, hydrologic transport and dry deposition phosphorus loading, will dictate phosphorus transport and fate in unit operations. Given the wide range of particles, particles were categorized based on categories of sediment (> 75μm), settleable (75 ~ 25 μm) and suspended (< 25μm) based on the one hour Imhoff settling test convention and mechanistic behavior. To prevent potential under-estimation of TP loads and mis-representation of the distribution of TP for source area watersheds, all samples were carried out manually capturing

the full cross-section of flow for discrete samples across each rainfall-runoff event. Duplicate 12-L samples were utilized to quantify particles size above 75 μm. Between 15 and 20 samples were taken for each event to ensure representative characterization across the entire hydrograph. The results of particulate phosphorus characterized by this study were compared with the data from other sources of the urban rainfall-runoff as shown in Table 2-3. Wet deposition of TP was not a significant source for the phosphorus levels found in urban runoff. Second, phosphorus levels reported by this study were higher than levels reported by other studies. Other than site specific effects, for example the use of phosphate-based admixtures in the watershed concrete pavement, one likely explanation may be the difference in sampling between this study and previous studies.

CONCLUSIONS

This study examined the influence of hydrology on urban runoff phosphorus partitioning, distribution of particulate phosphorus among sediment, settleable and suspended particles fractions, and dissolved phosphorus speciation from a research site in Baton Rouge, Louisiana. A number of Rainfall-runoff events were examined from 1088-m^2 urban source area watershed. The hydrologic characteristics of these events ranged from flow-limited to mass-limited events for TP and particulate transport. The equilibrium phosphorus distribution across a wide gradation of particles captured by hydrodynamic separation were examined and quantified based on TP mass and concentration.

This study is unique in that rainfall-runoff sampling strategy and phosphorus analysis methodology were addressed for the entire gradation of particulate matter transported, not just the suspended and dissolved fractions. Results indicate that depending on the hydrologic transport and antecedent dry period that a significant fraction of TP can be associated with the

sediment size fraction. Measured EMCs of TP from the site significantly exceeds common water quality standards (EPA 1986). Speciation results for the dissolved fraction indicate that phosphate is dominant with the forms of HPO_4^{2-} and $H2PO_4^{1-}$ and therefore these two species would dominate the bioavailability of dissolved phosphorus. Understanding partitioning and speciation of phosphorus as a function of hydrologic transport and time is crucial for designing unit operations and processes for source area watersheds. The dissolved fraction tends to be inversely related to hydrologic transport - lower dissolved fractions at higher flow rates and vice versa. While there were variations in hydrology during each individual event, the mean partition dissolved fractions ranged from 0.11 to 0.38. Distribution of particulate phosphorus between sediment, settleable and suspended particles was dependent on hydrology, which functioned as driving force for the transport of particles. At higher runoff flow rates, greater particulate phosphorus was entrained and mobilized. Equilibrium granulometric distribution showed that particulate-bound phosphorus association capacity ranging from 0.82 to 3.4 mg/g, increased with deceasing particle size. Small particles normally has larger specific surface area. Results from this study indicate that effective control of rainfall-runoff phosphorus from source area watersheds requires unit operations and processes that account for particulate-bound species, hydrologic transport and speciation of phosphorus.

REFERENCES

Allison, J.D., Brown, D.S. and Novo-Gradac, K.J. (1991). MINTEQA2/PRODEFA2, A Geochemical Assessment Model for Environmental Systems: Version 3.0 User's Manual. EPA/600/3-91/021, 115 pp.

APHA- American Public Health Association. (1998). Standard Methods for the Examination of Water and Wastewater, (20th Ed.) A.D. Eaton, L.S. Clesceri, A.E. Greenberg (Eds.), American Public Health Association, American Water Works Association and Water Environmental Federation, Washington, D.C.

Allen, T. (1981), Particle Size Measurement, 3rd ed. Chapman and Hall, London, UK.

Barlow, K., Nash, D. and Grayson, R., 2004. Investigating Phosphorus Interactions with Bed Sediments in a Fluvial Environment Using a Recirculating Flume and Intact Soil Cores. Water Research, 38, 3420-3430.

Barrett, M.S., R.D. Zuber, E.R. Collins, J.F. Malina, R.J. Charbeneau, & G.H. Ward. 1993. A Review and Evaluation of Literature Pertaining to the Quantity and Control of Pollution from Highway Runoff and Construction. Center for Research in Water Resources, Bureau of Engineering Research, University of Texas, Austin. CRWR 239.

Barrett, M.E., Malina, J.F., Charbeneau, R.J. and Ward, G.H. (1995). Characterization of Highway Runoff in Austin Texas area. Center for Research in Water Resources, Bureau of Engineering Research, University of Texas at Austin, 35 pp.

Barrett, M.E., Walsh, P.M., Malina, J.F. Jr. and Charbeneau, R.J., 1998. Performance of Vegetative Controls for Treating Highway Runoff. Journal of Environmental Engineering, 124(11), 1121-1128.

Bartone, D.M. and Uchrin, C.G., 1999. Comparison of Pollutant Removal Efficiency for Two Residential Storm Water Basins. Journal of Environmental Engineering, 125(7), 674-677.

Bowes, M.J., House, W.A., Hadgkinson, R.A. and Leach, D.V., 2005. Phosphorus-Discharge Hysteresis During Storm Events Along a Rivers Catchment: the River Swale, UK. Water Research, 29, 751-762.

Characklis, G.W. and Wiesner, M.R., 1997. Particles, Metals, and Water Quality Runoff from Large Urban Watershead. Journal of Environmental Engineering, 123(8), 753-759.

Comings, K.J., Booth, D.B. and Horner, R.R., 2000. Storm Water Removal by Two Wet Ponds in Bellevue, Washington. Journal of Environmental Engineering, 126(4), 321-330.

Correll, D. L. 1998. The role of phosphorus in the eutrophication of receiving waters: a review. J. Environ. Qual. 27:261-266.

Cowen, W.F., and Lee, G.F., 1973. Leaves as a source of phosphorus. Environ. Sci. Technol. 7(9), 853-854.

Culbert, H. and France, R. 1995. Laboratory prediction of phosphorus release from deciduous leaves to urban runoff. Water Quality Research Journal of Canada. 30(2), 243-246.

Dechesne, M., Barraud, S., and Bardin, J.P., 2005. Experimental assessment of stormwater infiltration basin evolution. Journal of Environmental Engineering, 131, 1090-1098.

Detenbeck, N.E. and Brezonik P.L., 1991. Phosphorus Sorption by Sediments from a Soft-Water Seepage Lake. Environmental Science & Technology, 25(3), 395-409.

Drapper, Rodger Tomlinson, and Philip Williams., 2000 Pollutant concentrations in road runoff: southeast queensland case study. Journal of Environmental Engineering, April, pp 313-320.

Drapper, D., Tomlinson, R. and Williams, P. (2000). Pollutant Concentrations in Road Runoff: Southeast Queensland Case Study. Journal of Environmental Engineering, American Society of Civil Engineers, Vol. 126, No.4, pp 313-320, (Apr).

Gächter, R., Steingruber, S.M., Reinhardt, M. and Wehrli, B., 2004. Nutrient Transfer from Soil to Surface Waters: Differences between Nitrate and Phosphate. Aquat. Sci., 66, 117-122.

Gächter, R., Ngatiah, J.M. and Stamm, C., 1998. Transport of Phosphate from Soil to Surface Waters by Preferential Flow. Environmental Science & Technology, 32(13), 1865-1869.

Gao, B., Walter, M.T., Steenhuis, T.S., Hogarth, W.L. and Parlange, J.Y., 2004. Rainfall Induced Chemical Transport from Soil to Runoff: Theory and Experiments. Journal of Hydrology, 295, 291-304.

Gray, J.R., Glysson, G.D., Turcios, L.M. and Schwarz, G.E. (2000). Comparability of Suspended-Sediment Concentration and Total Suspended Solids Data. United States Geological Survey, WRIR 11-4191, 14 pp.

Harwood, J.E., Hattingh, W.H.J. 1973. Colorimetric methods of analysis of phosphorus at low concentration in water. In Environmental Phosphorus Handbook; Griffith, E. J., Ed.; John Wiley & Sons: New York.

Helen Bennion, Stephen Juggins, and N. John Anderson. (1996). Environmental Science & Technology., VOL. 30, NO. 6, pp 2004-2007.

Helsel, D., Kim, J., Grizzard, T., Randall, C., and Hoehn, R. (1979). Land use influence on metals in storm drainage. J. Water Pollution Control Fed., 51(4), 709-717.

Huang, C.P., 1975. J. Colloid Interface Sci. 53, 178.

Huanxin, X., Presley, B.J. and Velinsky, D.J. 1997. Distribution and source of phosphorus in tidal river sediments in the Washington, DC area. Environmental Geology. 30(3/4), 224-230.

House, W.A. and Denison, F.H., 2002. Exchange of Inorganic Phosphate between River Waters and Bed-Sediments. Environmental Science & Technology, 36(20), 4295-4301.

Karthikeyan, K.G., Tshabalala, M.A., Wang, D. and Kalbasi, M., 2004. Solution Chemistry Effects on Orthophosphate Adsorption by Cationized Solid Wood Residues. Environmental Science & Technology, 38(3), 904-911.

Kayhanian, M., Singh, A., Suverkropp, C. and Borroum, S., 2003. Impact of annual average daily traffic on highway runoff pollutant concentrations. Journal of Environmental Engineering. November, 975-990.

Langmuir, Donald, 1997, Aqueous environmental geochemistry: New Jersey, Prentice-Hall, Inc., 600 p.

Marklund, A., Andersson, B. and Haglund, P., 2005. Traffic as a source of organophosphorus flame retardants and plasticizers in snow. 39(10), 3555-3562.

Metcalf & Eddy, Inc. 1991. Wastewater engineering: treatment, disposal, and reuse, 3rd ed. New York, NY: McGraw-Hill.

Morel, F.M., and Hering, J.G., 1993, Principles and applications of aquatic chemistry. New York, John Wiley & Sons, 588 p.

Morton, S.C., Glindemann, D. and Dewards, M.A., 2003. Phosphates, Phosphites, and Phosphides in Environmental Samples. Environmental Science & Technology.,VOL. 37, NO. 6, pp 1169-1174.

Murphy, J.; Riley, J. P. Anal. Chim. Acta 1962, 27, 31-36.

Novotny, Vladimir. 1992. Unit pollutant loads. Water Environ. Tech.

Owen P. Bricker. An Overview of the Factors Involved in Evaluating the Geochemical Effects of Highway Runoff on the Environment. US Geological Survey Open-File Report 98-630.

Premazzi, G., and Provoni, A. 1985. Internal P loading in lakes: A different approach to its evaluation. Hydrobiologia, Vol. 120, pp 23–33.

Pretty, J.N., Mason, C.F., Nedwell, D.B., Hine, R.E., Leaf, S. and Dils, R., 2003. Environmental Costs of Freshwater Eutrophication in England and Wales. Environmental Science & Technology., VOL. 37, NO. 2, pp 201-208.

Sansalone, J.J. and Buchberger, S.G., 1997. Partitioning and First Flush of Metals in Urban Roadway Storm Water. Journal of Environmental Engineering, American Society of Civil Engineers, Vol. 123. No. 2, February, pp 134-143.

Sansalone, J.J., Koran, J.M., Smithson, J.A. and Buchberger, S.G., 1998. Physical Characteristics of Urban Roadway Solids Transported During Rain Events. Journal of Environmental Engineering, American Society of Civil Engineers, Vol.124, No. 4, pp 427-440.

Schueler, T., 1987. Controlling urban runoff: a practical manual for planning and designing urban BMP. Metropolitan Washingto Council of Governments, Washington, D.c., 1-275.

Seo, D. and Canale, R.P., 1999. Analysis of Sediment Characteristics and Total Phosphorus Models for Shagawa Lake. Journal of Environmental Engineering, 125(4), 346-350.

Sharma, M.L., Herne, D.E., Byrne, J.D. and Kin, P.G. 1996. Nutrients discharge beneath urban lawns to a sandy coastal aquifer, perth, western Australia. Hydrogeology Journal. 4 (1), 103-117.

Snoeyink, V.L. and Jenkins, D., 1980. Water Chemistry. John Wiley & Son, Inc. New York 463 pp.

Spivakov, B.Y., Maryutina, T.A. and Muntau, H., 1999. Phosphorus Speciations in Water and Sediments. Pure Appl. Chem., 71(11), 2161-2176.

Thomson, N.R,. McBean, E.A., Snodgrass, W. and Mostrenko, I., 1997. Sample Size Needs for Characterization Pollutant Concentrations in Highway Runoff. Journal of Environmental Engineering, American Society of Civil Engineers, Vol. 123, No.10, pp 1061-1065 (Oct).

U.S. EPA, 1993. Handbook Urban Runoff Pollution. Office of Research and Development Washington, DC 20460. EPA/625/R-93/004 September. pp 6.

U.S. EPA, 1986. Quality Criteria for Water. Office of Water Regulation and Standards, US Government Printing Office (PB81-226759), Washington, DC 20460. EPA 440/5-86-001.

U.S. EPA, 1983. U.S. Environmental Protection Agency. Guidelines for the monitoring of urban runoff quality. EPA/600/2-83/124 (NTIS PB84-122902).

Vaze, J. and Chiew, F. H. S., 2004. Nutrient Loads Associated with Different Sediment Sizes in Urban Stormwater and Surface Pollutants. Journal of Environmental Engineering, American Society of Civil Engineers, APRIL, pp 391-396.

Vollenweider, R.A. and Kerekes, J., 1980. The loading concept as a basis for controlling eutrophication, philosophy and preliminary results of the OECD programme on eutrophication. Prog. Water Technol., 12, 5-38.

Wong, J.W.C. Chan, C.W.Y. and Cheung, K.C. 1998. Nitrogen and phosphorus leaching from fertilizer applied on golf course: lysimeter study. Water; Air; and Soil Pollution. 107, 335-345.

Aimin Zhou, Hongxiao Tang, Dongsheng Wang, 2005. Phosphorus adsorption on natural sediments: Modeling and effects of pH and sediment composition. Water Research 39, 1245-1254.

CHAPTER 3 IN-SITU REMOVAL MECHANISM AND POLLUTANT TRANSPORT MODELING OF PARTICULATE-BOUND PHOSPHORUS IN URBAN RAINFALL-RUNOFF

SUMMARY

This study investigated pollutant transport modeling of particulate-bound phosphorus in urban rainfall-runoff at the upper end of a small Cementitious Porous Pavement (CPP) watershed and in-situ removal mechanism and efficiency by hydrodynamic separator on the basis of representative sampling and appropriate P measurement. Such a study may help understanding how particulate bound fraction of phosphorus, which is a predominant over dissolved fraction, was transported in the urban rainfall-runoff events, evaluating phosphorus potential fate and bioavailability, and shedding sight on effective in-situ control of P which was considered a major cause of eutrophication.

Originated from regression model, P pollutant model of this research was developed by utilizing particulate matter transient loading over rainfall-runoff event coupled with P association capacity on particulate matters. Such a manner makes it possible to economically predict P loading and also facilitates better unit operation and process (UOP) selection.

The P removal mechanisms by hydrodynamic separator are a combination of dynamic screening and quiescent settling. Removal efficiencies of particulate bound phosphorus are pronouncedly dependent of size of particulate matter and distribution of particulate mass and hydrological parameters of the specific events. Generally, removal efficiency for overall particulate bound P was in the range of 10~50%, with highest removal efficiency for sediment bound P (normally more than 60%), medium removal efficiency for settleable bound P (mostly 30~60%) and lowest removal efficiency for suspended bound P (around 10%).

Results from this study indicate that P pollution model could be successfully applied for intra-event P transport in urban rainfall-runoff. Besides, hydrodynamic separation could effectively remove particulate-bound phosphorus. Nevertheless, additional urban rainfall-runoff P treatment is needed mainly because stringent discharge limit for P is promulgated and dissolved fraction of P is still of concern.

INTRODUCTION

Eutrophication could be attributed to excessive presence of nutrients (P and N) in a water body that stimulates algae bloom and oxygen depletion, which results in a less desirable water quality, thereby, affects the surrounding biota and water body's usage (e.g., aesthetics, recreation, fish maintenance and water supply) (Chau and Jin 1998). Discharge from non-point sources such as urban transportation land use rainfall-runoff has been recognized as major cause for pollution of surface waters (USEPA 1983; USEPA 1990; Duda 1993; Drapper et al. 2000; Ackerman and Schiff 2003). Due to the rapid urbanization and booming industrialization, non-point source of pollution which is detrimental to environment has been gradually increasing these years (Saget et al. 1996; Bertrand-Krajewski 1998; Brezonik and Stadelmann 2002; Jang et. al. 2005).

Contaminants (including P) from fertilizer in lawn use, atmospheric fallout, motor vehicles traffic, construction activities, animal waste, solid waste litter, and other anthropogenic sources accumulate on the built land surfaces may be washed off by sequent rainfall-runoff and received by adjacent surface waters, ground waters and ecosystems (Marklund et al. 2005; Akan et al. 2000). Perceived as a major source of pollutants that results in adverse environmental effects, urban rainfall-runoff has to comply with local and federal contaminant effluent limitations, as required by the National Pollutant Discharge Elimination System (NPDES).

P is the primary limiting nutrient in most lakes and reservoirs (Schindler 1977; Hecky and Kilham 1988). Intensive anthropogenic activities related to P use and dispersion such as urbanization, transportation, industrialization, development residential, and modernization of agriculture have placed a tremendous ecological stress on the receiving water bodies. Most of the lakes, rivers and estuaries around the world have increased levels of nutrients and other ecological harmful chemical compounds. In the continental USA, for example the mean TP concentration of stream water at 381 riverine sites was found to be 0.13 mg/L (Smith et al. 1987), which greatly exceeds the mesotrophic-eutrophic TP boundary of 0.075 mg/L recently proposed by Dodds et al. (1998). Table 3-1 lists concentration Level of TP (mg/L) of different trophic states. Smith et al. (1993) also showed that 48% of 410 water quality monitoring stations failed to meet the widely accepted US EPA (1986) standard of 0.1 mg/L. These low water quality data suggest that eutrophication is inevitable unless sources of P was treated and controlled effectively.

Table 3-1. Concentration Level of TP (mg/L) of different trophic states

	Concentration Level of TP (mg/L) of different trophic states			
	Oligotrophic (Low)	Mesotropic (intermediate)	Eutrophic (high)	Hypertropic (super-high)
Lakes (Vollenweider, 1980)	0.003 ~ 0.018	0.011 ~ 0.096	0.016 ~0.386	0.75 ~ 1.2
Lakes (Nurnberg, 1996)	< 0.01	0.01 ~ 0.03	0.03 ~ 0.1	> 0.1
Streams (Dodds et al., 1998)	< 0.025	0.025 ~ 0.075	> 0.075	NA
Coastal Marine (Hakanson, 1994)	< 0.01	0.01 ~ 0.03	0.03 ~ 0.04	> 0.04

There are two common inter-connected sources of P causing eutrophication in lakes or rivers: catchment (Deletic and Orr 2005; Sonstrom et al. 2002); internal release from particulate matter (Seo et al. 1999; Cerco 1995). To remediate water quality, some practice has been focus

on reducing sediment release of nutrients, for example utilization of active barriers (Hart et al. 2003), which is capable of containing nutrients by physiochemical adsorption or precipitation processes. However, even in cases where some promising results have been achieved, these are still the end-of-pipe strategy. More importantly, P temporally held on particulate matter has a great potential to release to the surrounding solution when the environmental parameters become favorable again such as low pH and anaerobic (Scarlatos 1997; Chen and Sheng 2005). Therefore P coming from transportation catchment (non-point source) and mobilized by urban rainfall-runoff needed treatment prior to receiving waters (Foy et al. 1996).

Effective P treatment selection depends on accurate monitoring of P loading and transport in urban rainfall-runoff. P always actively partitions between dissolved and particulate bound phase. Phosphorus can associate and distribute in whole size gradation of particulate matter transported by urban rainfall-runoff. The particle size distribution of particulate matter thus becomes a particularly important issue because it dictates mobility of the particles and pollutant concentrations associated with (Appan and Wang 2000). Given the wide size range of particulates in urban rainfall-runoff (from 1^{-} μm to $4{,}750^{+}$ μm) (Sansalone et al. 1998), particles are classified into categories of litter of gross debris (> 4750 μm), sediment (> 75 μm), settleable (75 ~ 25 μm) and suspended (< 25 μm) based on the solids mechanistic behavior and operational one hour Imhoff quiescent settling test (Lin and Sansalone 2004). Dissolved and particulate bound Phosphorus transport and loading in urban rainfall-runoff is a very complex phenomenon and is not yet well understood. The complexity of the problem is ascribable to many factors: a) different sampling strategy (manual or automatic sampling), which might fundamentally suggest the extent of representative sampling. It is not surprising to envision that automatic sampling would have difficulties to capture coarse fraction of particulate matter though the time span

between automatic samples could be very short; b) in-deterministic availability and buildup extent of atmospheric deposition with varying species of phosphorus; c) dynamic partitioning between dissolved and particulate bound phases due to physic-chemical interaction among rainfall-runoff and entrained dissolved solids, suspended solids, settleable solids and sediments solids; d) unique hydrodynamics of each and every rainfall-runoff event; e) different mobility and transformability of water and varying sizes of particles (Shinya et al. 2003; Zhou et al. 2005). The intricacy of monitoring P loading not only can partly explain the large discrepancy of TP data presented in literature but also would make people realize that analytical and mechanistic modeling of p transport in urban rainfall-runoff is too unrealistic to carry out. Therefore study on alternative modeling strategy, such as empirical correlation of particulate matter loading with mass of TP associated with, could become a suitable alternative.

Many P treatment methods with varying removal mechanism and efficiency have been investigated: infiltration and detention basin (Bartone and Uchrin 1999; Dechesne et al. 2005); constructed wetland system (Gervin and Brix 2001; Seo et al. 2005); vegetative controls (Barrett et al. 1998); stormtreat system (sedimentation tank) (Sonstrom et al. 2002); filtration with floating media filter (Visvanathan et al. 1996); urban wet detention ponds (Wu et al. 1996; Comings et al. 2000; Wang et al. 2004). Total P removal efficiencies are typically smaller than 50% and show a large variability. P treatability in urban rainfall-runoff is strongly influenced by sorption at surface of particulate matter and partition between the dissolved and particulate bound phase. Common particulate P removal mechanisms are sedimentation and filtration. Sedimentation generally needs large operational space which is limited in populated urban area. Possible contamination of underlying soil and groundwater is another problem which can not be neglected for application of sedimentation. While filtration processes are widely used, it

commonly encounters clogging which is characterized by the hydraulic resistance. Moreover, sand as a typical filter media can not achieve good P removal efficiency (Bubba et al. 2003; Forbes et al. 2004). To meet current and expected water quality requirement, advanced in-situ urban rainfall-runoff P treatment technologies and processes have to be investigated. Hydrodynamic separator attracted more and more attention due to its favorable features: flexibility to unsteady flow type of rainfall runoff; easiness to install, operate and maintain; work singly or in concert with other facilities; small footprint; potentially satisfactory particle removal efficiency, especially for coarse particle fractions.

Numerous research studies have been carried out on transport of phosphate from soil to runoff or subsurface flow (Gachter et al. 1998; Gachter et al. 2004; Gao et al. 2004; Mcdowell et al. 2002). However, studies on massive transport of phosphorus, especially temporal particulate bound phosphorus transport along rainfall runoff event, is not common. Moreover, the research on in-situ removal efficiency and mechanism of phosphorus in urban rainfall-runoff through hydrodynamic separator is even rare.

OBJECTIVES

P in situ transport in urban rainfall-runoff and on line removal by utilization of hydrodynamic separation as a physical unit operation would be investigated. There are four major objectives of this research. First, efforts would be emphasized on correctly monitor the transport and loading of urban rainfall-runoff P, especially particulate-bound P, which could only be obtained by means of representative sampling – flow weighted manual sampling. Second, temporal particulate-bound phosphorus and particulates transport would be correlated and modeled using power law by recognizing the similar profiles these two constituents developed over the hydrograph. Such a manner may allow reasonable particulate-bound phosphorus loading

prediction by using particulates as a surrogate on event or annual basis. Third, removal efficiencies of hydrodynamic separator would be presented by comparing influent and effluent in terms of TDP, suspended TP, settleable TP and sediment TP for a number of rainfall-runoff events. Finally, removal mechanism of particulate-bound phosphorus by hydrodynamic separator would be suggested.

BACKGROUND

Phosphorus is one of the major urban rainfall-runoff constituents that commonly occur in both soluble and particulate fractions. The concentrations of dissolved P in urban rainfall-runoff are typically lower than concentrations of particulate bound P (Jia and Sansalone). Such a phenomenon is usually the result of sorption of p on the particulate matters, whose surfaces are rich in metal oxides or minerals. The behavior, transport and ultimate environmental fate of phosphorus in urban rainfall-runoff depend largely on their sorption with the particulate matters. Sorption may be one of the most important chemical processes affecting mobility and bioavailability of contaminants in natural water systems (Drever 1997). Particulate matters contains varying amount of common minerals, such as Ca, Al and Fe, which are considered as good natural sorbents (Shinya et al. 2000). The fundamental theory applicable to p sorption on particulates is the electrical double layer, of which two types are recognized (Berner 1971; van Olphen, 1977). In the first type, sorption results from imperfections or ionic substitutions within the crystal lattice, which produces a positive electrical charge on the surface of particles. This charge is balanced by an excess concentration of ions of opposite charge (phosphate) attracted to the surface from the surrounding solution. The positively charged surface and adsorbed negative ions form the fixed layer and the mobile layer, respectively. Together they make up the electrical double layer. Another type of double layer occurs when, due to specific chemical forces, metal

ions sorbed at the surface of a particle become positively charged and form the fixed layer. In this type of double layer, the fixed charges on the surface vary as the composition of the solution changes. Phosphate could constitute the mobile layer by balancing the positive charge provided by metal ions on the fixed layer. In brief, surface of metal oxides becomes P adsorption sites due to the presence of a multiply charged cation, high positive surface charge densities at typical pH values of rainfall runoff (6 ~ 8), and the propensity to hydroxylate in aqueous systems. Most of P sorption on particulate matter is described as specific adsorption through ligand exchange with surface hydroxyl groups forming stable, inner sphere surface complexes (Sparks 2003). P can also combine with cations to form stable, sparingly soluble P mineral phase (Bohn et al. 1985). Therefore, potentially effective reactive particulate matter provides a geochemical environment that promotes both surface adsorption and precipitation reactions (Butkus and Grasso 2001). Extensive studies have been done on the p sorption on sediments (Zhou et a. 2005; Detenbeck and Brezonik 1991; Liu et al. 2002). Therefore removal of particulate bound P and particles is coupled together.

Monitoring P loading from urban rainfall-runoff could help better UOP selection of P removal. In order to economically predict P loading, rainfall-runoff P pollutant model would be used to analyze and provide insight into the control of non-point-source P loading. P pollutant power law model was developed by utilizing particulate matter transient loading over rainfall-runoff event coupled with P association capacity on particulate matters. Such an intuitive strategy of approaching the complicated P loading in urban rainfall-runoff would facilitate evaluating P source and transport and selecting appropriate treatment. The superiority of the P power law pollutant model to the more complex models for predicting P loading to receiving waters is its straightforwardness. In essence, the rainfall-runoff P pollutant model is developed

from regression model, which is mathematical equation that defines a dependent variable and one or more causal (independent) variables (Irish Jr. et a. 1998). Regression models are based on the assumption that the variation in rainfall-runoff water quality can be explained scientifically by measurable changes in other relevant variables that control the process. Rainfall-runoff regression models commonly use concentrations or mass loading of constituents as variables that are dependent upon runoff volume, rainfall intensity, traffic intensity, duration of the antecedent dry period, surrounding land use.

The traditional approaches of pollution control at the end-of-pipe are seen as less desirable in the context of more stringent environmental regulations and the escalating costs of waste management (Shonnard et al. 2003). One answer to the dual needs of sustained economic growth and a healthy environment is pollution prevention before it reaches reservoir.

In the past decade, there has been an increased focus on mitigating the detrimental effects of rainfall-runoff pollutants on receiving waters. To some extent, the physical structures used to moderate and abate peak runoff flows from developed areas, such as wet detention ponds, dry retention areas and swales, have been found to be fairly successful at removing rainfall-runoff contaminants. However, in regions where high levels of runoff pollutant removal are required to sensitivity of receiving waters, or in selected urban locations where space constraints limit the construction of detention or retention facilities, more effective and feasible contaminant removal techniques are required. Because predominant urban runoff P is associated with particles, devices that use physical filtration (e.g. sand filters) have been implemented as a means of improving runoff quality. Sand filters, however, have not received widespread use for P removal, largely because of two constraints: first, they require careful design and periodic maintenance to ensure

consistent hydraulic performance, and secondly, they were testified to be ineffective at removing soluble P runoff pollutants (Bubba et al. 2003; Forbes et al. 2004).

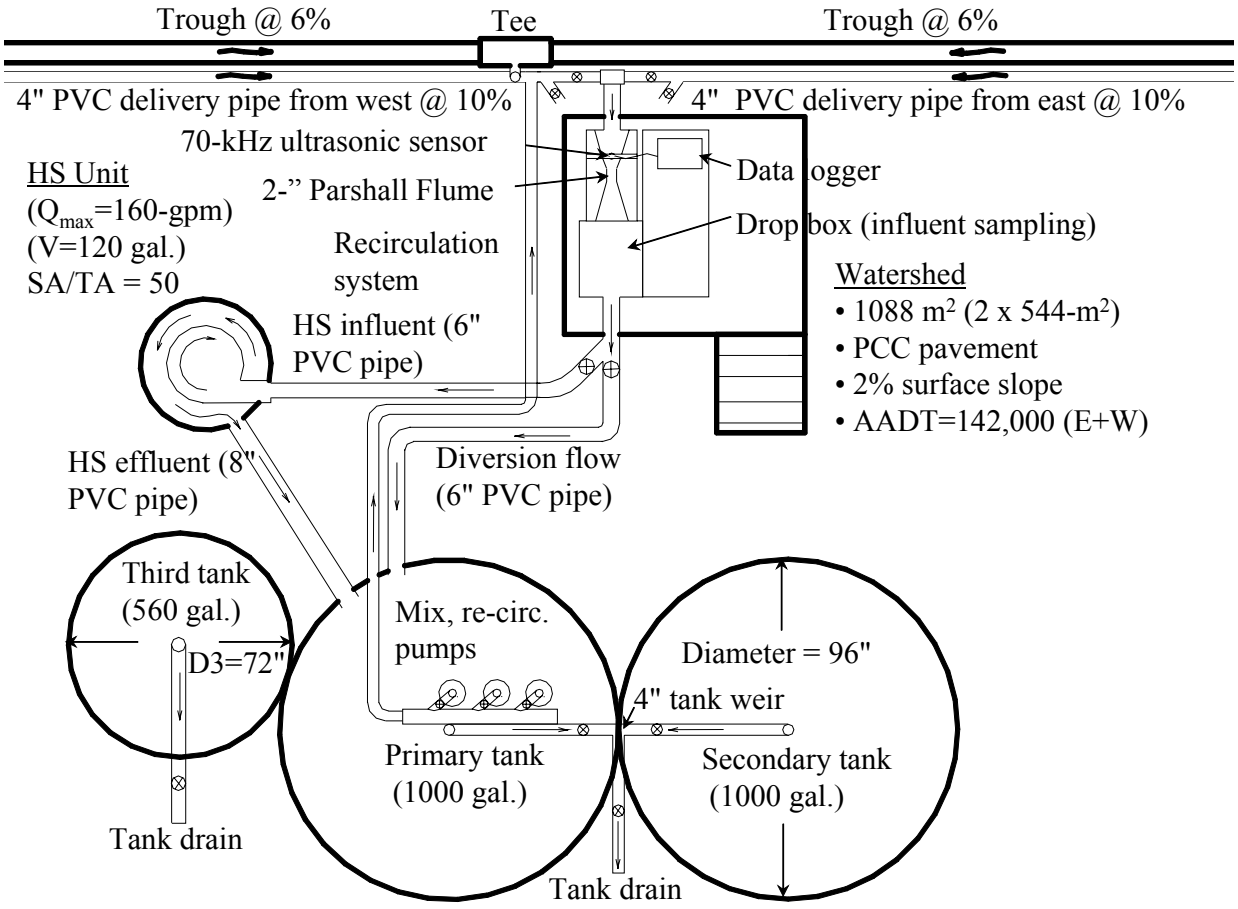

Figure 3-1: Plan view of Baton Rouge rainfall-runoff Catchment Site.

Hydrodynamic separator has become one of the popular means of removing some portions of particles (P associated) carried by urban rainfall-runoff prior to final discharge. As a physical unit operation, hydrodynamic separation (HS) hydrodynamic unit can be characterized as tangential flows into a cylindrical vessel, which in turn creates a rotary flow regime. Figure 3-1 is a schematic illustration of the HS hydrodynamic system at the research site.

The hydrodynamic separation deflects and removes particles and particulate-bound phosphorus in the hydrodynamic separator as an in-situ, real-time unit operation. The separation and containment chamber consists of a containment sump in the lower section and an upper

deflective screen section. Particulate matters are separated within the chamber using a deflective screen allowing the filtered water to pass through to a volute annular area and to the outlet overflow weir. The water and associated particulate-bound phosphorus left within the separation chamber are kept in continuous motion by the energy generated by the hydraulic difference and rotating flow. Such a matter has the effect of preventing the separation screen from being clogged by the particulate matter separated from the inflow. The particulate matter ultimately settles into the containment sump and finer particles (settleable and suspended) removed and trapped in the volute section.

METHODOLOGY

Discrete flow weighted grabbed samples were taken from influent and effluent of hydrodynamic separator throughout the entire rainfall-runoff event. The detailed description of rainfall runoff research site configuration and sampling procedure was demonstrated at a companion article (Jia and Sansalone).

TOTAL PHOSPHORUS (TP) ANALYSIS

There are numerous analytical procedures for TP reported in the literature. Currently employed methods are adapted from methods used for soil, solid waste, and wastewater quality analyses (Standard Methods 1998). The ascorbic acid method is used to detect orthophosphate as recommended by other researchers (Harwood and Hattingh 1973; Murphy and Riley 1962). The persulfate digestion was used to measure TP by converting all forms of phosphorus to orthophosphate. Measurement of particle-bound phosphorus in rainfall-runoff involves three steps: 1) Particulate/solution separation; 2) Acid digestion and conversion particulate bound phosphorus to dissolved phosphate; 3) Analytical measurement of the dissolved phosphate using colorimetric reagent.

Given the wide size range of particulates in urban rainfall-runoff, particles are classified into categories of sediment (> 75 μm), settleable (75 ~ 25 μm) and suspended (< 25 μm) based on the one hour Imhoff settling test convention and mechanistic behavior. The discrete grabbed samples provide information on temporal extreme values as well as the on-line variation of runoff constituents during a runoff event. To prevent potential under-estimation of particulate TP loads and subsequent mis-representation of the distribution of TP, all discrete samples are carried out manually capturing the full cross-section of flow and sampling throughout the entire rainfall-runoff event. Duplicate 12-L samples were utilized to quantify particles size above 75 μm (sediment) and duplicate 1-L samples were used to quantify finer particles: settleable and suspended. Between 15 and 20 samples were taken to ensure representative characterization across the entire hydrograph for each event.

EFFICIENCY OF TP REMOVAL BY HS

Based on mass loading, the general form of removal efficiency of TP by HS is written as:

$$\Delta = \frac{M_{in} - M_{eff}}{M_{in}} * 100\% \qquad \text{Equation 3-1}$$

where, Δ is the TP removal percent by HS, M_{in} is the TP influent to HS mass loading (g) and M_{eff} is the TP effluent of HS mass amount (g). M_{in} and M_{eff} were calculated and integrated from curve of TP concentrations versus runoff volume. Since HS itself contains certain amount of volume (about 450 L), the general form of TP removal efficiency becomes problematic of overestimation especially for the event with relatively small amount of runoff volume, for example 1672 L of October 14 event. Therefore revised form of TP removal efficiency was utilized as:

$$\Delta = \frac{M_{in}\frac{V_{eff}}{V_{in}} - M_{eff}}{M_{in}\frac{V_{eff}}{V_{in}}} * 100\% \qquad \text{Equation 3-2}$$

where, V_{in} and V_{eff} were rainfall runoff volume (L) of influent to HS and effluent of HS, respectively.

RESULTS

CHARACTERISTICS OF RAINFALL-RUNOFF EVENTS

Mass or Flow Limited of Constituents

To overcome limitation of event mean concentration (EMC) of only single value for whole event and provide the temporal variation of constituents (particulate matter or P) along runoff hydrograph, concept of mass limited or flow limited are introduced (Sansalone and Buchberger 1997). Such a concept originated from the distinction of comparisons of normalized values of constituents mass and rainfall runoff volumes. Mass limited event refers to the event with disproportionately large amount of mass of a constituent transported during the runoff hydrograph, while flow limited event means that the linear relationship between the normalized mass of a constituent and the normalized runoff volume. Normalized cumulative mass of constituents are often plotted against normalized cumulative runoff volume to indicate an event mass limited or flow limited.

$$\frac{m'(t)}{v'(t)} \geq 1 \qquad \text{Equation 3-3}$$

where m'(t) and v'(t) refer to normalized cumulative constituents mass or normalized cumulative runoff volume, respectively.

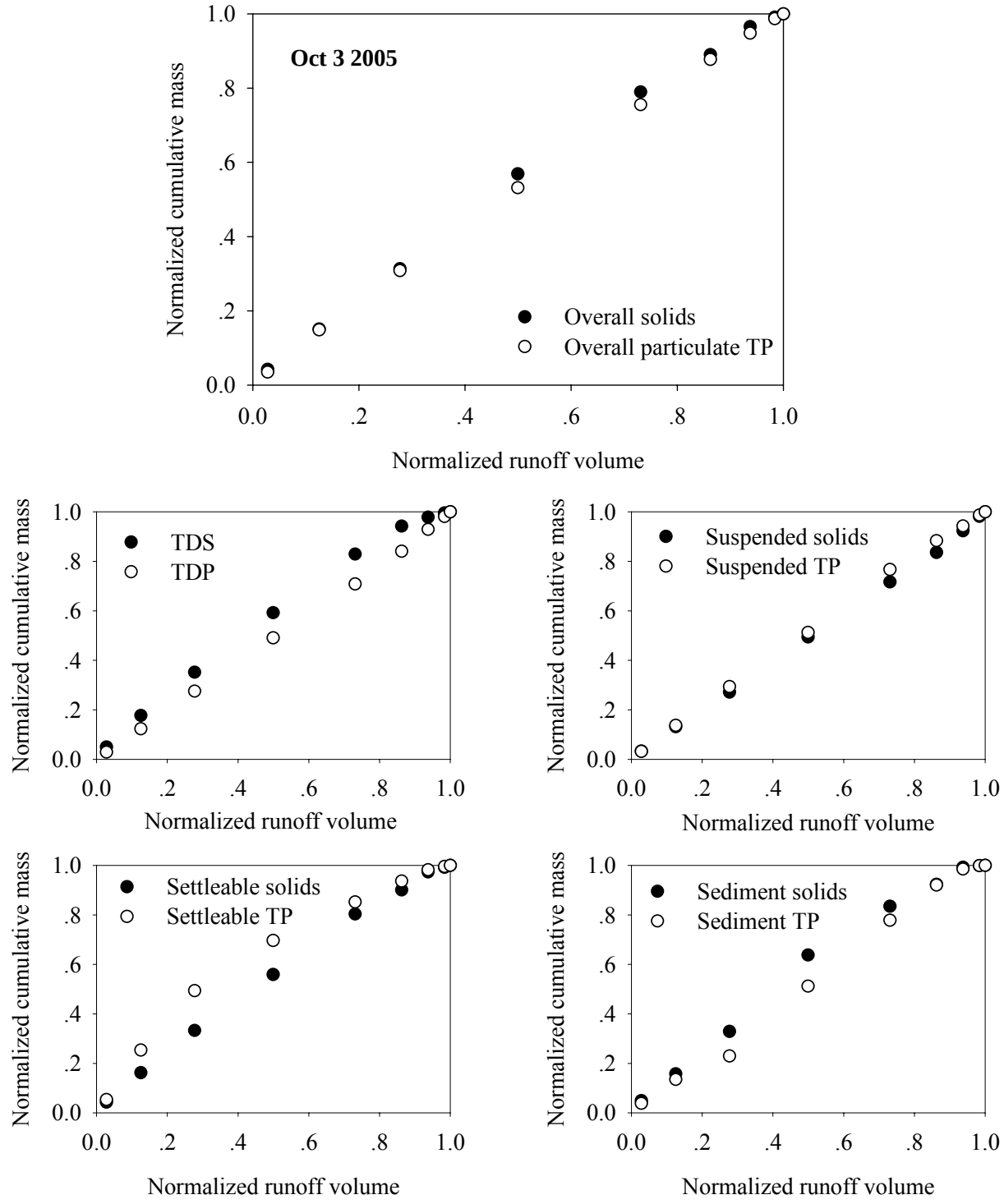

Figure 3-2. Non-dimensional particulate matter and TP associated versus normalized runoff volume for Oct 3 2005 event.

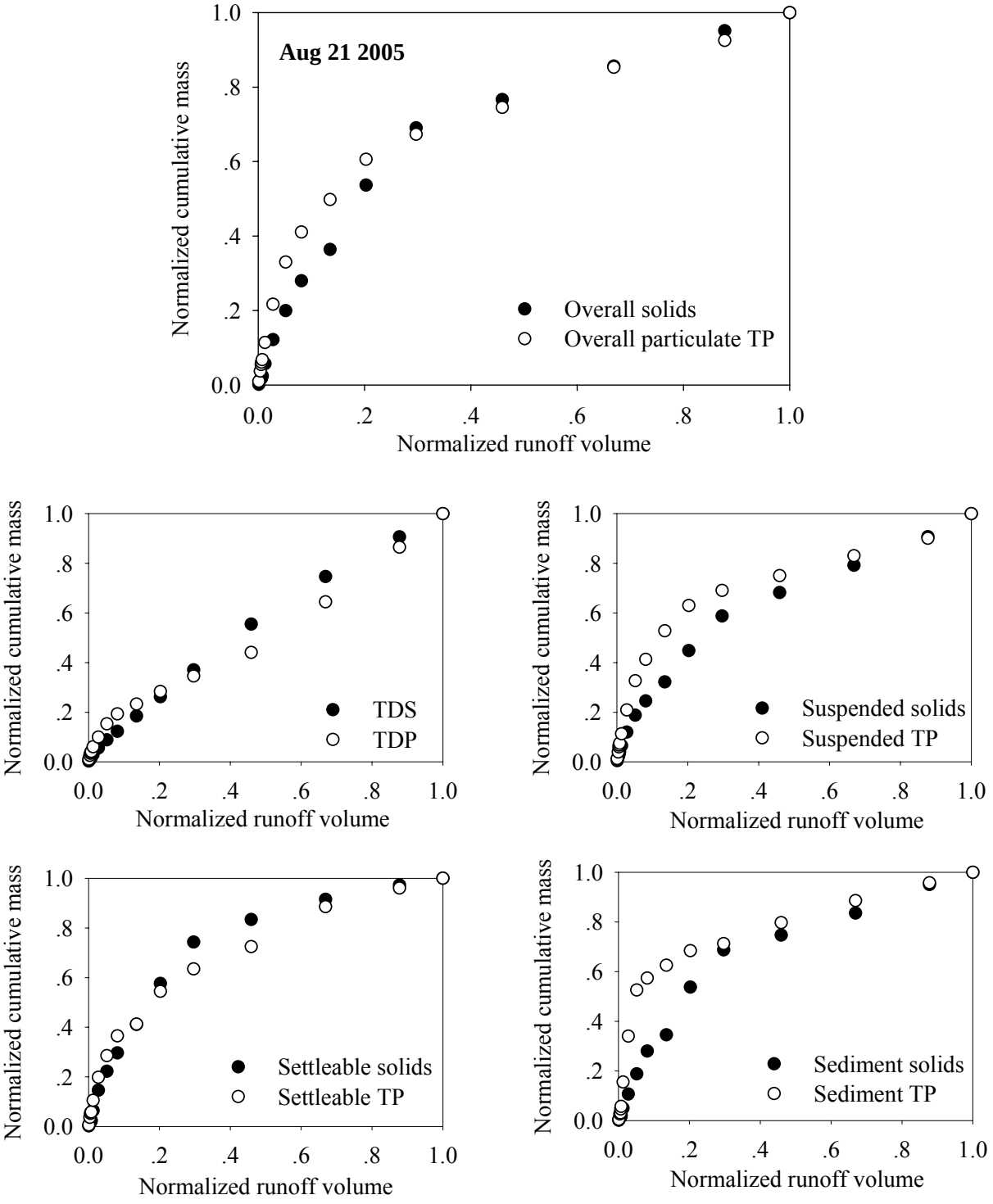

Figure 3-3. Non-dimensional particulate matter and TP associated versus normalized runoff volume for August 21 2005 event.

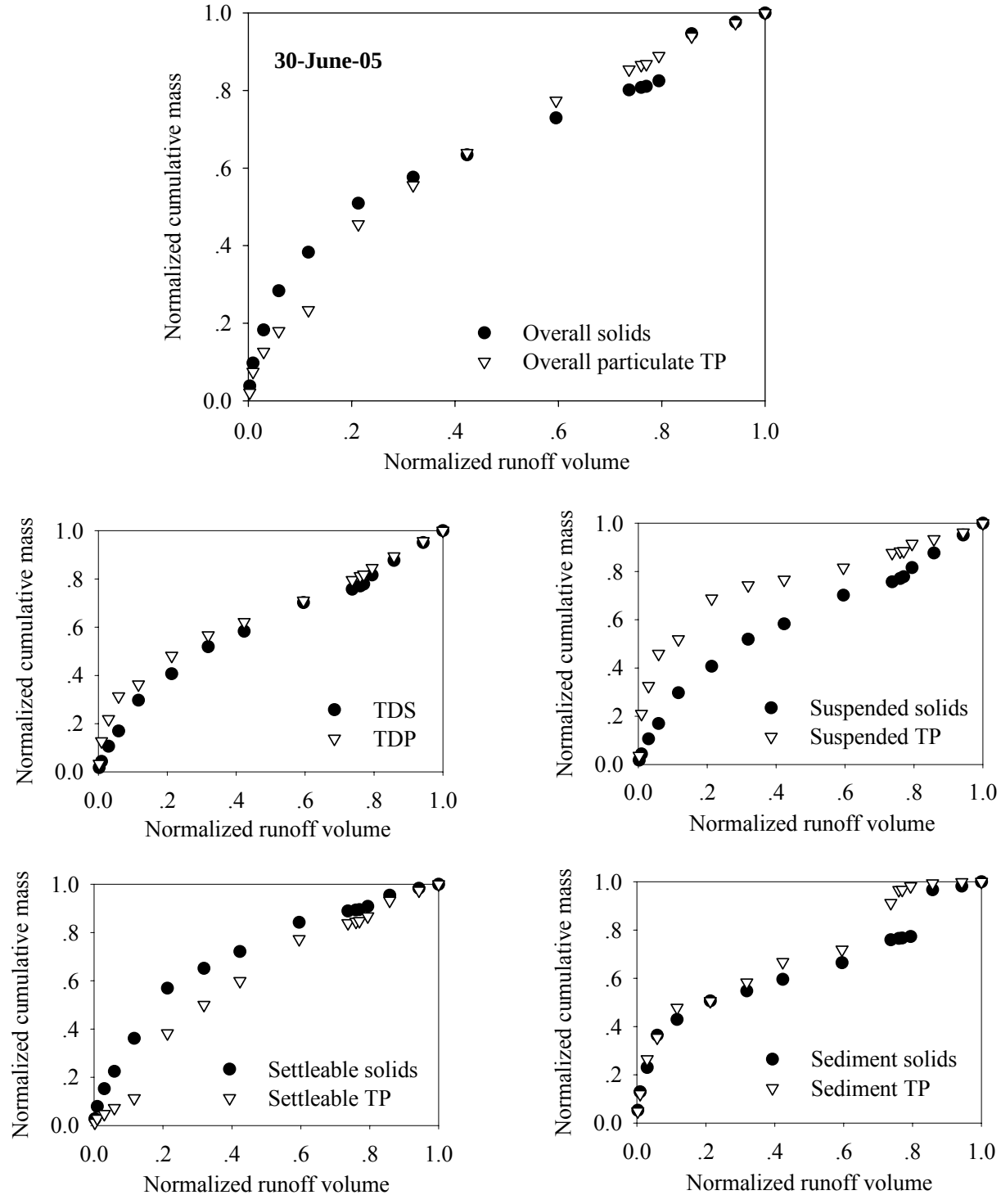

Figure 3-4. Non-dimensional particulate matter and TP associated versus normalized runoff volume for June 30 2005 event.

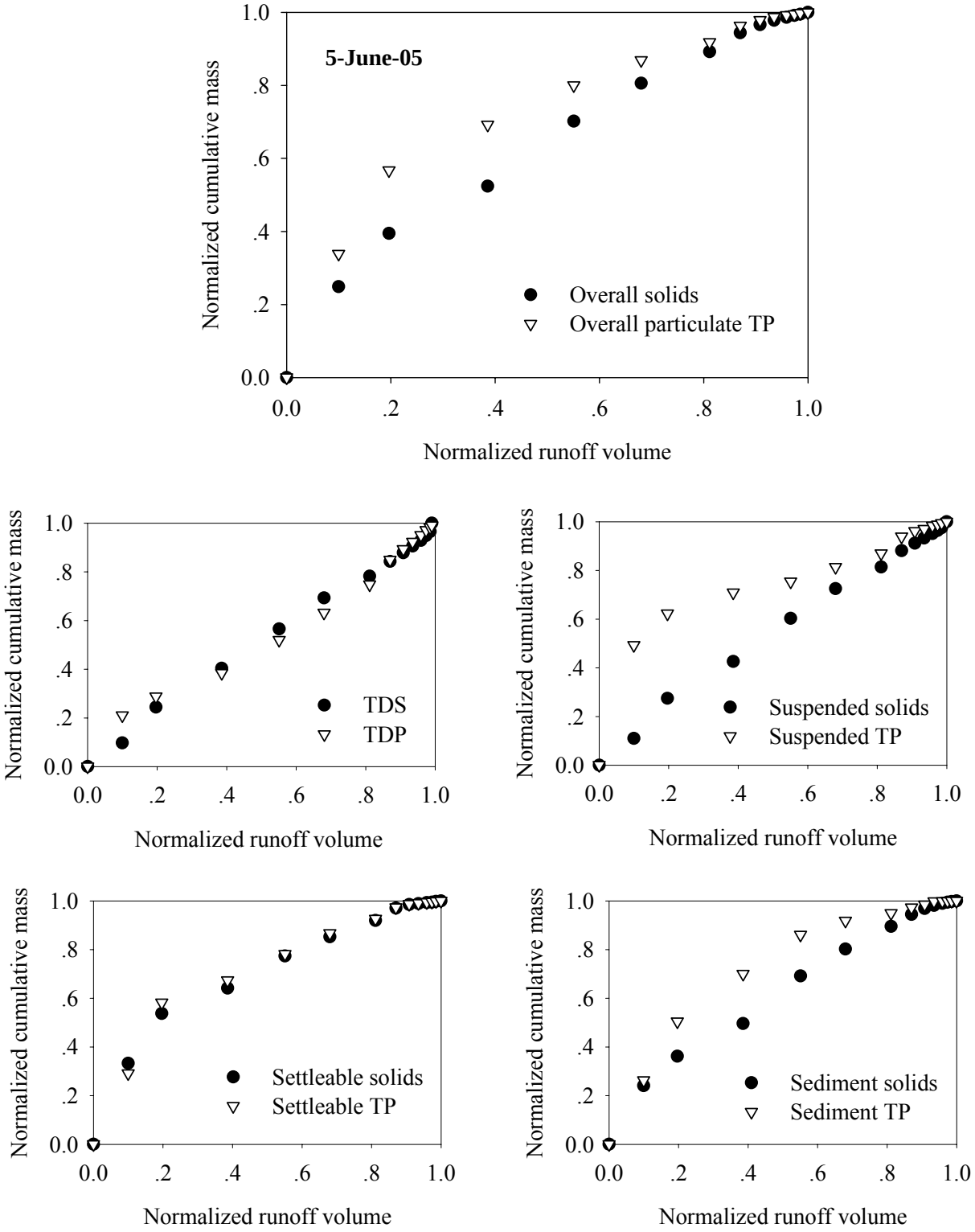

Figure 3-5. Non-dimensional particulate matter and TP associated versus normalized runoff volume for June 5 2005 event.

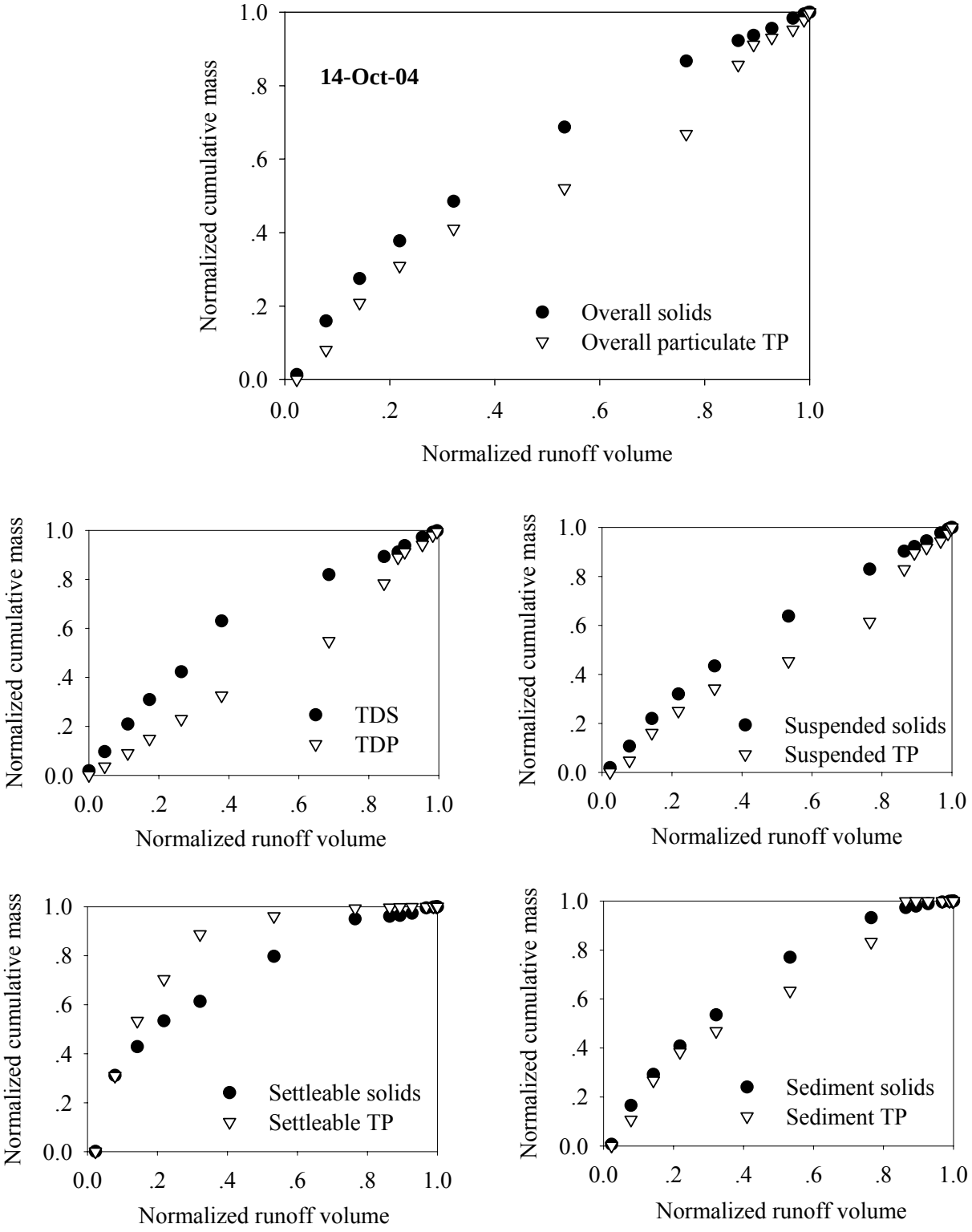

Figure 3-6. Non-dimensional particulate matter and TP associated versus normalized runoff volume for October 14 2004 event.

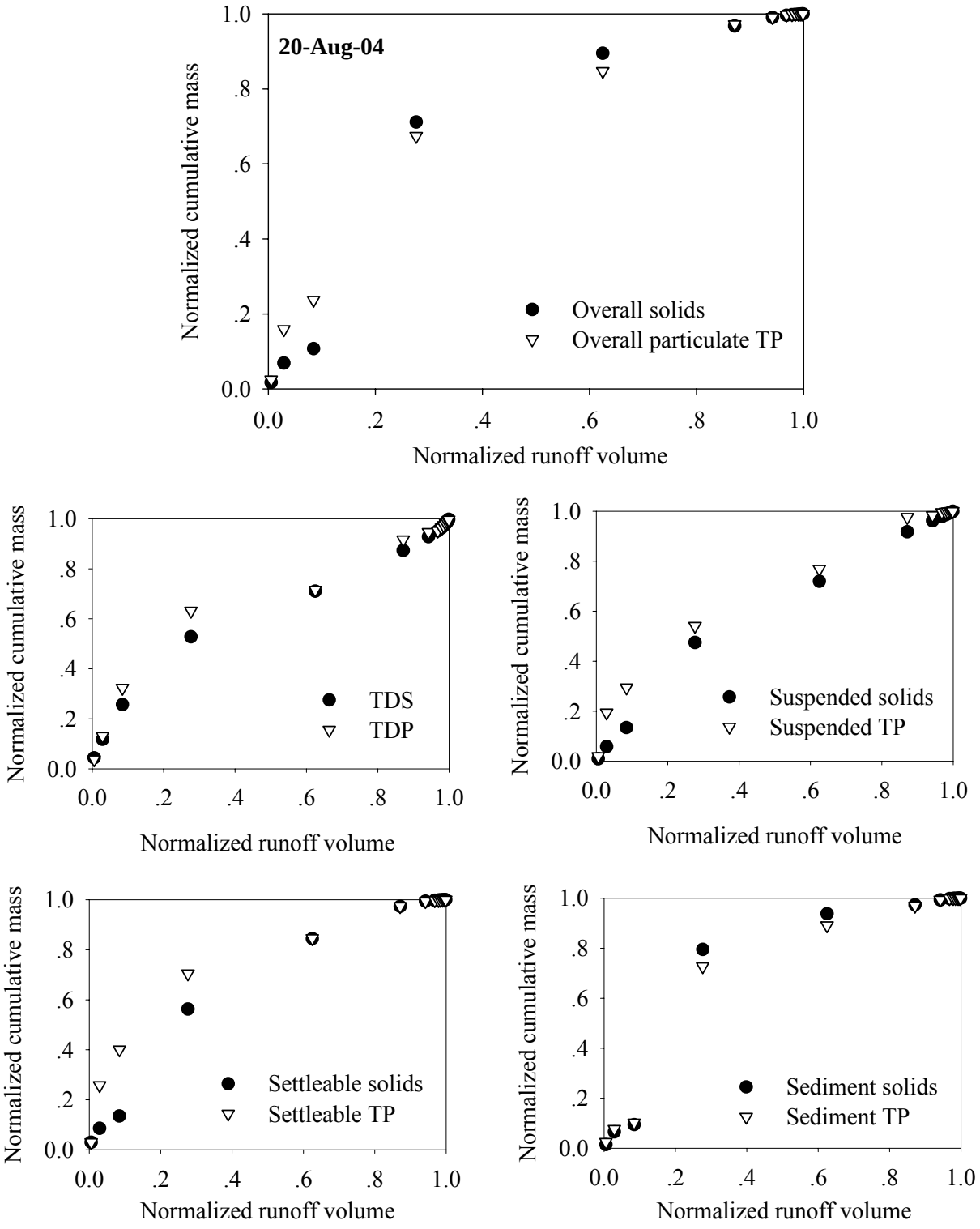

Figure 3-7. Non-dimensional particulate matter and TP associated versus normalized runoff volume for August 20 2004 event.

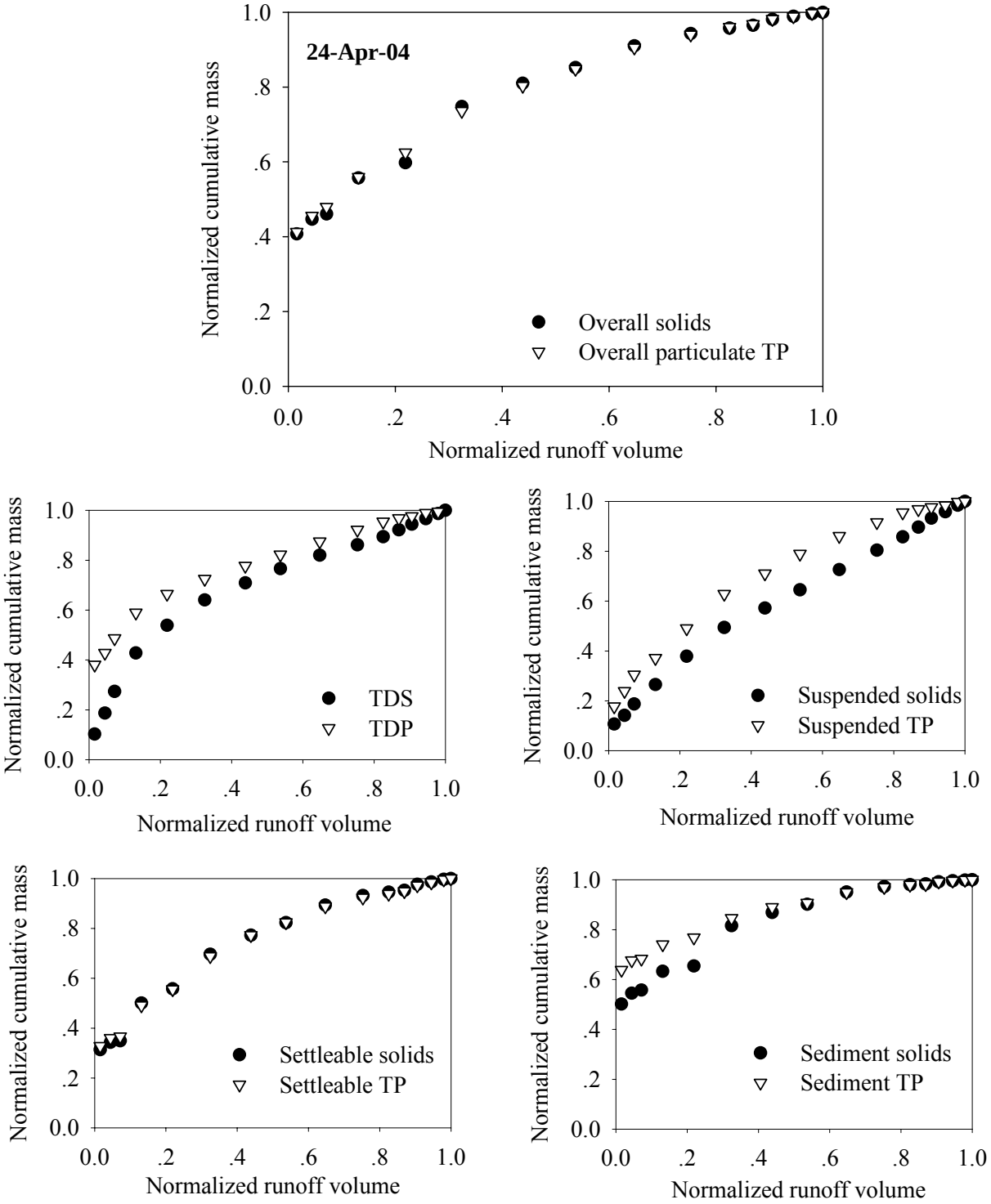

Figure 3-8. Non-dimensional particulate matter and TP associated versus normalized runoff volume for April 24 2004 event.

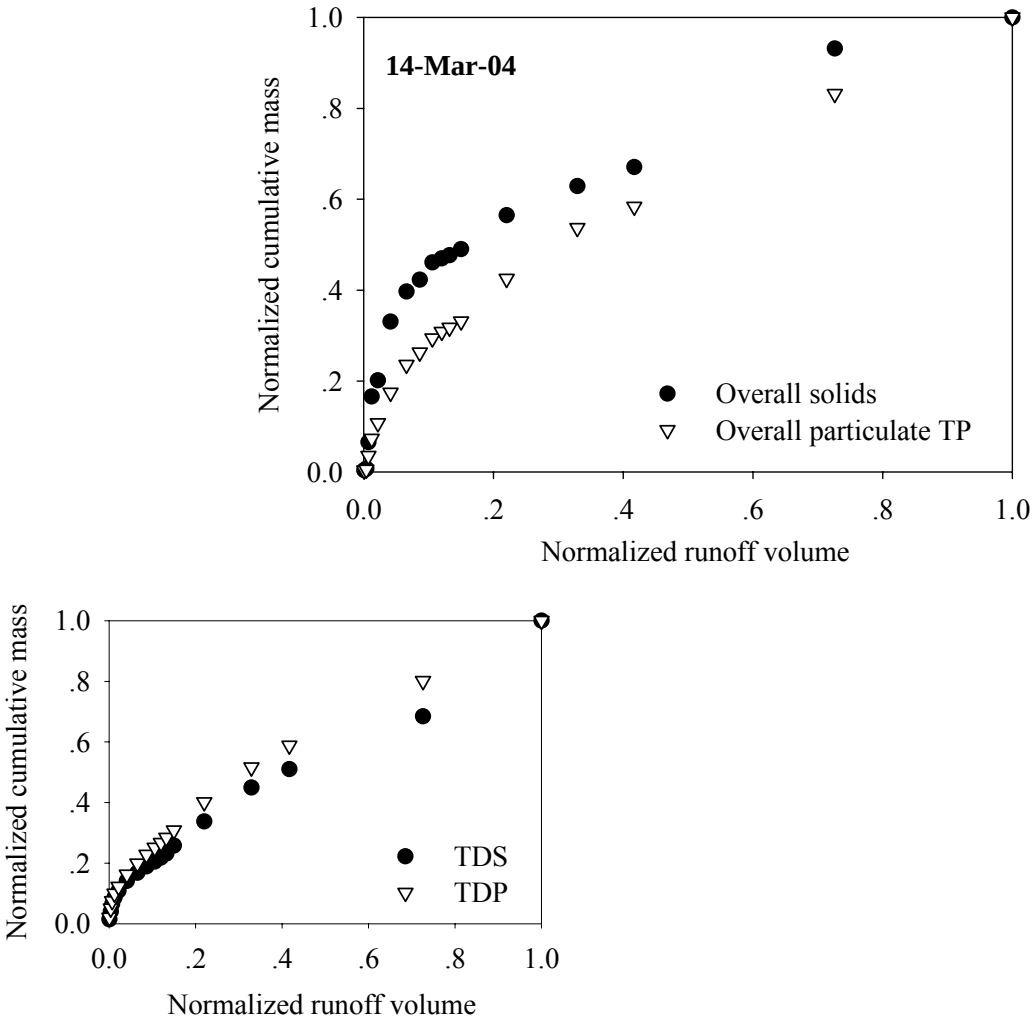

Figure 3-9. Non-dimensional particulate matter and TP associated versus normalized runoff volume for March 14 2004 event.

According to such definitions of mass limited and flow limited of constituents, normalized cumulative particulate matter and P were plotted against normalized cumulative runoff volume. The results were shown in Figure 3-2, Figure 3-3, Figure 3-4, Figure 3-5, Figure 3-6, Figure 3-7, and Figure 3-8. The characteristics of mass limited or flow limited of particulate matter and P were summarized in Table 3-2 and Table 3-3 respectively. It is apparent that the characteristics of particulate matter are same as the corresponding P associated with though the distributions of normalized cumulative mass of particulate matter and P showed some discrepancy. Such a finding indicates that particulate mass transport, mass limited or flow

limited, would dictate the features of transport of P associated with. Therefore, particulate matter, which is an economically measurable constituent of rainfall runoff, could be utilized as a surrogate of P loading. Such a matter would be very useful in terms of effective prediction.

Table 3-2. Summary of characteristics of mass limited or flow limited for particulate matter temporal transported in rainfall-runoff events.

	TDS	Suspended	Settleable	Sediment	Overall
Oct 3 05	F	F	M	F	F
Aug 21 05	F	M	M	M	M
Jun 30 05	M	M	M	M	M
Jun 5 05	F	F	M	M	M
Oct 14 04	F	F	M	M	F
Aug 20 04	M	M	M	M	M
Apr 24 04	M	M	M	M	M
Apr 14 04	F	NA	NA	NA	M

Table 3-3. Summary of characteristics of mass limited or flow limited for Total dissolved P and particulate bound TP transported in rainfall-runoff events.

	TDP	Suspended TP	Settleable TP	Sediment TP	Overall
Oct 3 05	F	F	M	F	F
Aug 21 05	F	M	M	M	M
Jun 30 05	M	M	M	M	M
Jun 5 05	F	M	M	M	M
Oct 14 04	F	F	M	M	F
Aug 20 04	M	M	M	M	M
Apr 24 04	M	M	M	M	M
Apr 14 04	F	NA	NA	NA	M

It is evident that non-dimensional cumulative mass of sediments and settleables and associated P were consistently nonlinear to the non-dimensional cumulative runoff volume,

therefore they are pronouncedly mass limited. For majority of events, suspended particulate matter and P associated with demonstrated mass limited feature. Conversely, suspended particulate matter and dissolved solids for some events showed flow limited phenomena. In brief, most of the events is predominant with mass limited feature.

P Specific Capacities on Particulate Matter

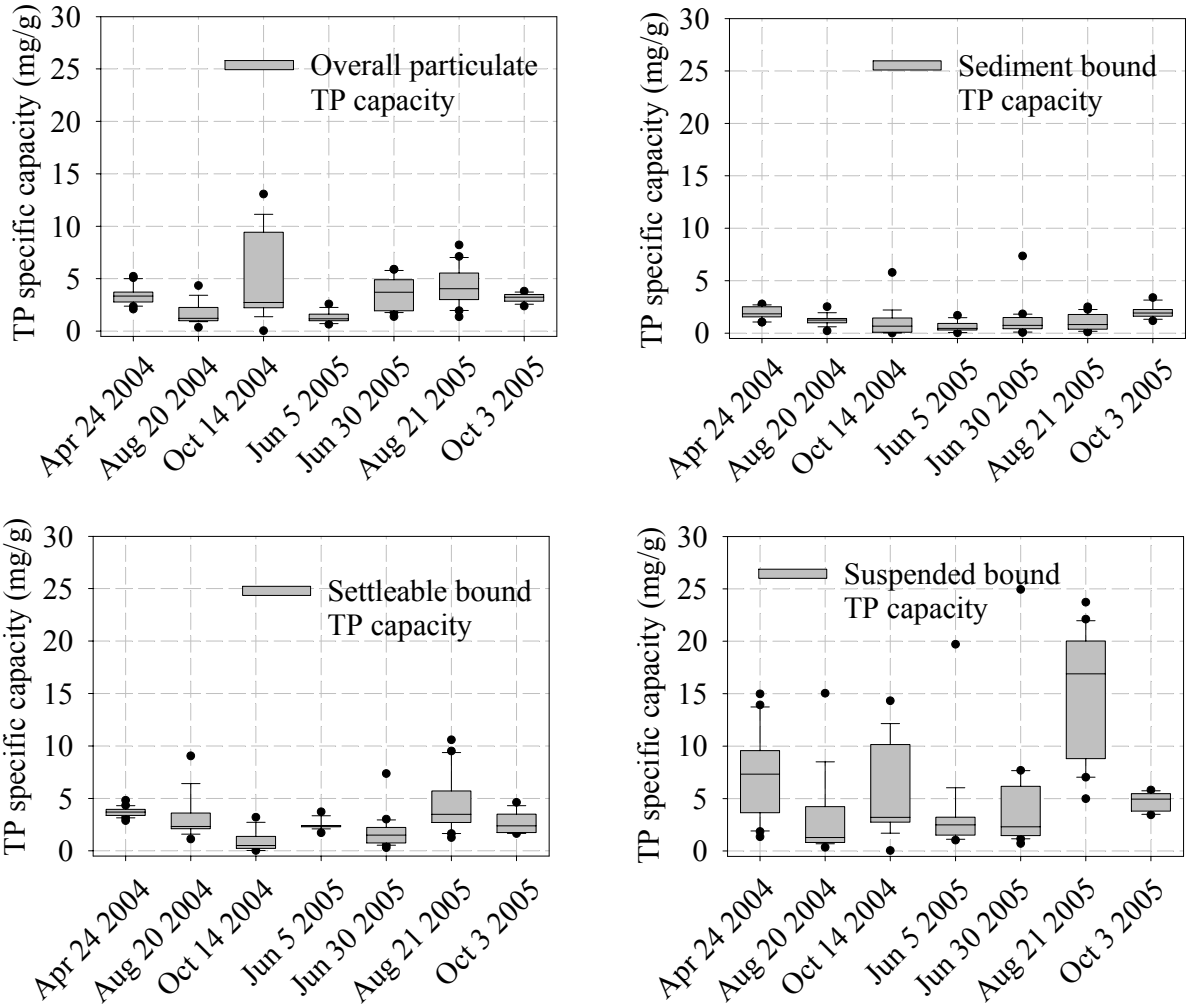

Figure 3-10. Temporal TP specific capacity on particulate matter.

Temporal P specific capacities on particulate matter (mg/g) based each event were depicted in Figure 3-10. P specific capacities on particulate matter for all the samples of influent to HS were plotted and formed each of the vertical boxes which are composed of the median, 10^{th}, 25^{th}, 75^{th}, and 90^{th} percentile. Comparatively, majority of P specific capacities on overall

particulate matter were in the range of 4 to 5 mg/g. P specific capacities on sediments were nearly 2 mg/g and on settleables about 3 to 4 mg/g. P specific capacities on suspended particulate matter were the highest and with most of them were just smaller than 10 mg/g. It is concluded that particulate matter temporally transported by urban rainfall runoff can associated a limited range of P. It is also suggested that finer particulate matter has better P specific capacities because of its large value of specific surface area.

P POLLUTANT POWER LAW MODEL

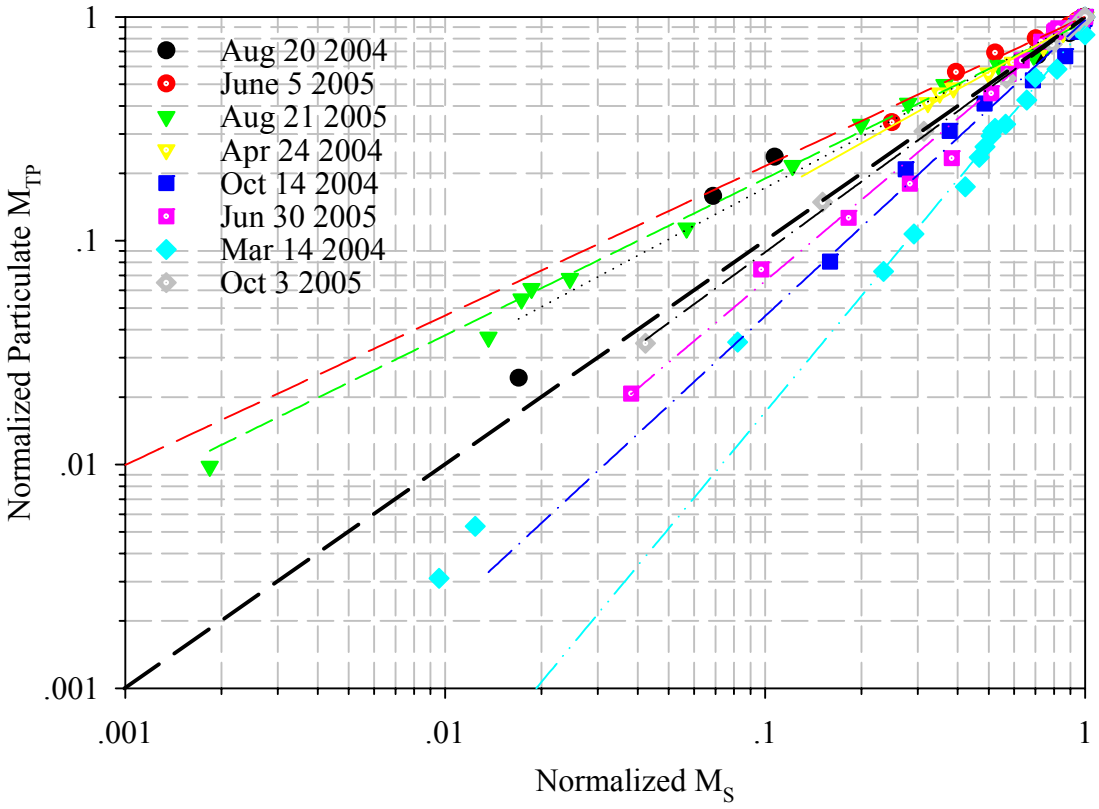

Figure 3-11. Power law application on correlating normalized particulate matter and associated TP. The constants and correlation coefficients of power law were shown in Table 3-4.

Based on the findings that a) particulate matter and P associated with followed same mass limited or flow limited feature, and b) P specific capacities on particulate matter were in limited range, power law equation was suggested to correlate the normalized cumulative mass loading for particulate matter (M_s) and P associated with (M_{TP}):

$$M_{TP} = \alpha M_S^{\beta}$$ Equation 3-4

where constant α is the indicator of P specific capacity and constant β reflects the curvature of curve. The P pollutant model has been tested for the P loadings for several actual rainfall-runoff events monitored and the results were depicted in Figure 3-11. All the constants used in the model and correlation coefficients were shown in Table 3-4. The high values of correlation coefficients suggest most of the experimental data could be successfully represented by the power law model. This indicates the model derived could be used to predict mass loadings particulate bound P through measurement of particulate matter measurement from the urban rainfall runoff.

Table 3-4. Constants and correlation coefficients of Power law applied on correlation of normalized particulate matter mass and TP associated.

Power Law	Mass limited event (β > 1)				flow limited event (β < 1)			
	Jun 5 05	Aug 21 05	Aug 20 04	Apr 24 04	Oct 3 05	Oct 14 04	Jun 30 05	Mar 14 04
α	1.003	0.95	0.988	0.986	0.989	0.967	1.057	0.908
β	0.668	0.7	0.76	0.798	1.047	1.323	1.205	1.724
R^2	0.995	0.994	0.989	0.992	0.999	0.983	0.982	0.982

REMOVAL EFFICIENCIES AND MECHANISM OF HS

Both concentrations of dissolved and particulate-bound fractions of phosphorus measured by discrete samples in urban rainfall-runoff commonly exceed water quality criteria of 0.1 mg/L recommended by EPA 1986 on rainfall-runoff event basis (Jia and Sansalone). In addition, particulate matters are designated to three categories, sediments, settleables and suspended according to their easiness of treatability and difference of physical properties. Therefore the in-situ rainfall-runoff treatments have to address sediments bound, settleables bound and suspended bound and dissolved phosphorus.

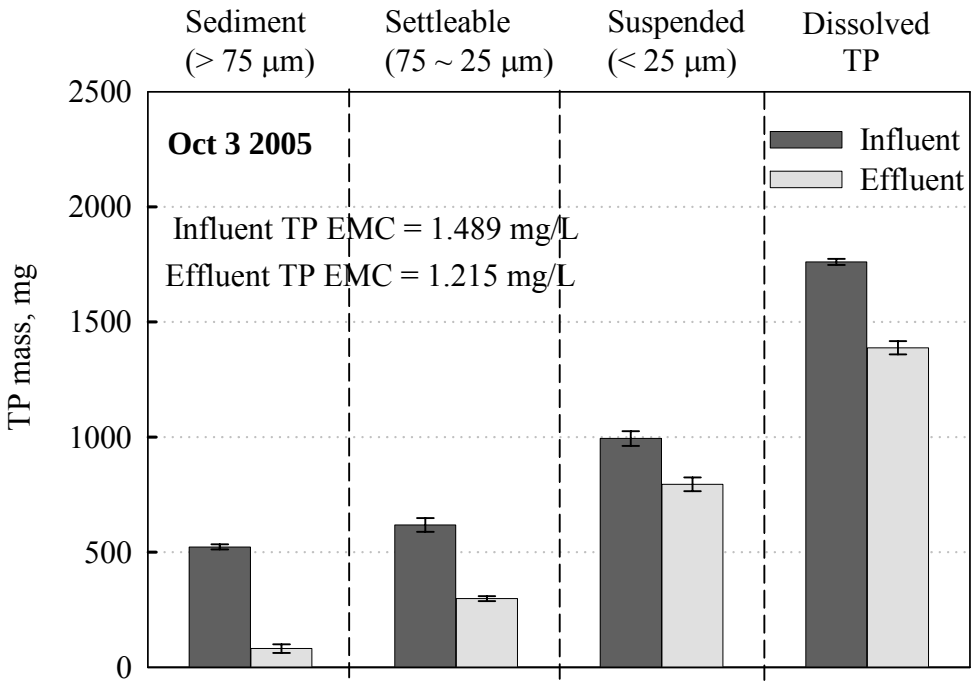

Figure 3-12. TP removal by HS for event Oct 3 2005

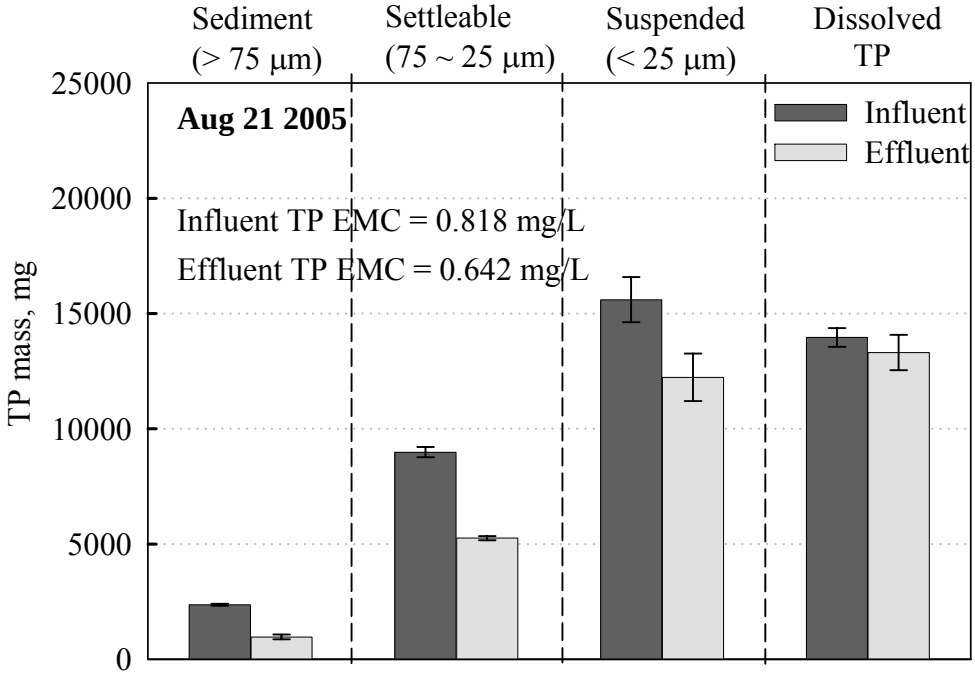

Figure 3-13. TP removal by HS for event Aug 21 2005

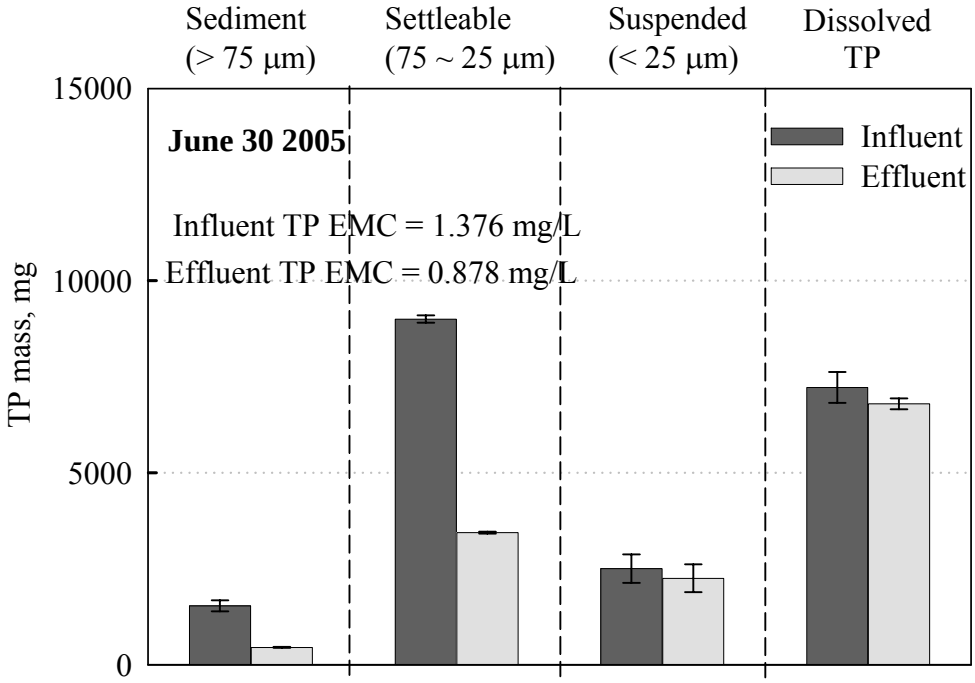

Figure 3-14. TP removal by HS for event June 30 2005

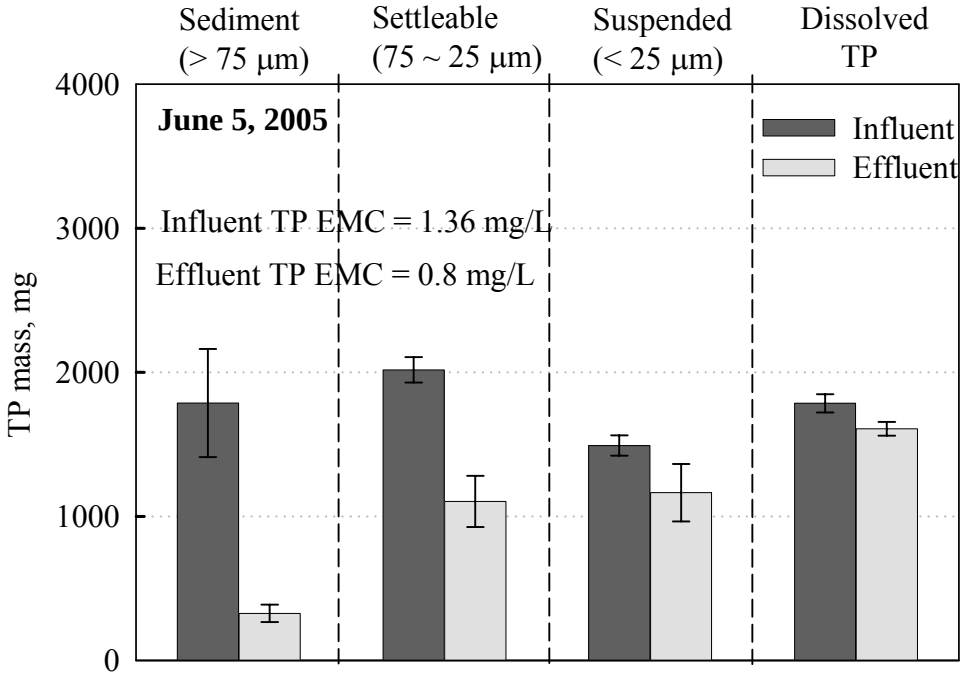

Figure 3-15. TP removal by HS for event June 5 2005

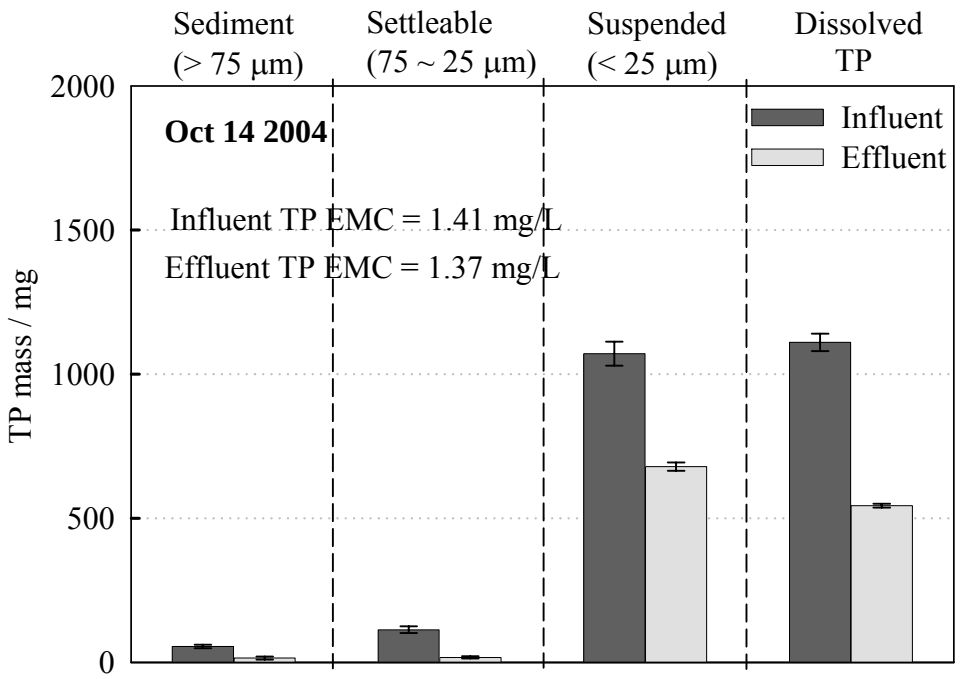

Figure 3-16. TP removal by HS for event Oct 14 2004

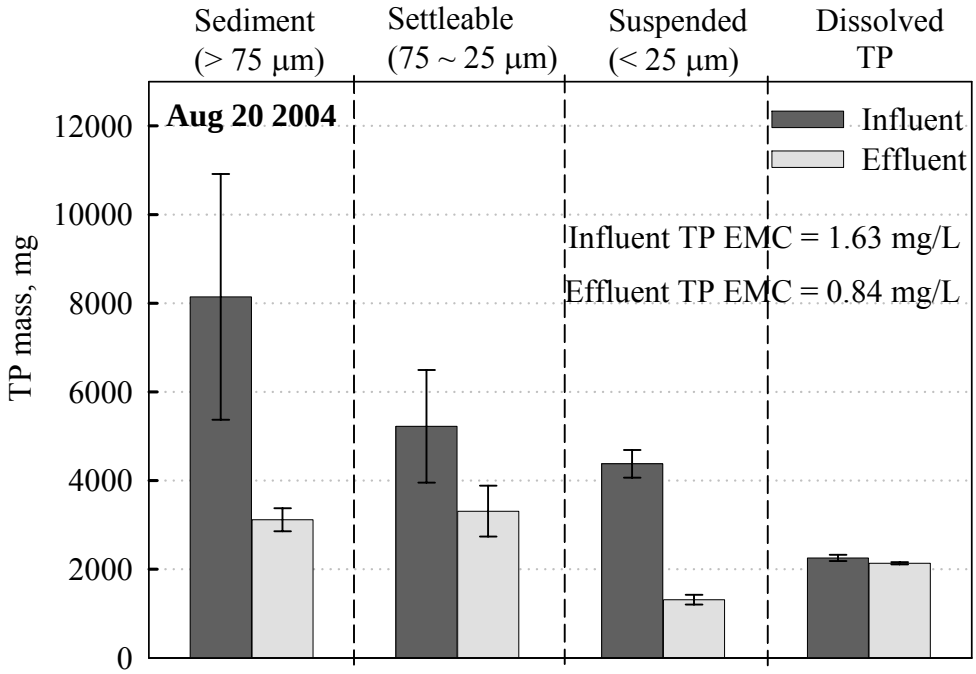

Figure 3-17. TP removal by HS for event Aug 20 2004

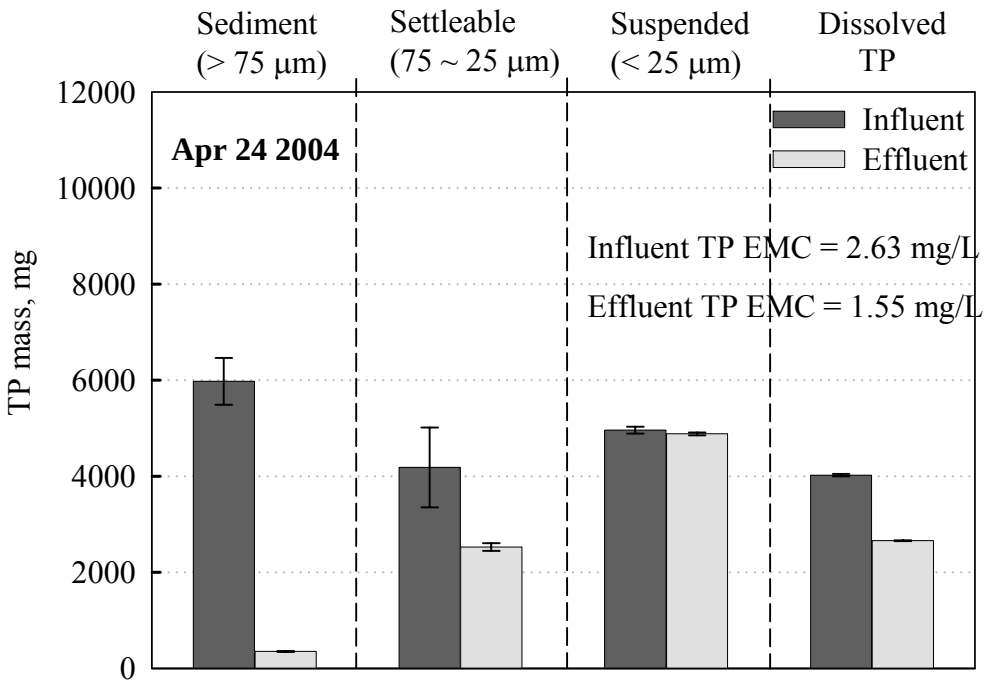

Figure 3-18. TP removal by HS for event Apr 24 2004.

Table 3-5. Summary of TP removal efficiency by HS.

	TP Removal efficiency by HS				
Event	Sediment bound	Settleable bound	Suspended bound	Dissolved	Overall
Mar 14 2004	12.6%			-2.0%	7.7%
Apr 24 2004	93.6%	34.7%	1.0%	10.6%	40.8%
Aug 20 2004	59.9%	33.6%	71.3%	0.8%	48.8%
Oct 14 2004	68.4%	84.8%	1.3%	10.6%	12.7%
June 5 2005	81.7%	45.3%	21.9%	9.9%	40.6%
June 30 2005	70.7%	61.8%	10.2%	5.9%	36.2%
Aug 21 2005	58.6%	40.9%	20.7%	3.6%	21.5%
Oct 3 2005	80.7%	40.1%	0.8%	2.2%	18.4%

Event Means Concentrations (EMC) and Mass loading comparisons of influent to HS and effluent of HS by means of sediment bound fraction, settleable bound fraction, suspended bound fraction and dissolved fraction through hydrodynamic separation were depicted in Figure 3-12,

Figure 3-13, Figure 3-14, Figure 3-15, Figure 3-16, Figure 3-17 and Figure 3-18. Results of total phosphorus removal efficiencies summarized in Table 3-5. As the first rainfall runoff event studied for phosphorus, March 14 2004 event was presented as only particulate and dissolved fraction. The overall TP removal efficiencies were in range of 10~50% for all the rainfall runoff events studied. Sediment bound TP removal efficiencies varied from about 60% to 94%, majorities of settleable bound TP removal efficiencies differed 30% to 60%, suspended bound TP removal efficiencies were generally smaller than 20% with exception of the value of 71.3% for Aug 20 2004 event, which a pronounced mass limited event with high intensity, short duration and single hydrograph peak. Typical dissolved P removal efficiencies fell into less than 10%. In brief, the results indicated that removal percent of sediment-bound phosphorus is highest, settleable-bound phosphorus moderate, and suspended-bound phosphorus and dissolved phosphorus to a varying lower extent. Such an overall performance is not surprising because removal mechanisms of hydrodynamic separation include hydrodynamic screening and vortex settling, both of which primarily depend on particle size. The coarser of particulate matter, the more pronounced of effect of screening and settling. Rainfall runoff flow rate caused by rainfall intensity and hydraulic difference could be another factor which influence particulate bound TP removal efficiency by HS. However it would be too early to argue about how flow rate affected particulate bound TP removal efficiency by HS due to the limited number of rainfall runoff events studied. Even considering that, the differences of the sediment bound, settleable bound, suspended bound and dissolved TP removal efficiencies are evidently significant. Therefore hydrodynamic separation can be utilized as in-situ primary pre-treatment dealing with particles and particulate-bound phosphorus, especially for sediment and settleable fractions. Alleviation of the clogging problem in the subsequent filtration process is another advantage could be taken.

With respect to adsorptive filtration applied to achieve higher P removal efficiency if required, amorphous oxide coated media filter could be applied following HS unit operation because of their good adsorption capacity and high hydraulic conductivity. Such a combination of operations would ensure that concentrations of effluent P is low enough for discharge to surrounding surface waters.

IMPLICATIONS AND DISCUSSION

Transport of particulate bound P during the urban rainfall runoff is a complicated phenomenon. In addition to P always dynamically partitioning between dissolved and particulate bound phase, appropriate sampling strategy forms the corner stone to represent what was really occurring in the rainfall runoff. Due to the small opening mouth of sampling tube for the most automatic samplers, incomplete representation of particulate matter, especially settleable and sediment fractions, could be inferred. Another shortcoming of automatic sampling is that particulate matter as a whole was normally obtained by the difference of before and after fractionation through 0.45 μm membrane filter using dozens ml of runoff solution, to which experimental error could be high.

Conversely, manual sampling across the full flow direction through wide open mouth container could overcome the inability of capturing coarse particles. Additionally, replicate sediment fraction was sieved and quantified by 12 L containers, duplicate settleable and suspended fractions were obtained from 1 L quiescent settling test, which allow the minimal experimental error by operating large volume of solution and concomitant large value of particulate mass. Finally, the identification of three categories of particulate matter (sediments, settleables and suspended) and P associated with would address the treatability and select the best unit operations and processes (UOPs).

CONCLUSIONS

On the basis of representative manual sampling and appropriate particulate bound P measurement in terms of sediment bound fraction, settleable bound fraction and suspended fraction, this study investigated pollutant transport modeling of particulate-bound phosphorus in urban rainfall-runoff at the upper end of a small Cementitious Porous Pavement (CPP) watershed and in-situ removal mechanism and efficiency by hydrodynamic separator. Such a study would help understanding how particulate bound fraction of phosphorus, which is a predominant over dissolved fraction, was transported in the urban rainfall-runoff events, evaluating phosphorus potential fate and bioavailability, and shedding sight on effective in-situ control of P which was considered a major cause of eutrophication.

Developed from regression model, P pollutant model based on power law equation was triggered by the finding the transient loadings of particulate matter and P associated with followed the same characteristics of mass limited or flow limited. In addition, P association capacities on particulate matters were also found in the limited range. The high values correlation coefficients by applying the model indicate that the simple power law equation gained success in correlating temporal mass loads of particulate matter and P contained. Such a manner makes it possible to economically predict P loading through measuring the more assessable particulate matter and also facilitates better unit operation and process (UOP) selection.

The P removal mechanisms by hydrodynamic separator are a combination of dynamic screening and quiescent settling. Removal efficiencies of particulate bound phosphorus are pronouncedly dependent of size of particulate matter and distribution of particulate mass and hydrological parameters of the specific events. Generally, removal efficiency for overall

particulate bound P was in the range of 10~50%, with highest removal efficiency for sediment bound P (normally more than 60%), medium removal efficiency for settleable bound P (mostly 30~60%) and lowest removal efficiency for suspended bound P (around 10%).

Results from this study indicate that P pollution model could be successfully applied for intra-event P transport in urban rainfall-runoff. Besides, hydrodynamic separation could effectively remove particulate-bound phosphorus. Nevertheless, additional urban rainfall-runoff P treatment is needed mainly because stringent discharge limit for P is promulgated and dissolved fraction of P is still of concern.

REFERENCES

Ackerman, D. and Schiff, K., 2003. Modeling Storm Water Mass Emissions to the Southern California Bight. Journal of Environmental Engineering, 129(4), 308-317.

Akan, A.O., Schafran, G.C., Pommerenk, P. and Harrell, L.J., 2000. Modeling Storm - Water Runoff Quantity and Quality from Marine Drydocks. Journal of Environmental Engineering, 126(1), 5-11.

APHA- American Public Health Association. (1998). Standard Methods for the Examination of Water and Wastewater, (20th Ed.) A.D. Eaton, L.S. Clesceri, A.E. Greenberg (Eds.), American Public Health Association, American Water Works Association and Water Environmental Federation, Washington, D.C.

Appan, A. and Wang, H., 2000. Sorption Isotherms and Kinetics of Sediment Phosphorus in a Tropical Reservoir. Journal of Environmental Engineering, 126(11), 993-998.

Barrett, M.E., Walsh, P.M., Malina, J.F. Jr. and Charbeneau, R.J., 1998. Performance of Vegetative Controls for Treating Highway Runoff. Journal of Environmental Engineering, 124(11), 1121-1128.

Barrett, M.E., Irish, L.B. Jr., Malina, J.F. Jr. and Charbeneau, R.J., 1998. Characterization of Highway Runoff in Austin, Texas, Area. Journal of Environmental Engineering, 124(2), 131-137.

Bartone, D.M. and Uchrin, C.G., 1999. Comparison of Pollutant Removal Efficiency for Two Residential Storm Water Basins. Journal of Environmental Engineering, 125(7), 674-677.

Berner, R.A., 1971. Principles of chemical sedimentology. New York, McGraw-Hill, Inc. pp 240.

Bertrand-Krajewski, J.-L., Chebbo, G., Saget, A., 1998. Distribution of pollutant mass vs volume in stormwater discharges and the first flush phenomenon. Water Res. 32(8), 2341-2356.

Bohn, H., B. McNeal, and G. O'Connor. 1985. Soil Chemistry. 2nd ed. John Wiley & Sons, New York.

Brezonik, P.L. and Stadelmann, T.H., 2002. Analysis and predictive models of stormwater runoff volumes, loads and pollutants concentrations from watersheds in the Twin Cities metropolitan area, Minnesota, USA. Water Res. 36, 1743-1757.

Bubba, M.D., Arias, C.A. and Brix, H., 2003. Phosphorus Adsorption Maximum of Sands for Use as Media in Subsurface Flow Constructed Reed Beds as Measured by the Langmuir Isotherm. Water Research, 37, 3390-3400.

Butkus, M.A. and Grasso, D., 2001. The Nature of Surface Complexation: A Continuum Approach. Environmental Geology, 40, 446-453.

Cerco, C.F., 1995. Response of Chesapeake Bay to Nutrient Load Reductions. Journal of Environmental Engineering, 121(8), 549-557.

Chau, K.W. and Jin, H., 1998. Eutrophication Model for a Coastal Bay in Hong Kong. Journal of Environmental Engineering, 124(7), 628-638.

Chen, X.J. and Sheng, Y.P., 2005. Three-Dimensional Modeling of Sediment and Phosphorus Dynamics in Lake Okeechobee, Florida: Spring 1989 Simulation. Journal of Environmental Engineering, 131(3), 359-374.

Comings, K.J., Booth, D.B. and Horner, R.R., 2000. Storm Water Removal by Two Wet Ponds in Bellevue, Washington. Journal of Environmental Engineering, 126(4), 321-330.

Dechesne, M., Barraud, S., and Bardin, J.P., 2005. Experimental assessment of stormwater infiltration basin evolution. Journal of Environmental Engineering, 131, 1090-1098.

Deletic, A and Orr, David W., 2005. Pollution buildup on road surfaces. Journal of Environmental Engineering, 131, 49-59.

Detenbeck, N.E. and Brezonik P.L., 1991. Phosphorus Sorption by Sediments from a Soft-Water Seepage Lake. Environmental Science & Technology, 25(3), 395-409.

Dodds, W.K., Jones, J.R., Welch, E.B., 1998. Suggested classification of stream trophic state: distribution of temperate stream types by chlorophyll, total nitrogen, and phosphorus. Water Research 32, 1455-1462.

Drapper, D., Tomlinson, R. and Williams, P., 2000. Pollutant Concentrations in Road Runoff: Southeast Queensland Case Study. Journal of Environmental Engineering, 126(4), 313-320.

Drever, J.I., 1997. The geochemistry of natural waters (3rd ed.): New York, Prentice-Hall, pp 436.

Duda, A.M., 1993. Addressing nonpoint sources of water pollution must become an international priority. Water Sci. Technol. 28, 1-11.

Forbes, M.G., Dickson, K.R., Golden, T.D., Hudak, P. and Doyle, R.D., 2004. Dissolved Phosphorus Retention of Light-Weight Expanded Shale and Masonry Sand Used in Subsurface Flow Treatment Wetlands. Environmental Science & Technology, 38(3), 892-898.

Foy, R.H., Gibson, C.E., Champ, T., 1996. The effectiveness of restricting phosphorus loading from sewage treatment works as a means of controlling eutrophication in Irish lakes. In: Giller, P.S., Miller, A.A. (Eds), Disturbance and Recovery of Ecological Systems. Royal Irish Academy, Dublin, Ireland, 134-152.

Gachter, R., Ngatiah, John M., Stamm, C., 1998. Transport of phosphate from soil to surface waters by preferential flow. Environmental Science & Technology. 32(13), 1865-1869.

Gachter, R., Steingruber, S.M., Reinhardt, M. and Wehrli, B., 2004. Nutrient Transfer from Soil to Surface Waters: Differences between Nitrate and Phosphate. Aquat. Sci., 66, 117-122.

Gao, B., Walter, M.T., Steenhuis, T.S., Hogarth, W.L. and Parlange, J.Y., 2004. Rainfall Induced Chemical Transport from Soil to Runoff: Theory and Experiments. Journal of Hydrology, 295, 291-304.

Gervin, L. and Brix, H., 2001. Removal of Nutrients from Combined Sewer Overflows and Lake Water in a Vertical-Flow Constructed Wetland System. Water Science and Technology, 44(11-12), 171-176.

Hakanson, L., 1994. A review of effect-dose-sensitivity models for aquatic ecosystems. Internationale Revue der Gesamten Hydrobiologie 79, 621-667.

Hart, B., Roberts, S., James, R., Taylor, J., Donnert, D. and Furrer, R., 2003. Use of Active Barriers to Reduce Eutrophication Problems in Urban Lakes. Water Science and Technology, 47(7-8), 157-163.

Harwood, J.E., Hattingh, W.H.J. 1973. Colorimetric methods of analysis of phosphorus at low concentration in water. In Environmental Phosphorus Handbook; Griffith, E. J., Ed.; John Wiley & Sons: New York.

Hecky, R.E., Kilham, P., 1988. Nutrient limitation of phytoplankton in freshwater and marine environments: a review of recent evidence on the effects of enrichment. Limnology and Oceanography 33, 796-822.

Irish, L.B. Jr., Barrett, M.E., Malina, J.F. and Charbeneau, R.J., 1998. Use of Regression Models for Analyzing Highway Storm-Water Loads. Journal of Environmental Engineering, 124(10), 987-993.

Jang, Am, Youngwoo Seo and Paul L. Bishop. 2005. The removal of heavy metals in urban runoff by sorption on mulch. Environmental Pollution. 133, 117-127.

Liu, M., Hou, L., Xu, S., Ou, D. Yang, Y., Zhang, B. and Liu, Q., 2002. Adsorption of phosphate on Tidal Flat Surface Sediments from the Yangtze Estuary. Environmental Geology, 42, 657-665.

Marklund, A., Andersson, B., and Haglund, P., 2005. Traffic as a source of organophosphorus flame retardants and plasticizers in snow. Environ. Sci. & Technol. 39(10), 3555-3562.

McDowell, R., Sharpley, A. and Withers, P., 2002. Indicator to Predict the Movement of Phosphorus from Soil to Subsurface Flow. Environmental Science & Technology, 36(7), 1505-1509.

Murphy, J.; Riley, J. P. Anal. Chim. Acta 1962, 27, 31-36.

Nurnberg, G.K., 1996. Trophic state of clear and colored, soft-and hard-water lakes with special consideration of nutrients, anoxia, phytoplankton and fish. Lakes and Reservoir Management 12, 432-447.

Saget, A., Chebbo, G., Bertrand-Krajewski, J.-L., 1996. The first flush in sewer systems. Water Sci. Technol. 33(9), 101-108.

Sansalone, J.J. and Buchberger, S.G., 1997. Partitioning and First Flush of Metals in Urban Roadway Storm Water. Journal of Environmental Engineering, American Society of Civil Engineers, Vol. 123. No. 2, February, pp 134-143.

Sansalone, J.J., Koran, J.M., Smithson, J.A. and Buchberger, S.G., 1998. Physical Characteristics of Urban Roadway Solids Transported During Rain Events. Journal of Environmental Engineering, American Society of Civil Engineers, Vol.124, No. 4, pp 427-440.

Scarlatos, P.D., 1997. Experiments on Water-Sediment Nutrient Partitioning Under Turbulent, Shear and DiffusiveConditions. Water, Air, and Soil Pollution, 99, 411-425.

Schindler, D.W., 1977. Evolution of phosphorus limitation in lakes. Science. 195, 260-262.

Seo, D. and Canale, R.P., 1999. Analysis of Sediment Characteristics and Total Phosphorus Models for Shagawa Lake. Journal of Environmental Engineering, 125(4), 346-350.

Seo, D.C., Cho, J.S., Lee, H.J., and Heo, J.S., 2005. Phosphorus Retention Capacity of Filter Media for Estimating the Longevity of Constructed Wetland. Water Research, 39, 2445-2457.

Shinya, M., Tsuchinaga, T., Kitano, M., Yamada, Y. and Ishikawa, M., 2000. Characterization of Heavy Metal and Polycyclic Aromatic Hydrocarbons in Urban Highway Runoff. Water Science and Technology, 42(7-8), 201-208.

Shinya, M., Tsuruho, K. and Ishikawa, M., 2003. Evaluation of Factors Influencing Diffusion of Pollutant Loads in Urban Highway Runoff. Water Science and Technology, 47(7-8), 227-232.

Shonnard, D.R., Allen, D.T., Nguyen, N., Austin, S.W. and Hesketh, R., 2003. Green Engineering Education through a U.S. EPA/Academia Collaboration. Environmental Science & Technology, 37(23), 5453-5462.

Smith, R.A., Alexander, R.B., Lanfear, K.J., 1993. Stream water quality in the conterminous United States – Status and Trends of Selected Indicators during the 1980s (Water Supply Paper 2400.). US Geological Survey.

Smith, R.A., Alexander, R.B., Wolman, M.G., 1987. Water-quality trends in the nation's rivers. Science 235, 1507-1615.

Sonstrom, R.S., Clausen, J.C. and Askew, D.R., 2002. Treatment of Parking Lot Stormwater Using a StormTreat System. Environmental Science & Technology, 36(20), 4441-4446.

Sparks, D.L., 2003. Environmental Soil Chemistry, Academic Press, Amsterdam.

U.S. EPA, 1983. Results of the national urban runoff program. NTIS # PB84-1855345, Washington, D.C.

U.S. EPA, 1986. Quality Criteria for Water. Office of Water Regulation and Standards, US Government Printing Office (PB81-226759), Washington, DC 20460. EPA 440/5-86-001.

U.S. EPA, 1990. National water quality inventory – 1998 report to congress, EPA 440-4-90-003. Washington, D.C.

Van Olphen, H., 1977. An introduction to clay colloid chemistry (2nd ed.). New York, Wiley-Interscience, 318 p.

Visvanathan, C., Werellagama, D.R.I.B., and Aim, R.B., 1996. Surface water pretreatment using floating media filter. Journal of Environmental Engineering, 122,25-33.

Vollenweider, R.A. and Kerekes, J. 1980. The loading concept as a basis for controlling eutrophication, philosophy and preliminary results of the OECD programme on eutrophication. Prog. Water Technol., 12, 5-38.

Wang, G.T., Chen, S., Barber, M.E. and Yonge, D.R., 2004. Modeling Flow and Pollutant Removal of Wet Detention Pond Treating Stormwater Runoff. Journal of Environmental Engineering, 130(11), 1315-1321.

Wu, J.S., Holman, R.E. and Dorney, J.R., 1996. Systematic Evaluation of Pollution Removal by Urban Wet Detention Ponds. Journal of Environmental Engineering, 122(11), 983-988.

Zhou, A.M., Tang, H.X., and Wang D.S. 2005. Phosphorus adsorption on natural sediments: Modeling and effects of pH and sediment composition. Water Research 39, 1245-1254.

CHAPTER 4 BATCH EQUILIBRIA FOR PHOSPHORUS ADSORPTION ON ALUMINUM OXIDE COATED MEDIA

SUMMARY

Adsorption of phosphorus (P) from synthetic rainfall-runoff onto highly porous aluminum oxide coated media (AOCM) was investigated as a function of initial phosphate concentrations, solution pH, ionic strength, adsorbent media size and the presence of co-existing ions such as calcium, sulfate and nitrate. The P adsorption experiments were carried out across a range of typical rainfall-runoff conditions: variable initial phosphorus concentrations from 0 to 25 mg/L; solution pH range of 5 to 9; ionic strength range of 0.0005 to 0.2 M; three varying media size suitable for potential filter use; and influence of co-existence of multi-component ions. Phosphorus adsorption increased with decreasing AOCM adsorbent size and slightly acidic pH. While calcium enhanced P adsorption by forming ternary complexes, sulfate inhibited P adsorption by competing for available adsorption sites. Ionic strength and nitrate has little effect on P adsorption. Low desorption potential, which resulted from strong bonding between P and AOCM, was also obtained under typical experimental conditions.

The adsorption data were successfully fit to Freundlich, Langmuir and Langmuir-Freundlich isotherm equations. Maximum P adsorption capacity of AOCM was 2.5 [mg/g]. The highly porous and lightweight AOCM contained 4.59±0.94 mg of aluminum oxide per mg of expanded clay substrate and resulted in P adsorption capacity that was very favorable. The equilibria parameters derived using these isotherm models could be used to infer the batch adsorption performance and fixed bed adsorption results for more complex rainfall-runoff system. Based on adsorption by AOCM, phosphorus concentrations could be reduced to a suitable level for discharge to natural surface waters.

INTRODUCTION

As one of the essential elements on earth, phosphorus has been regarded as the major growth limiting nutrient. However excessive amount of phosphorus in water bodies such as urban streams and lake reservoirs is directly responsible for eutrophication (algal blooms, depletion of dissolved oxygen and deterioration of water quality). Eutrophication is considered as one of the most important environmental problems. A better understanding of the detrimental influence of eutrophication caused by phosphorus has led to more stringent regulation of phosphorus level in receiving waters and stimulated the demand for more efficient and cost effective removal of phosphorus. The maximum contaminant level (MCL) of phosphorus in lake reservoirs was 0.1 mg/L as recommended by EPA (1986). Complying with this standard is apparently difficult considering the significant amounts of waters and discharges around the world that exceed this level. Figure 4-1 and Figure 4-2 illustrate total dissolved phosphorus (TDP) and total phosphorus (TP) ranges of eight rainfall-runoff events captured from the Baton Rouge research site. Results from these figures illustrate that while concentrations of TDP typically represent a smaller proportion of total P, TDP levels alone exceed MCL for TP. Removal of phosphorus from urban rainfall-runoff has become a priority in many areas of the USA for suitable discharge to receiving waters.

A variety of physical operations and biological/chemical processes have been investigated for the treatment of phosphorus from water. Each of these operations and processes has its own advantage and disadvantage. Conventional physical methods targeting on removal of predominant particulate-bound fraction of phosphorus, such as quiescent settling, have proved to be in most cases marginally satisfactory (Clark et al. 1997) if operated as a single primary unit operation when considering TP discharge levels that are 0.10 mg/L or lower.

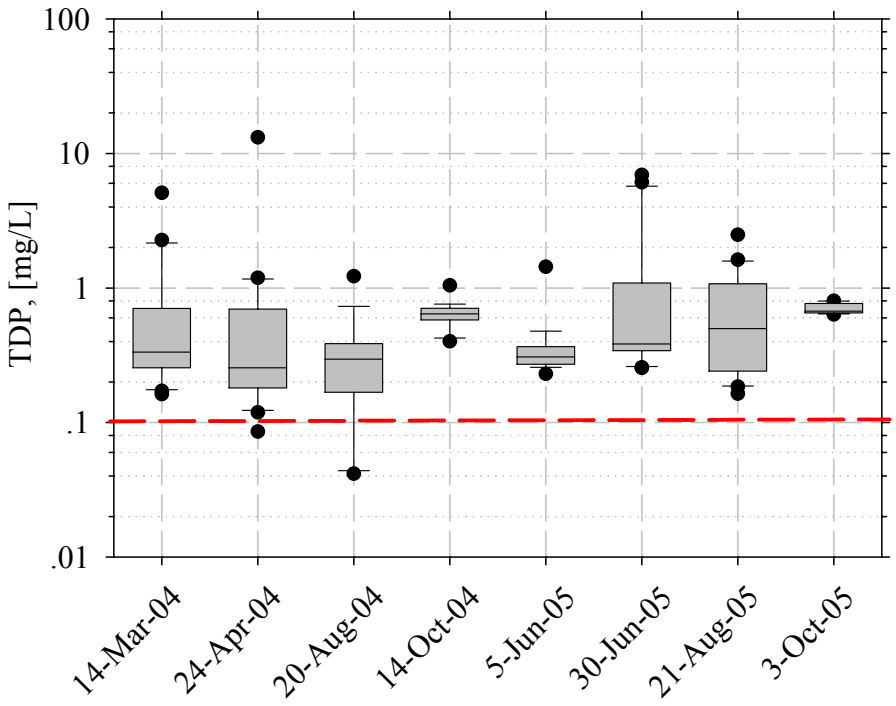

Figure 4-1. TDP Ranges of urban rainfall runoff on an event basis.

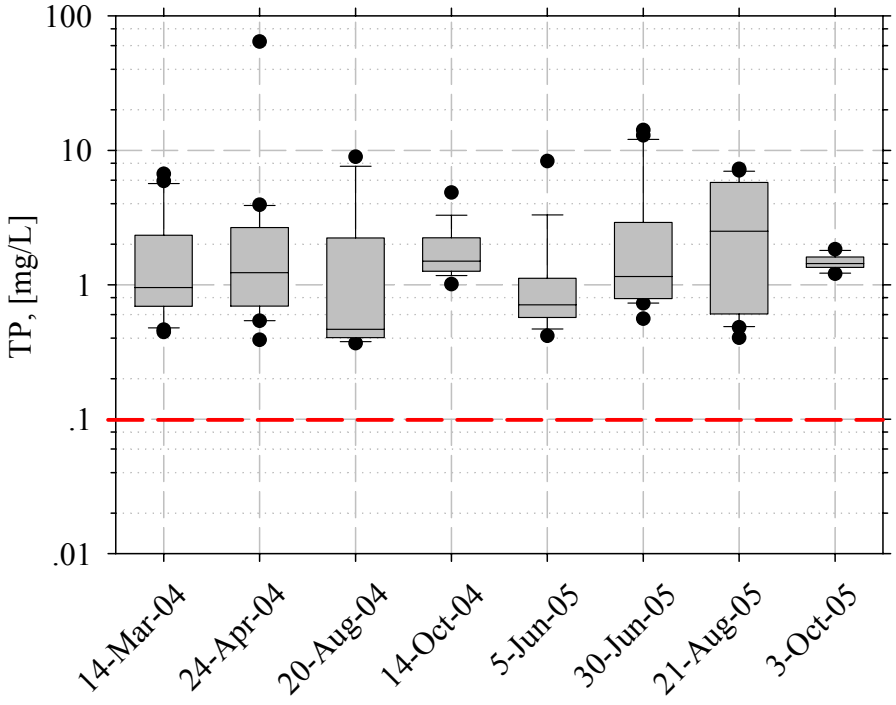

Figure 4-2. TP Ranges of urban rainfall runoff on an event basis.

Advanced physical methods such as reverse osmosis and electrodialysis are more effective, but far less economical and maintainable given complex rainfall-runoff phenomena; which may hinder their widespread use (Omoike and Vanloon 1999; Sakakibara and Nakajima 2002). Enhanced biological treatment can remove higher percentage of TP, but these processes even for "natural" systems encounter operational difficulties and have challenges of maintainability. Alternatively, physical or chemical adsorption processes by metal oxides (Al and Fe), have advantages for adsorbing or precipitating phosphorus even at low TDP concentration but generally require some form of primary treatment to reduce unsteady flows and reduce particulate loadings before adsorption/precipitation. Direct precipitation of phosphorus by Ca and Mg are less commonly employed because of handling difficulties, production of large amount of sludge and generally requires some level of secondary treatment before direct discharge to surface waters. (Stumm and Morgan 1981; Clark et al. 1997; Sawada et al. 2003). Generally all of these advanced process systems require some form of upstream primary treatment for quantity and quality control.

Economical sorption materials for effective phosphorus removal from aqueous solution such as urban rainfall-runoff, has attracted great attention lately. A range of adsorbents has been investigated for phosphate adsorption, including: aluminas (Gangoli and Thodos 1973), aluminum hydroxide (Galinada and Yoshida 2004), aluminum oxide (Huang 1977), synthetic boehmite (Tang et al. 1996), gibbsite (Gimsing et al. 2004), goethite (Juang and Chung 2004; Rietra et al. 2001), amorphous calcium silicate (Southam et al. 2003), polymeric hydrogels (Kofinas and Kioussis 2003), fly ash (Deborah and Marcia 1979), iron oxide tailings (Zeng et al. 2004) and blast furnace slag (Hisashi et al. 1986). It was found that lower concentrations of

phosphorus [1 mg/L] can be removed by activated alumina (Donnert and Salecker, 1999a; Donnert and Salecker, 1999b).

Routinely applied in chemical process industries for the separation of species from liquid streams, knowledge of adsorption phenomena at the solid-liquid interface is crucial for understanding the fate and transport of environmental contaminants, which commonly come into contact with surfaces that provide sites with which ions and molecules interact (Ioannidis and Anderko 2001). Sorption by aluminum species is credited to the presence of Al-OH and functional groups on the mineral surface (Shin et al. 2004). Given the complexity of surface composition and structure, many interactions are likely to occur, including specific chemical adsorption (surface complexation involved with ligand exchange) and precipitation; nonspecific physical adsorption (ion exchange relevant to electrostatic forces) driven by the surface charge and surface area of adsorbent. When surface complexation phenomenon occurs, the surface complexes formed can be classified as inner and outer sphere complexes depending on the type of affinity of phosphate to an active surface site. Formation of these surface complexes is mostly dependent on the degree of surface protonation and/or dissociation. Johnson et al. (2002) used P NMR to study the adsorption of phosphate on γ-Al_2O_3 and concluded that the adsorption is complex, with evidence of outer- and inner- sphere complexes and surface precipitation.

Aluminum oxide coated media (AOCM) represents a group of aluminum oxide coated or impregnated substrates with high porosity and large specific surface area were developed to selectively bind the phosphorus anion onto and into the media matrix, permitting subsequent removal from an aqueous stream. This engineered media must fulfill requirements of economy, provide a medium of desired hydraulic conductivity, provide desired P adsorption capacity, reduce P concentrations to targeted levels, and be able to retain the P without desorption.

OBJECTIVES

This study had three objectives. In the first objective of this study, AOCM equilibrium adsorption capacities were evaluated in terms of dissolved phosphorus removal, using data collected from rainfall-runoff in Baton Rouge, LA as a basis for TP and TDP levels. The second objective is to characterize the effects of TDP adsorbate concentration, solution pH, ionic strength, media size and presence of enhancing and competing ions such as calcium, sulfate and nitrate on equilibrium adsorption. The third objective was to examine adsorption data utilizing Langmuir, Freundlich and Langmuir-Freundlich isotherm models to indicate possible adsorption mechanisms and provide guidance for adsorption cartridge design.

BACKGROUND

Adsorption, which has been extensively used in industrial processes for a variety of separation and purification purposes, is envisaged as a prominent method of treating dissolved P, measured as total dissolved phosphorus (TDP) in rainfall-runoff or snowmelt. Specifically, solute adsorption onto metal oxides can be ascribed to the amphoteric surface, on which surface functional groups are most commonly represented by hydrolyzed species (Stumm and Morgan 1996). The acid-base reactions on the surface are simply illustrated.

$$XOH = H^+ + XO^- \qquad \text{Equation 4-1}$$

$$XOH + H^+ = XOH_2^+ \qquad \text{Equation 4-2}$$

Bulk electrolytes can react with these groups to form ion pairs or covalent bounds. The affinity of phosphate for (hydr)oxide surfaces depends on the complexing capacity of anions, which allows binding to surface groups by ligand exchange reactions, and attractive or repulsive electrostatic interactions with the charged (hydr)oxide surfaces (Stumm, 1987; Antelo et al. 2005). If only electrostatic interactions are involved, outer sphere complexes are formed. For

instance, if the oxide surface has a steady positive charge, the balancing anions located in the double layer can be exchanged with the anions of the bulk electrolyte.

$$A_{1s}^{-} + A_2^{-} \Leftrightarrow A_1^{-} + A_{2s}^{-} \qquad \text{Equation 4-3}$$

If a specific interaction occurs, the adsorbed species are directly bound to the oxide surface, and inner-sphere complexes are formed. This occurs when oxygen atoms of the phosphate ions displace the surface hydroxyl groups and the water molecules coordinated with aluminum. Additional mechanisms might be involved, including ligand adsorption as the result of an exchange with hydroxyl groups and metal-ligand adsorption to form ternary complexes. Ligand adsorption as the result of an exchange with hydroxyl groups can be represented.

$$X-OH + L^{-} = X-L + OH^{-} \qquad \text{Equation 4-4}$$

$$2X-OH + L^{-} = X_2-L^{+} + 2OH^{-} \qquad \text{Equation 4-5}$$

As a consequence of ligand exchange adsorption, solution pH is expected to increase because the hydroxyl ions are released from the oxidic adsorbent. Phosphate replaces singly coordinated OH^- groups and then reorganizes into a very stable bi-nuclear bridge between cations (Bohn et al. 1985). This chemisorption process is coupled with the release of OH^- ions, hence the process is favored by lower pH values (Stumm 1987; Altundogan and Tumen 2001). Metal-ligand adsorption by formation of form ternary complexes can be represented as follows.

$$X-OH + L^{-} + Me^{z+} = X-L-Me^{z+} + OH^{-} \qquad \text{Equation 4-6}$$

$$X-OH + L^{-} + Me^{z+} = X-OMe-L^{(z-2)+} + H^{+} \qquad \text{Equation 4-7}$$

Concerning adsorption on aluminum oxides, a formation of inner-sphere complexes is probable (Bleam et al. 1991) and at low pH there is some evidence suggesting outer-sphere complexes and surface precipitation as $AlPO_4$ (Johnson et al. 2002). The combined effects of pH and ionic

strength result in higher phosphate adsorption in acidic media at most ionic strengths, but result in lower phosphate adsorption under higher pH, and with more basic media (Antelo et al. 2005).

MULTI-COMPONENT INTERACTIONS

Interaction between dissolved P and various co-existing ions that are typically observed in rainfall-runoff may affect the adsorption of P on AOCM and thereby the mobility and bioavailability of P. The interaction of ions during simultaneous adsorption may be caused by direct competition for adsorptive sites and the influence of ion adsorption on the surface charge leading to either synergistic effects in terms of adsorption (e.g. calcium and phosphate) or to competitive effects (e.g. sulfate and phosphate). Rietra et al. (1999) showed that phosphate has a higher adsorption affinity than sulfate in competitive conditions despite the ability of sulfate to form inner-sphere complexes. Calcium was found to significantly enhance phosphate adsorption to iron oxides through co-adsorption (Rietra et al. 2001).

Complexation reactions at the surface of AOCM induce more complexity than corresponding reactions in homogeneous solution. The co-adsorption of several anions does not only imply a competition for available surface sites, but does affect the surface equilibrium by altering the surface charge (Butkus and Grasso 2001). In practical situations, multi-component competition may increase the complexity of anion interactions at the AOCM water interface. Such complex systems frequently occur, and the magnitude of these competitive interactions must be clarified to better predict behavior of P adsorption on AOCM and identify those anions more likely to be affected during transport in the presence of other anions. Given the environmental importance of phosphorus across a wide range of ionic strength and co-existing ions observed in rainfall-runoff, studying the effects of ionic strength and coexisting ions on P adsorption by AOCM becomes very important.

METHODS AND MATERIALS

ISOTHERM MODELING

Adsorption capacities at equilibrium, Q_e [mg/g], were determined according to the mass balance between the sorbent phase and sorbate phase after introducing AOCM into the batch reactor.

$$Q_e = \frac{V}{m}(C_0 - C_e) \qquad \text{Equation 4-8}$$

In this expression C_0 [mg/L] is the initial solute concentration, C_e [mg/L] the concentration of solute at equilibrium, *m* (g) the mass of AOCM, and V(L) the solution volume. This equation is also known as the line of operation which is illustrated in Figure 4-3.

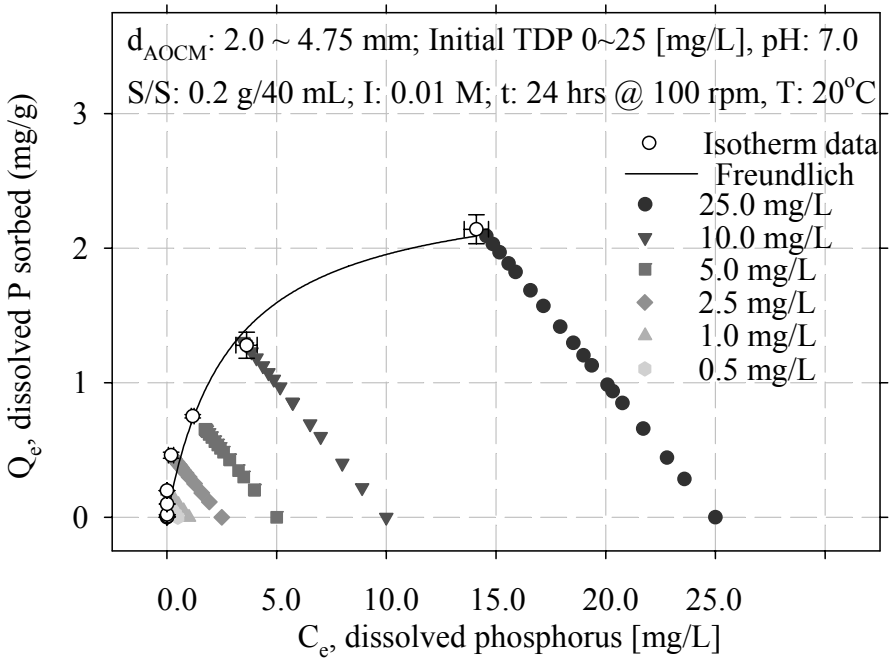

Figure 4-3. Operational lines for AOCM adsorption of TDP.

Adsorption data were examined using Freundlich (Freundlich and Heller 1939), Langmuir (Langmuir 1918) or integrated Langmuir-Freundlich (L-F) isotherms. Although Freundlich and Langmuir isotherms were first introduced about seven decades ago, they still

remain the two most commonly used adsorption isotherm equations (Kinniburg 1986). The selections of these three isotherm models was based on the ability of each model to successfully fit a wide variety of adsorption conditions imposed by the experimental matrix, the ability to provide a physical interpretation based on model parameter results and the relative simplicity of the isotherm equations. All the three isotherm equations were transformed to linear forms so their parameters could be determined by linear regression. Model parameters were also examined with the aid of non-linear regression using least-squares to acquire the optimized estimate of isotherm model parameters.

The Freundlich isotherm was utilized as a non-ideal adsorption model describing systems that exhibit nonlinear increases in adsorption with adsorbate concentration. The Freundlich isotherm model assumes that the adsorbent surface is heterogeneous and the surface sites have different adsorption potentials. Due to the heterogeneous surface of oxide coated media and subsequent heterogeneous surface affinity distribution and multi-layer adsorption, it was hypothesized that the Freundlich isotherm has a clear physical basis for application to phosphorus adsorption by AOCM. The Freundlich model form for a single adsorbent (non-competitive) is expressed as follows.

$$Q_e = K_F C_e^{\,n} \qquad \text{Equation 4-9}$$

In this expression K_F is an empirical constant indicating media adsorption capacity; and *n* is an empirical constant reflecting the isotherm profile curvature.

In contrast to Freundlich, the Langmuir isotherm was also examined based on the alternate hypothesis that all adsorbates compete for a single population of uniform monolayer sites. That suggests all reactive sites of the sorbent have same affinity for the sorbate. The expression for the Langmuir model utilized in this study is as follows.

$$Q_e = \frac{Q_m b C_e}{1 + b C_e} \qquad \text{Equation 4-10}$$

In this expression, Q_m is the maximum adsorption capacity, [mg/g] and *b* is an empirical constant [L/mg]. One of the essential characteristics of the Langmuir equation is that it can be expressed in terms of a dimensionless constant called the equilibrium parameter ($R_{L,I}$), which can be beneficially used to predict whether a sorption system is favorable or unfavorable in batch processes (Lin and Juang, 2002). The parameter is described by the following equation.

$$R_{L,I} = \frac{1}{1 + b C_i} \qquad \text{Equation 4-11}$$

In this expression C_i is the highest initial solute concentration (mg/L), and *b* is the Langmuir constant. The value of $R_{L,I}$ indicates whether the isotherm is irreversible ($R_{L,I} = 0$), favorable ($0 < R_{L,I} < 1$), linear ($R_{L,I} = 1$) or unfavorable ($R_{L,I} > 1$).

In contrast to Freundlich and Langmuir models, the integrated Langmuir-Freundlich isotherm is essentially a Freundlich isotherm, which represents the asymptotic property to approach an adsorption at high concentration (Kinniburg 1986). Therefore the integrated Langmuir-Freundlich isotherm would like be suitable a wider range of experimental conditions. The Langmuir-Freundlich (L-F) equation is expressed as follows.

$$Q_e = \frac{K_{LF} C_e^{\lambda}}{1 + \theta C_e^{\lambda}} \qquad \text{Equation 4-12}$$

In this expression K_{LF}, θ and λ are the L-F constants.

SORBENT MEDIA

Sorbent media utilized in this study was a specific form of AOCM. This media was prepared from clay material and aluminum oxide. Clay expanded with a blowing agent was fired into bricks at 1000^0C . The cooled bricks were crushed and sieved to yield to produce three size ranges of substrate: 0.85 ~ 2 mm, 2 ~ 4.75 mm and 4.75 ~ 9.5 mm using ASTM standard sieves No. ¼ inch (4.75-mm opening), No. 10 mesh (2.00-mm opening) and No. 20 mesh (0.85-mm

opening). The resulting substrate is a stable, highly porous material, lightweight media of low organic content. The sorbent substrate was then coated with an aluminum salt to produce the sorbent media (AOCM) utilized in this study. The effect of media size of AOCM on phosphorus adsorption was examined using these three size categories: 0.85 ~ 2 mm; 2 ~ 4.75 mm and 4.75 ~ 9.5 mm by sieving. Such a size range of AOCM is suitable for the potential adsorption cartridge filter usage.

SORPTION EQUILIBRIA

The stock phosphate solution (100 mg/L PO_4^{3-}) was prepared and calibrated by dissolving 143.3 mg anhydrous potassium dihydrogen orthophosphate (KH_2PO_4) into 1.0 L of de-ionized water. By dilution from the stock solution, synthetic rainfall-runoff of specific initial working phosphate concentrations used to obtain adsorption data were set as: 0.0, 0.05; 0.10; 0.50; 1.0; 2.5; 5.0; 10.0; 25.0 [mg/L] or 0.0, 0.53; 1.05; 5.26; 10.53; 26.32; 52.63; 105.26; 263.16 [μmol/L], respectively. Such a selection of phosphorus concentration range is based on the measurement of TDP ranging from 0.01 mg/L to 13.2 mg/L, and TP ranging from 0.4 mg/L to 66.6 mg/L for rainfall-runoff from urban Baton Rouge, LA. The event-based statistical distribution of these concentrations is shown in Figure 4-1 and Figure 4-2.

Ionic strength was fixed at 0.01 M using KCl. Solution pH was adjusted and maintained to 7 throughout the adsorption experiment by the dropwise addition of 0.02 N HCl or 0.02 N KOH. No buffer was added to avoid possible competition for sorption sites. Precisely measured amounts (0.200 dry grams) AOCM and 40 ml of working phosphate solution were added in a 50 ml polyethylene centrifuge tube. A value of 10% to about 30% adsorption for the highest solute concentration utilized was selected as the criterion for the sorbent-solution ratio used (0.2g/40 ml = 1/200) (USEPA 1987). The mixture was shaken on a horizontal bench shaker at a rate of 100

rpm and adsorption was carried out at 20 ± 2ºC until adsorption equilibrium was achieved. Equilibrium was confirmed by the consistent residual phosphate concentrations of last two consecutive measurements (at half an hour interval). The contents in the centrifuge tube were then filtered through 0.45 μm filter and the total dissolved phosphate concentration (PO_4^{3-}) in the filtrate was measured using the ascorbic acid method (Standard Method 1998 of 4500-P-E for wastewater which is equivalent to USEPA method 365.2). The amount of solute sorbed was calculated from the difference between the initial and equilibrium solute concentrations. All measurements were duplicated and demonstrated high repeatability with experimental error controlled within 5%. All calibrations were based on six standards over the range of sample concentrations with the coefficient of determination (R^2) greater than 0.99. All chemicals used were analytical reagent grade.

SOLUTION PH AND INITIAL TDP CONCENTRATION

To test the influence of solution pH on phosphorus sorption, synthetic rainfall-runoff was prepared at pH 5, 6, 7, 8 and 9 with variable initial TDP concentration (0 ~ 25 mg/L) and different solution ionic strength (0.0005 ~ 0.2 M KCl). The pH range was determined based on measured pH ranges in rainfall-runoff that ranged from slightly less than 6 to slightly greater than 8 (Sansalone and Buchberger 1997, Sansalone et al. 1998, Sansalone et al 2005). During the adsorption reaction time, the pH of the reactants was adjusted every 2 hours and kept constant by titration of 0.02 N HCl or 0.02 N KOH.

IONIC STRENGTH EFFECT

The range of ionic strengths in rainfall-runoff has been measured to range from 0.0008 to 0.17 M (Sansalone et al. 1998, Sansalone et al. 2005). Therefore ionic strength was adjusted to

0.0005, 0.005, 0.01 and 0.2 M with KCl for the range of initial phosphate concentration (0 ~ 25 mg/L) and range of pH (5 ~ 9).

ROLE OF DESORPTION

Desorption of TDP is a significant concern for any media deployed to adsorb TDP from rainfall-runoff. Therefore desorption was measured for the media immediately after adsorption was completed. After an adsorption run, deionized water (40 ml) with no TDP was added to media in a batch reactor. The solution pH was fixed at 7.0 for the 24 hour desorption period. After shaking for 24 hours, the TDP content in the aqueous solution was measured again by ascorbic acid method. The amount of TDP desorbed was calculated from the difference between the beginning and end of the desorption experiment.

Table 4-1. Parameters of Langmuir, Freundlich and Langmuir-Freundlich isotherm equations for effect of pH on P adsorption by AOCM. Experiments were carried out: initial P concentrations 0; 0.05; 0.1; 0.5; 1.0; 2.5; 5.0; 10.0; 25 [mg/L]; AOCM size 2 ~ 4.75 mm; pH from 5 to 9; ionic strength 0.01 M KCl; sorbent solution ratio 0.2g/40ml; shaking rate 100 rpm for 24 hours; ambient temperature 20^0C.

Solution pH	Langmuir			Freundlich			Langmuir-Freundlich			
	b	Q_m	R^2	K_F	n	R^2	λ	θ	K_{LF}	R^2
pH 5	0.57	2.72	0.93	0.96	0.38	0.96	0.44	0.11	1.09	0.96
pH 6	0.78	2.38	0.92	1.09	0.28	0.98	0.42	0.13	1.08	0.98
pH 7	0.34	2.52	0.96	0.72	0.41	0.98	0.51	0.13	0.82	0.98
pH 8	0.38	1.91	0.94	0.61	0.37	0.98	0.40	0.04	0.64	0.98
pH 9	0.09	1.60	0.99	0.18	0.74	0.99	1.18	0.05	0.13	0.99

COMPETITION WITH COMMON IONS IN RAINFALL-RUNOFF

Common ions commonly identified in urban rainfall-runoff are calcium (Ca^{2+}), sulfate (SO_4^{2-}) and nitrate (NO_3^-). These ions can have a positive or negative effect on phosphorus adsorption by AOCM. The role of these common ions on AOCM adsorption of TDP was examined based on concentration ranges measured in urban rainfall-runoff; calcium (15 mg/L),

sulfate (35 mg/L) and nitrate (5 mg/L) (Dean et al. 2005). Each of these ions was introduced individually to the adsorption solution.

RESULTS

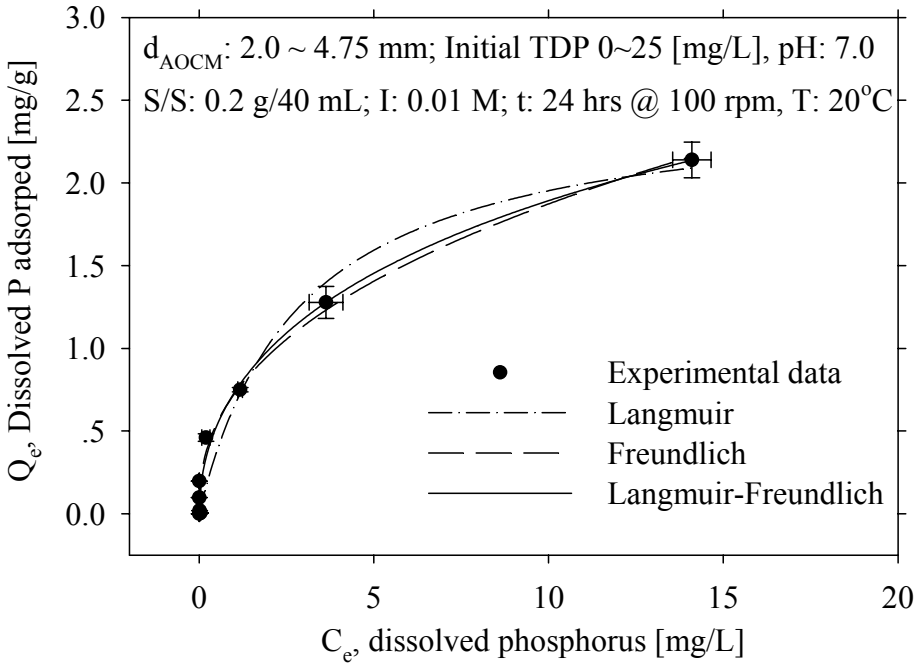

Figure 4-4. Illustration of P adsorption by AOCM modeled by Langmuir, Freundlich and Langmuir-Freundlich isotherms. The model parameters are summarized in Table 4-1.

TDP adsorption by AOCM was modeled by Langmuir, Freundlich and Langmuir-Freundlich isotherm equations and summarized in Figure 4-4. Experiment was carried out: initial P concentrations 0; 0.05; 0.1; 0.5; 1.0; 2.5; 5.0; 10.0; 25 [mg/L]; AOCM size 2 ~ 4.75 mm; pH 7; ionic strength, I = 0.01 M KCl; sorbent-solution ratio, s/s ratio: 0.2g/40ml; shaking rate of 100 rpm for 24 hours; ambient temperature, T = 20^0C. The parameters of three isotherm models are summarized in Table 4-1. Coefficients of determination, R^2, which is a measure of the goodness of fit were 0.96, 0.98 and 0.98 for Langmuir, Freundlich and Langmuir-Freundlich isotherm respectively. The high values of R^2 indicate the satisfactory representation of the experimental data and fit of three models. Comparatively, Freundlich and Langmuir-Freundlich (L-F)

equations fit closely the experimental data and both are generally slightly better than Langmuir. Considering the physical mechanism of P adsorption on AOCM and simplicity of Freundlich isotherm, it would be used as the primary isotherm model in this study. In addition, P adsorption on AOCM is a favorable process which is confirmed by equilibrium parameter ($R_{L,I}$) located between 0 and 1.

INFLUENCE OF AOCM SIZE (D_{AOCM})

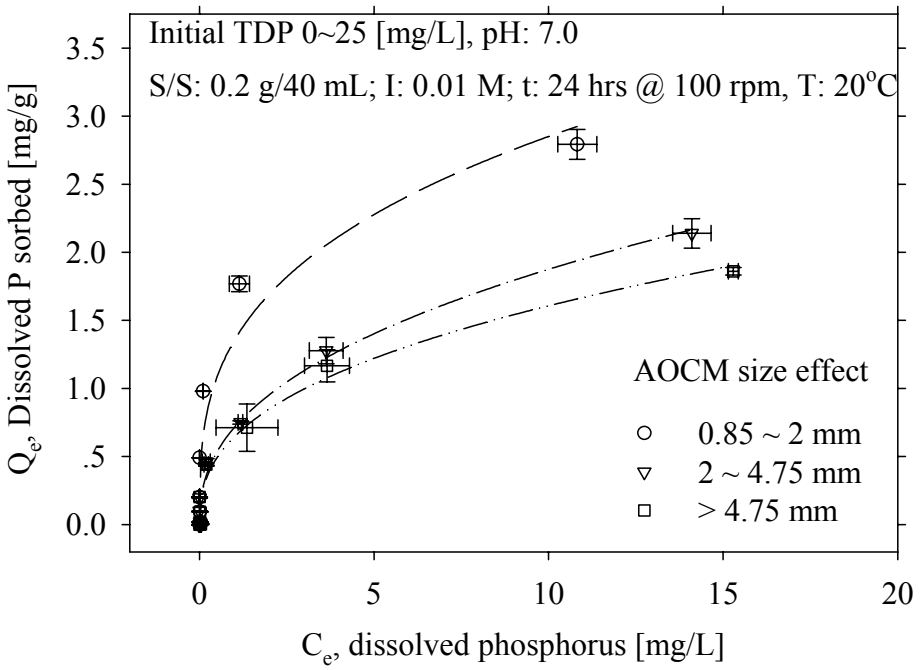

Figure 4-5. Effect of AOCM size on P adsorption. Measured data were fit by a Freundlich isotherm and corresponding parameters are summarized in Table 4-2.

The adsorbent media size has a considerable effect on TDP adsorption. With media adsorption, an important characteristic is the surface area available for sorption, which is in part related to the size and porosity of the media. Finer particles have a greater specific surface area (SSA) than larger particles by definition. This is the case for the AOCM with an SSA of 282.23 ± 22.53, 268.72 ± 24.56, 235.16 ± 5.95 m^2/g for AOCM size ranges of 0.85 ~ 2 mm; 2 ~ 4.75 mm and 4.75 ~ 9.5 mm respectively. The influence of AOCM size on P adsorption is illustrated

in Figure 4-5. Results were modeled using a Freundlich isotherm and corresponding parameters are summarized in Table 4-2. Values of K_F, an indicator of adsorption capacity, were 1.35, 0.72 and 0.65 for AOCM size of 0.85 ~ 2 mm; 2 ~ 4.75 mm and 4.75 ~ 9.5 mm, respectively. Examination of the data using the Langmuir isotherm model with results summarized in Table 4-2 also confirmed the same phenomena; the values of Q_m were 2.71, 2.52 and 2.13 mg/g for AOCM size of 0.85 ~ 2 mm; 2 ~ 4.75 mm and 4.75 ~ 9.5 mm, respectively. Since adsorption is a surface phenomenon, the smaller adsorbent sizes offer comparatively larger surface areas and hence higher phosphorus removal is obtained at equilibrium. Medium AOCM size range (2 ~ 4.75 mm) was primarily studied since, contact time, hydraulic conductivity of the media bed and head loss are all important parameters when selecting a media size.

Table 4-2. Parameters of Langmuir, Freundlich and Langmuir-Freundlich isotherm equations for effect of AOCM size on P adsorption by AOCM. Experiments were carried out: initial P concentrations 0; 0.05; 0.1; 0.5; 1.0; 2.5; 5.0; 10.0; 25 [mg/L]; pH 7; ionic strength 0.01 M KCl; sorbent solution ratio 0.2g/40ml; shaking rate 100 rpm for 24 hours; ambient temperature 20^0C.

Size (mm)	Langmuir			Freundlich			Langmuir-Freundlich			
	b	Q_m	R^2	K_F	n	R^2	λ	θ	K_{LF}	R^2
0.85 ~ 2	2.83	2.71	0.92	1.35	0.32	0.89	0.74	1.41	4.36	0.93
2 ~ 4.75	0.34	2.52	0.96	0.72	0.41	0.98	0.51	0.13	0.82	0.98
4.75 ~ 9.5	0.38	2.13	0.96	0.65	0.40	0.97	0.55	0.21	0.81	0.98

INFLUENCE OF SOLUTION PH AND INITIAL TDP CONCENTRATION

The influence of solution pH on sorption of phosphorus by AOCM at I = 0.01 M, 0.2 M, 0.005 M and 0.0005 M are summarized in Figure 4-6. Solution pH consistently illustrated a strong effect on P adsorption on AOCM under each of the four different ionic strength levels. As the solution pH increased, the Freundlich sorption parameters and maximum sorption capacity decreased systematically. Maximum P adsorption was obtained at pH of 5.

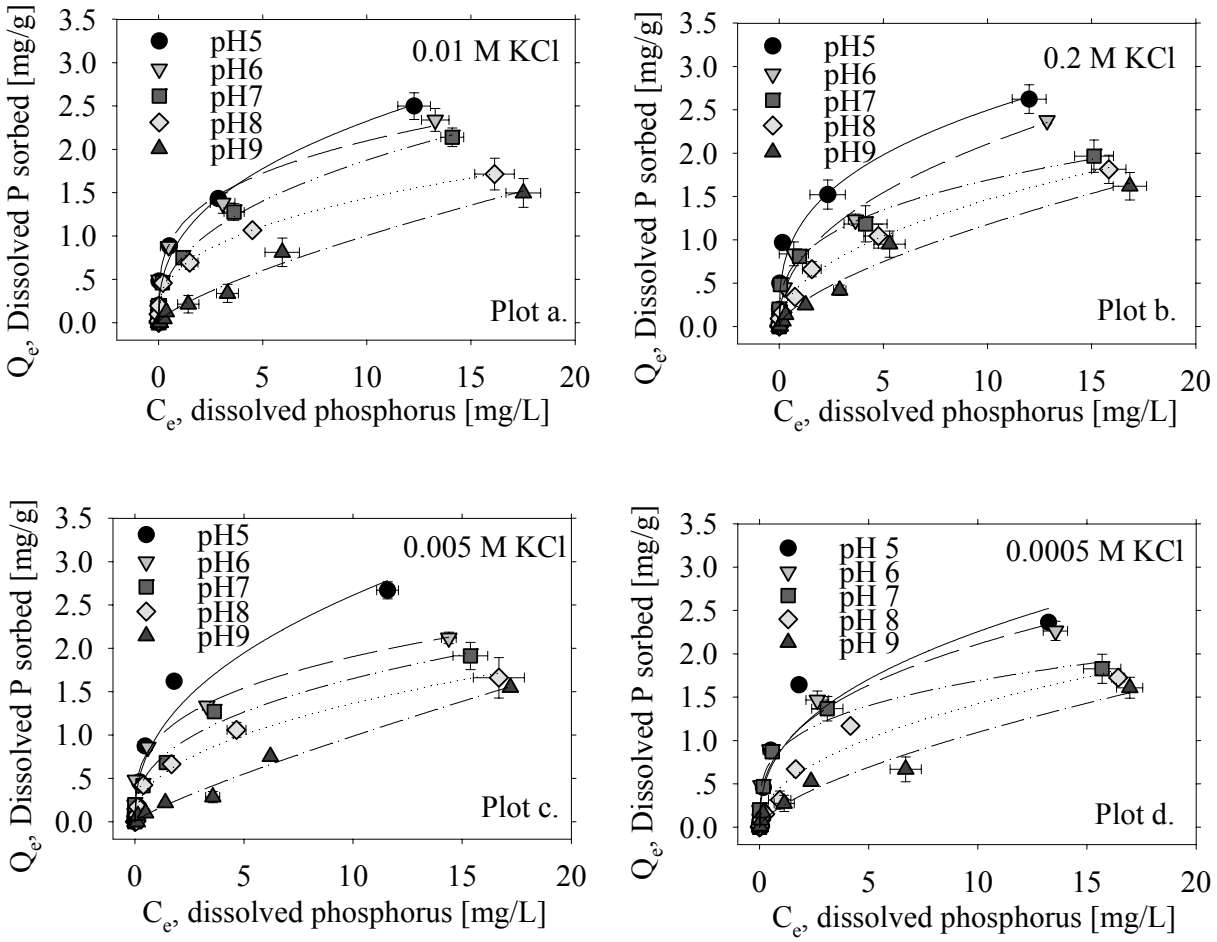

Figure 4-6. Effects of pH on TDP adsorption by AOCM at ionic strength, I of 0.01 M, 0.2 M, 0.005 M and 0.0005 M, respectively. Experiments were carried out at: initial P concentrations 0; 0.05; 0.1; 0.5; 1.0; 2.5; 5.0; 10.0; 25 [mg/L]; media size, d_{AOCM}: 2 ~ 4.75 mm; sorbent/solution ratio, s/s: 0.20 g/40 ml; contact time, t: 24 hours at 100 rpm; ambient temperature, T: 20^0C. The data were fit by a Freundlich isotherm and corresponding parameters are summarized in Table 4-3 and Table 4-4. Model fit of data resulted in R^2 values that ranged from 0.90 to 0.99.

Phosphate exists and dissociates in water as follows:

$H_3PO_4 \Leftrightarrow H^+ + H_2PO_4^-$ $K_1 = 10^{-2.16}$ Equation 4-13

$H_2PO_4^- \Leftrightarrow H^+ + HPO_4^{2-}$ $K_2 = 10^{-7.21}$ Equation 4-14

$HPO_4^{2-} \Leftrightarrow H^+ + PO_4^{3-}$ $K_3 = 10^{-12.32}$ Equation 4-15

where K_1, K_2 and K_3 are thermodynamic dissociation constants. In the aqueous urban rainfall-runoff, various types of protonated phosphate species, $H_2PO_4^-$, HPO_4^{2-} and PO_4^{3-}, are formed depending on pH. In the pH range of 2 to 10, dissolved phosphate exists mainly in the form of

$H_2PO_4^-$ (Huang 1975; Karthikeyan et al 2004). The point of zero charge (PZC) of adsorbent has an important role in the physical-adsorption phenomenon, which is found to be about 11 for AOCM (Jia and Sansalone).

Table 4-3. Parameters of Freundlich isotherm for effect of ionic strength 0.01 M and 0.2 M KCl on P adsorption by AOCM. Experiments were carried out at: initial P concentrations 0; 0.05; 0.1; 0.5; 1.0; 2.5; 5.0; 10.0; 25 [mg/L]; AOCM size 2 ~ 4.75 mm; sorbent solution ratio 0.2g/40ml; shaking rate 100 rpm for 24 hours; ambient temperature 20^0C.

Solution pH	Freundlich (Media size 2 ~ 4.75 mm)					
	Ionic strength 0.01 M KCl			Ionic strength 0.2 M KCl		
	K_F	n	R^2	K_F	n	R^2
pH 5	0.96	0.38	0.96	1.16	0.33	0.96
pH 6	1.09	0.28	0.98	0.75	0.45	0.98
pH 7	0.72	0.41	0.98	0.79	0.33	0.97
pH 8	0.61	0.37	0.98	0.47	0.49	0.99
pH 9	0.18	0.74	0.99	0.26	0.65	0.98

Table 4-4. Parameters of Freundlich isotherm for effect of ionic strength 0.005 M and 0.0005 M KCl on P adsorption by AOCM. Experiments were carried out at: initial P 0; 0.05; 0.1; 0.5; 1.0; 2.5; 5.0; 10.0; 25 [mg/L]; AOCM size 2 ~ 4.75 mm; sorbent solution ratio 0.2g/40ml; shaking rate 100 rpm for 24 hours; ambient temperature 20^0C.

Solution pH	Freundlich (Media size 2 ~ 4.75 mm)					
	Ionic strength 0.005 M KCl			Ionic strength 0.0005 M KCl		
	K_F	n	R^2	K_F	n	R^2
pH 5	0.98	0.43	0.95	0.89	0.4	0.9
pH 6	0.94	0.31	0.98	0.91	0.37	0.95
pH 7	0.68	0.39	0.98	0.91	0.27	0.98
pH 8	0.49	0.45	0.98	0.47	0.48	0.96
pH 9	0.14	0.84	0.99	0.24	0.66	0.97

The value of PZC for AOCM indicates that surface of AOCM would be positively charged under the studying pH range, which would promote the adsorption of $H_2PO_4^-$ ion. Besides, P Chemisorption on AOCM process, ligand adsorption as the result of an exchange with

hydroxyl groups or metal-Ligand adsorption to form ternary complexes, is coupled with the release of OH^- ions which also suggests that slightly acidic environment is favorable. The sorption of phosphorus followed Freundlich isotherm very well under different pH and ionic strength conditions. Most of the correlation coefficients are larger than 0.95 and Freundlich isotherm parameters were shown in Table 4-3 and Table 4-4.

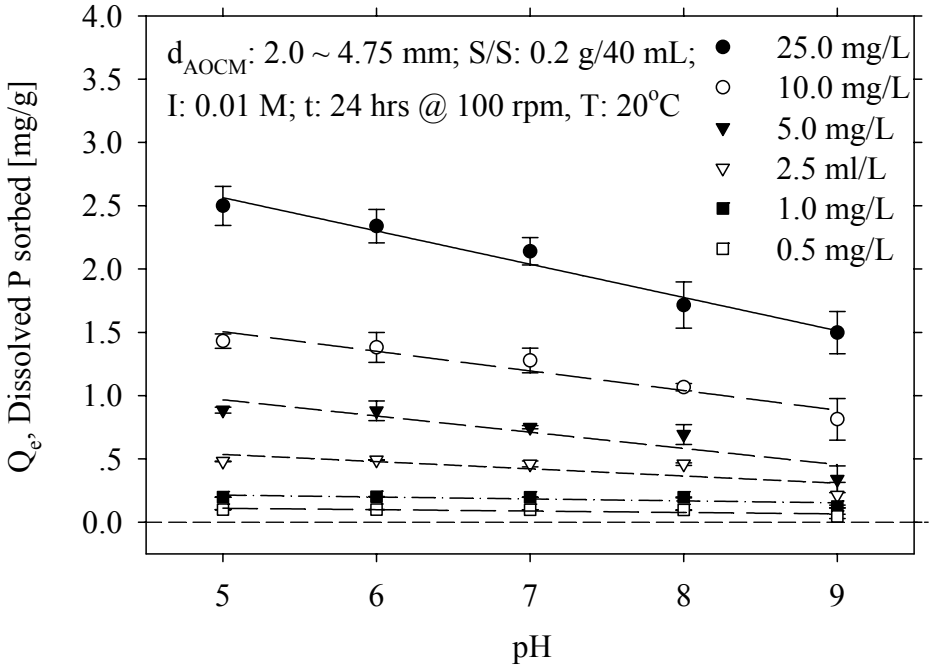

Figure 4-7. Summary of the influence of initial TDP concentration on adsorption capacity by AOCM as a function of pH.

Figure 4-7 highlights the effect of variation of initial phosphorus concentration on adsorption capacity by AOCM at different pH. It is apparent that P adsorption capacities increase with high initial P concentrations in the P concentration range. Besides, the slopes of the regression straight lines suggest that pH has more effects on adsorption capacity at higher P concentration than lower P concentration and it also confirms high pH is unfavorable for P adsorption on AOCM.

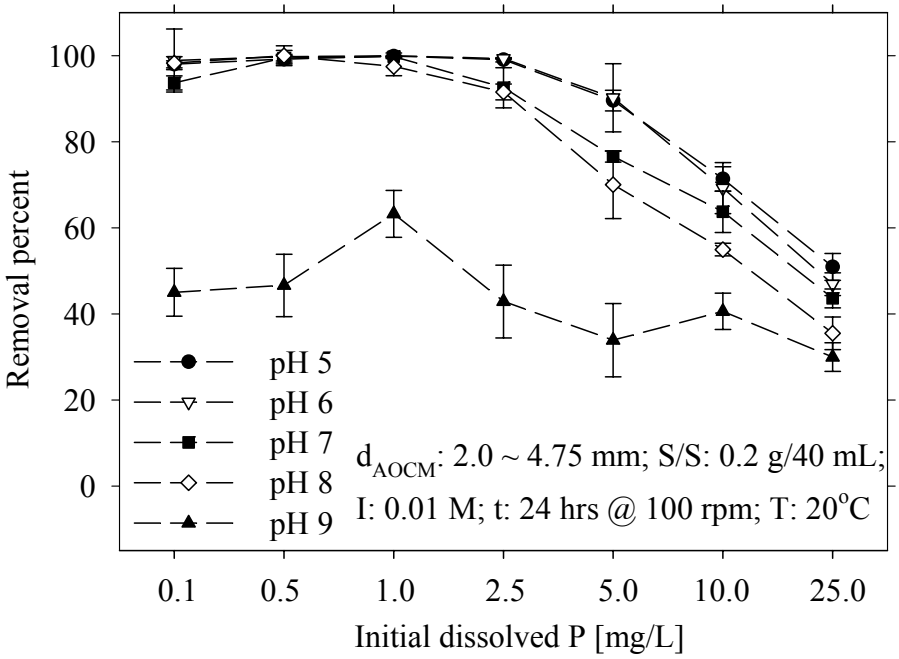

Figure 4-8. TDP concentration reduction (%) by AOCM as a function of initial TDP concentration @ t = 0. Experiments were carried out with a solid/solution ratio of 0.20 g/40 mL, I: 0.01 M KCl; d_{AOCM} range: 2 ~ 4.75 mm; t: 24 hours at 100 rpm; ambient temperature, T: 20^0C.

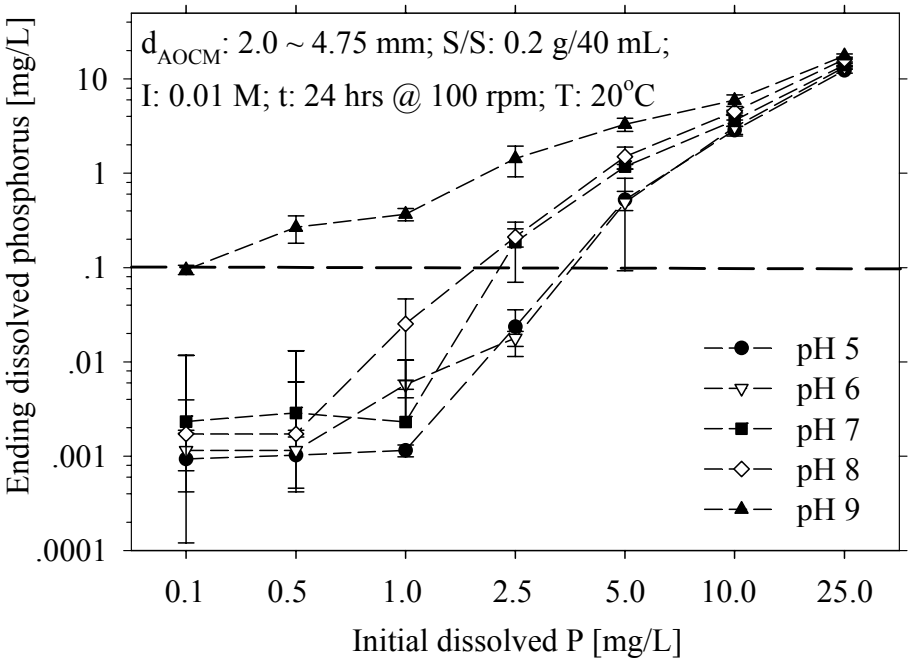

Figure 4-9. Comparison of initial (t = 0) and equilibrium (t = 24 hours) TDP concentrations. Experiments were carried out with a solid/solution ratio of 0.20 g/40 mL, I: 0.01 M; d_{AOCM} range: 2 ~ 4.75 mm; t: 24 hours at 100 rpm; ambient temperature, T: 20^0C.

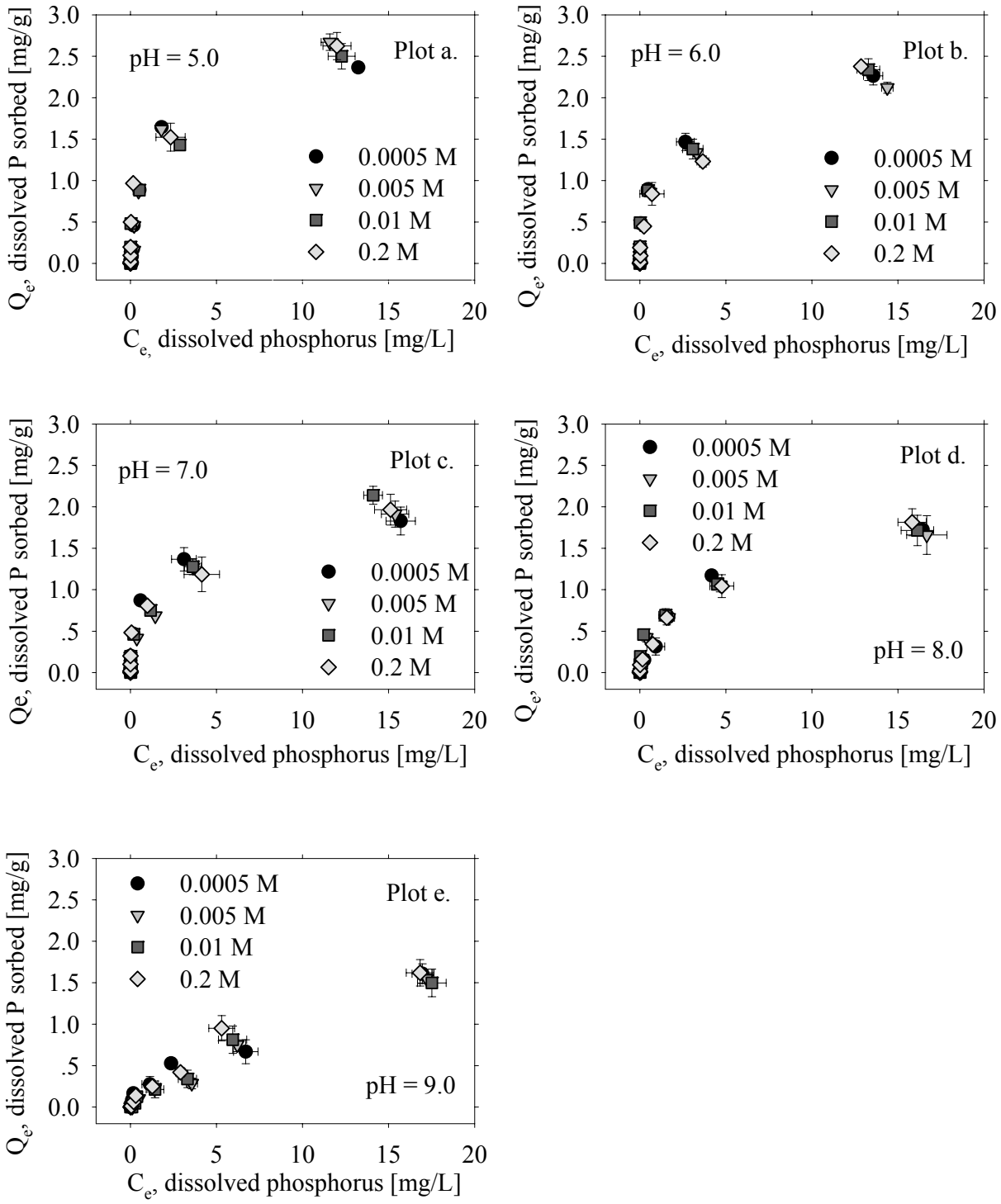

Figure 4-10. Effects of ionic strength on P equilibrium adsorption by AOCM at constant pH levels of 5, 6, 7, 8, 9. Experiments were carried out at: initial P concentrations 0; 0.05; 0.1; 0.5; 1.0; 2.5; 5.0; 10.0; 25 [mg/L]. Experiments were carried out with a solid/solution ratio of 0.20 g/40 mL; d_{AOCM} range: 2 ~ 4.75 mm; t: 24 hours at 100 rpm; ambient temperature, T: 20^0C.

Figure 4-8 and Figure 4-9 depicts the removal percent of P adsorption by AOCM and comparison of starting and ending P concentrations. Most of the ending P concentrations were below 0.1 mg/L for starting P concentrations below 2.5 mg/L and pH from 5 to 8 with 90 percent removal or even higher.

Ending P concentrations were between 0.1 to 15 mg/L for starting P concentrations between 2.5 to 25 mg/L and pH from 5 to 8 with 35 to 95 percent removal.
Removal percent ranges from to 35 to 65 for all the P concentrations at pH 9. Considering event mean concentration (EMC) of P in urban rainfall-runoff is typically below 2 mg/L, AOCM demonstrate very good P adsorption capacity for low P concentration.

INFLUENCE OF SOLUTION IONIC STRENGTH

The effects of the solution ionic strength on P adsorption by AOCM at pH 5, 6, 7, 8 and 9 were illustrated in Figure 4-10. Ionic strength in the study range (0.0005 ~ 0.2 M KCl) appears to have insignificant effect on phosphorus adsorption. The effects of the solution ionic strength are usually analyzed in terms of the type of complexes that phosphate can form with the surface. If phosphate forms outer sphere complexes, then background ions would compete for the adsorption sites. Therefore a decrease in the phosphate adsorption would be observed when ionic strength is increases.

Conversely, if phosphate forms inner sphere complexes and is directly coordinated to sorbent surfaces, then background ions would be less likely in competing for the adsorption sites. Therefore, phosphate adsorption would be less affected by altering the ionic strength (Sparks 2003). Macroscopically, inner-sphere sorption is suggested by the fact that uptake is unaffected by changes in ionic strength (Juang & Chung 2004) and occurs below PZC, where the surface of AOCM is positively charged.

INFLUENCE OF DESORPTION

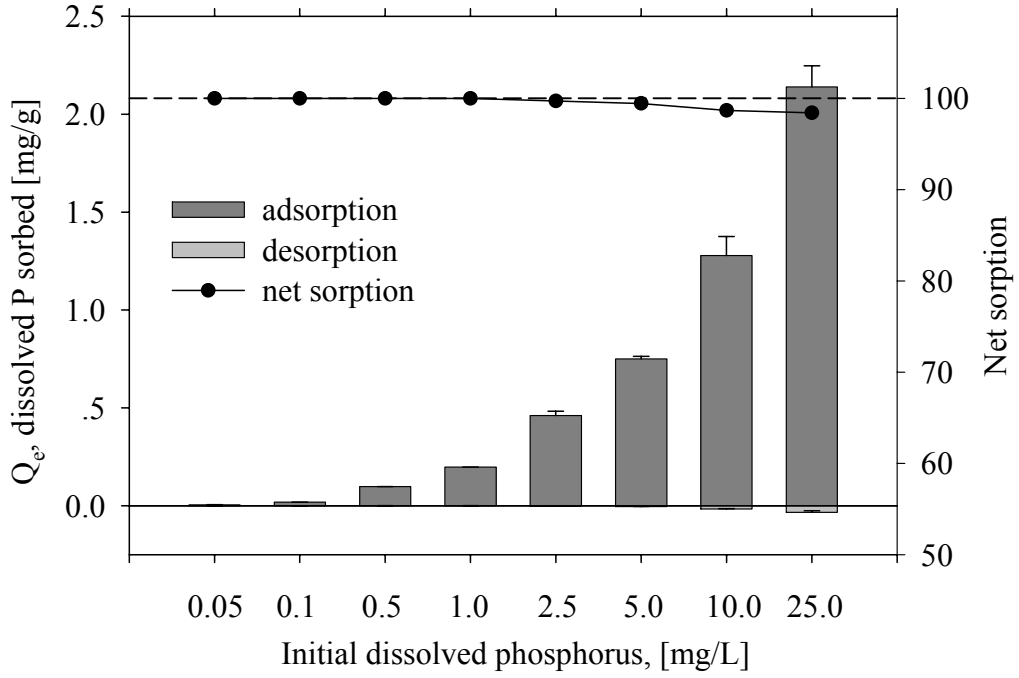

Figure 4-11. Desorption of TDP from AOCM. As with sorption experiments, desorption experiments were carried out with a solid/solution ratio of 0.20 g/40 mL, I: 0.01 M; d_{AOCM} range: 2 ~ 4.75 mm; t: 24 hours at 100 rpm; ambient temperature, T: 20^0C.

Effect of desorption experiment was performed under similar controlled conditions to check the reversibility in the adsorption process and result was shown in Figure 4-11.

Release of previously sorbed P from AOCM were insignificant in for the whole study P concentration range (0 ~ 25 mg/L) at pH of 7. Such a favorable desorption result indicates P adsorption on AOCM is mainly chemical adsorption and the bond between phosphorus and the affinity sites on the surface of AOCM is strong.

INFLUENCE OF COMPETING IONS

With interaction with coexisting ions such as Calcium, Sulfate and Nitrate, adsorption of phosphorus in synthetic urban rainfall-runoff on AOCM has been found to be important and may significantly affect P mobility and bioavailability. The extent of this interaction normally depends on the ion relative concentration range, affinity of the anions for the surface, the change

in the surface potential upon adsorption and solution pH. Anion adsorption at the oxide water interfaces is commonly interpreted as a surface complexation mechanism in which anionic solute binds to the site of reaction on the surface to form either an inner-sphere or ion-pair complex.

Table 4-5. Parameters of Freundlich isotherm for effect of Ca (15 mg/L) and Sulfate (35 mg/L) presence on P adsorption by AOCM. Experiments were carried out: initial P 0; 0.05; 0.1; 0.5; 1.0; 2.5; 5.0; 10.0; 25 [mg/L]; AOCM size 2 ~ 4.75 mm; ionic strength 0.01 M KCl; sorbent solution ratio 0.2g/40ml; shaking rate 100 rpm for 24 hours @ 20^0C.

Solution pH	Freundlich (Media size 2 ~ 4.75 mm; Ionic strength 0.01 M KCl)					
	Ca 15 mg/L			Sulfate 35 mg/L		
	K_F	n	R^2	K_F	n	R^2
pH 5	0.93	0.44	0.96	0.78	0.38	0.98
pH 6	0.92	0.35	0.99	0.57	0.4	0.99
pH 7	0.84	0.37	0.98	0.52	0.43	0.99
pH 8	0.63	0.42	0.99	0.22	0.66	0.99
pH 9	0.46	0.51	0.99	0.05	1.08	0.98

Table 4-6. Parameters of Freundlich isotherm for effect of concentrations of Ca and Sulfate presence on P adsorption by AOCM. Experiments were carried out at: initial dissolved Phosphorus 0; 0.05; 0.1; 0.5; 1.0; 2.5; 5.0; 10.0; 25 [mg/L]; pH 7; ionic strength 0.01 M KCl; d_{AOCM} 2 ~ 4.75 mm; sorbent solution ratio 0.2g/40ml; shaking rate 100 rpm for 24 hours; ambient temperature 20^0C.

Freundlich (Media size 2 ~ 4.75 mm; Ionic strength 0.01 M KCl; pH 7)							
Effect of Ca concentration				Effect of Sulfate concentration			
Calcium	K_F	n	R^2	Sulfate	K_F	n	R^2
0 mg/L	0.71	0.42	0.98	0 mg/L	0.71	0.42	0.98
5 mg/L	0.84	0.36	0.98	10 mg/L	0.56	0.46	0.99
15 mg/L	0.84	0.37	0.98	35 mg/L	0.52	0.43	0.99
45 mg/L	0.92	0.35	0.99	105 mg/L	0.48	0.43	0.99

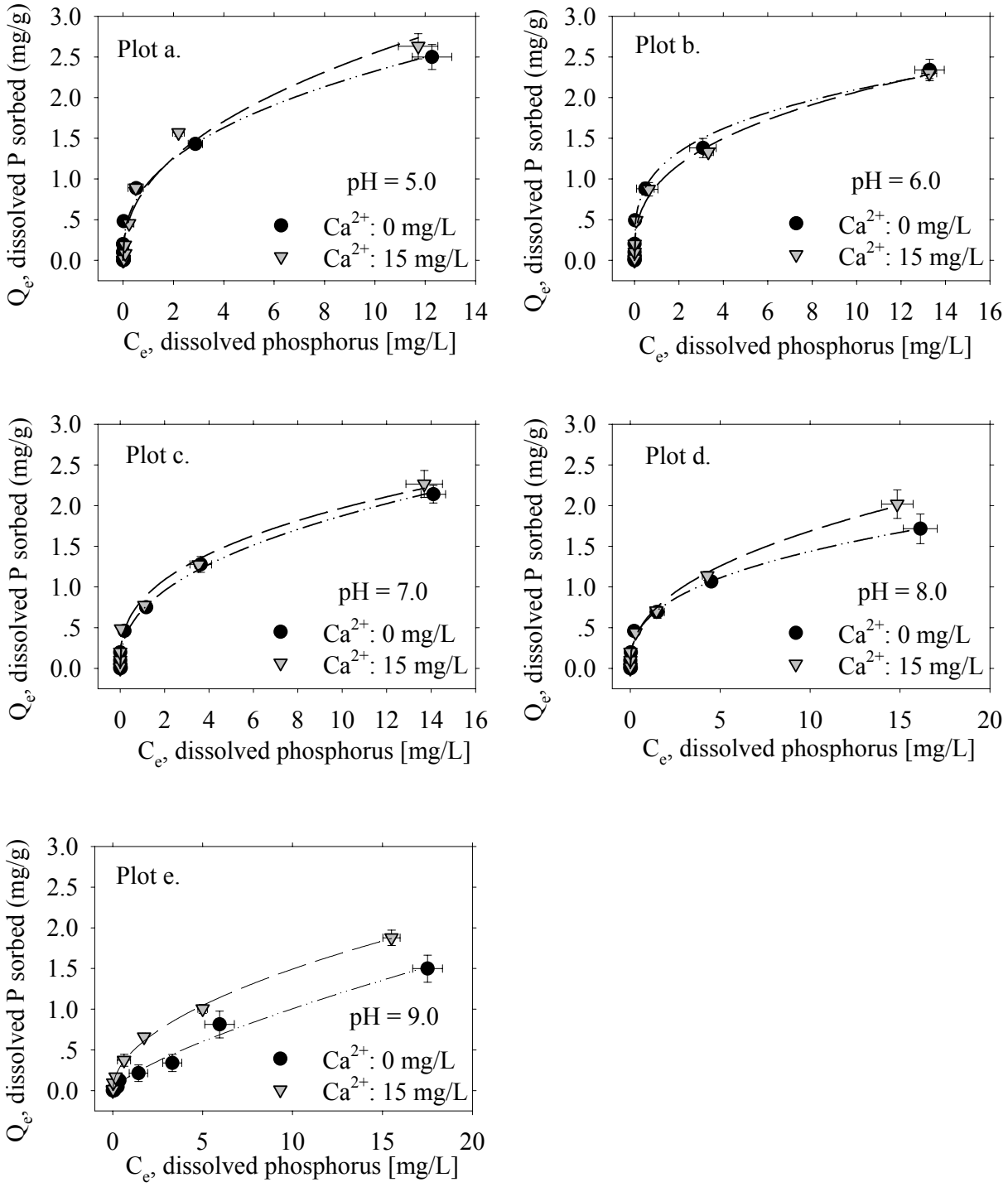

Figure 4-12. Influence of calcium (at 15 mg/L) on AOCM adsorption of TDP. Experiments were carried out at: initial P concentrations 0; 0.05; 0.1; 0.5; 1.0; 2.5; 5.0; 10.0; 25 [mg/L], solid / solution ratio of 0.20 g/40 mL, I: 0.01 M; d_{AOCM} range: 2 ~ 4.75 mm; t: 24 hours at 100 rpm; ambient temperature, T: 20^0C. The data were fit to Freundlich isotherm and parameters are summarized in Table 4-5 and Table 4-6.

INFLUENCE OF CA^{2+}

Adsorption of phosphorus on AOCM was compared in the presence and absence of Calcium (15 mg/L) at pH 5, 6, 7, 8 and 9 shown in Figure 4-12.

Phosphate was strongly bound on AOCM in the low pH range (5 ~ 7) and the presence of Calcium has slightly increased phosphorus adsorption in the acidic and neutral environment. Phosphate was weakly bound on AOCM in the high pH range (8~9) and the presence of Calcium has significantly increased phosphorus adsorption in the base environment.

The varying promotion of phosphate adsorption with the presence of Calcium was attributed to the formation of ternary surface complexes involving both Calcium and phosphate simultaneously.

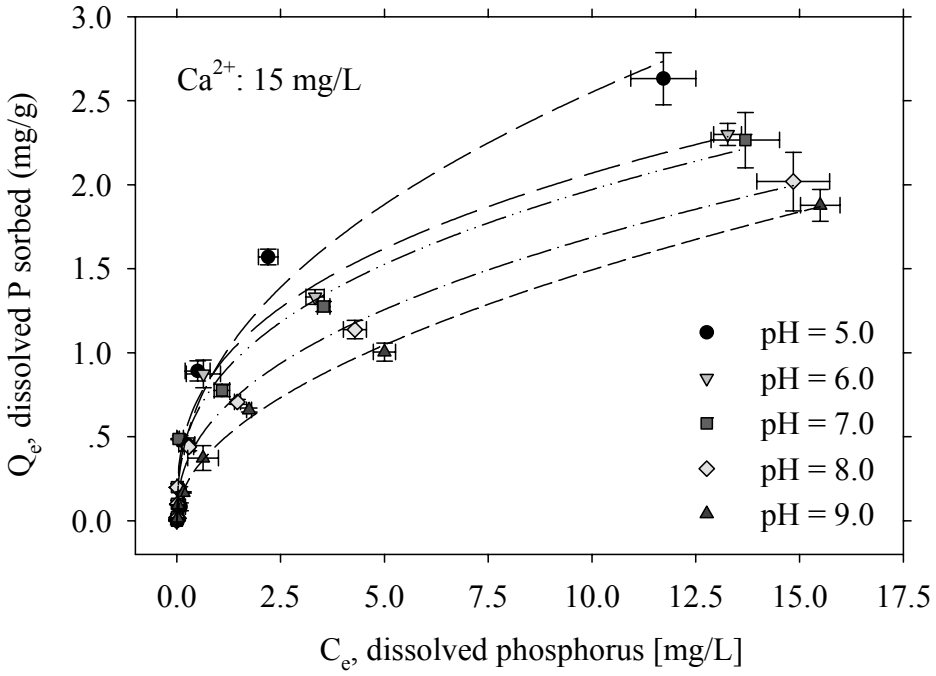

Figure 4-13. Influence of pH with the presence of Ca (15 mg/L) on P adsorption capacity by AOCM. Experiments were carried out at: initial P concentrations 0; 0.05; 0.1; 0.5; 1.0; 2.5; 5.0; 10.0; 25 [mg/L]. Experiments were carried out with a solid/solution ratio of 0.20 g/40 mL, I: 0.01 M; d_{AOCM} range: 2 ~ 4.75 mm; t: 24 hours at 100 rpm; ambient temperature, T: 20^0C. Data were modeled with a Freundlich isotherm and corresponding parameters are shown in Table 4-5.

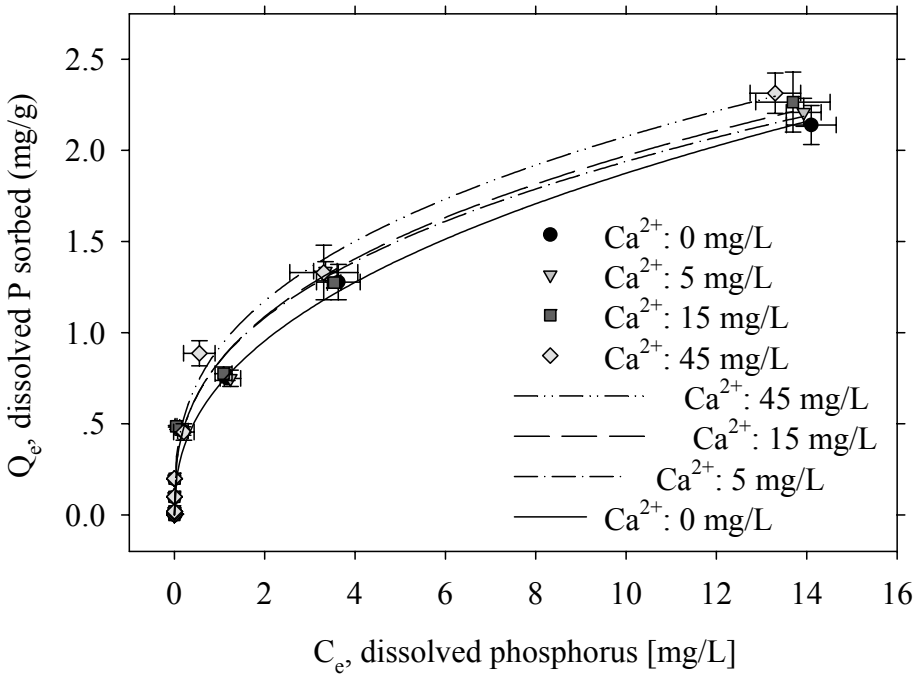

Figure 4-14. Influence of Ca^{2+} concentration on adsorption capacity of AOCM for TDP. Experiments were carried out at: initial P concentrations 0; 0.05; 0.1; 0.5; 1.0; 2.5; 5.0; 10.0; 25 [mg/L]. Experiments were carried out with a solid/solution ratio of 0.20 g/40 mL, I: 0.01 M; d_{AOCM} range: 2 ~ 4.75 mm; t: 24 hours at 100 rpm; ambient temperature, T: 20^0C. The data were modeled by a Freundlich isotherm and corresponding parameters are summarized in Table 4-6.

Effect of pH with presence of Ca (15 [mg/L]) on P adsorption capacity by AOCM was depicted in Figure 4-13. Higher solution pH still leads to lower adsorption capacity, which agreed with the result without presence of Ca. The experimental data were successfully fitted by Freundlich model and parameters were shown in Table 4-5.

Effect of varying Ca concentration (5, 15, 45 mg/L) presented on P adsorption capacity by AOCM was shown in Figure 4-14. Apparently, the more Ca added, the more significant enhancing effect on P adsorption. The experimental data were successfully fitted by Freundlich model and parameters were shown in Table 4-6.

COMPETITIVE EFFECT OF NITRATE AND SULFATE

The influence of nitrate (5 mg/L) on P adsorption capacity by AOCM was depicted in Figure 4-15. The difference between P adsorption capacities for all the initial P concentration without and with addition of Nitrate (5 mg/L) are insignificant statistically, therefore low concentration of Nitrate in urban rainfall-runoff has trivial effect on P adsorption on AOCM.

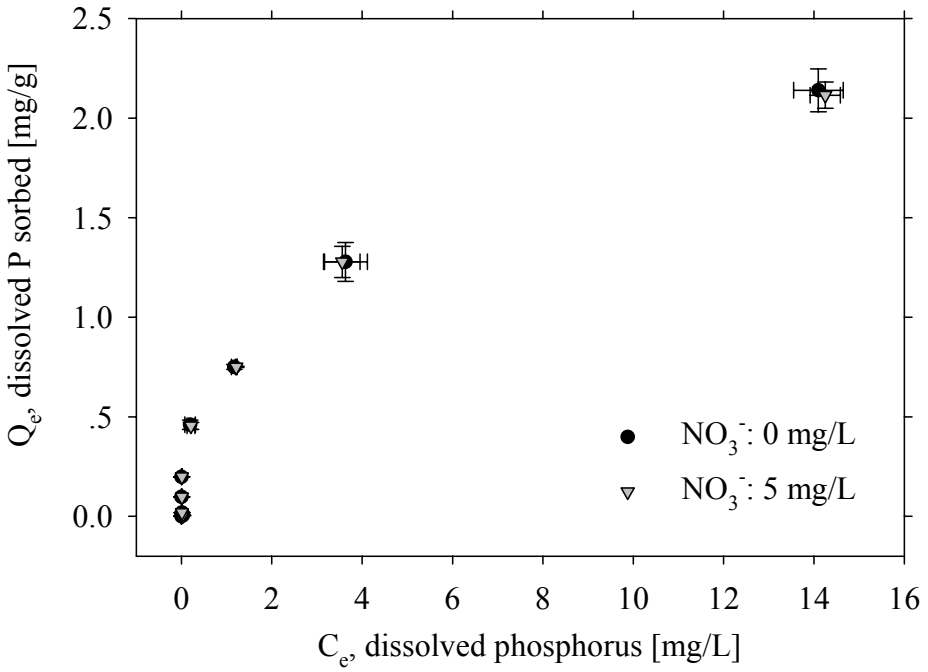

Figure 4-15. Influence of nitrate (at 5 mg/L) on AOCM adsorption capacity for TDP. Experiments were carried out at: initial P concentrations 0; 0.05; 0.1; 0.5; 1.0; 2.5; 5.0; 10.0; 25 [mg/L]. Experiments were carried out with a solid/solution ratio of 0.20 g/40 mL, I: 0.01 M; d_{AOCM} range: 2 ~ 4.75 mm; t: 24 hours at 100 rpm; ambient temperature, T: 20^0C.

Adsorption of phosphorus on AOCM was compared in the presence and absence of Sulfate (35 mg/L) at pH 5, 6, 7, 8 and 9 shown in Figure 4-16. For all the pH values, Sulfate showed apparent competition on P adsorption. Both phosphate and sulfate have been found to be adsorbed on oxide surface through ligand exchange (Pigna and Violante 2003; Wu et al. 2003; Yao and Milero 1996). They might compete for common adsorptive sites of oxides surfaces.

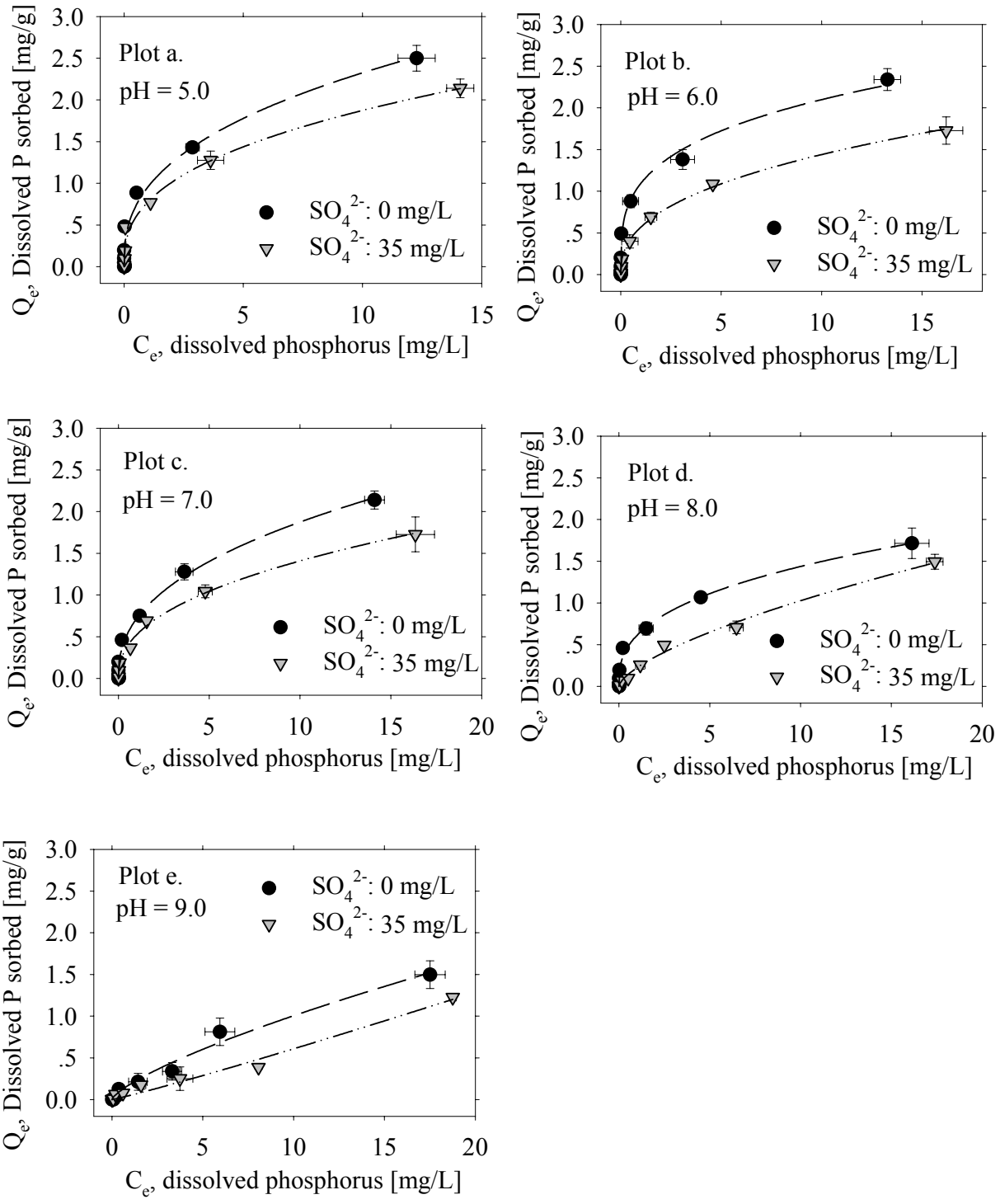

Figure 4-16. Influence of SO_4^{2-} (at 35 mg/L) on AOCM adsorption of TDP at pH 5, 6, 7, 8, 9 respectively. Experiments were carried out at: initial P concentrations 0; 0.05; 0.1; 0.5; 1.0; 2.5; 5.0; 10.0; 25 [mg/L]. Experiments were carried out with a solid/solution ratio of 0.20 g/40 mL, I: 0.01 M; d_{AOCM} range: 2 ~ 4.75 mm; t: 24 hours at 100 rpm; ambient temperature, T: 20^0C. The data were modeled with a Freundlich isotherm and corresponding parameters are shown in Table 4-5 and Table 4-6.

The competition was related to ligand kind, anion concentration, number of surface groups and system pH. All of these would affect the relative affinity with Al oxides, ligand existing state and chemical equilibrium.

From the results obtained in this research, we may conclude that most of sites on Al oxides surface had affinity to both sulfate and phosphate. The occupation of sulfate caused the number of available sites to decrease and reduce the amount of P sorption. The adsorption of sulfate also results in the increasing of negative charge quantity on Al oxides surface, and hydroxyl released into solution caused the pH to increase. All these directly restrain the phosphate adsorption with the presence of sulfate.

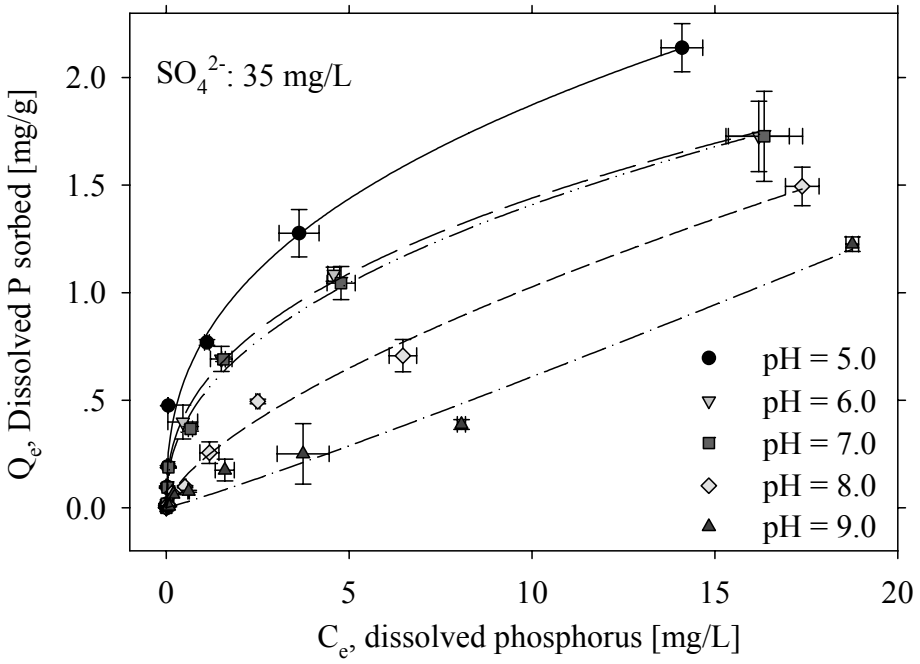

Figure 4-17. Influence of pH with the presence of SO_4^{2-} (at 35 mg/L) on AOCM adsorption capacity of TDP. Experiments were carried out at: initial P concentrations 0; 0.05; 0.1; 0.5; 1.0; 2.5; 5.0; 10.0; 25 [mg/L]. Experiments were carried out with a solid/solution ratio of 0.20 g/40 mL, I: 0.01 M; d_{AOCM} range: 2 ~ 4.75 mm; t: 24 hours at 100 rpm; ambient temperature, T: 20^0C. The data were modeled with a Freundlich isotherm and corresponding parameters are shown in Table 4-5.

Effect of pH with presence of Sulfate (35 [mg/L]) on P adsorption capacity by AOCM was depicted in Figure 4-17. Higher solution pH still leads to lower adsorption capacity, which agreed with the result without presence of Sulfate. The experimental data were successfully fitted by Freundlich model and parameters were shown in Table 4-5. Effect of varying Sulfate concentration (10, 35, 105 mg/L) presented on P adsorption capacity by AOCM was shown in Figure 4-18. Apparently, the more Sulfate added, the more significant suppressing effect on P adsorption. The experimental data were successfully fitted by Freundlich model and parameters were shown in Table 4-6.

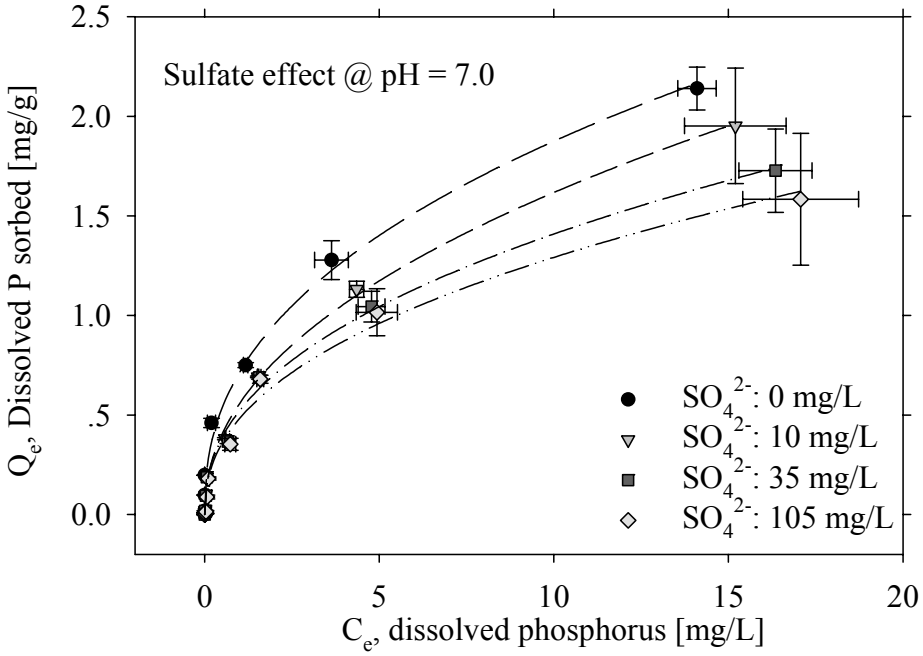

Figure 4-18. Influence of SO_4^{2-} concentration on AOCM adsorption capacity of TDP. Experiments were carried out at: initial P concentrations 0; 0.05; 0.1; 0.5; 1.0; 2.5; 5.0; 10.0; 25 [mg/L]. Experiments were carried out with a solid/solution ratio of 0.20 g/40 mL, I: 0.01 M; d_{AOCM} range: 2 ~ 4.75 mm; t: 24 hours at 100 rpm; ambient temperature, T: 20^0C. The data were modeled with a Freundlich isotherm and corresponding parameters are shown in Table 4-6.

EFFICIENCY OF FOREIGN IONS

The more addition of competing or enhancing ions, the greater magnitude of phosphate adsorption capacity variation would be. The ability of foreign ions to compete with or enhance

phosphate adsorption on AOCM can be illustrated by plotting efficiency of foreign ions calculated using the following expression given by Deb and Datta (1967):

$$Efficiency\ of\ foreign\ ions\ (\%) = \left(\frac{P\ sorbed\ with\ \ foreign\ ions}{P\ sorbed\ when\ added\ alone} - 1\right) * 100 \qquad \text{Equation 4-16}$$

Figure 4-19 summaries efficiency of foreign ions Ca^{2+}, Nitrate and Sulfate. Calcium was found to enhance and Sulfate was found to suppress the adsorption of P on AOCM at the typical pH, ionic strength range and EMC of P range in urban rainfall-runoff. Nitrate showed trivial effect on adsorption of p on AOCM. Though Sulfate and Nitrate showed some effect on inhibiting P adsorption on AOCM, the reduction of P removal could be inappreciable due to the low concentration range of these competing ions in urban rainfall-runoff and compensated by Ca^{2+}.

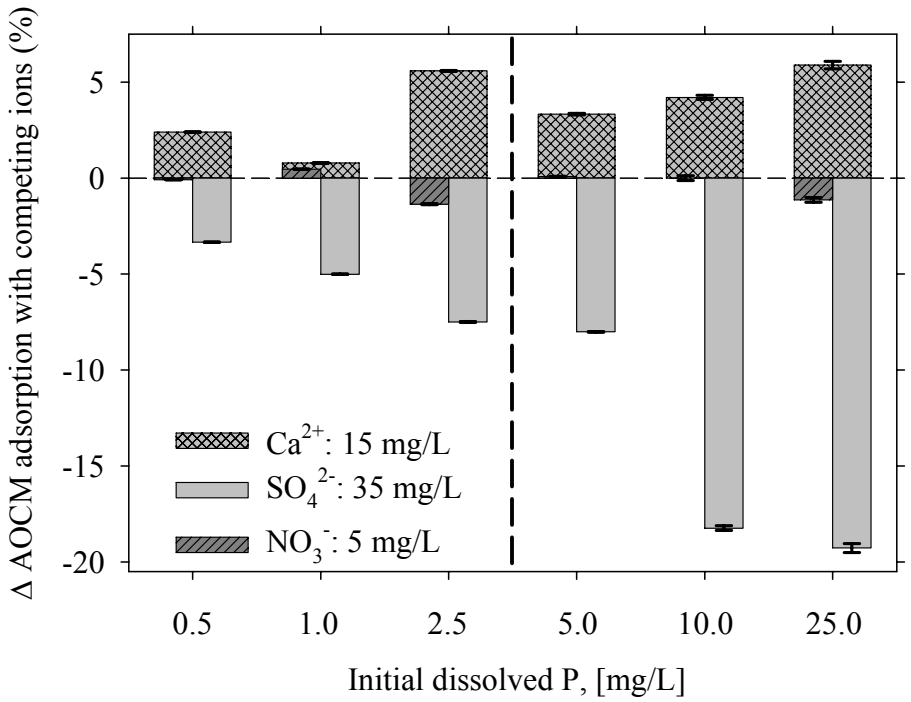

Figure 4-19. Influence of coexisting ions on AOCM adsorption of TDP at initial P concentrations 0.5; 1.0; 2.5; 5.0; 10.0; 25 [mg/L]. Experiments were carried out with a solid/solution ratio of 0.20 g/40 mL, I: 0.01 M; d_{AOCM} range: 2 ~ 4.75 mm; t: 24 hours at 100 rpm; ambient temperature, T: 20^0C.

IMPLICATIONS

Generally, it is hard to distinguish adsorption from surface precipitation because these two processes are coupled together in most cases. However dependable adsorption isotherm needs minimize precipitation effect. In some phosphate adsorption studies, precipitation can be apparently observed or strongly inferred. Sufficiently high anion concentrations or high ratio of P to Al strongly suggest that precipitation is bound to occur. Therefore this study adopted low P concentration range (which also corresponds to the typical values found in urban rainfall-runoff) and low ratio of P to Al to emphasize adsorption.

Compared with waste water, urban rainfall-runoff contains more variable concentrations of P. The adsorbent developed need be flexible to treat concentrations of P down to 0.1 mg/L. Therefore, treated P concentration limit has to be considered in addition to removal efficiency to adequately delineate the applicability of adsorbent.

CONCLUSIONS

Obtaining reliable adsorption equilibrium is crucial since the isotherms so derived generally were utilized as the corner stone for further adsorption design and engineering application. The adsorption of phosphate on AOCM has been found to be strongly dependent on pH and maximum removal efficiencies have been obtained at slightly acidic conditions. Phosphorus adsorption was shown to increase with decreasing AOCM adsorbent size. While Calcium enhanced P adsorption by forming ternary complexes, Sulfate inhibited P adsorption by competing for the common active sites. Ionic strength and Nitrate has little effect on P adsorption. Low desorbability, which likely resulted from strong bonding between P and AOCM, was also obtained under experimental conditions. The use of AOCM for adsorption of phosphorus from aqueous solution has a prominent advantage because very porous substrate

facilitates fully contact between phosphorus and AOCM. Good adsorption capacities were obtained for the typical conditions of urban rainfall runoff. Thus it is concluded that AOCM is a low-cost while effective adsorbent for phosphorus adsorption. Easy availability and high adsorption capacity make AOCM superior to the other adsorbents for phosphate removal. It is also found Freundlich isotherm could successfully represent data of P adsorption on AOCM. Upon treatments by AOCM, phosphorus concentrations could be reduced to a suitable level for discharge into natural surface waters, which suggests the promising application of AOCM.

REFERENCES

Aksoyoglu, S. and Radioanal, J., 1989. Nucl. Chem. 134(2), 393-403.

Antelo, J., Avena, M., Fiol, S., Lopez, R. and Arce, F., 2005. Effects of pH and Ionic Strength on the Adsorption of Phosphate and Arsenate at the Goethite-Water Interface. Journal of Colloid and Interface Science, 285, 476-486.

APHA- American Public Health Association. (1998). Standard Methods for the Examination of Water and Wastewater, (20th Ed.) A.D. Eaton, L.S. Clesceri, A.E. Greenberg (Eds.), American Public Health Association, American Water Works Association and Water Environmental Federation, Washington, D.C.

Altundogan, H.S. and Tumen, F., 2001. Removal of Phosphates from Aqueous Solutions by Using Bauxite I: Effect of pH on the Adsorption of Various Phosphates. Journal of Chemical Technology and Biotechnology, 77, 77-85.

Bleam, W.F., Pfeffer, P.E., Goldberg, S., Taylor, R.W. and Dudley, R., 1991. A ^{31}P Solid-State Nuclear magnetic Resonance Study of Phosphate Adsorption at the Boehmite/Aqueous Solution Interface. Langmuir, 7, 1702-1712.

Bohn, H., B. McNeal, and G. O'Connor. 1985. Soil Chemistry. 2nd ed. John Wiley & Sons, New York.

Butkus, M.A. and Grasso, D., 2001. The Nature of Surface Complexation: A Continuum Approach. Environmental Geology, 40, 446-453.

Clark, T., Stephenson, T. and Pearce, P.A., 1997. Water Research. 31(10) 2557-2563.

Dean, C.M, Sansalone, J.J., Cartledge, F.K. and Pardue J.H. 2005. Influence of Hydrology on Rainfall-Runoff Metal Element Speciation.

Deb, D.L., and Datta, N.P., 1967. Plant Soil. 26, 303-316.

Deborah, L.V. and Marcia, H.B. (1979). High-calcium flyash for tertiary phosphorus removal. Wat. Swge Wks., 6, 62-104.

Donnert, D. and Salecker, M., 1999a. Elimination of phosphorus from waste water by crystallization. Environ. Technol. 20, 735-742.

Donnert, D. and Salecker, M., 1999b. Elimination of phosphorus from municipal and industrial waste water. Water Sci. Technol. 40, 195-202.

Freundlich, H. and Heller, W. 1939. J. Am. Chem. Soc. 61, 2228.

Galinada, W. and Yoshida, H. 2004. Intraparticle diffusion of Phosphates in OH-type strongly basic ion exchanger. AICHE Journal. 50(11), 2806-2815.

Gangoli, N. and Thodos, G. (1973). Phosphorus adsorption studies. J. Wat. Pollut. Control Fed., 45(4).

Gimsing, A.L., Borggaard, O.K. and Sestoft, P., 2004. Modeling the Kinetics of the Competitive Adsorption and Desorption of Glyphosate and Phosphate on Goethite and Gibbsite and in Soils. Environmental Science & Technology, 38(6), 1718-1722.

Hisashi, Y., Mitsu, K., Kazuo, S. and Masakazu, H.A. (1986). A fundamental research on phosphate removal by using slag. Wat. Res. 20(5), 547-557.

Huang, C.P., 1975. J. Colloid Interface Sci. 53, 178.

Huang, C.P., 1977. Removal of phosphate by powdered alumina oxide adsorption. J. Wat. Pollut. Control Fed. 49(8), 1811-1817.

Ioannidis, S. and Anderko, A., 2001. Equilibrium Modeling of Combined Ion-Exchange and Molecular Adsorption Phenomena. Ind. Eng. Chem. Res., 40, 714-720.

Karthikeyan, K.G., Tshabalala, M.A., Wang, D. and Kalbasi, M., 2004. Solution Chemistry Effects on Orthophosphate Adsorption by Cationized Solid Wood Residues. Environmental Science & Technology, 38(3), 904-911.

Kofinas, P. and Kioussis, D.R., 2003. Reactive Phosphorus Removal from Aquaculture and Poultry Productions Systems Using Polymeric Hydrogels. Environmental Science & Technology, 37(2), 423-427.

Johnson, B.B., Ivanov, A.V., Antzutkin, O.N. & Forsling, W. 2002. ^{31}P nuclear magnetic Resonance study of the adsorption of phosphate and phenyl phosphate on γ-Al_2O_3. Langmuir, 18, 1104-1111.

Juang, R.S. and Chung, J.Y., 2004. Equilibrium Sorption of Heavy Metals and Phosphate from Single- and Binary- Sorbate Solutions on Goethite. Journal of Colloid and Interface Science, 275, 53-60.

Kinniburg, D.G., 1986. General purpose adsorption isotherms. Environ. Sci. Technol. 20, 895-904.

Langmuir, I. 1918. The adsorption of gases on plane surface of glass, mica and platinium. J. Am. Chem. Soc. 40, 1361.

Lin, S.-H., and Juang, R.-S., 2002. Heavy metal removal from water by sorption using surfactant-modified montmorillonite. J. Hazard. Mater. 92(3), 315-326.

Omoike, A.I. and Vanloon, G.W., 1999. Water Research. 33(17), 3617-3627.

Pigna, M. and Violante, A., 2003. Adsorption of Sulfate and Phosphate on Andisols. Communications in Soil Science and Plant Analysis, 34(15-16), 2099-2113.

Riemam, W. and Walton, H., 1970. Ion exchange in analytical chemistry, International series of monographs in analytical chemistry. Vol. 38, Pergamon, Oxford.

Rietra, R.P., Hiemstra, T. and van Riemsdijk, W.H., 1999. Sulfate adsorption on goethite. J. colloid Interface Sci. 218, 511-521.

Rietra, R.P., Hiemstra, T. and van Riemsdijk, W.H., 2001. Interaction between Calcium and Phosphate Adsorption on Goethite. Environmental Science & Technology, 35(16), 3369-3374.

Sakakibara, Y. and Nakajima, H., 2002. Phosphate Removal and Recovery by a Novel Electrolytic Process. Water Science and Technology, 46(11), 147-152.

Sansalone, J.J. and Buchberger, S.G., 1997. Partitioning and First Flush of Metals in Urban Roadway Storm Water. Journal of Environmental Engineering, American Society of Civil Engineers, Vol. 123. No. 2, February, pp 134-143.

Sansalone, J.J., Koran, J.M., Smithson, J.A. and Buchberger, S.G., 1998. Physical Characteristics of Urban Roadway Solids Transported During Rain Events. Journal of Environmental Engineering, American Society of Civil Engineers, Vol.124, No. 4, pp 427-440.

Sawada, K., Abdel-Aal, N., Sekino, H. and Satoh, K., 2003. Adsorption of Inorganic Phosphates and Organic Polyphosphonate on Calcite. The Royal Society of Chemistry, 342-347.

Shin, E.W., Han, J.S., Jang, M., Min, S.H., Park, J.K. and Rowell, R.M., 2004. Phosphate Adsorption on Aluminum-Impregnated Mesoporous Silicates: Surface Structure and Behavior of Adsorbents. Environmental Science & Technology, 38(3), 912-917.

Southam, D.C., Lewis, T.W., McFarlane, A.J. and Johnston, J.H., 2003. Amorphous Calcium Silicate as a Chemisorbent for Phosphate. Current Applied Physics, 4, 355-358.

Sparks, D.L., 2003. Environmental Soil Chemistry, Academic Press, Amsterdam.

Stumm, W. and Morgan J.J. 1996. Aquatic chemistry. Wiley-Interscience: New York.

Stumm, W. 1987. Aquatic surface chemistry: Chemical processes at the particle-water interface. John Wiley & Sons, New York.

Stumm, W. and Morgan. J.J. 1981. Aquatic chemistry. An introduction emphasizing chemical equilibria in natural waters, 2nd ed. New York, Wiley.

Tang, W.P., Shima, O., Ookubo, A. and Ooi, K., 1997. A Kinetic Study of Phosphate Adsorption by Boehmite. Journal of Pharmaceutical Sciences, 86(2), 230-235.

U.S. EPA, 1986. Quality Criteria for Water. Office of Water Regulation and Standards, US Government Printing Office (PB81-226759), Washington, DC 20460. EPA 440/5-86-001.

USEPA. 1987. Technical Resource Document. Batch-type procedures for estimating soil adsorption of chemicals. EPA/530-SW-87-006-F

Wu, C.H., Lin, C.F. and Lo, S.L., 2003. Modeling Competitive Adsorption of Chromate, Sulfate, and Selenate on -Al_2O_3: Comparison Between the Triple-Layer Model and a Freundlich-Type Multi-Component Isotherm. Journal of the Chinese Institute of Environmental Engineering, 13(2), 87-94.

Yao, W. and Milero, F.J., 1996. Adsorption of Phosphate on Manganese Dioxide in Seawater. Environmental Science & Technology, 30(2), 536-541.

Zeng, L., Li, X. and Liu, J., 2004. Adsorptive Removal of Phosphate from Aqueous Solutions Using Iron Oxide Tailings. Water Research, 38, 1318-1326.

CHAPTER 5 PARAMETRIC EVALUATION OF RAINFALL-RUNOFF PHOSPHORUS ADSORPTION KINETICS ON ALUMINUM OXIDE COATED MEDIA

SUMMARY

While engineered media such as aluminum oxide coated media (AOCM) has been deployed in packed-bed and cartridge systems for adsorption of phosphorus in rainfall-runoff or snowmelt loadings, there is little information on adsorption kinetics and mechanisms. In this study the kinetics of phosphate, P (measured as total dissolved phosphorus, TDP) adsorption by AOCM was measured using synthetic rainfall-runoff and a batch-type flow through process. The specific AOCM was very porous and lightweight clay substrate, coated with aluminum oxide. Kinetics were examined as a function of a number of parameters. These parameters included initial phosphate concentration of 0.5 to 5 mg/L; pH levels from 5 to 9; ionic strength at 0.01 M; sorbent/solution ratio of 1 g/2L to 10 g/2 L; three media sizes that ranged from 0.85 mm to 9.5 mm, surface loading rates that ranged from 40 to 170 L/(min-m^2); and presence of co-existing ions of Ca^{2+}, SO_4^{2-} and NO_3^{1-}.

Sorption kinetics were examined based on several model categories: (1) boundary layer phenomena using a pseudo first-order reaction and pseudo second-order reaction model; (2) based on diffusion phenomena using parabolic diffusion and intraparticle diffusion models, and (3) based on empirical Elovich and power law models. Given the reactive and porous properties of the AOCM both reaction kinetics and diffusion mechanisms played a role in adequately describing the data. Results indicated that the pseudo second order model outperformed other models and that intraparticle diffusion model described the first hour TDP adsorption kinetics.

Higher adsorption kinetics were observed at lower initial P concentrations, slightly acidic conditions, high surface loading rate and high sorbent solution ratio. The presence of NO_3^{1-}or the

variability of ionic strength had an insignificant effect on kinetics. While Ca^{2+} accelerated kinetics by synergism, SO_4^{2-} inhibited kinetics through competition for common sites. The results of this study are summarized in terms of utilizing pseudo second order kinetics and intraparticle diffusion to predict the kinetics of AOCM behavior in packed-bed or cartridge treatment design, application and simulation of performance of pilot- or full- scale systems.

INTRODUCTION

Elevation of phosphate (P) concentration above common regulatory and ecological specifications for nutrients in lakes, ponds and streams, accelerates eutrophication. Eutrophication continues to be a global environmental problem through deterioration of the quality of surface water thereby restricting use for fisheries, recreation, and drinking water (USEPA 1998). Bloom of algae and depletion of dissolved oxygen in water bodies are just two results of eutrophication caused by excessive of P input. Abundant supply of nutrients (especially P) comes from point source (industrial and domestic waste waters) or non-point rainfall-runoff source (leaves, fertilizers, detergents, animal wastes and anthropogenic activities pertinent to P use and discharge) (Vollenweider 1989). In Europe and USA, much work has been done to reduce point-source inputs of nutrients from industrial and municipal wastewater (Baker et al. 1998; Chaudhary et al. 2002; Oguz et al. 2003), but the problems associated with non-point sources such as rainfall-runoff are still of major concern and more challenging to manage (Duda 1993).

Eutrophication has attracted growing attention over the last decade and more stringent water standard for P has been promulgated. To prevent the development of biological nuisances, and to control accelerated eutrophication, research and regulation have suggested that total phosphates as total phosphorus (TP) should not exceed 0.05 [mg/L] in any stream at the point

where the stream enters any lake or reservoir, and less than 0.025 [mg/L] within a lake or reservoir (USEPA 1986). A desired goal for the prevention of plant nuisances in streams or other flowing waters not discharging directly to lakes or impoundments is 0.1 [mg/L] total P (USEPA 1986). Levine and Schindler (1989) suggested that the critical concentration of P above which the growth of algae and other aqueous plants accelerates, is 0.01 [mg/L] for dissolved reactive P (DRP) and 0.02 [mg/L] for total phosphorus (TP). In Berlin, future stringent phosphorus regulations are expected, set to a limit of 0.05 [mg/L] in the receiving water bodies in order to prevent increased algae growth (Genz et al. 2004). Therefore, as a key contributor to eutrophication, the TP concentration of rainfall-runoff with a typical range of 0.5 to 2 mg/L (Dean et al 2005) has to be decreased significantly by efficient and cost effective treatment.

In order to comply with the various limits set for P, numerous efforts for P (both TP and TDP) removal in terms of physical, biological and chemical operations and processes have been taken and reported. Each of the operations and processes has its own advantage and disadvantage. Conventional physical methods targeting on removal of predominant particulate-bound fraction of phosphorus, such as quiescent settling, have proved to be in most cases barely satisfactory if operated singly considering the demanding phosphorus discharge level (0.1 [mg/L]). Under quiescent settling TP removal efficiency is low from 10% to 50% (Clark et al. 1997) and the higher efficiencies are likely a result of TDP partitioning to particulate matter that is separated by settling. Alternate approaches include physical and chemical phenomena of adsorption and precipitation in the presence of engineered media. For example, adsorption on aluminum oxide includes physical and chemical processes. Both can be rapid, occurring within minutes or hours of contacting (Tang et al. 1996; Forbes et al. 2004). After initial stage, slower reactions continue to remove phosphate from solution for periods of from several days to

months. Later stage removal of phosphate has been attributed to physically-adsorbed P shifting to chemically-adsorbed forms, diffusion of phosphate adsorbed on the surface of porous media to positions inside the matrix, and precipitation of crystalline Al-phosphates (Nichols 1983). In the present study, phosphorus removal kinetics by AOCM have been evaluated. Media such as AOCM, with large surface area, microporous characteristic and reactive chemical nature of their surfaces have made such media potential adsorbents for the removal of P. However, AOCM behavior requires examination under controlled conditions when considering application of the media for full-scale use. Kinetics provide crucial information in assessing the feasibility of AOCM for rainfall-runoff P adsorption.

OBJECTIVES

The goal of this study was to quantify the adsorption kinetics of AOCM for TDP. In order to achieve this goal there were a number of objectives. The first objective was to measure adsorption kinetics by means of differential column batch reactors (DCBR) as a function of selected chemical, loading, and media parameters. There parameters included initial TDP concentration of 0.5 to 5 mg/L; pH levels from 5 to 9; ionic strength at 0.01 M; sorbent/solution ratio of 1 g/2L to 10 g/2 L; three media sizes that ranged from 0.85 mm to 9.5 mm, surface loading rates that ranged from 40 to 170 L/(min-m^2); and presence of co-existing ions of Ca^{2+}, SO_4^{2-} and NO_3^{1-}. The second objective was to use this DCBR experiments to determine the rate-limiting step as well as kinetic parameters describing mass transfer resistances due to film diffusion (D_f) and effective intraparticle diffusion (D_{ei}) (combination of pore diffusion (D_f) and surface diffusion (D_s)). The final objective was to examine the applicability of kinetic models (pseudo first-order kinetic, pseudo second-order kinetic, Elovich kinetic, potential driving

kinetic, power law, intra-particle diffusion, parabolic diffusion) to simulate and analyze adsorption processes of P on AOCM by describing the rate and mechanism of adsorption.

BACKGROUND

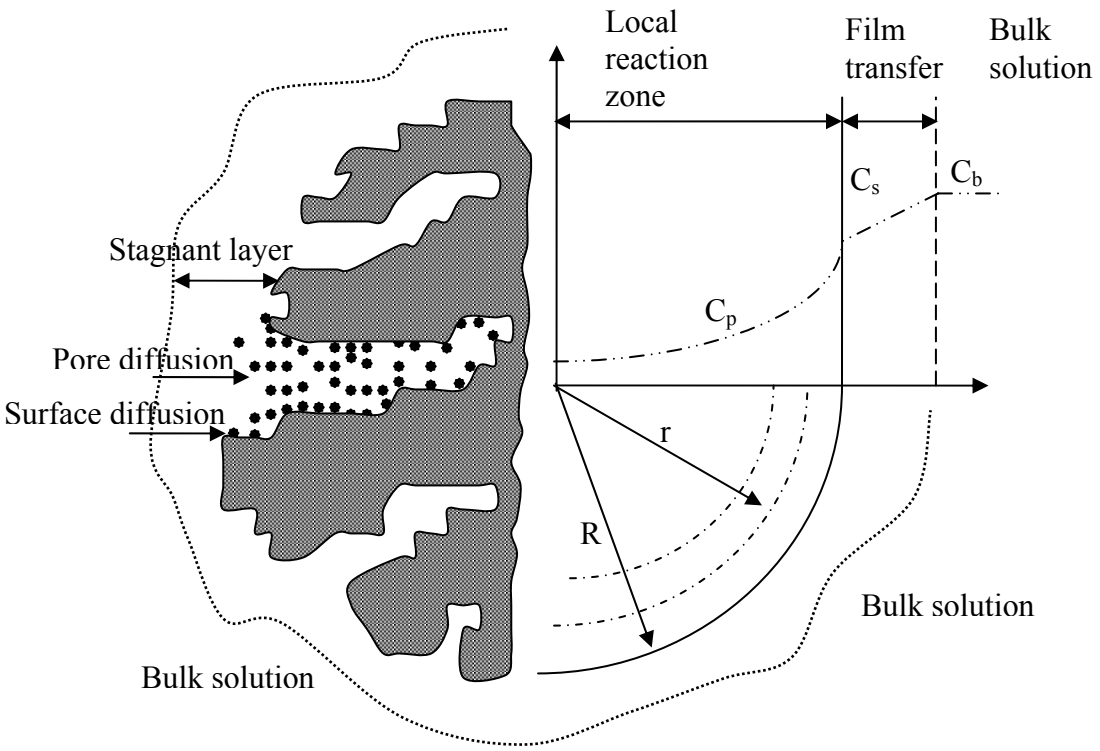

Figure 5-1. Schematic plot of P transport from the bulk solution onto porous AOCM (adapted from Badruzzaman et al. 2004; Notthakun et al. 1989).

Urban rainfall-runoff is a complicated environmental system which is abundant of frequent interactions among anions, cations, dissolved organics and charged surface of particulate matter. Generally, interaction between organic compounds and hydrophobic surfaces are dominated by relatively weak dispersion forces, and the adsorption can be considered reversible. In contrast, interactions between phosphate and aluminum species (functional groups on surface of AOCM) are dominated by the formation of strong inner sphere complexes and to a lesser extent by weaker ion exchange reactions (Kim and Kirkpatrick 2004; Hu et al. 2004; De-Bashan and Bashan 2004; Altundogan and Tumen 2001). The contending mechanisms of the

complicated kinetics of P sorption on AOCM are diffusion and adsorption reaction (Ippolito et al. 2003; Koretsky 2000).

It is assumed that phosphate adsorption on AOCM involves a sequential and/or parallel progression through four steps (Sperlich et al. 2005; Badruzzaman et al. 2004; Hatfield et al. 1996): diffusion through the bulk solution, film diffusion, intraparticle diffusion (including surface and pore diffusion), and adsorption reaction on the sorbent surface schematically shown in Figure 5-1. The relative importance of each step is generally variable. However, the bulk solution diffusion and surface adsorption steps are typically rapid and thus not rate-limiting. Sorbate flux through the stagnant film surrounding the sorbent material is directly proportional to the linear concentration gradient across the film and the film mass transfer coefficient (D_f). The magnitude of D_f is dictated by the flow regime around the sorbent material (generally inferred from bulk hydrodynamics) and the sorbent physical indices such as size, shape, roughness, porosity, surface area and surface charge. Intraparticle diffusion may be within the pore space (i.e. pore diffusion) or along the sorbent surface within the pores (i.e. surface diffusion). In many cases it is difficult to differentiate pore diffusion from surface diffusion, therefore lumped effective intraparticle diffusion is normally adopted.

KINETICS MODELS

With respect to kinetic modeling, three classes of models were examined. Two models were based on boundary layer reaction phenomena; the pseudo first-order kinetics and pseudo second-order kinetics models. Two models were based on diffusion phenomena; the intra-particle diffusion and parabolic diffusion models. Two models were empirical; the Elovich model and the power law models. Each of these models finds common application for describing mass transfer phenomena.

BOUNDARY LAYER MODELS

The adsorption of P on AOCM can be controlled by diffusion across a stagnant boundary layer with the mass transfer driving force as a concentration differential (House et al. 2002). Therefore the boundary layer model can be written based on the following equations.

$$\frac{dC_t}{dt} = \frac{D_m}{\gamma\theta}(C_t - C_s) \qquad \text{Equation 5-1}$$

$$\gamma = 2500/v \qquad \text{Equation 5-2}$$

$$\theta = \frac{V_t}{A_s} \qquad \text{Equation 5-3}$$

Where C_t is the P concentration at the bulk solution, C_s is the P concentration at the AOCM surface (assumed to be constant), D_m is the P molecular diffusion coefficient, γ is the thickness of stagnant film in μm, v is the bulk recirculating velocity of solution in cm/s, θ is the effective depth of solution which is calculated by V_t the bulk volume and A_s the total surface area of AOCM. The boundary layer model has solution in the following form.

$$C_t = C_0 \exp(-k_b t) + C_e(1 - \exp(-k_b t)) \qquad \text{Equation 5-4}$$

In these expressions the concentration (C_t) is a function of initial concentration (C_0) and simulated final equilibrium concentration (C_e) as well as a rate constant ($k_b = D_m/(\gamma\theta)$. For the ease of visual examination and linear regression, the equation could be rearranged to the following form.

$$C_t = (C_0 - C_e)\exp(-k_b t) + C_e \qquad \text{Equation 5-5}$$

Parameters C_e and k_b can be obtained by fitting boundary layer model with the experimental data. Therefore D_m can be calculated and a comparison of experimental and simulated C_e can also be carried out. The boundary layer equation can be combined with the following two mass balance equations.

$$q_e = \frac{V_t}{m}(C_0 - C_e) \qquad \text{Equation 5-6}$$

$$q_t = \frac{V_t}{m}(C_0 - C_t)$$ Equation 5-7

The boundary layer model solution can therefore be rewritten in the following form.

$$\frac{q_t}{q_e} = 1 - \exp(-k_b t)$$ Equation 5-8

In this expression q_e [mg/g] is adsorption capacities at equilibrium, q_t [mg/g] is adsorption capacities at time *t*, m (g) the mass of AOCM, and V_t(L) the solution volume.

PSEUDO FIRST ORDER MODEL

The pseudo-first order model (Kobya 2002) is expressed in the following form.

$$\frac{dq_t}{dt} = k_1(q_e - q_t)$$ Equation 5-9

In this expression q_e and q_t are the adsorption capacity [mg/g] at equilibrium and at reaction time *t*, respectively; and k_1 is the rate constant (min^{-1}) for pseudo first-order adsorption. The integration of Eqn. 9 yields Eqn. 10.

$$\frac{q_t}{q_e} = 1 - \exp(-k_1 t)$$ Equation 5-10

The plot of q_t vs. t by pseudo first-order model would follow an exponential increase to an asymptotic level. Since the pseudo first-order model is of the boundary layer model form, only pseudo first-order model would be presented in this study.

PSEUDO-SECOND ORDER MODEL

The pseudo second-order kinetic adsorption rate equation (Kobya 2002) is written in the following form.

$$\frac{dq_t}{dt} = k_2(q_e - q_t)^2$$ Equation 5-11

For the boundary conditions when t = 0 q_t = 0, and t = t q_t =q_t, the integration of Eqn. 11 will yield Eqn. 12.

$$q_t = \frac{q_e t}{\frac{1}{q_e k_2} + t}$$ Equation 5-12

A hyperbolic equation (q_t=c_1t/(c_2+t)) can be used for non-linear curve fitting. Parameters q_e and k_2 were obtained from a and b respectively.

ELOVICH MODEL

The Elovich model has been used to describe the kinetics of adsorption and desorption of various inorganic materials on many adsorbents (Sparks 1995; Sparks 1999). The Elovich model can be expressed in the following form.

$$\frac{dq_t}{dt} = \alpha e^{-\beta q_t}$$ Equation 5-13

In the above equation α and β are Elovich model constants, which can be determined by curve fitting.

POWER EQUATION MODEL

The power law equation is an empirical equation of the following form.

$$q_t = a t^b$$ Equation 5-14

The power law equation can be used to empirically correlate P adsorption capacity as a function of time with model parameter constants *a* and *b*.

INTRA-PARTICLE DIFFUSION MODEL

Despite the common application of models based on reaction kinetics or empirical models, neither class of model can identify the diffusion mechanism(s) that occurs during the adsorption process.

Therefore kinetics data are also commonly examined using intra-particle diffusion models. (Kostura et al. 2005; Karaca et al. 2004; Ozacar 2003; Ruixia et al. 2002)

$$q_t = k_p t^{0.5} + y_0$$ Equation 5-15

In this expression k_p is the intraparticle diffusion rate constant and y_0 intercept of the model line which indicates the thickness of the boundary layer. The closer of value of y_0 approaches zero, the greater the applicability of the intra-particle diffusion model. Higher values of k_p often indicates quicker and better adsorption as a result of improved bonding between P and AOCM.

PARABOLIC DIFFUSION

Another diffusion model commonly utilized is parabolic diffusion model (Pavlatou and Polyzopoulos 1988; House et al. 1995, Liu et al 2005).

$$(q_t / q_e)/t = (4/\pi^{0.5})/(D_m / r^2)^{0.5}(t^{-0.5}) - D_m / r^2 \qquad \text{Equation 5-16}$$

This expression can be simplified as follows.

$$(q_t / q_e)/t = \xi * t^{-0.5} - \psi \qquad \text{Equation 5-17}$$

where r is the media radius, ξ and ψ model constants. Nonlinear regressions and a least-squares analysis were conducted to determine the optimized constants for all the models.

METHODOLOGY AND MATERIALS

SORBENT MEDIA

Sorbent media utilized in this study was a specific form of AOCM. This media was prepared from clay material and aluminum oxide. Clay expanded with a blowing agent was fired into bricks at 1000^0C . The cooled bricks were crushed and sieved to yield to produce three size ranges of substrate: 0.85 ~ 2 mm, 2 ~ 4.75 mm and 4.75 ~ 9.5 mm using ASTM standard sieves No. ¼ inch (4.75-mm opening), No. 10 mesh (2.00-mm opening) and No. 20 mesh (0.85-mm opening). The resulting substrate is a stable, highly porous material, lightweight media of low organic content. The sorbent substrate was then coated with an aluminum salt to produce the sorbent media (AOCM) utilized in this study.

The effect of media size of Aluminum Oxide Coated Media on phosphorus adsorption was examined using these three size categories: 0.85 ~ 2 mm; 2 ~ 4.75 mm and 4.75 ~ 9.5 mm by sieving. Such a size range of AOCM is suitable for potential adsorption cartridge filter or packed-bed applications.

DIFFERENTIAL COLUMN BATCH REACTOR (DCBR)

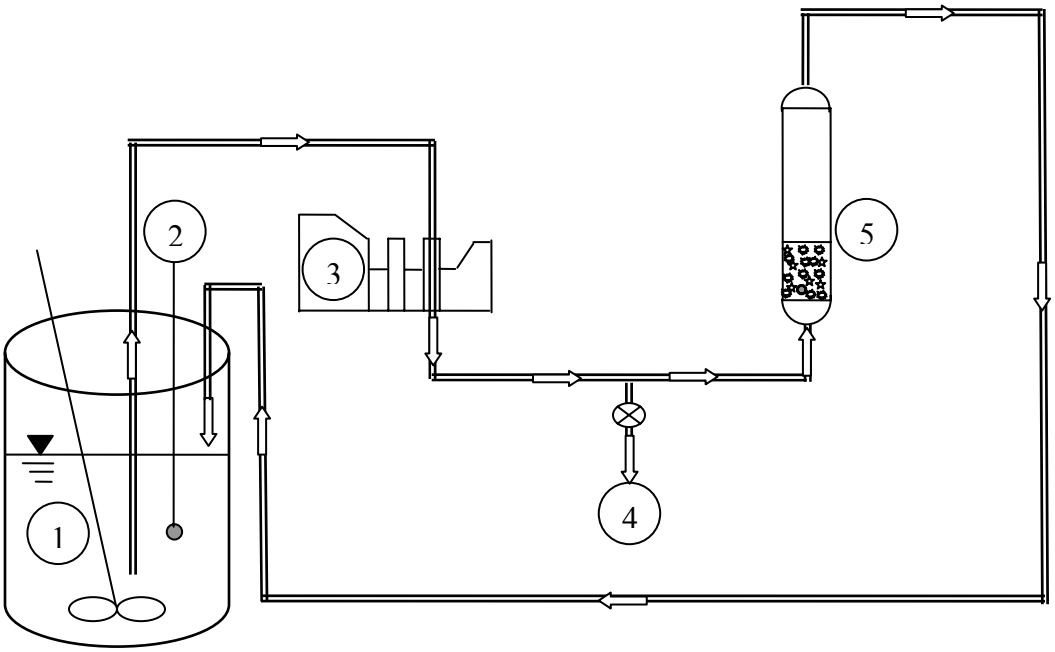

1: P recirculating container (2.0 L); 2: Influent pH meter and recorder
3: Recirculating peristaltic pump; 4: Sampling port
5: P adsorption column filled by AOCM

Figure 5-2. Schematic experimental configuration of P adsorption kinetics on porous AOCM.

Differential column batch reactors (DCBR) with internal diameter of 4.5 cm and length of 8 cm were used to determine phosphate (measured as TDP) adsorption kinetics at ambient temperature of 20 ± 2ºC. The phosphate test solution from a continuously and completely-mixed feed container (2.0 L), was recirculated through the DCBR filled by a defined amount of AOCM at the desired flowrate as shown in Figure 5-2.

After startup, aliquots (5 ml) of replicate samples were collected at predetermined time intervals (normally in range of 5 to 15 minutes) from the sampling ports. Immediately after sampling, the samples were then filtered through 0.45 μm filter and the total dissolved phosphate concentration (PO_4^{3-}) in the filtrate was measured using the ascorbic acid method (Standard Method 1998 of 4500-P-E for wastewater which is equivalent to USEPA method 365.2). Amounts of the adsorbed P were calculated by integrating the effluent concentrations with time

given the known influent time and P concentration. During the experiment, solution pH in the feed container was kept at the required value by 0.02 N KCL or 0.02 N NaOH.

PARAMETRIC INFLUENCE ON SORPTION KINETICS

Sorption kinetics for P was evaluated for selected parameters. There parameters included initial phosphate concentrations of 0.5 to 5 mg/L; pH levels from 5 to 9; ionic strength at 0.01 M; sorbent/solution ratio of 1 g/2L to 10 g/2 L; three media sizes that ranged from 0.85 mm to 9.5 mm, surface loading rates that ranged from 40 to 170 L/(min-m^2); and presence of co-existing ions of Ca^{2+}, SO_4^{2-} and NO_3^{1-}.

Solution pH was adjusted to value of 5 to 9 and kept constant during experiment using 0.02 N HCl or 0.02 KOH. The volume addition of HCl or KOH is negligible compared to the whole recirculation volume of P solution.

The value of pH was determined by the observation of pH ranging mainly from 6 to 8 in urban rainfall-runoff (Sansalone et al 1998). Ionic strength varies from 0.0008 to 0.17 M in urban rainfall-runoff (Sansalone et al. 2005). 0.01 M KCl was chosen as a representative mean ionic strength when studying the effect of ionic strength on P adsorption on AOCM.

Three size ranges of Aluminum Oxide Coated Media, 0.85 ~ 2 mm, 2 ~ 4.75 mm and 4.75 ~ 9.5 mm, were tested on P adsorption kinetics. Competitive or enhanced sorption kinetics was studies by introducing typical ions in urban rainfall-runoff such as Ca^{2+}, SO_4^{2-} and NO_3^{1-}.

RESULTS

MODEL COMPARISON OF AOCM ADSORPTION KINETICS FOR P

Experimental data of TDP adsorption on AOCM as a function of time were analyzed by applying the kinetic models such as pseudo first-order reaction, pseudosecond-order reaction, Elovich, power law and parabolic diffusion.

Figure 5-3 and Figure 5-4 illustrate the results for initial P concentration 0.5 mg/L and 5 mg/L simulated by these models. The experiments were carried out at solution pH of 7.0; ionic strength, I of 0.01M KCl; sorbent/solution, s/s of 10g/2L; and the surface loading rate was 65 L/(m^2-min). The parameters corresponding to each model were shown in Table 5-1 and Table 5-2 respectively.

R^2, which is a measure of the goodness of fit, were 0.99, 0.99, 0.7, 0.94 and 0.91 for pseudo first-order reaction, pseudo-second-order reaction, Elovich, power law and parabolic diffusion respectively for an initial P concentration 0.5 mg/L.

R^2 were 0.92, 0.97, 0.72, 0.96 and 0.97 for the pseudo first-order reaction model, pseudo second-order reaction model, Elovich model, power law model and parabolic diffusion model respectively for an initial P concentration 5 mg/L. Comparatively, the pseudo second-order reaction fits the data and has a clear reaction mechanism and therefore was selected as the primary model in this study.

Table 5-1. Parameters of reaction models of P adsorption kinetics on AOCM by pseudo first order, pseudo second order, Elovich and power equations. Experiments were carried out at: AOCM size 2 ~ 4.75 mm; initial dissolved phosphorus 5 and 0.5 mg/L; pH 7; 0.01M KCl; Sorbent/solution = 10g/2L; Surface loading 65 L/(m^2-min).

P [mg/L]	P adsorption by AOCM reaction kinetics											
	Pseudo first order			Pseudo second order			Elovich			Power		
	q_e	k_1	R^2	q_e	k_2	R^2	β	A	R^2	a	b	R^2
5	0.60	0.03	0.92	0.66	0.06	0.97	25.3	120.5	0.72	0.17	0.22	0.96
0.5	0.10	0.06	0.99	0.12	0.55	0.99	142.9	13.0	0.70	0.02	0.33	0.94

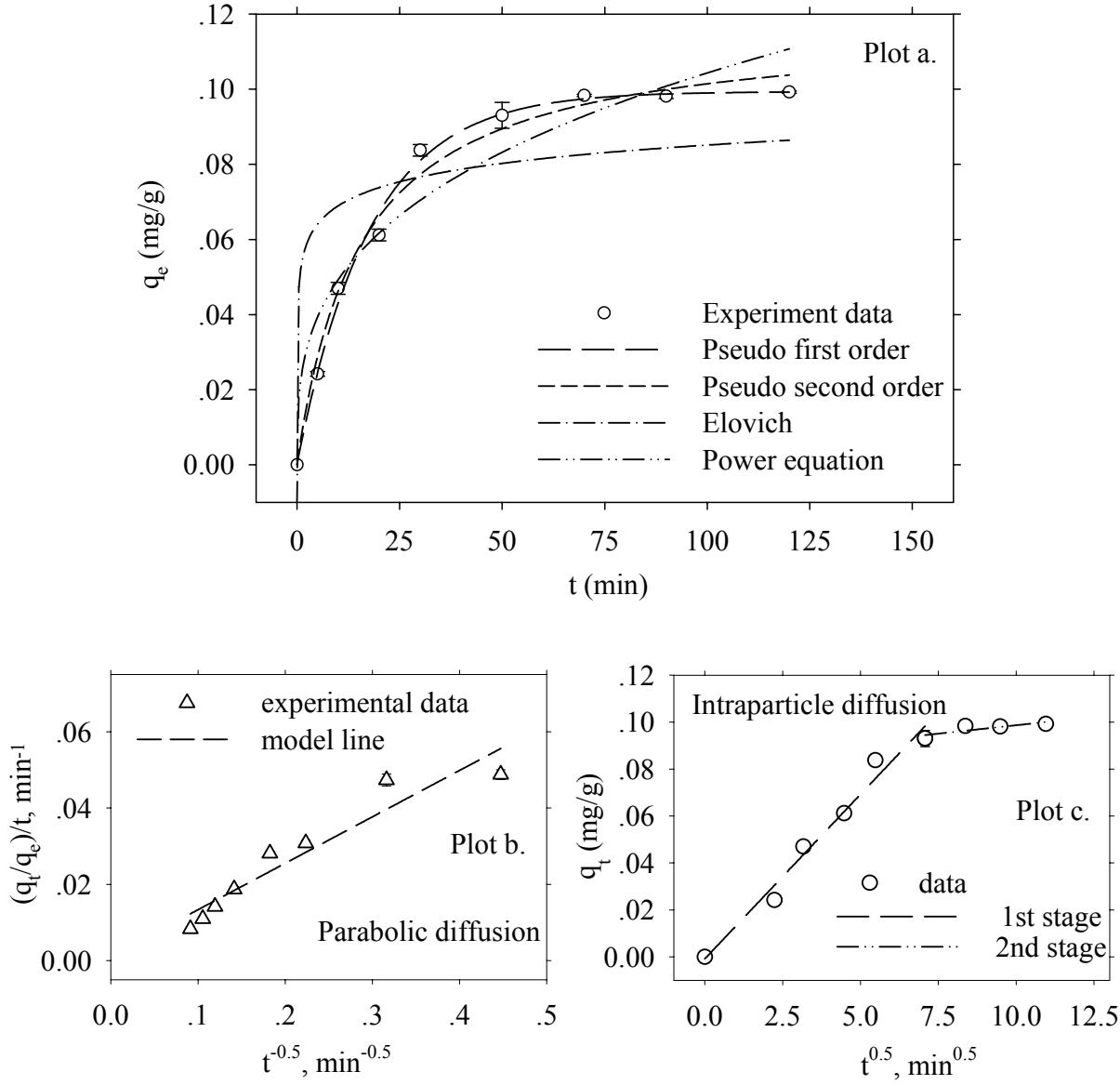

Figure 5-3. Illustrations of P adsorption kinetics on AOCM modeled by pseudo first order, pseudo second order, Elovich; power law; parabolic; intraparticle diffusion equations. Experiments were carried out at: initial dissolved phosphorus 0.5 mg/L; pH 7; 0.01M KCl; Sorbent/solution = 10g/2L; Surface loading 65 L/(m^2-min). The parameters corresponding to each model were shown in Table 5-1 and Table 5-2.

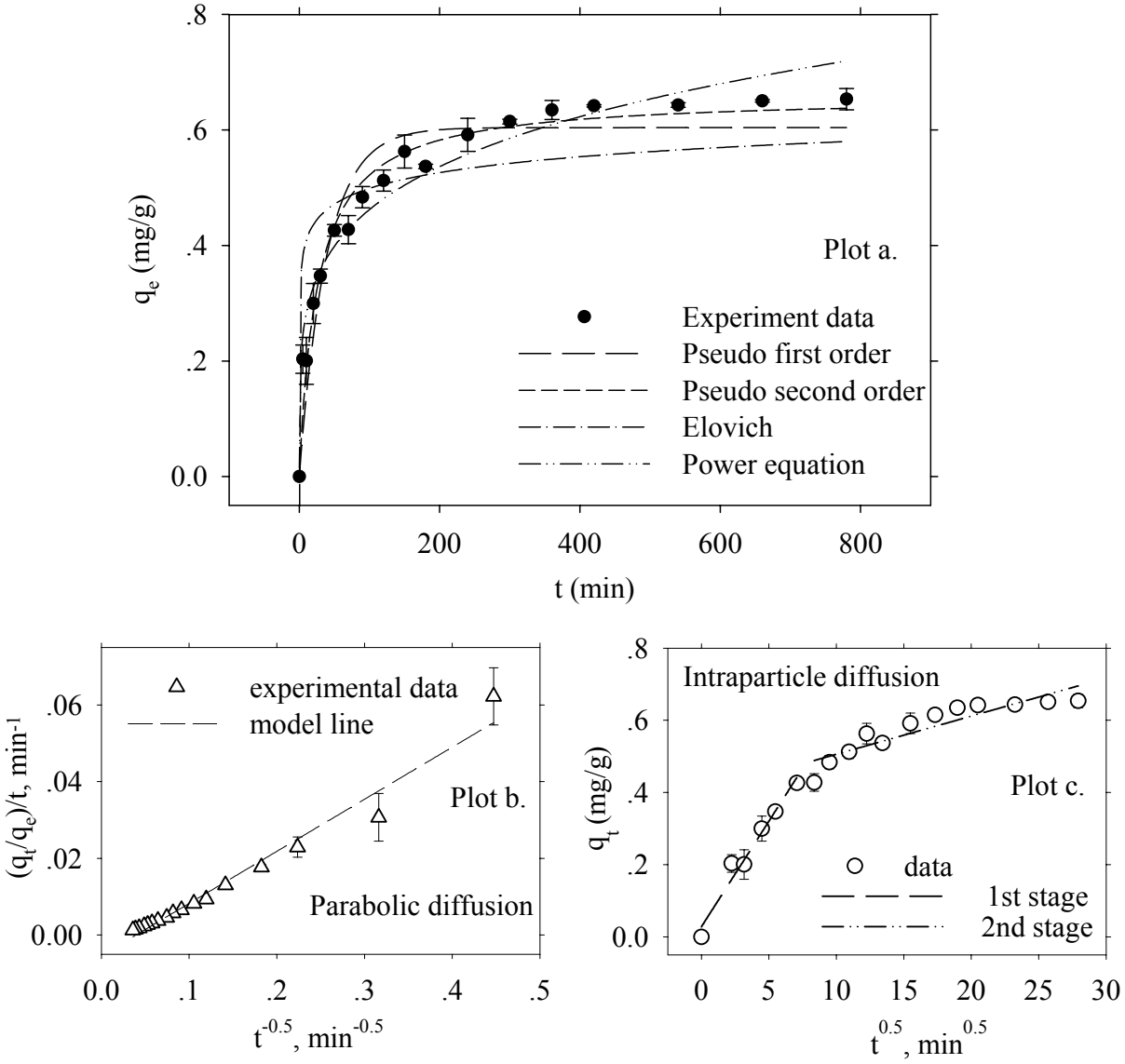

Figure 5-4. Illustrations of P adsorption kinetics on AOCM modeled by pseudo first order, pseudo second order, Elovich; power law; parabolic; intraparticle diffusion equations. Experiments were carried out at: initial dissolved phosphorus 5 mg/L; pH 7; 0.01M KCl; Sorbent/solution = 10g/2L; Surface loading 65 L/(m^2-min). The parameters corresponding to each model were shown in Table 5-1 and Table 5-2.

Table 5-2. Parameters of diffusion models of P adsorption kinetics on AOCM by Parabolic; Intraparticle diffusion equations. Experiments were carried out at: AOCM size 2 ~ 4.75 mm; initial dissolved phosphorus 5 and 0.5 mg/L; pH 7; 0.01M KCl; Sorbent/solution = 10g/2L; Surface loading 65 L/(m^2-min).

P [mg/L]	P adsorption by AOCM diffusion kinetics								
	Parabolic diffusion			Intraparticle diffusion model					
				First stage			Second stage		
	ζ	ψ	R^2	y_0	k_p	R^2	y_0	k_p	R^2
5	0.1358	0.0054	0.97	0.0277	0.0585	0.97	0.4002	0.0106	0.824
0.5	0.0012	0.1217	0.907	-0.001	0.014	0.977	0.0843	0.0014	0.711

However, the pseudo second-order kinetic model can not distinguish the diffusion mechanism during the adsorption process. Thus, the kinetics data were also examined with an intra-particle diffusion model also shown in Figure 5-3 and Figure 5-4. The intra-particle model illustrates two stages for both the initial P concentration of 0.5 mg/L and 5 mg/L. The kinetics transition time between stages occurred about one hour after the P adsorption started for both initial concentrations. The parameters corresponding to intra-particle model are summarized in Table 5-1 and Table 5-2. R^2 were 0.98 and 0.97 in the first stage for initial P concentration of 0.5 mg/L and 5 mg/L respectively. R^2 were 0.71 and 0.82 in the second stage for initial P concentration of 0.5 mg/L and 5 mg/L respectively. According to intra-particle model, film and intraparticle diffusion as well as adsorption reaction mechanisms are involved. The adsorption process can be broken down into several steps if bulk diffusion to the film layer is negligible. External film diffusion is the first step. The second step is adsorption, proceeding at a rate controlled by intra-particle diffusion; the third step establishes the final equilibrium. It is clear from the intra-particle plots in Figure 5-3 an Figure 5-4 that the intra-particle diffusion model applies effectively during the initial one hour of the sorption process. Hence, it is suggested that

intra-particle diffusion controls the limiting rate of phosphorus sorption on AOCM which otherwise is described by the pseudo second-order kinetic model.

Table 5-3. Parameters of pseudo second order equation for P adsorption kinetics by AOCM.

Category and conditions of effects		Pseudo second order kinetics			
		q_e	k_2	R^2	Experiment conditions
Size Effect (mm)	0.85~2	0.695	0.073	0.946	P: 5 [mg/L]; pH 7; 65 L/(m^2-min); Ionic strength: 0.01 M KCl; Sorbent/solution = 10g/2L
	2~4.75	0.659	0.058	0.972	
	4.75~9.5	0.649	0.051	0.976	
Concentration Effect [mg/L]	5	0.659	0.058	0.972	AOCM 2~4.75 mm; pH 7; 65 L/(m^2-min); Ionic strength: 0.01 M KCl; Sorbent/solution = 10g/2L
	2.5	0.437	0.15	0.992	
	1	0.222	0.356	0.981	
	0.5	0.117	0.552	0.988	
pH effect	5	0.921	0.036	0.971	P: 5 [mg/L]; AOCM 2~4.75 mm; 65 L/(m^2-min); Ionic strength: 0.01 M KCl; Sorbent/solution = 10g/2L
	6	0.91	0.034	0.952	
	7	0.659	0.058	0.972	
	8	0.565	0.063	0.971	
	9	0.162	1.4	0.655	
Surface Loading Effect (L/(m^2-min))	170	0.196	1.286	0.997	P: 0.5 [mg/L]; pH 7; AOCM 2~4.75 mm; Ionic strength: 0.01 M KCl; Sorbent/solution = 5g/2L
	85	0.217	0.495	0.989	
	65	0.235	0.231	0.99	
	40	0.211	0.205	0.996	
Sorbent Solution Ratio effect	10g/2L	0.117	0.552	0.988	P: 0.5 [mg/L]; pH 7; AOCM 2~4.75 mm; Ionic strength: 0.01 M KCl; 65 L/(m^2-min)
	5g/2L	0.235	0.231	0.99	
	4g/2L	0.23	0.216	0.99	
	2g/2L	0.293	0.287	0.992	
	1g/2L	0.389	0.211	0.982	
Ca effect [mg/L]	45	0.673	0.073	0.96	P: 5 [mg/L]; pH 7; 65 L/(m^2-min); Ionic strength: 0.01 M KCl; 10g/2L; AOCM 2~4.75 mm
	15	0.68	0.06	0.948	
	0	0.659	0.058	0.972	
Ionic strength Effect (KCl)	0.01 M	0.659	0.058	0.972	P: 5 [mg/L]; pH 7; 65 L/(m^2-min); Ionic strength: 0.01 M KCl; 10g/2L; AOCM 2~4.75 mm
	0	0.641	0.088	0.967	
Nitrate effect [mg/L]	0	0.659	0.058	0.972	P: 5 [mg/L]; pH 7; 65 L/(m^2-min); Ionic strength: 0.01 M KCl; 10g/2L; AOCM 2~4.75 mm
	5	0.602	0.054	0.949	
	25	0.636	0.027	0.986	
Sulfate effect [mg/L]	0	0.659	0.058	0.972	P: 5 [mg/L]; pH 7; 65 L/(m^2-min); Ionic strength: 0.01 M KCl; 10g/2L; AOCM 2~4.75 mm
	10	0.542	0.084	0.988	
	35	0.536	0.06	0.957	
	105	0.572	0.021	0.954	

EFFECT OF AOCM SIZE ON P ADSORPTION KINETICS

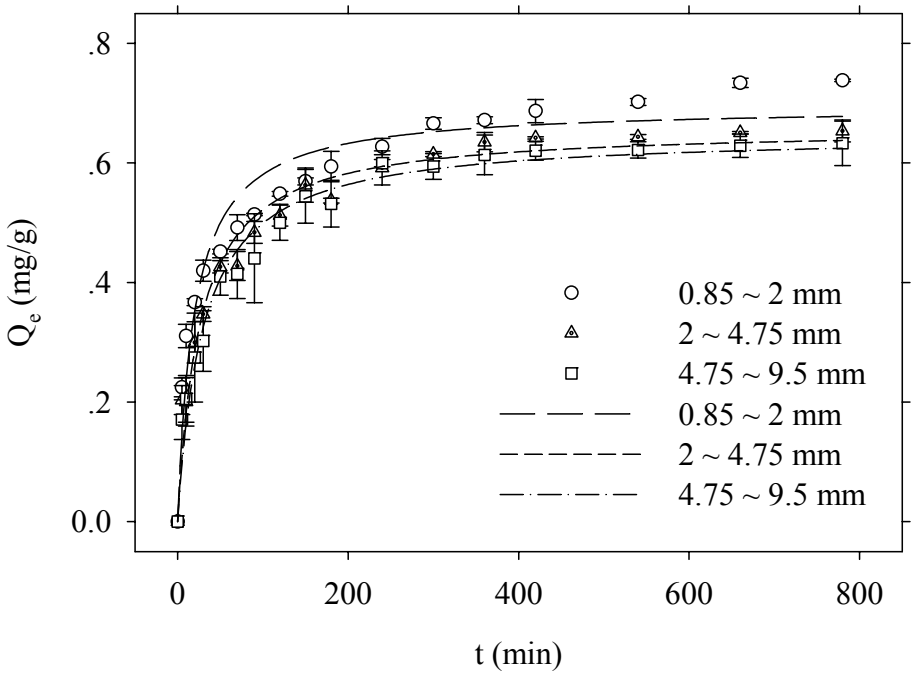

Figure 5-5. Size effect on P adsorption kinetics on AOCM. Experiments were carried out: Initial dissolved phosphorus 5 mg/L; pH 7; 0.01M KCl; Sorbent/solution = 10g/2L; Surface loading 65 L/(m^2-min). Experimental data were fitted by pseudo second order kinetics model and the parameters related were shown in Table 5-3.

Experimental kinetic data describing P sorption on AOCM as a function of AOCM size is summarized in Figure 5-5. The data were compared to pseudo second-order kinetics and corresponding parameters are summarized in Table 5-3.

Comparison between data and models yielded R^2 values that were 0.946, 0.972 and 0.976 for AOCM size of 0.85 ~ 2 mm, 2 ~ 4.75 mm and 4.75 ~ 9.5 mm respectively. The equilibrium adsorption capacities from model simulations were 0.695, 0.659 and 0.649 [mg/g] for AOCM size of 0.85 ~ 2 mm, 2 ~ 4.75 mm and 4.75 ~ 9.5 mm respectively. The increasing values of adsorption capacities with deceasing AOCM size by flow through kinetics agree with the result found from batch-type isotherm studies. The reaction rate constants from model simulated were 0.073, 0.058 and 0.051 g/(mg-min) for AOCM size of 0.85 ~ 2 mm, 2 ~ 4.75 mm and 4.75 ~ 9.5 mm, respectively.

These results indicate that P adsorption kinetics increase with finer AOCM size. If head loss and hydraulic conductivity are not constraints for a particular application, adsorption would be enhanced with the 0.85 ~ 2 mm adsorbent size. The smaller adsorbent sizes would provide comparatively larger surface area per mass and volume and hence higher adsorption kinetics are obtained. Since many rainfall-runoff applications require considerations of minimal head loss and higher hydraulic conductivity, the medium AOCM size range (2 ~ 4.75 mm) was primarily examined.

EFFECT OF SURFACE LOADING ON P ADSORPTION KINETICS

Experimental kinetics data illustrating P adsorption on AOCM as a function of surface loading are depicted in Figure 5-6. The data were compared to a pseudo second-order kinetics model and corresponding parameters are summarized in Table 5-3.

Model comparisons of the data were strong with R^2 values exceeding 0.98 for all four surface loadings. Results indicate that one hour was required surface loadings of 170, 85 and 65 L/(min-m^2) to reach equilibrium with P concentration levels close to zero. About three hours was required for surface loading of 40 L/(min-m^2) to reach equilibrium with P concentration level close to zero.

Equilibrium adsorption capacities for the four surface loadings were comparable, which suggests the good experimental repetition. The simulated reaction rate constants are 1.286, 0.495, 0.231 and 0.205 g/(mg-min) for 170, 85, 65 and 40 L/(min-m^2), respectively.

At higher recirculating flow rate, the surface of Aluminum Oxide Coated Media would be renovated by recirculating phosphorus solution more frequently. Hence the more reaction probabilities would occur. A surface loading rate of 65 L/(min-m^2) was primarily utilized in this study.

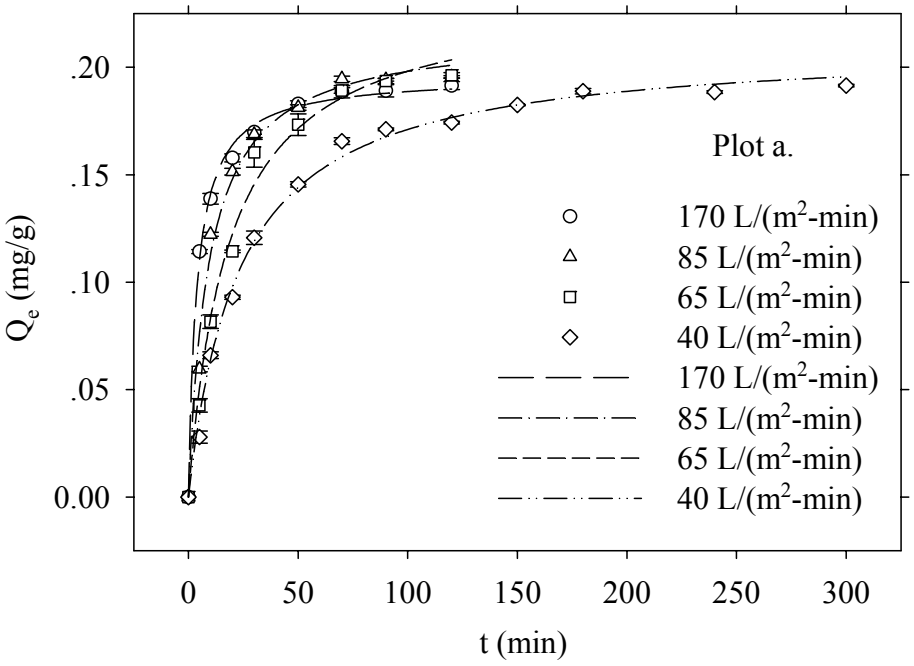

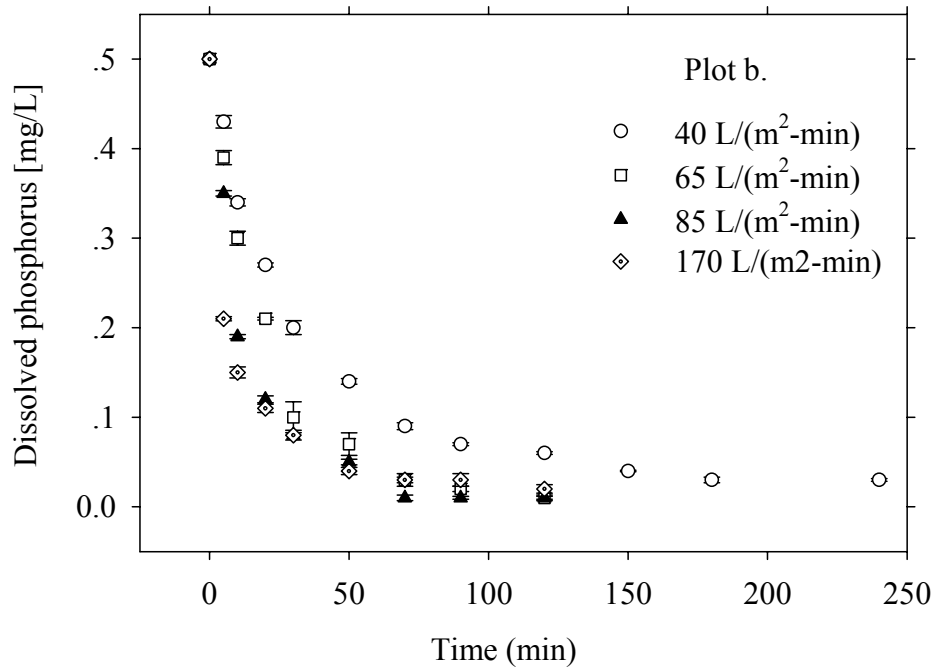

Figure 5-6. Surface loading effect on P adsorption kinetics on AOCM. Experiments were carried out: Initial dissolved phosphorus 0.5 mg/L; AOCM size 2 ~ 4.75 mm; pH 7; ionic strength 0.01M KCl; Sorbent/solution = 10g/2L. Experimental data were fitted by pseudo second order kinetics model and the parameters related were shown in Table 5-3.

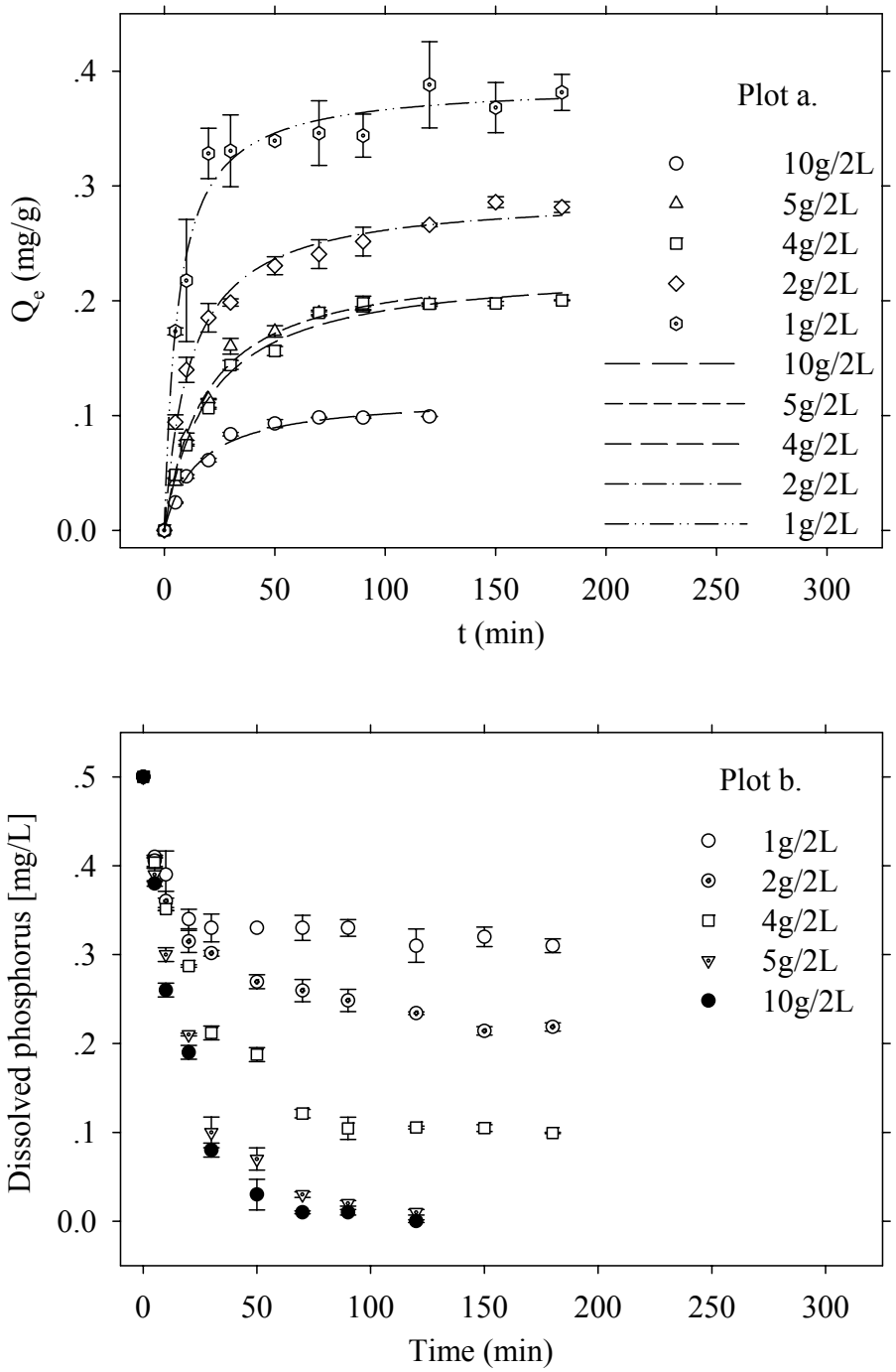

Figure 5-7. Sorbent solution ratio effect on P adsorption kinetics by AOCM. Experiments were carried out: Initial dissolved phosphorus 0.5 mg/L; size 2 ~ 4.75 mm; pH 7; ionic strength 0.01M KCl; Surface loading 65 L/(m^2-min). Experimental data were fitted by pseudo second order kinetics model and the parameters related were shown in Table 5-3.

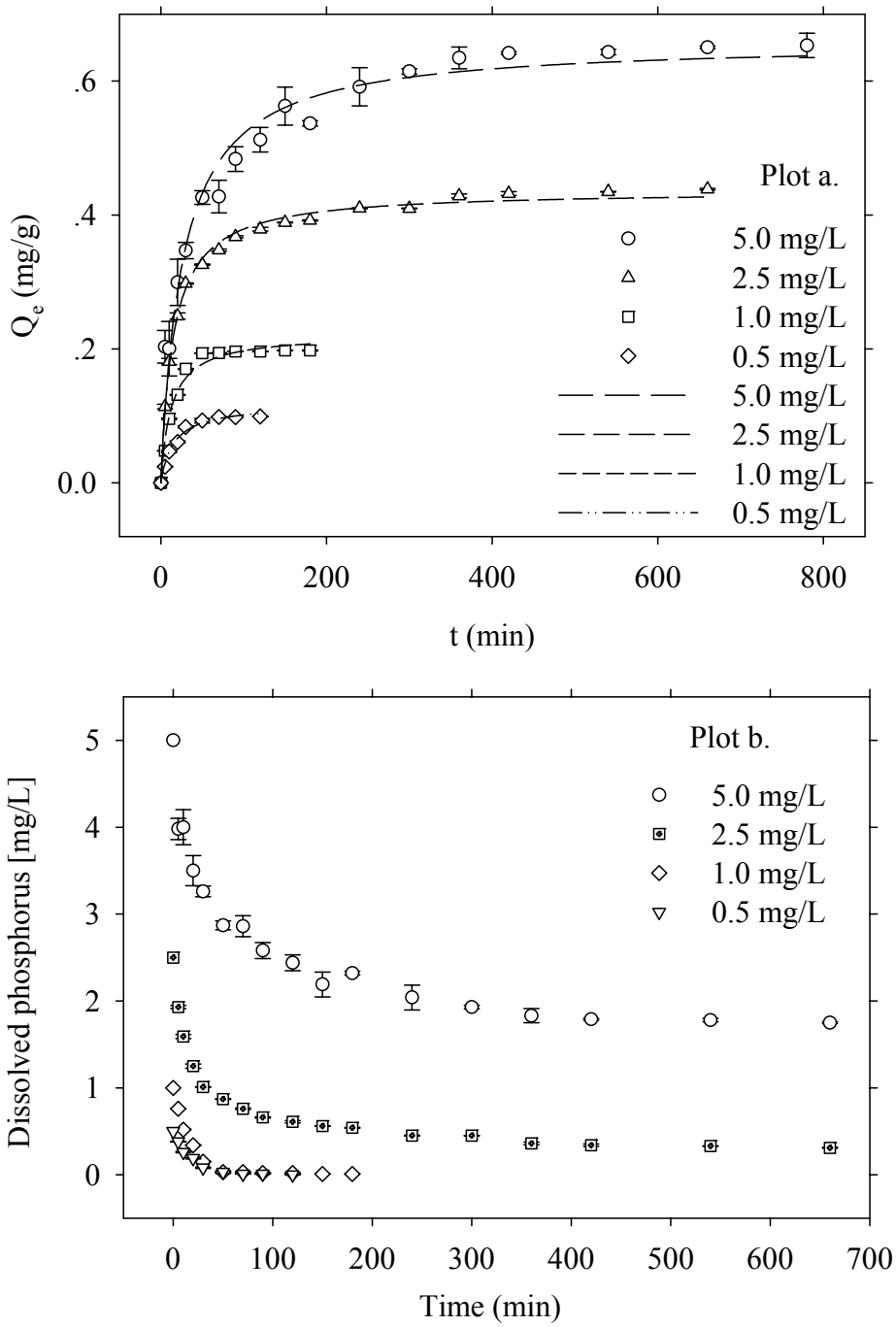

Figure 5-8. Concentration effect on P adsorption kinetics by AOCM. Experiments were carried out: size 2 ~ 4.75 mm; pH 7; 0.01M KCl; Sorbent/solution = 10g/2L; Surface loading 65 L/(m^2-min). Experimental data were fitted by pseudo second order kinetics model and the parameters related were shown in Table 5-3.

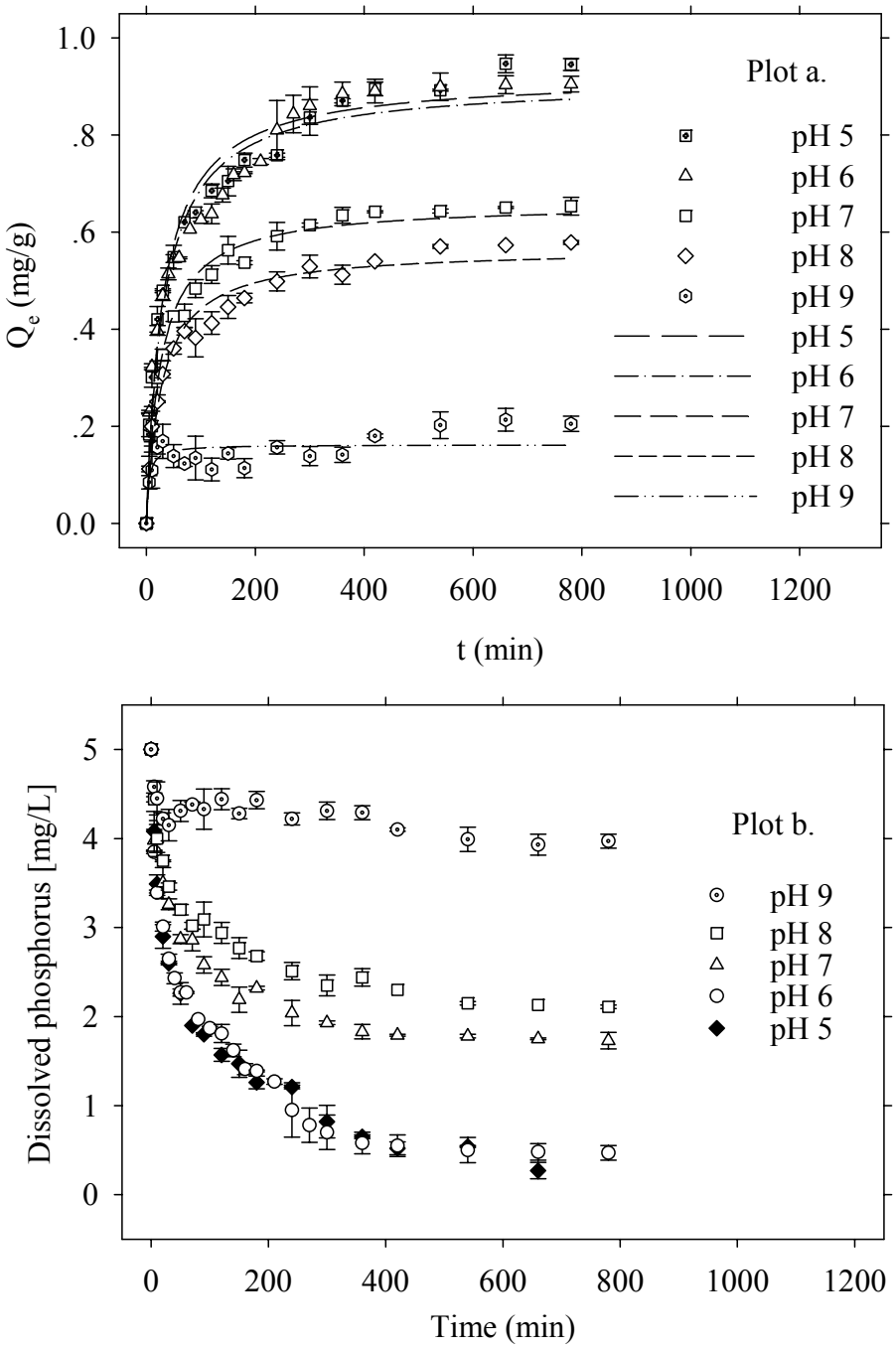

Figure 5-9. pH effect on P adsorption kinetics by AOCM. Experiments were carried out: Initial dissolved phosphorus 5 mg/L; size 2 ~ 4.75 mm; 0.01M KCl; Sorbent/solution = 10g/2L; Surface loading 65 L/(m^2-min). Experimental data were fitted by pseudo second order kinetics model and the parameters related were shown in Table 5-3.

EFFECT OF SORBENT/SOLUTION RATIO (S/S) ON P ADSORPTION KINETICS

Kinetics data describing P adsorption on AOCM as a function of sorbent/solution ratio was depicted in Figure 5-7. The data were compared to a pseudo second-order kinetics model and corresponding parameters are summarized in Table 5-3. Model comparisons of the data were strong with R^2 values exceeding 0.98 for all five s/s ratios. Equilibrium was reached in 30 minutes for the highest s/s ratio and equilibrium times increased for lower s/s ratios, reaching 150 minutes for the smallest s/s ratio. The ending equilibrium P concentrations were near zero for s/s ratios of 10 g/2 L and 5 g/2 L, while ending equilibrium P concentrations were above 0.1 mg/L for sorbent solution ratio 4 g/2 L, 2 g/2 L and 1 g/2 L. It is suggested that appropriate s/s ratios are very critical to ensure a targeted ending equilibrium P concentration. Low s/s ratios not only lead to slower kinetics but also concomitant high ending equilibrium P concentration. Equilibrium adsorption capacities increased from 0.117 [mg/g] to 0.389 [mg/g] as s/s ratios decreased from 10 g/2 L to 1 g/2 L. Such a phenomenon occurred because of limited P loadings which come from P concentration of 0.5 mg/L in 2 L solution. The s/s ratio of 10 g/2 L was the primarily focus of this study.

EFFECT OF CONCENTRATION ON P ADSORPTION KINETICS

Kinetic data describing phosphorus adsorption on AOCM as a function of concentration are depicted in Figure 5-8. The data were compared to a pseudo second-order kinetics model and corresponding parameters are summarized in Table 5-3.

Model comparisons of the data were strong with R^2 values exceeding 0.97 for all four concentration levels from 0.5 to 5 mg/L. Approximately 30 minutes were required to reach equilibrium for a P concentration of 0.5 mg/L while about 6 hours were required to reach equilibrium for a P concentration of 5 mg/L. The common kinetics profile was that initially very

fast kinetics was followed by slower kinetics. The ending equilibrium P concentrations were approximately 0 mg/L and 1.75 mg/L for the starting P concentration of 0.5 mg/L and 5 mg/L, respectively. The adsorption kinetic rate constants were 0.058, 0.15, 0.356 and 0.552 g/(mg-min)for P influent concentration of 5 mg/L, 2.5 mg/L, 1 mg/L and 0.5 mg/L respectively. It is apparent that lower P concentrations favor faster kinetics. The equilibrium adsorption capacities were 0.659, 0.437, 0.222 and 0.117 [mg/g] for P influent concentration of 5 mg/L, 2.5 mg/L, 1 mg/L and 0.5 mg/L respectively.

The equilibrium adsorption capacities declined with deceasing P influent concentrations because a single s/s ratio was used for all the different P influent concentrations. P concentrations of 0.5 mg/L and 5 mg/L were the primarily focus of this study.

EFFECT OF PH ON P ADSORPTION KINETICS

Kinetic data representing the influence of pH on P adsorption kinetics with AOCM are summarized in Figure 5-9. The data were compared to a pseudo second-order kinetics model and corresponding parameters are summarized in Table 5-3.

Model comparisons of the data were strong with R^2 values exceeding 0.95 for pH values of 5.0, 6.0, 7.0 and 8.0 and 0.66 for a pH of 9.0. Modeled kinetic rate constants for pH values of 5.0 and 6.0 were 0.036 and 0.034 g/(mg-min), which are very comparable. Modeled kinetic rate constants for pH of 8.0 and 9.0 were also very comparable, 0.063 and 1.4 g/(mg-min), respectively.

The modeled kinetic rate constant for pH value of 7.0 was 0.058 4 g/(mg-min), intermediate to the other rate constant values. Equilibrium adsorption capacities were 0.921, 0.91, 0.659, 0.565 and 0.162 [mg/g] and ending equilibrium P concentration were 0.27, 0.35, 1.75, 2.13 and 3.93 [mg/L] for pH of 5.0, 6.0, 7.0, 8.0 and 9.0 respectively.

The results of P adsorption kinetics are consistent with findings of P adsorption isotherms. Results indicate that pH has a strong effect on P adsorption capacities. With the primary pH range of 6 to 8 in urban rainfall-runoff (Sansalone and Buchberger 1997, Sansalone et al 2005) a solution pH of 7 was the primarily focus of this study.

EFFECT OF IONIC STRENGTH ON P ADSORPTION KINETICS

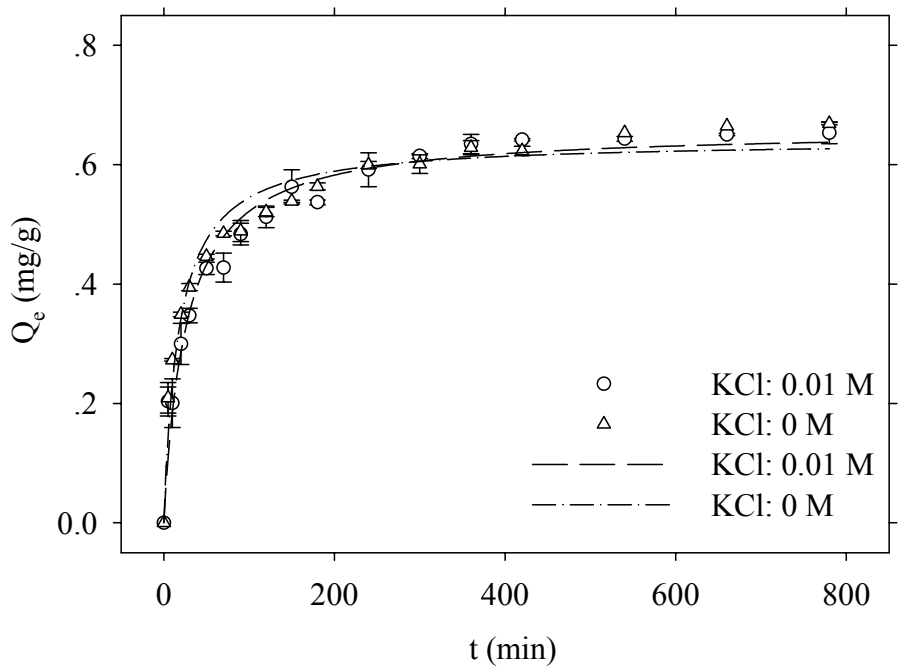

Figure 5-10. Ionic strength effect on P adsorption kinetics by AOCM. Experiments were carried out: Initial dissolved phosphorus 5 mg/L;size 2 ~ 4.75 mm; pH 7; Sorbent/solution = 10g/2L; Surface loading 65 L/(m^2-min). Experimental data were fitted by pseudo second order kinetics model and the parameters related were shown in Table 5-3.

Kinetics data as a function of solution ionic strength effects on P adsorption kinetics for AOCM is depicted in Figure 5-10. These data were compared to a pseudo second-order kinetics model and corresponding parameters are summarized in Table 5-3. Results indicate that P adsorption kinetics data mingled together and modeled lines were hardly distinguishable. Results indicate that ionic strength effects in the typical range observed for rainfall-runoff had an insignificant effect on P adsorption kinetics by AOCM.

EFFECT OF CA^{2+} ON P ADSORPTION KINETICS

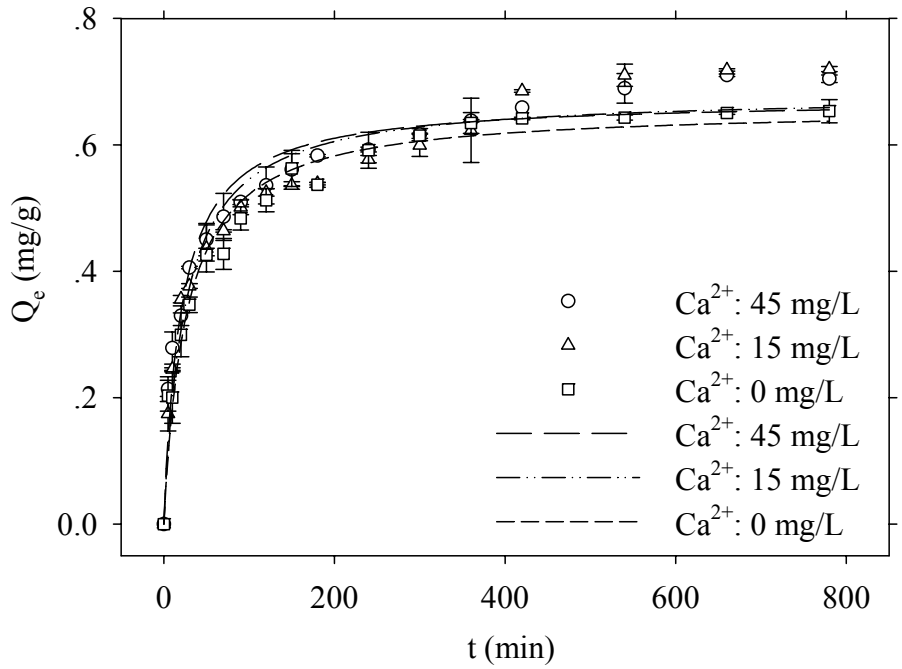

Figure 5-11. Calcium effect on P adsorption kinetics by AOCM. Experiments were carried out: Initial dissolved phosphorus 5 mg/L; size 2 ~ 4.75 mm; pH 7; 0.01M KCl; Sorbent/solution = 10g/2L; Surface loading 65 L/(m^2-min). Experimental data were fitted by pseudo second order kinetics model and the parameters related were shown in Table 5-3.

Kinetic data illustrating the influence of Ca^{2+} on P adsorption kinetics by AOCM is depicted in Figure 5-11. The data were compared to a pseudo second-order kinetics model and corresponding parameters are summarized in Table 5-3. Results indicated that the difference of P adsorption kinetics data with and without the presence of Ca^{2+} were very small, although P adsorption kinetics with the presence of Ca^{2+} were slightly improved as compared to results without the presence of Ca^{2+}. The primary reason is that relatively low concentrations of P and Ca^{2+} can not produce accelerated kinetics though adsorption capacities were enhanced as shown with isotherm data. The secondary reason is that a neutral pH environment (7.0) inhibited formation of ternary complexes, thus the P adsorption kinetics was not strengthened significantly.

EFFECT OF SO_4^{2-} ON P ADSORPTION KINETICS

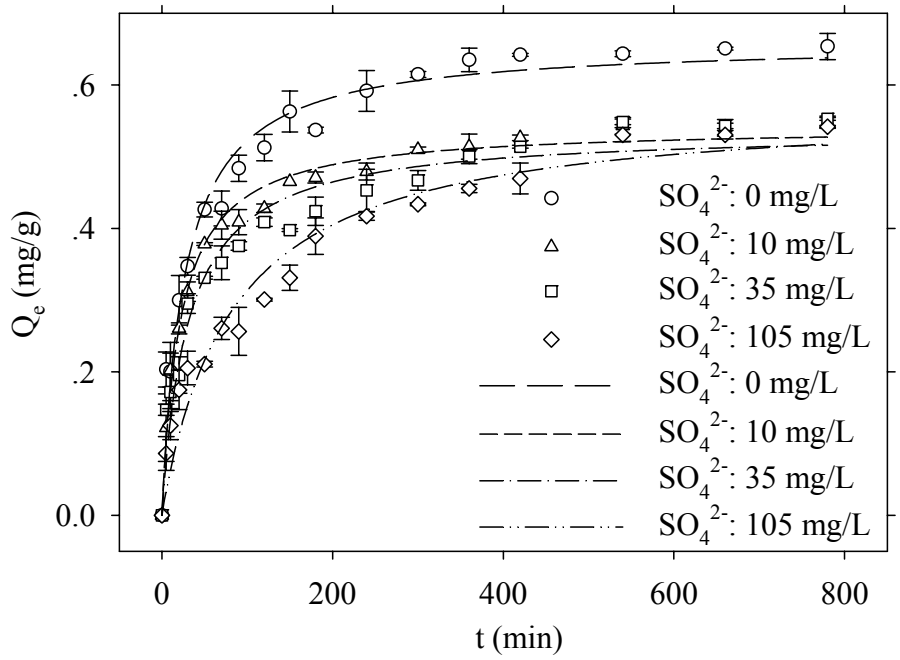

Figure 5-12. Sulfate effect on P adsorption kinetics by AOCM. Experiments were carried out: Initial dissolved phosphorus 5 mg/L; size 2 ~ 4.75 mm; pH 7; 0.01M KCl; Sorbent/solution = 10g/2L; Surface loading 65 L/(m^2-min). Experimental data were fitted by pseudo second order kinetics model and the parameters related were shown in Table 5-3.

Kinetic data for the influence of SO_4^{2-} on P adsorption kinetics with AOCM are depicted in Figure 5-12. The data were compared to a pseudo second-order kinetics model and corresponding parameters are summarized in Table 5-3.

Results indicate that there are differences in P adsorption kinetics with and without the presence of SO_4^{2-}. P adsorption capacities decreased as follows: 0.66, 0.54, 0.54 and 0.57 [mg/g] for 0, 10, 35 and 105 [mg/L] SO_4^{2-} addition. The results were slightly lower than findings for equilibrium isotherms which were 0.75, 0.69, 0.69, 0.67 [mg/g], respectively and measured at 24 hours. Results indicate that the presence of increasing levels of SO_4^{2-} increasingly reduced P adsorption kinetics by AOCM because SO_4^{2-} can compete with PO_4^{3-} for the common adsorptive sites.

EFFECT OF NO_3^{1-} ON P ADSORPTION KINETICS

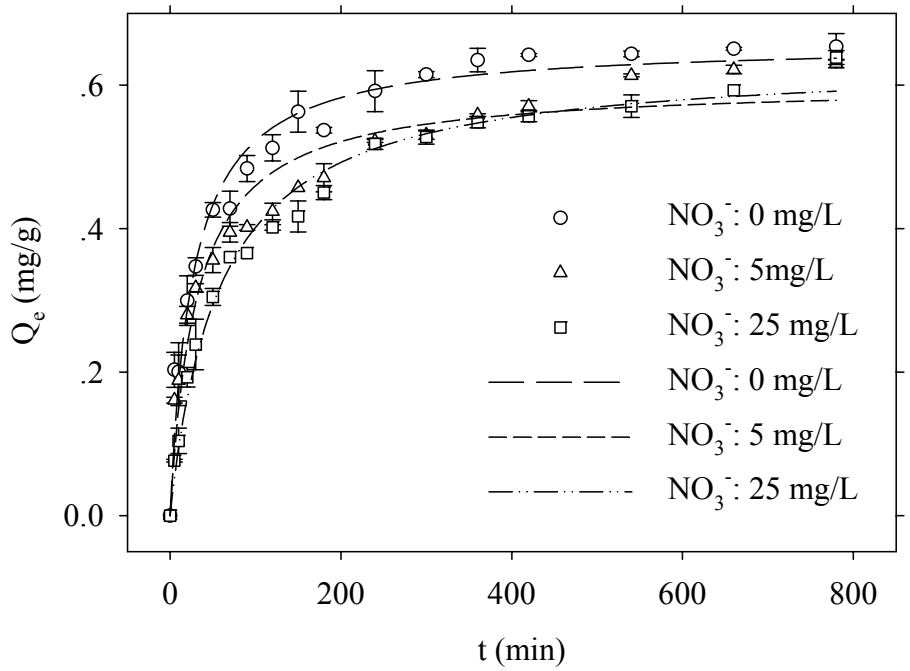

Figure 5-13. Nitrate effect on P adsorption kinetics by AOCM. Experiments were carried out: Initial dissolved phosphorus 5 mg/L; size 2 ~ 4.75 mm; pH 7; 0.01M KCl; Sorbent/solution = 10g/2L; Surface loading 65 L/(min-m^2). Experimental data were fitted by pseudo second order kinetics model and the parameters related were shown in Table 5-3.

Kinetics data illustrating the role of NO_3^{1-} on P adsorption kinetics on AOCM is depicted in Figure 5-13. The data were compared to a pseudo second-order kinetics model and corresponding parameters are summarized in Table 5-3.

Results indicate that P adsorption on Aluminum Oxide Coated Media as a function of time were only slightly inhibited with increasing concentrations of NO_3^{1-} and the differences in equilibrium adsorption capacities on Aluminum Oxide Coated Media are similar, 0.659, 0.602 and 0.636 [mg/g] for 0, 5 and 25 [mg/L] of NO_3^{1-} addition, respectively. Such a slight variation of P adsorption kinetics on Aluminum Oxide Coated Media with presence of nitrate suggested that effect of nitrate is insignificant.

EFFECTIVE INTRAPARTICLE DIFFUSION COEFFICIENT, D_{EI}

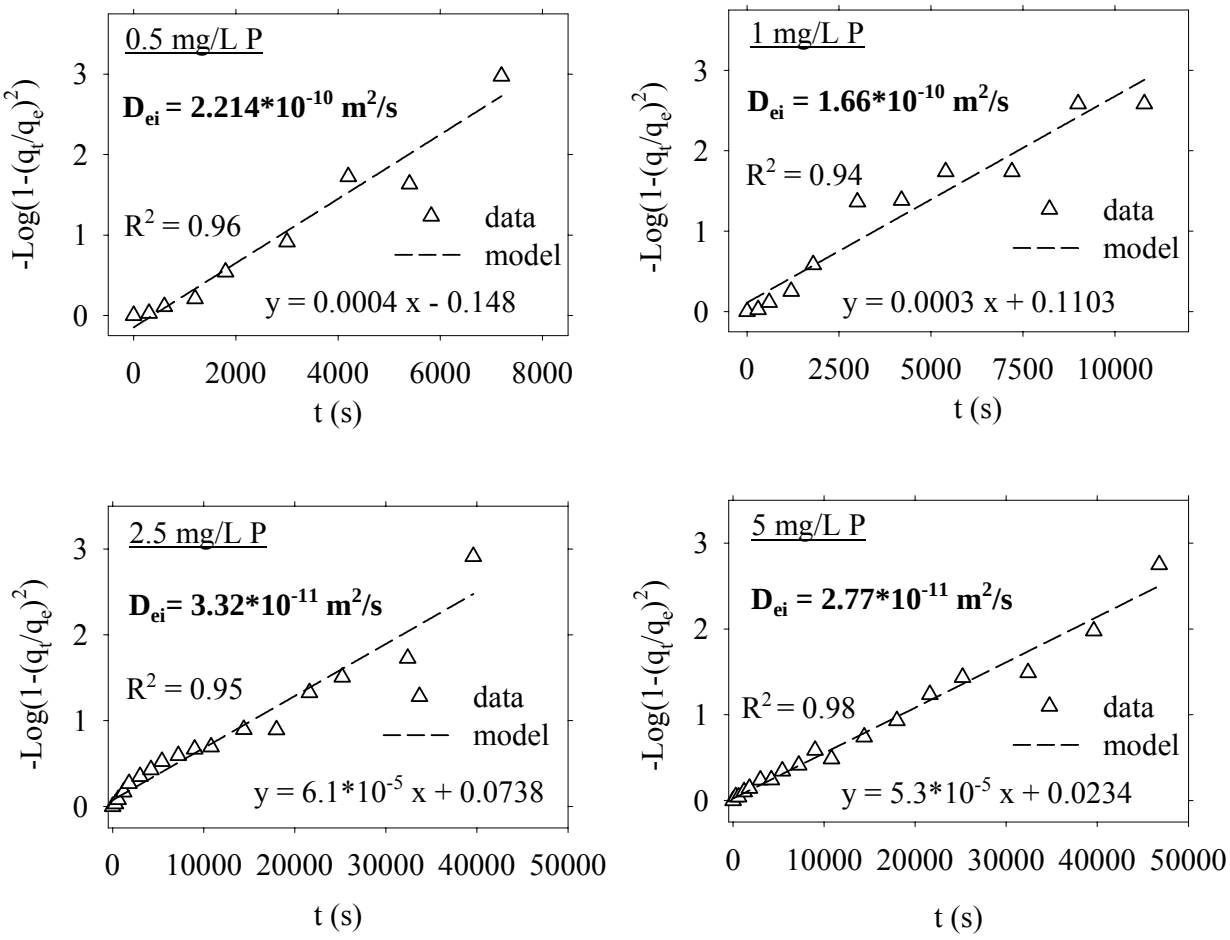

Figure 5-14. Evaluation of effective intraparticle diffusion coefficients by Boyd's method at P concentrations 0.5; 1; 2.5; 5 mg/L respectively. Experiments were carried out at pH 7; ionic strength 0.01 M KCl; AOCM size 2 ~ 4.75 mm (size mean 3.1 mm); surface loading rate 65 L/(m^2-min); sorbent solution ratio 10g/2L. Data were fitted by Boyd's method and corresponding parameters were shown in Table 5-4.

Table 5-4. Summary of film diffusion coefficients (D_f), effective intra particle diffusion coefficients (D_{ei}), pore diffusion coefficients (D_p) at two concentrations of phosphorus.

C_0	C_e	K_1	$t_{1/2}$	D_f Half time method	D_{ei} Boyd's method	D_p Half time method	D_p Parallel pore model
[mg/L]	[mg/L]	min^{-1}	min	(cm^2/s)	(cm^2/s)	(cm^2/s)	(cm^2/s)
5	1.730	0.0254	27.29	3.78E-06	2.77E-07	4.40E-07	0.8 ~ 2.4 E-08
0.5	0.008	0.0563	12.31	1.80E-04	2.21E-06	9.76E-07	

The effective intraparticle diffusion coefficients, $D_{ei,}$ based on P adsorption capacity by AOCM were evaluated by Boyd's method (Boyd et al. 1947; Hano et al. 1997; Urano and Tachikawa 1991):

$$-\log\{1-(\frac{q_t}{q_e})^2\} = \frac{4\pi^2 D_{ei} t}{2.3D^2} \qquad \text{Equation 5-18}$$

In this expression q_t is the amount of P adsorbed at time t, q_e the equilibrium P amount adsorbed and q_t/q_e represents adsorption coverage, D is mean geometric diameter of AOCM of the 2 ~ 4.75 mm size range (0.31 cm utilized) and the media shape was assumed to be spherical. The value of D_{ei} were obtained from slope of the plots of $-\log(1-(q_t/q_e)^2)$ versus t. Figure 5-14 illustrates plots of $-\log(1-(q_t/q_e)^2)$ versus t at four different initial concentrations. Values of D_{ei} ranging from 0.277×10^{-6} to 2.2×10^{-6} cm^2/s for initial P concentration 5 mg/L and 0.5 mg/L, respectively are summarized in Table 5-4. Boyd's method is applicable for the present study since the relationships between $-\log(1-(q_t/q_e)^2)$ and t were linear and all the R^2 values are larger than 0.94.

PORE DIFFUSIVITY BY PARALLEL PORE MODEL

According to the parallel pore model (Klug and Alexander 1956), the pore diffusivity (D_p) can be related to the molecular diffusivity (D_m) in the liquid phase:

$$D_p = \frac{\varepsilon}{100\zeta} D_m \qquad \text{Equation 5-19}$$

In this expression, ε is the particle porosity of AOCM which is 0.54±0.02 measured by ASTM C 642-97 (2004), ζ is the tortuosity of AOCM pores, which is usually between 2 and 6 for oxide type adsorbents. D_m value for $H_2PO_4^-$ was reported as 8.79×10^{-6} cm^2/s in water at ambient temperature (Edwards and Huffman 1959). Therefore D_p is approximately $(0.8 \sim 2.4)\times10^{-8}$ cm^2/s. Pore diffusivities were comparable to effective intraparticle diffusivities in terms of magnitude, therefore it is suggested that pore diffusion contributed more than surface diffusion to

the overall intraparticle diffusion and pore diffusion is the rate limiting step for the intraparticle diffusion.

PORE AND FILM DIFFUSIVITY BY HALF TIME EQUATIONS

The rate limiting step of the adsorption process can be elucidated using the first order kinetic data (Helfferich, 1962). Suggested by Asher and Pankow (1991), the first-order rate constant (K_1) and two half time equations can be used to obtain pore diffusion coefficients D_p, cm^2/s and film diffusion coefficient D_f, cm^2/s, assuming the spherical geometry of an adsorbent .

$$t_{1/2} = -\frac{\ln(0.5)}{K_1} \qquad \text{Equation 5-20}$$

$$t_{1/2} = \frac{0.0075D^2}{D_p} \qquad \text{Equation 5-21}$$

$$t_{1/2} = \frac{0.115D\delta}{D_f} \times \frac{C_0}{C_e} \qquad \text{Equation 5-22}$$

In this expression $t_{1/2}$ is the time needed to remove the phosphorus concentration to half the initial concentration in seconds, C_0 and C_e are the initial and equilibrium concentrations of the phosphorus respectively, δ is the thickness of the stagnant film adjacent to the surface of adsorbent, which is assumed as 0.001 cm.

The values of D_{ei}, D_p and D_f were calculated for different initial concentrations by a variety methods such as Boyd's method, half time method and parallel pore method. By comparison of results presented in Table 5-4, film diffusion coefficients (D_f) are at least one order magnitude larger than effective intraparticle diffusion coefficients (D_{ei}), which suggest that film mass transfer occurred very fast and is not the rate limiting step. Pore diffusion coefficients (D_p) calculated from the half time method and parallel pore method showed consistent results. In addition the comparable level of effective intra particle diffusion coefficients and pore diffusion coefficients suggest that pore diffusion is the rate limiting step for the overall mass transfer

process of P adsorption by AOCM. The determination of pore diffusion as primary diffusion step also help with elucidating the applicability of intraparticle diffusion model.

IMPLICATIONS AND DISCUSSION

P adsorption kinetics on AOCM was studied with the goal of identifying media behavior to selected common rainfall-runoff parameters. P adsorption kinetics with AOCM was determined to be integrated diffusion and reaction processes. Typically diffusion can be enhanced by adequate mixing, heterogeneous surfaces and high contacting area. AOCM is a preferred media from a number of physical characteristics including high porosity, very lightweight and large pore size distribution. All of these characteristics facilitate diffusion processes. Adsorption reactions for P on AOCM are dictated by pH, species of P and functional groups on AOCM. The neutral to slightly acidic pH range of urban rainfall-runoff for source area watersheds, is conducive to rapid adsorption kinetics and good adsorption capacities.

CONCLUSIONS

Both of the reaction kinetics and the diffusion mechanism were applied to adequately describe P adsorption kinetics by AOCM. The measured data were best described using a pseudo second-order reaction model fitted for the overall range of kinetics data and the intraparticle diffusion model best predicted the first hour of P adsorption kinetics.

The kinetics of P adsorption on AOCM was fast for the typical urban rainfall runoff conditions, with the reactions completed within the first few hours, sometimes even within minutes. Finer size of AOCM showed quicker P kinetics. The higher initial P concentration, the longer reaction time and vice versa. The high surface loading rate and the higher sorbent solution ratio, the better kinetics could be obtained. Lower pH not only promotes faster adsorption but also ensure higher adsorption capacity. Ionic strength and Nitrate have little effect on P

adsorption kinetics. While Calcium accelerates noticeable P adsorption kinetics by forming ternary complexes, Sulfate inhibited appreciable P adsorption kinetics by competition for common sites. Adsorption capacities obtained from recirculating kinetics agree with the batch adsorption isotherm findings.

Pore diffusion was suggested as rate limiting step for P adsorption kinetics on AOCM by comparison of film diffusion, effective intra particle diffusion and pore diffusion through half time method, parallel pore method and Boy'd method.

REFERENCES

Altundogan, H.S. and Tumen, F., 2001. Removal of Phosphates from Aqueous Solutions by Using Bauxite I: Effect of pH on the Adsorption of Various Phosphates. Journal of Chemical Technology and Biotechnology, 77, 77-85.

APHA- American Public Health Association. 1998. Standard Methods for the Examination of Water and Wastewater, (20th Ed.) A.D. Eaton, L.S. Clesceri, A.E. Greenberg (Eds.), American Public Health Association, American Water Works Association and Water Environmental Federation, Washington, D.C.

Asher, W.E. and Pankow, J.F. 1991. Prediction of gas/water mass transport coefficients by a surface renewal model. Environ. Sci. Technol. 25, 1294-1300.

ASTM C 642-97, 2004. Test method for density, absorption, and voids in Hardened Concrete, ASTM Annual Book.

Badruzzaman, M., Westerhoff, P. and Knappe, D.R.U. 2004. Intraparticle diffusion and adsorption of arsenate onto granular ferric hydroxide (GFH). Water Research, 38, 4002-4012.

Baker, M.J., Blowes, D.W. and Ptacek, C.J., 1998. Laboratory Development of Permeable Reactive Mixtures for the Removal of Phosphorus from Onsite Wastewater Disposal Systems. Environmental Science & Technology, 32(15), 2308-2316.

Boyd, G.E., Adamson, A.W., and Meyers, L.S. 1947. The exchange adsorption of ions from aqueous solution by organic zeolites. II. Kinetics. J. Am. Chemical Soc., 69, 2836.

Chaudhary, D.S., Vigneswaran, S., Jegatheesan, V., Ngo, H.H., Moon, H., Shim, W.G. and Kim, S.H., 2002. Granular Activated Carbon (GAC) Adsorption in Tertiary Wastewater Treatment: Experiments and Models. Water Science and Technology, 47(1), 113-120.

Clark, T., Stephenson, T. and Pearce, P.A., 1997. Water Research. 31(10) 2557-2563.

Dean, C.M, Sansalone, J.J., Cartledge, F.K. and Pardue J.H. 2005. Influence of Hydrology on Rainfall-Runoff Metal Element Speciation.

De-Bashan, L.E. and Bashan, Y., 2004. Recent Advances in removing Phosphorus from Wastewater and its Future Use as Fertilizer. Water Research, 38, 4222-4246.

Duda, A.M., 1993. Addressing nonpoint sources of water pollution must become an international priority. Water Sci. Technol. 28, 1-11.

Edwards, O.W. and Huffman, E.O. 1959. J. Phys. Chem. 63, 1830-1833.

Forbes, M.G., Dickson, K.R., Golden, T.D., Hudak, P. and Doyle, R.D., 2004. Dissolved Phosphorus Retention of Light-Weight Expanded Shale and Masonry Sand Used in Subsurface Flow Treatment Wetlands. Environmental Science & Technology, 38(3), 892-898.

Genz, A., Kornmüller, A. and Jekel, M., 2004. Advanced Phosphorus Removal from Membrane Filtrates by Adsorption on Activated Aluminum Oxide and Granulated Ferric Hydroxide. Water Research, 38, 3523-3530.

Hano, T., Takanashi, H., Hirata, M., Urano, K. and Eto, S., 1997. Removal of Phosphorus from Wastewater by Activated Alumina Adsorbent. Wat. Sci. Tech., 35(7), 39-46.

Hatfield, K., Burris, D.R. and Wolfe, N.L., 1996. Analytical model for heterogeneous reactions in mixed porous media. Journal of Environmental Engineering. 676-684.

Helfferich, F. 1962. Ion exchange. McGraw Hill, New York. 299-319.

House, W.A., Dension, F.H. and Armitage, P.D., 1995. Comparison of the uptake of inorganic phosphorus to a suspended and stream bed sediment. Water Res. 29, 767-779.

House, W.A. and Denison, F.H., 2002. Exchange of Inorganic Phosphate between River Waters and Bed-Sediments. Environmental Science & Technology, 36(20), 4295-4301.

Hu, H., Li, X., He, J. and Liu, F., 2004. Secondary Adsorption of Phosphate on Aluminum Oxides Surfaces as Influenced by Several Organic Acids. Journal of Plant Nutrition, 27(4), 637-649.

Ippolito, J.A., Barbarick, K.A., Heil, D.M., Chandler, J.P. and Redente, E.F., 2003. Phosphorus Retention Mechanisms of a Water Treatment Residual. J. Environ. Quality, 32, 1857-1864.

Karaca, S., Gürses, A., Ejder, M. and Acikyildiz, M., 2004. Kinetic Modeling of Liquid-Phase Adsorption of Phosphate on Dolomite. Journal of Colloidal and Interface Science, 277, 257-263.

Kim, Y. and Kirkpatrick, J., 2004. An Investigation of Phosphate Adsorbed on Aluminum Oxyhydroxide and Oxide Phases by Nuclear Magnetic Resonance. European Journal of Soil Sciences, 55, 243-251.

Klug, H.P. and Alexander, L.E. 1956. X-ray diffraction procedure for polycrystalline sand amorphous materials. John Wiley & Sons: New York. P 491.

Kobya, M., Demirbas, E. et al. (2002). Adsorption kinetic models applied to Nichel ions on hazelnut shell activated carbons. Adsorption Science & Technology, 20 (2), 179-188.

Koretsky, C., 2000. The Significance of Surface Complexation Reactions in Hydrologic Systems: A Geochemist's Perspective. Journal of Hydrology, 23, 127-171.

Kostura, B. Kulveitova, H. and Lesko J. 2005. Blast furnace slags as sorbents of phosphate from water solutions. Water Research. 39, 1795-1802.

Levine, S.L. and Schindler, D.W. 1989. Phosphorus, nitrogen and carbon dynamics of experimental lake 303 during recovery from eutrophication. Can. J. Fish Aquat. Sci. 46, 2-10.

Liu, D.F., Sansalone, J.J. and Cartledge, F.K. 2005. Adsorption kinetics for urban rainfall-runoff metals by composite oxide-coated polymeric media. Journal of Environmental Engineering, 1168-1177.

Nichols, D.S. J. Water Pollut. Control Fed. 1983, 55(5), 495-505.

Notthakun, S. Crittenden, J.C., Hand, D.W., El-behlil, A.M., Arora, H., Vaitheswaran, K., 1989. Prediction of granular activated carbon process performance using mass transfer models. Proceedings of a Technology Transfer Conference: Design and Use of Granular Activated Carbon-Practical Aspects, Denver, CO, AWWA Research Foundation.

Oguz, E., Gurses, A. and Yalcin, M., 2003. Removal of Phosphate from Waste Waters by Adsorption. Water, Air, and Soil Pollution, 148, 279-287.

Ozacar, M., 2003. Equilibrium and kinetic modelling of adsorption of phosphorus on calcined alunite. Adsorption 9(2): 125-132.

Pavlatou, A. and Polyzopoulos N.A., 1988. The role of diffusion in the kinetics of phosphate desorption: the relevance of the Elovich equation. J. Soil Sci. 39, 425-436.

Ruixia, L., Jinlong, G., Hongxiao, T., 2002. Adsorption of fluoride, phosphate and arsenate ions on a new type of ion exchange fiber. J. Colloid Interface Sci. 248, 268-274.

Sansalone, J.J. and Buchberger, S.G., 1997. Partitioning and First Flush of Metals in Urban Roadway Storm Water. Journal of Environmental Engineering, American Society of Civil Engineers, Vol. 123. No. 2, February, pp 134-143.

Sansalone, J.J., Koran, J.M., Smithson, J.A. and Buchberger, S.G., 1998. Physical Characteristics of Urban Roadway Solids Transported During Rain Events. Journal of Environmental Engineering, American Society of Civil Engineers, Vol.124, No. 4, pp 427-440.

Sansalone, J.J., Zheng, T. 2005. Transient rainfall-runoff loadings to a partial exfiltration system: implications for urban water quantity and quality. Journal of Environmental Engineering, 1155-1167.

Sparks, D. L., 1995. Environmental Soil Chemistry, Academic Press, San Diego.

Sparks, D. L., 1999. "Kinetics and mechanisms of chemical reaction at the soil mineral/water interface," In: Soil Physical Chemistry, 2nd ed., Sparks D. L. eds., CRC Press.

Sperlich, A., Werner, A., Benz, A., Amy, G., Worch, E. and Jekel, M., 2005. Breakthrough Behavior of Granular Ferric Hydroxide (GFH) Fixed-Bed Adsorption Filters: Modeling and Experimental Approaches. Water Research, 39, 1190-1198.

Tang, W.P., Shima, O., Ookubo, A. and Ooi, K., 1997. A Kinetic Study of Phosphate Adsorption by Boehmite. Journal of Pharmaceutical Sciences, 86(2), 230-235.

Urano, K. and Tachikawa, H., 1991. Process Development for Removal and Recovery of Phosphorus from Wastewater by a New Adsorbent II: Adsorption Rates and Breakthrough Curves. Ind. Eng. Chem. Res., 30, 1897-1899.

U.S. EPA, 1986. Quality Criteria for Water. Office of Water Regulation and Standards, US Government Printing Office (PB81-226759), Washington, DC 20460. EPA 440/5-86-001.

USEPA, 1998. National Water Quality Inventory, Report to congress; EPA841-R00-001. National service center for environmental publications. Cincinnati, OH.

Vollenweider, R.A., 1989. Global problems of eutrophication and its control. In conservation and management of lakes, Salanki, J., Herodek, S., Eds.; Symposium Biologica Hungarica Vol. 38; Akademiai Kiado: Budapest, pp 19-41.

CHAPTER 6 PHOSPHORUS ADSORPTION BREAKTHROUGH FROM ALUMINUM OXIDE COATED MEDIA

SUMMARY

Breakthrough of phosphate from aluminum oxide coated packed bed columns was examined for aluminum oxide coated media (AOCM) using synthetic rainfall-runoff. Breakthrough curve (BTC) characteristics and suitability of AOCM as a subsequent adsorptive-filtration process for effluent from primary unit operations such as a hydrodynamic separator containing low concentrations in both particulate bound phosphorus and particulate matter were examined.

This research presents two mechanistic and two empirical BTC models respectively for phosphate (P) measured as total dissolved phosphorus (TDP) for transport and adsorption in heterogeneous AOCM column which is important for the design and prediction of full-scale systems.

The mechanistic Langmuir model and mechanistic Freundlich model incorporate one dimensional mass balance and transport equation based on packed bed, simplified intraparticle Linear Driving Force (LDF) mass transfer model, nonlinear isotherm models (Langmuir/Freundlich) and corresponding initial and boundary conditions. The pertinent parameters of mechanistic models were determined by independent results of batch type isotherm and flow through kinetics of P adsorption on AOCM studied or through formulated correlations. The reliability of mechanistic models were verified for their capability to simulate a suite of BTC data. The empirical Thomas model and empirical bed-depth-service-time (BDST) model resulted in similar results after mathematical derivation. The applicability of the empirical models was confirmed by high R^2 values.

BTC of P adsorption on AOCM demonstrated typical "S-shaped" curves. The number of bed volumes at breakthrough (N_{bt}) is several hundred, and number of bed volume at exhaustion (N_{ex}) are of double or triple the breakthrough value. Smaller AOCM size leads to better BTC due to higher contacting area. Good BTC favors with slightly acidic pH, low P concentration and low surface loading. Enhancement effect from Ca addition and inhibition effect from sulfate presence were not very significant because levels of interacting concentrations were low. The maximum adsorption capacities calculated from BTC are generally smaller than values from adsorption isotherm mainly because of shorter contact time.

In brief, results of BTC indicate that AOCM are capable of efficient and effective P treatment for rainfall runoff. BTC models, especially mechanistic models, would provide valuable and cost effective information in guiding design and operation of full-scale adsorption columns.

INTRODUCTION

The excessive use, discharge and dispersion of phosphate-containing compounds, given that phosphorus is a primary limiting nutrient in most lakes and reservoirs (Schindler 1977; Hecky and Kilham 1988), has exerted a tremendous ecological influence on the receiving water bodies and accelerated eutrophication which is characterized by bloom of algae and depletion of dissolved oxygen.

Rainfall-runoff contains elevated concentration of P which is pertinent to intensive anthropogenic activities such as urbanization, transportation, industrialization, development residential, and modernization of agriculture. In the last two decades, the growing legislative requirements on effluent discharges created an impetus for non-point source control of P and highlighted the demand for effective urban rainfall-runoff P treatment methods.

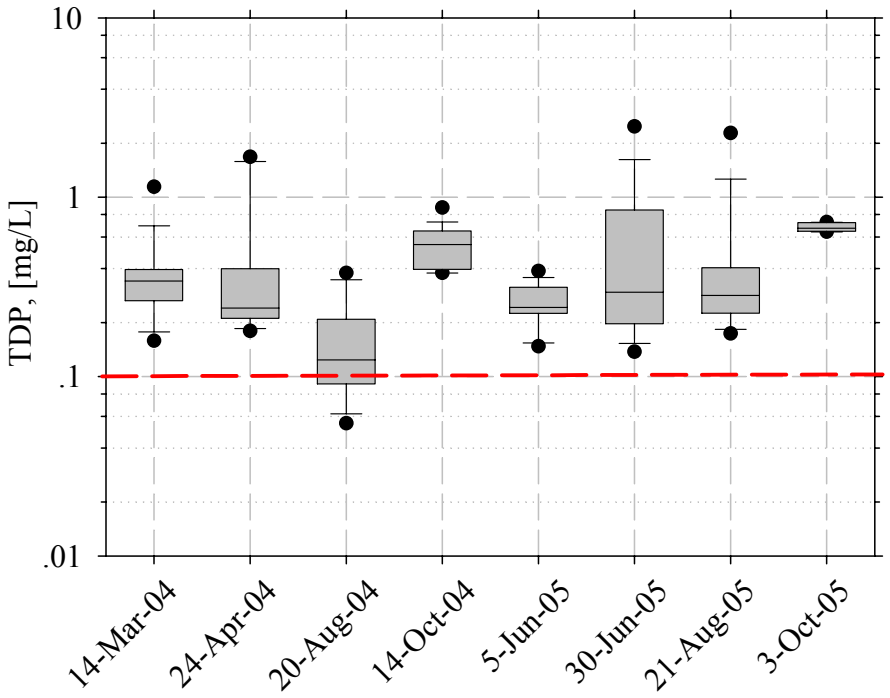

Figure 6-1. TDP Ranges of urban rainfall runoff effluent of hydrodynamic separator.

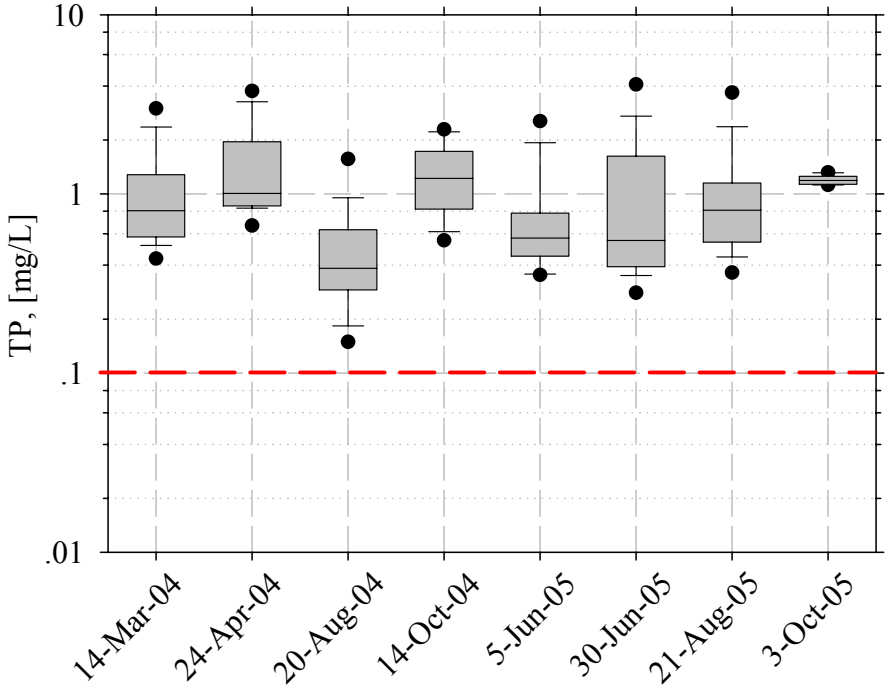

Figure 6-2. TP Ranges of urban rainfall runoff effluent of hydrodynamic separator.

In order to comply with discharge limitations of P, numerous biological, physical and chemical operations and processes for P removal from solution have been investigated and applied. Each of the operations and processes has its own advantage and disadvantage. One unit process is chemical adsorption by metal oxides of aluminum or iron. Such unit processes have potential viability due to their strong affinity for sorbing P even at low P concentrations. Therefore chemical adsorption becomes an effective and attractive process applicable to urban rainfall-runoff P treatment.

Aluminum oxide coated media (AOCM) with large surface area, microporous characteristic and chemical nature of their surface have made them potential adsorbents for the removal of P from rainfall-runoff. Some of the important advantages of AOCM over the other adsorbents are high adsorption capacity, low-cost, ready availability and sustainable supply, good selectivity, sufficient chemical durability and physical strength with low desorption potential for chemical adsorption phenomena that are generally irreversible under ambient rainfall-runoff conditions. Breakthrough curves through lab-scale fixed-bed P adsorption on AOCM would provide crucial information in assessing the feasibility of AOCM for actual rainfall-runoff P removal.

Numerous research studies have been carried out in an attempt to develop and assess new adsorbent for P removal. The major problem is that only scattered fixed-bed data are available and most of the data are based on batch equilibrium systems. The direct application of batch isotherm data for designing and adsorption systems often encounters problems and inferences from such data may lead to false direction without proper interpretation (Sperlich et al. 2005). The primary reason is that flow through an adsorption column is not at equilibrium. The extent of adsorption in flow through adsorption is dependent of diffusion, flow regimes and contacting

patterns (Burris et al. 1996). Consequently, carrying out lab-scale flow through and adsorption test becomes particularly appropriate prior to the full-scale design.

In addition to minimize operating and maintenance costs and to maximize treatment effectiveness, modeling the P adsorption on AOCM would provide valuable insights on the mechanism and necessary guidance on scale-up and operation strategies. P adsorption systems with AOCM could operate singly or preferably with other pretreatment technologies such as primary clarifiers or hydrodynamic separator as primary treatment. For in-situ rainfall-runoff treatment, systems are generally designed to operate under lower hydraulic gradients to treat and/or remove P in rainfall-runoff through gravitational flow.

In this study, we investigated the treatment of P in synthetic rainfall-runoff under the assumption that most of the particulate matter and particulate-bound P had been removed through some form of physical or hydrodynamic unit operation. As such, this bench-scale upflow adsorption column with a packed-bed of AOCM represents a secondary unit process that follows a primary unit operation in order to provide P effluent concentration below 0.1 mg/L prior to discharging to receiving waters. It is assumed that some form of primary unit operation treatment will attenuate primary influent to generate steadier flow for the AOCM adsorption system. Figure 6-1 and Figure 6-2 showed total dissolved phosphorus (TDP) and total phosphorus (TP) concentration ranges of hydrodynamic separator effluent.

OBJECTIVES

This study had a series of three objectives with respect to quantifying P adsorption breakthrough behavior of AOCM. The first objective was to investigate adsorption capacities of AOCM from breakthrough curves and verify the feasibility of AOCM as a potentially effective P adsorbent in flow-through situations. The second objective was to examine the breakthrough

behavior for a series of typical rainfall-runoff conditions on AOCM adsorption performance such as initial loading P concentration, surface loading rates, solution pH and presence of Ca^{2+}, SO_4^{2-}. The influence of media size was also examined in this parameter evaluation. The final goal was to simulate BTC by empirical and mechanistic models. The ability to predict BTC data through specific empirical and mechanistic models was assessed by coefficients of determination.

BACKGROUND

It is essential to understand mass transfer mechanisms in order to design a cost effective and efficient adsorption system. Usually four fundamental steps would occur for transport and reaction of adsorbate to a very porous adsorbent (Sperlich et al. 2005; Badruzzaman et al. 2004; Lee et al. 2003; Hatfield et al. 1996; Bai et al. 1996). These steps are:

1. bulk solution transport. The adsorbate is first transported from the bulk solution to the hydrodynamic boundary layer surrounding the adsorbent. The hydrodynamic boundary layer is assumed to be stationary and very thin. Depending on the velocity of bulk solution, this transport will occur either by diffusion or turbulent mixing.

2. film (external) transport. The adsorbate would then pass through the hydrodynamic boundary layer to the active surface sites of the adsorbent. Transport through the hydrodynamic boundary layer is dependent on the molecular diffusion and the thickness of the boundary layer.

3. intraparticle (internal) transport. After passing through the boundary layer, the adsorbate would diffuse through the pores or diffuse along the surface of pores to adsorptive sites. Depending on molecular diffusion, size of pores and chemical nature of pore surfaces, this intraparticle transport integrates pore diffusion through the solution in the pores and diffusion along the adsorbent surface before adsorption takes place.

4. adsorption and ultimate equilibrium. This final chemical reaction step is normally very fast.

Comparing the four steps, bulk transport and adsorption are rarely, if ever, rate-limiting steps. The transport mechanisms of concern, therefore, are external film diffusion and internal (intraparticle) diffusion. Previous work in this dissertation for P adsorption kinetics on AOCM indicates that pore diffusion is the rate limiting step.

BREAKTHROUGH CURVES AND MASS TRANSFER ZONE

Typically, the breakthrough curve profile follows an "S" shape when the effluent adsorbate concentration is plotted against elapse time or equivalent numbers of bed volume treated. The breakthrough point occurs when the effluent adsorbate concentration reaches a pre-determined maximum concentration, which depends on the treatment requirement and specific effluent concentration. Generally the specific effluent concentration is defined as the 5% or 10% of the influent concentration, or set to a specific effluent concentration, for example, 0.05 mg/L for TDP. The adsorption column may be considered exhausted when the effluent adsorbate concentration equals 90% or 95% of the influent concentration (Liu et al. 2005). In the adsorption column, the length of the mass transfer zone (MTZ) is a function of the hydraulic loading rate applied to the column, adsorbate concentration, solution pH, concentrations of enhancing and competing ions. Surface structure, surface area, and surface charge all have an impact on the MTZ profile. Bulk density, porosity and packing of adsorbent media also have an impact on the length of MTZ by affecting flow rates and flow pattern. For example, fast surface-loading rate, high adsorbate concentration and inappropriate solution pH, would cause the length of MTZ to be greater than the adsorption bed depth, resulting in rapid breakthrough. Therefore the adsorbate could not be removed completely by the adsorbent before the adsorbate moved out

of the adsorbent bed depth. For many breakthrough curves, the length of the mass transfer zone is expressed as follows (Metcalf and Eddy 2003).

$$H_{MTZ} = 2H\left[\frac{N_{ex} - N_{bt}}{N_{ex} + N_{bt}}\right] \qquad \text{Equation 6-1}$$

In this expression, H_{MTZ} is the length of mass transfer zone (m); H is the height of the adsorption column (m); N_{ex} is the number of bed volume at exhaustion; and $N_{bt}$is the number of bed volume at breakthrough.

BTC MODELING

Two empirical models (Thomas model and bed-depth-service-time (BDST) model) and two mechanistic models (mechanistic Freundlich model and mechanistic Langmuir model) were investigated for BTC of P adsorption on AOCM.

Thomas Model

This model developed by Thomas, which is widely used in the design of fixed bed adsorption systems, is summarized as follows. (Reynolds and Richards 1996; Lin and Huang 2000; Fu and Viraraghavan 2003; Thirunavukkarasu 2003):

$$\frac{C_t}{C_0} = \frac{1}{1 + \exp\left[\frac{k}{F}(Q_e m - C_0 V_b N_{BV})\right]} \qquad \text{Equation 6-2}$$

In this expression C_t is the effluent adsorbent concentration, [mg/L], C_0 is the influent adsorbent concentration, [mg/L], k is the Thomas rate constant, L/(min-mg), F is the volumetric flow rate, L/min.; Q_e is the overall adsorption capacity, [mg/g]; m is the dry mass of adsorbent, g; V_b is the bed volume, L; and N_{BV} is the number of bed volumes. In this study, nonlinear regression and a least-squares algorithm was utilized to examine the best estimate of constants k and Q_e for the Thomas model.

Bed-Depth-Service-Time (BDST) Model

The bed-depth-service-time model (Hutchins 1973; Srivastava et al. 1997; Jusoh et al. 2002) can be expressed as follows.

$$t = \frac{N_0 H}{C_0 u} - \frac{1}{kC_0} \ln\left(\frac{C_0}{C_t} - 1\right) \qquad \text{Equation 6-3}$$

In this expression t is the service time, min; H the adsorption bed depth, cm; N_0 is the adsorption capacity in mg of adsorbate based on mL of adsorbent, u is the superficial velocity, cm/min; k is the rate constant of adsorption (L/(min-mg); C_0 is the influent phosphorus concentration; and C_t is the effluent phosphorus concentration. After rearrangement by considering the adsorption column physical configurations and bed density, the BDST model can be converted to the Thomas model. Therefore this study would only use Thomas model instead of BDST model as an empirical model for the data simulation and prediction because of its simplicity.

Mechanistic Freundlich Model

The governing one-dimensional mass balance and transport equation (Brosillon et al. 2001) for predicting the P adsorption for a column filled with AOCM is as follows.

$$\varepsilon \frac{\partial C}{\partial t} + u\varepsilon \frac{\partial C}{\partial z} = -\rho \frac{\partial q}{\partial t} \qquad \text{Equation 6-4}$$

In this expression, ρ is the adsorption bed density, ε the bed void fraction, u the superficial velocity of feed influent, t the operating time, and z the distance from the inlet of the adsorption column and C and q are the phosphorus concentration in the liquid and solid phase, respectively. Assumptions associated with the mass balance and transport equation are as follows: a) mass transfer by convection is significant while radial and axial dispersions are insignificant; b) the flow pattern is ideal plug flow and flow rate is stable; c) No other reactions take place in the

column except adsorption; d) temperature in the column is uniform and invariant with time. The initial and boundary conditions associated with the mass balance equation are as follows.

$$C = 0 \ @t = 0 \ \ for \ 0 \le z \le H$$ Equation 6-5

$$C = C_0 \ @z = 0 \ \ for \ t > 0$$ Equation 6-6

In this expression H is the adsorption column height and C_0 is the feed phosphorus concentration in the liquid phase. The adsorption rate of phosphorus can be described by the following linear driving force model in terms of the overall liquid phase volumetric mass transfer coefficient.

$$\rho \frac{\partial q}{\partial t} = K_L a(C - C^*)$$ Equation 6-7

In this expression C is the P concentration in the bulk liquid phase, C^* is the P liquid phase concentration in equilibrium with the solid phase concentration q, a is the mass transfer area per unit volume of the bed, and K_L is the overall liquid phase mass transfer coefficient. $K_L a$ can be designated as the volumetric mass transfer coefficient in the liquid phase.

Taking account of wave propagation theory (Chern and Chien 2001), the introduction of the feed generates a self-sharpening wave. Because of the finite mass transfer rate, the self sharpening wave will eventually evolve into a constant pattern traveling at a constant velocity. In the constant pattern wave, the ratio of P concentrations in the liquid and solid phases is constant.

$$\frac{q}{C^*} = \frac{q_0}{C_0}$$ Equation 6-8

After rearrangement the following expression is generated.

$$C^* = \frac{q}{q_0} C_0$$ Equation 6-9

In this expression q_0 is the P concentration in the solid phase, which is in equilibrium with the feed solution P concentration, C_0. The Freundlich adsorption isotherm was taken into account for correlating P concentration in the liquid and solid phase as follows.

$$q = K_F C^n \qquad \text{Equation 6-10}$$

After combining the Freundlich isotherm, constant wave model, and linear driving force model into the fundamental mass balance and transport models, in addition to boundary and initial conditions, the following equation can be obtained and used to predict the breakthrough curve.

$$t = t_{1/2} + \frac{\rho K_F {C_0}^{n-1}}{K_L a}[\int_{1/2}^{y} \frac{1}{y - y^{1/n}} dy] \qquad \text{Equation 6-11}$$

In this expression y is the dimensionless effluent concentration of P (equal to C/C_0), $t_{1/2}$ is the half time for y = 1/2, which is obtained from the breakthrough experimental data. Overall volumetric mass transfer coefficient $K_L a$ can be obtained from fitting breakthrough experimental data by regression (Tien 1994).

$$\frac{dq}{dt} = K_L a(q_e - q) \qquad \text{Equation 6-12}$$

Mechanistic Langmuir Model

Derivation of mechanistic Langmuir model followed the same strategy of mechanistic Freundlich model except a Langmuir non linear isotherm was utilized.

$$q = \frac{q_m bC}{1 + bC} \qquad \text{Equation 6-13}$$

The following equation was obtained and used to predict the breakthrough curve (adapted from Cookson 1969; Yoshida et al. 2004).

$$N_{BV} = (\varepsilon + 1000\rho \frac{q_{e0}}{C_0}) - \frac{(1000\rho \frac{q_{e0}}{C_0})u}{K_f aH}[\ln \frac{0.5}{1-y} + (1 + \frac{1}{bC_0}) \ln \frac{1-y}{y}] \qquad \text{Equation 6-14}$$

where N_{BV} is the number of bed volume, ε adsorption bed porosity, ρ adsorption bed density, g/ml, C_0 phosphorus loading concentration, mg/L, q_{e0} adsorbent capacity in equilibrium with C_0 in terms of Langmuir isotherm, mg/g, K_f mass transfer coefficient, cm/s, *a* surface area per unit

volume of packing, cm^2/cm^3, H, adsorption column height, b, constant in the Langmuir isotherm, y, ratio of P effluent concentration to influent concentration. Mass transfer coefficient K_f was correlated by Eqn. 15, Eqn. 16 and Eqn. 17 (Lee et al. 2000; Ko et al. 2001; Cookson 1969).

$$\frac{K_f}{u} = \frac{1.26Sc^{-2/3}\,\mathrm{Re}^{-2/3}}{\varepsilon} \qquad \text{Equation 6-15}$$

$$S_c = \frac{\mu}{\rho_w D_m} \qquad \text{Equation 6-16}$$

$$\mathrm{Re}_d = \frac{Du\rho_w\varepsilon}{60\mu} \qquad \text{Equation 6-17}$$

Where:

Sc: The dimensionless Schmidt number

Re_d: The dimensionless Reynolds number

ε: bed porosity

u superficial velocity cm/s

μ: dynamic viscosity of water (1.009×10^{-2} g/cm-sec)

ρ_w: the density of water (1 g/cm^3)

D_m: Phosphate molecular diffusion coefficient 8.79×10^{-6} cm^2/s (Edwards and Huffman 1959)

D: inner diameter of adsorption bed, cm;

u: superficial velocity (cm/min);

METHODOLOGY AND MATERIALS

EXPERIMENTAL PROCEDURE FOR COLUMN BREAKTHROUGH

Phosphorus adsorption on AOCM column under continuous loading was investigated and presented as breakthrough curves, which is plotted by the ratio of effluent concentration (C_e) to influent concentration (C_0) against the bed volume numbers (equivalent to cumulative volume)

of synthetic urban rainfall-runoff flowing through the column. The column design is illustratively shown in Figure 6-3.

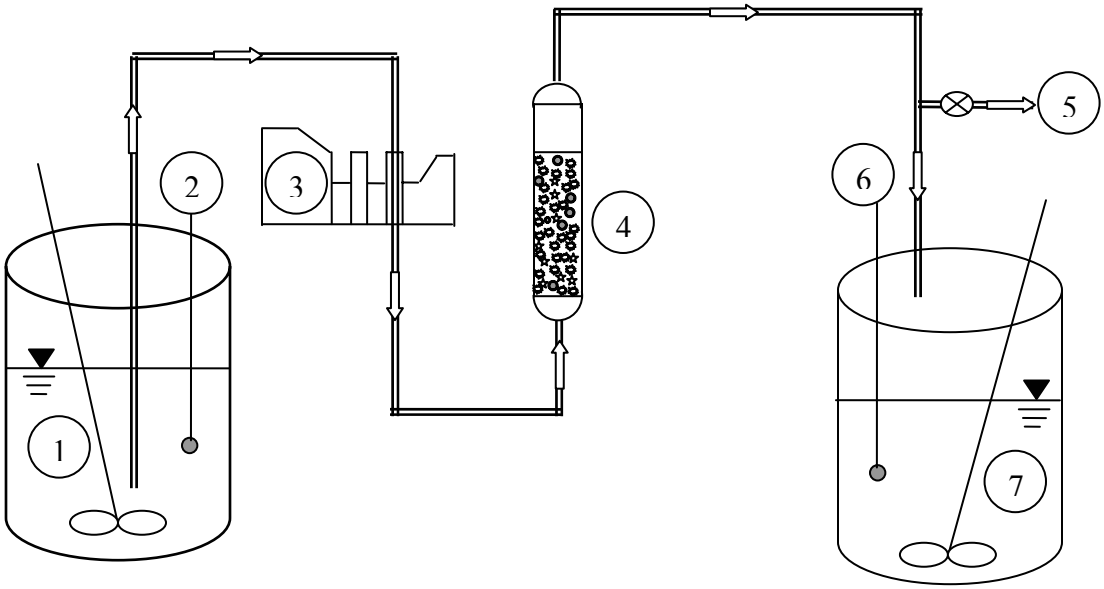

1: P feed tank (20 L);
2: Influent pH meter and recorder
3: Peristaltic pump;
4: P adsorption column filled by AOCM
5: Sampling port;
6: Effluent pH meter and recorder
7: Effluent tank (20 L)

Figure 6-3. Schematic experimental configuration of P adsorption breakthrough on AOCM.

Column experiments are carried out in Teflon PFA column with internal diameters of 4.5 cm and length of 8 cm. The column diameter of 4.5 cm is based on maintaining a column diameter to media diameter ratio (D/d) greater than 12 without the introduction of significant influence on axial velocity profiles and wall skin friction in laboratory columns (Chellam and Wiesner 1993). Packed bed length is dependent on media capacity to keep a reasonable breakthrough time. The main component of the experimental configuration type is a packed-bed reactor column in which media is loaded to measure the breakthrough capacity. Screens with fine aperture were placed at the bottom and top of the column to prevent the loss of AOCM during the test. Accurately measured 40 g desiccated AOCM was used in adsorption experiments. The

porosity of the column was determined by comparing the column weight before and after saturation and was verified by the measured volume of water added to just saturate the column. Influent P concentration was set up as the desired value. The influent is stored in a 20-L polypropylene container. The constant influent upflow feed to the column is supplied by use of a multi-channel peristaltic pump. Once the pump is calibrated, column runs are initiated, monitored and terminated through the pump. The influent pH is adjusted to a specified value and controlled with an accuracy of ± 0.2 pH units. The Effluent pH is measured and recorded at 10 to 30-minutes interval to quantify any pH drift. Sampling of column effluent is timed such that the breakthrough curve (BTC) can be clearly defined from a sufficient number of data points. The periodic effluent samples collected were measured by HACH DR/2000 Spectrophotometer for phosphorus content using ascorbic acid method (Standard Method 1998).

Mass of P retained was determined by integration of breakthrough curves.

FLOW RATES AND FLOW REGIME

The range of influent flow rates of column runs is based on real-time range of rainfall-runoff surface loadings. For example, a design flow of 50 L/(m^2-min) is utilized for the peak of 1-year return event at an experimental site treating overland flow (Sansalone and Buchberger 1997). Therefore the surface loading rates used in this study range from 20 to 65 L/m^2-min. Since the internal diameter of column is 4.5 cm, the equivalent influent flow rates will be 30 to 100 ml/min and superficial velocities 2 to 6.5 cm/min. This loading rate range is typical of many urban rainfall-runoff conditions where unit operation and process such as a partial exfiltration reactor (PER) are applied for in-situ treatment. The decision to utilize a peak flow typical of a hydrograph from a moderately high intensity rainfall-runoff event as compared for example to a 1-month return event will under-estimate PER breakthrough capacity. Bench-scale results from

other researchers using columns packed with GAC and wastewater influent had improved breakthrough capacity as hydraulic loading rates were lowered (Reed et al. 1996)
The flow regime is computed by the Reynolds number as in Eqn. 17 discussed earlier. Reynolds number for all the tested conditions were slightly greater than 1, therefore flow was located in turbulent regime which is close to the typical situation of rainfall-runoff.

A variety of conditions was carried out to study their effects on BTC. Three sizes of AOCM (0.85 ~ 2 mm; 2 ~ 4.75 mm; 4.75 ~ 9.5 mm) were tested for the effect of size of adsorbent. Surface loading rates ranged from 20 to 65 L/(m^2-min). Influent pH varied from 6 to 8 adjusted by 0.1 N HCl and 0.1 N NaOH. Influent P concentrations differed from 1 to 5 mg/L. Ions such as Calcium and Sulfate were introduced to the P adsorption column by AOCM to investigate competitive or enhancing effect. All the conditions used were consistent with typical values of urban rainfall-runoff.

RESULTS

The breakthrough curves (BTC) for P adsorption on AOCM were constructed under different conditions by plotting the normalized effluent concentration (C/C_0) versus equivalent number of bed volumes (BV). BTC fitted by Bed-Depth-Service-Time (BDST) or Thomas model, mechanistic Freundlich model and mechanistic Langmuir model was illustrated in Figure 6-4. Experiment was carried out at influent P 0.5 mg/L; pH7; ionic strength 0.01M KCl; AOCM size 2 ~ 4. 75 mm; surface loading 40 L/(m^2-min). All the BTC experimental conditions and primary results were summarized in Table 6-1. The parameters corresponding to each model were shown in Table 6-2, Table 6-3, and Table 6-4 respectively. The bed volumes for breakthrough and exhaustion were 221 and 673 respectively.

Table 6-1. Summary of BTC experimental conditions and primary results.

Effect	size	Conc.	Surface loading	pH	Ca^{2+}	SO_4^{2-}	H	N_{bt}	N_{ex}	q_e
	mm	mg/L	L/(m^2-min)		mg/L	mg/L	cm			mg/g
size	**0.85 ~ 2**	0.5	40	7	0	0	4.06	440	810	0.4533
	2 ~ 4.75	0.5	40	7	0	0	5.12	221	673	0.3588
	4.75 ~ 9.5	0.5	40	7	0	0	4.33	142	492	0.3021
Conc.	2 ~ 4.75	**0.5**	40	7	0	0	4.33	221	673	0.3588
	2 ~ 4.75	**1**	40	7	0	0	4.33	125	452	0.4663
	2 ~ 4.75	**2.5**	40	7	0	0	4.33	19	332	0.7133
	2 ~ 4.75	**5**	40	7	0	0	4.33	8	182	0.7352
surface loads	2 ~ 4.75	0.5	**20**	7	0	0	4.33	387	831	0.4540
	2 ~ 4.75	0.5	**40**	7	0	0	4.33	221	673	0.3588
	2 ~ 4.75	0.5	**65**	7	0	0	4.33	184	523	0.2885
pH	2 ~ 4.75	0.5	40	**6**	0	0	4.33	426	913	0.5255
	2 ~ 4.75	0.5	40	**7**	0	0	4.33	221	673	0.3588
	2 ~ 4.75	0.5	40	**8**	0	0	4.33	96	391	0.2048
Ca^{2+}	2 ~ 4.75	0.5	40	7	**15**	0	4.33	228	681	0.3779
SO_4^{2-}	2 ~ 4.75	0.5	40	7	0	**35**	4.33	124	625	0.3278

Table 6-2. Parameters of Thomas model for BTC data fitting.

	C_0	BV	m	F	k	Q_e	R^2
	mg/L	L	g	L/min	L/(min-mg)	mg/g	
40 L/(m^2-min); pH7; 2 ~ 4.75 mm; 0.5 mg/L	0.5	0.065	40	0.0625	0.0204	0.3559	0.995
40 L/(m^2-min); pH7; 2 ~ 4.75 mm; 1 mg/L	1	0.065	40	0.0625	0.0131	0.4633	0.996
40 L/(m^2-min); pH7; 2 ~ 4.75 mm; 2.5 mg/L	2.5	0.065	40	0.0625	0.0048	0.7341	0.995
40 L/(m^2-min); pH7; 2 ~ 4.75 mm; 5 mg/L	5	0.065	40	0.0625	0.0050	0.5931	0.994
20 L/(m^2-min); pH7; 2 ~ 4.75 mm; 0.5 mg/L	0.5	0.065	40	0.03	0.0082	0.4497	0.994
65 L/(m^2-min); pH7; 2 ~ 4.75 mm; 0.5 mg/L	0.5	0.065	40	0.1	0.0382	0.2957	0.996
40 L/(m^2-min); pH8; 2 ~ 4.75 mm; 0.5 mg/L	0.5	0.065	40	0.0625	0.0282	0.1995	0.994
40 L/(m^2-min); pH6; 2 ~ 4.75 mm; 0.5 mg/L	0.5	0.065	40	0.0625	0.0152	0.5257	0.992
40 L/(m^2-min); pH7; 4.75~ 9.5 mm; 0.5 mg/L	0.5	0.077	40	0.0625	0.0197	0.3023	0.997
40 L/(m^2-min); pH7; 0.85 ~ 2 mm; 0.5 mg/L	0.5	0.061	40	0.0625	0.0230	0.4537	0.989
Ca 15mgL added; 40 L/(m^2-min); pH7; 2 ~ 4.75 mm; 0.5 mg/L	0.5	0.065	40	0.0625	0.0172	0.3962	0.995
SO4 35mgL added; 40 L/(m^2-min); pH7; 2 ~ 4.75 mm; 0.5 mg/L	0.5	0.065	40	0.0625	0.0158	0.3490	0.995

Table 6-3. Parameters of Mechanistic Freundlich model for BTC data fitting.

	$t_{1/2}$	BV	ρ_b	K_F	n	K_La	R^2
	min	ml	g/ml			1/min	
40 L/(m^2-min); pH7; 2 ~ 4.75 mm; 0.5 mg/L	440	65	0.62	0.72	0.41	0.0023	0.926
40 L/(m^2-min); pH7; 2 ~ 4.75 mm; 1 mg/L	280	65	0.62	0.72	0.41	0.0037	0.982
40 L/(m^2-min); pH7; 2 ~ 4.75 mm; 2.5 mg/L	180	65	0.62	0.72	0.41	0.0056	0.837
40 L/(m^2-min); pH7; 2 ~ 4.75 mm; 5 mg/L	75	65	0.62	0.72	0.41	0.0114	0.977
20 L/(m^2-min); pH7; 2 ~ 4.75 mm; 0.5 mg/L	1400	65	0.62	0.72	0.41	0.0011	0.921
65 L/(m^2-min); pH7; 2 ~ 4.75 mm; 0.5 mg/L	200	65	0.62	0.72	0.41	0.0044	0.765
40 L/(m^2-min); pH8; 2 ~ 4.75 mm; 0.5 mg/L	250	65	0.62	0.61	0.37	0.0047	0.773
40 L/(m^2-min); pH6; 2 ~ 4.75 mm; 0.5 mg/L	675	65	0.62	1.09	0.28	0.0016	0.858
40 L/(m^2-min); pH7; 4.75~9.5 mm; 0.5mg/L	375	77	0.53	0.65	0.4	0.0029	0.894
40 L/(m^2-min); pH7; 0.85 ~ 2 mm; 0.5 mg/L	625	61	0.66	1.35	0.32	0.0016	0.945
Ca 15mgL added; 40 L/(m^2-min); pH7; 2 ~ 4.75 mm; 0.5 mg/L	500	65	0.62	0.84	0.37	0.0021	0.905
SO4 35mgL added; 40 L/(m^2-min); pH7; 2 ~ 4.75 mm; 0.5 mg/L	420	65	0.62	0.52	0.43	0.0026	0.823

Table 6-4. Parameters of Mechanistic Langmuir model for BTC data fitting.

	q_m	b	ε	ρ_b	u	K_f	Re	R^2
	mg/g			g/ml	cm/min	cm/min		
40 L/(m^2-min); pH7; 2 ~ 4.75 mm; 0.5 mg/L	2.52	0.34	0.74	0.62	4	0.0085	21.6	0.90
40 L/(m^2-min); pH7; 2 ~ 4.75 mm; 1 mg/L	2.52	0.34	0.74	0.62	4	0.0085	21.6	0.98
40 L/(m^2-min); pH7; 2 ~ 4.75 mm; 2.5 mg/L	2.52	0.34	0.74	0.62	4	0.0085	21.6	0.80
40 L/(m^2-min); pH7; 2 ~ 4.75 mm; 5 mg/L	2.52	0.34	0.74	0.62	4	0.0085	21.6	0.70
20 L/(m^2-min); pH7; 2 ~ 4.75 mm; 0.5 mg/L	2.52	0.34	0.74	0.62	2	0.0067	10.8	0.89
65 L/(m^2-min); pH7; 2 ~ 4.75 mm; 0.5 mg/L	2.52	0.34	0.74	0.62	6.5	0.0104	35.1	0.79
40 L/(m^2-min); pH8; 2 ~ 4.75 mm; 0.5 mg/L	1.91	0.3	0.74	0.62	4	0.0085	21.6	0.82
40 L/(m^2-min); pH6; 2 ~ 4.75 mm; 0.5 mg/L	2.38	0.68	0.74	0.62	4	0.0085	21.6	0.94
40 L/(m^2-min); pH7; 4.75~9.5 mm; 0.5mg/L	2.13	0.38	0.78	0.53	4	0.0082	22.7	0.89
40 L/(m^2-min); pH7; 0.85 ~ 2 mm; 0.5 mg/L	2.71	0.5	0.72	0.66	4	0.0086	21	0.82
Ca 15mgL added; 40 L/(m^2-min); pH7; 2 ~ 4.75 mm; 0.5 mg/L	2.79	0.28	0.74	0.62	4	0.0085	21.6	0.84
SO4 35mgL added; 40 L/(m^2-min); pH7; 2 ~ 4.75 mm; 0.5 mg/L	2.04	0.28	0.74	0.62	4	0.0085	21.6	0.84

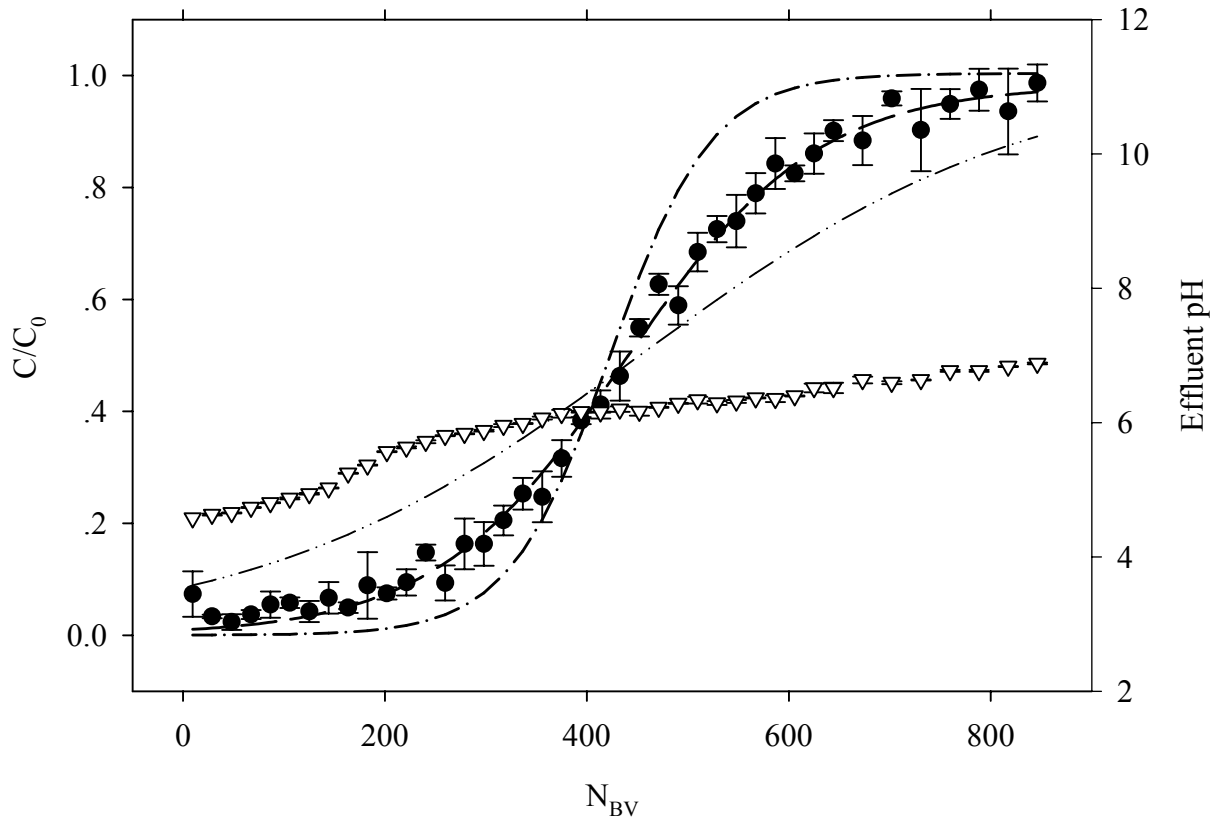

Figure 6-4. Illustration of Breakthrough curve fitted by Bed-Depth-Service-Time (BDST) or Thomas model, mechanistic Langmuir model and mechanistic Freundlich model, respectively. Experiment was carried out: influent P 0.5 mg/L; pH7; ionic strength 0.01M KCl; AOCM size 2 ~ 4. 75 mm; surface loading 40 L/(m^2-min). The parameters corresponding to each model were shown in Table 6-2, Table 6-3 and Table 6-4.

The effluent pH gradually increased from about 5 to 7 which happened to be the pre-setup influent value. The variation of effluent pH under this experimental condition represented the typical pattern of pH change during BTC process for P adsorption on AOCM except the ending pH would reach to pH 6 or 8 when the influent pH value was set as 6 or 8. Therefore it was suggested that effluent pH would start at about 5 and reach same value of influent pH at exhaustion capacity of AOCM. The high value of correlation coefficient of Thomas model (0.995) indicates that Thomas model could represent data very well. The correlation coefficients for mechanistic Freundlich and mechanistic Langmuir were 0.926 and 0.9 respectively which

suggest that these two models were very successful in predicting data. Comparatively, mechanistic Freundlich model followed the data trend better than mechanistic Langmuir model.

EFFECT OF SIZE OF AOCM

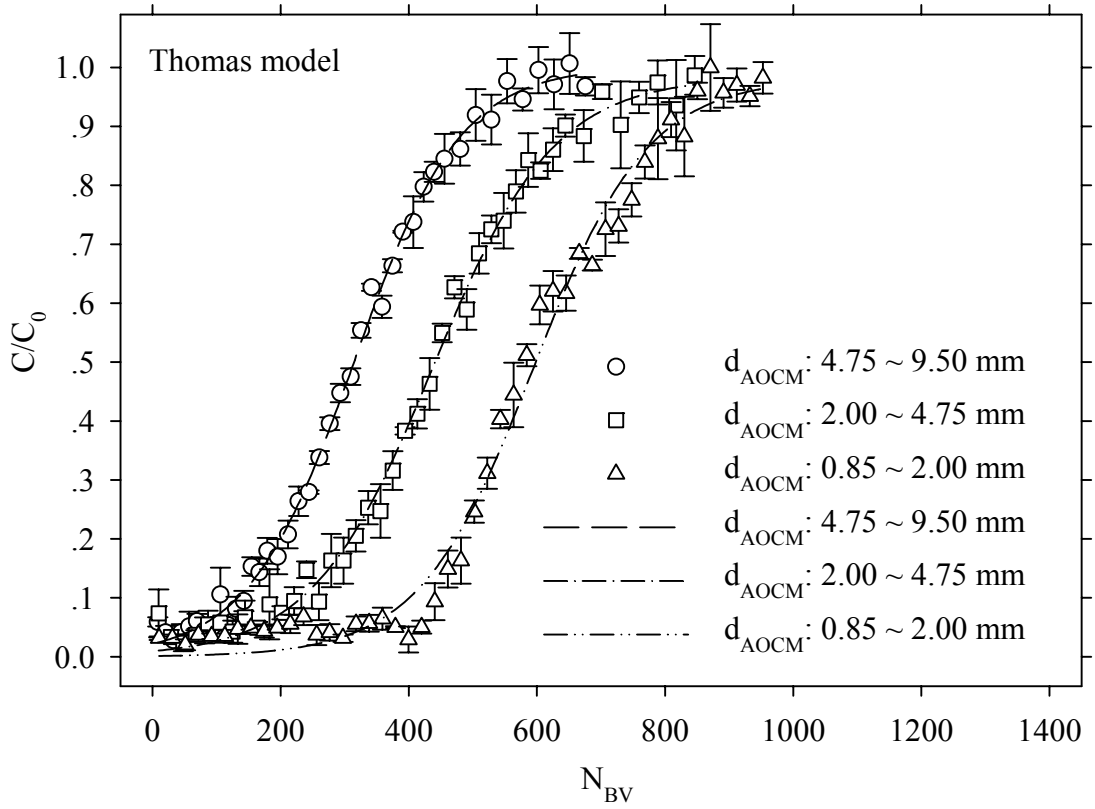

Figure 6-5. Size effect on BTC of P adsorption on AOCM fitted by Thomas model. Experiments were carried out: size 0.85~2 mm, 2~4. 75 mm, 4.75~9.5 mm; surface loading 40 L/(m^2-min). P 0.5 mg/L; pH7; 0.01M KCl. The parameters related to the model were shown in Table 6-2.

Size effect on BTC of P adsorption on AOCM was depicted in Figure 6-5. The numbers of bed volume of breakthrough were 440, 221 and 142 and the numbers of bed volume of exhaustion were 810, 673 and 492 for size of AOCM of 0.85 ~ 2 mm, 2 ~ 4.75 mm and 4.75 ~ 9.5 mm respectively. Apparently, better BTC occurred at smaller size of AOCM. Conceived as a surface phenomenon, adsorption would be enhanced with finer adsorbent size. The smaller adsorbent sizes would provide comparatively larger surface areas and hence higher adsorption capacities were obtained. Adsorption capacities from BTC were 0.4523, 0.3588 and 0.3021 mg/g

for size of AOCM of 0.85 ~ 2 mm, 2 ~ 4.75 mm and 4.75 ~ 9.5 mm respectively. Medium AOCM size range (2 ~ 4.75 mm) was primarily studied in this work.

EFFECT OF P CONCENTRATION

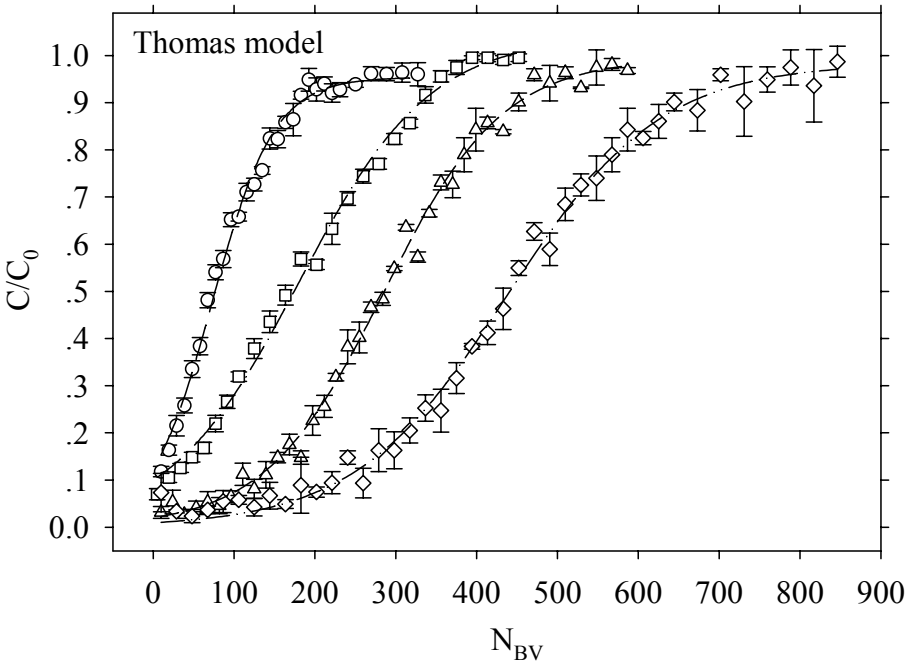

Figure 6-6. Influent P concentration effect on BTC of P adsorption on AOCM fitted by Thomas model. Experiments were carried out: influent P 0.5 mg/L, 1 mg/L, 2.5 mg/L, 5 mg/L respectively; pH7; 0.01M KCl; AOCM size 2 ~ 4. 75 mm; surface loading 40 L/(m^2-min). The parameters related to the model were shown in Table 6-2.

Influent P concentration effect on BTC of P adsorption on AOCM was shown in Figure 6-6. The numbers of bed volume of breakthrough were 8, 19, 125 and 221 and the numbers of bed volume of exhaustion were 182, 332, 452 and 673 for P concentration of 5 mg/L, 2.5 mg/L, 1 mg/L and 0.5 mg/L respectively. Clearly, increasing the influent concentration significantly reduced the predicted service time and better BTC results favors lower concentrations. Under the same residence time and other corresponding conditions, high concentrations of P may already flow our of adsorption bed before sufficiently contacting AOCM because certain amount of AOCM may not suffice the high loading of P mass. Nonetheless, adsorption capacities from

BTC were 0.7352, 0.7133, 0.4663 and 0.3588 mg/g for P concentration of 5 mg/L, 2.5 mg/L, 1 mg/L and 0.5 mg/L respectively. P concentration of 0.5 mg/L was primarily studied in this work.

EFFECT OF SURFACE LOADING RATE

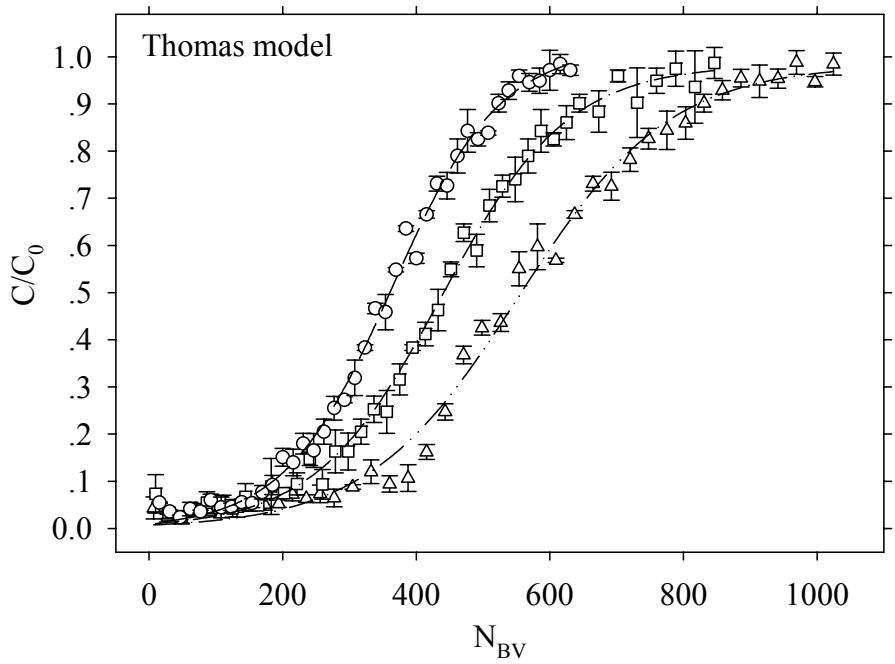

Figure 6-7. Surface loading effect on BTC of P adsorption on AOCM fitted by Thomas model. Experiments were carried out: surface loading 20, 40, 60 L/(m^2-min) respectively; P 0.5 mg/L; pH value of 7; 0.01M KCl; size 2 ~ 4. 75 mm. The parameters related were shown in Table 6-2.

Variation of the adsorbed P amount and BTC at different surface loading rates was determined and shown in Figure 6-7. The numbers of bed volume of breakthrough were 387, 221 and 184 and the numbers of bed volume of exhaustion were 831, 673 and 523 for surface loading of 20 L/(m^2-min), 40 L/(m^2-min), 65 L/(m^2-min) respectively. Evidently, the removal of P exhibited better performance at lower surface loading of 20 L/(m^2-min). The lower surface loading, as expected, induces more effective P removal due to the higher empty bed contact time (EBCT). EBCT were 2.2, 1.1 and 0.7 min for surface loading of 20 L/(m^2-min), 40 L/(m^2-min), 65 L/(m^2-min) respectively. The curves of similar shape at different surface loading rates suggest

that the rate determining step of adsorption is the intraparticle diffusion. Moderate surface loading of 40 L/(m^2-min) was mainly studies in this work.

EFFECT OF SOLUTION PH

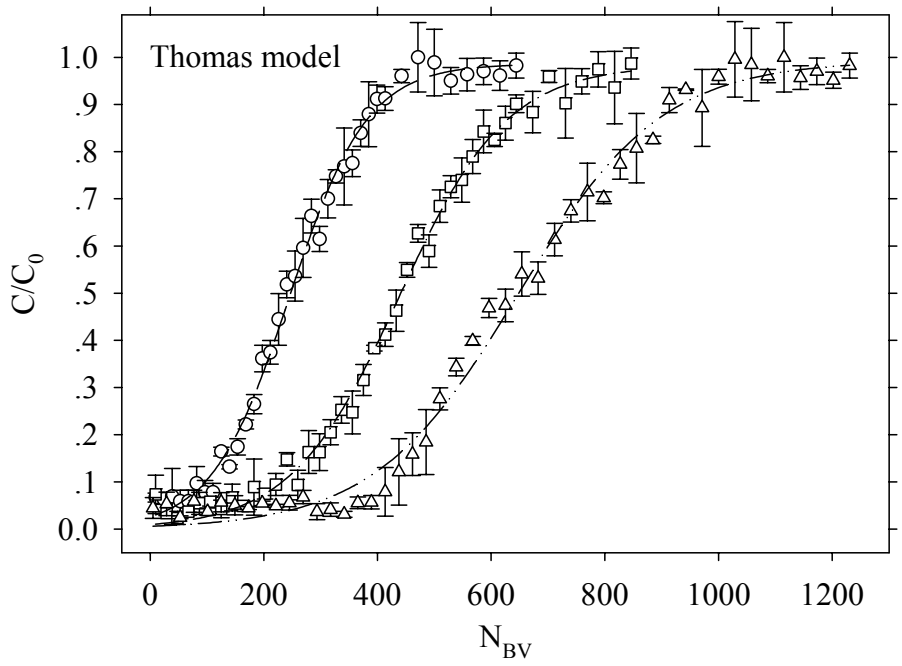

Figure 6-8. pH effect on BTC of P adsorption on AOCM fitted by Thomas model. Experiments were carried out: pH 6, 7, 8 respectively; influent P 0.5 mg/L; 0.01M KCl; size 2 ~ 4. 75 mm, surface loading 40 L/(m^2-min). The parameters related to the model were shown in Table 6-2.

Variation of BTC of P adsorption on AOCM at different solution pH was depicted in Figure 6-8. The numbers of bed volume of breakthrough were 426, 221 and 96 and the numbers of bed volume of exhaustion were 913, 673 and 391 for solution pH of 6, 7 and 8 respectively. Evidently, the removal of P exhibited better performance at slightly acidic pH of 6. Slightly acidic pH, as expected, induces more effective P removal due to the chemisorption characteristics of AOCM favoring low pH.

EFFECT OF COEXISTING IONS

Difference of BTC performance with presence of coexisting ions such as Calcium and Sulfate were depicted in Figure 6-9.

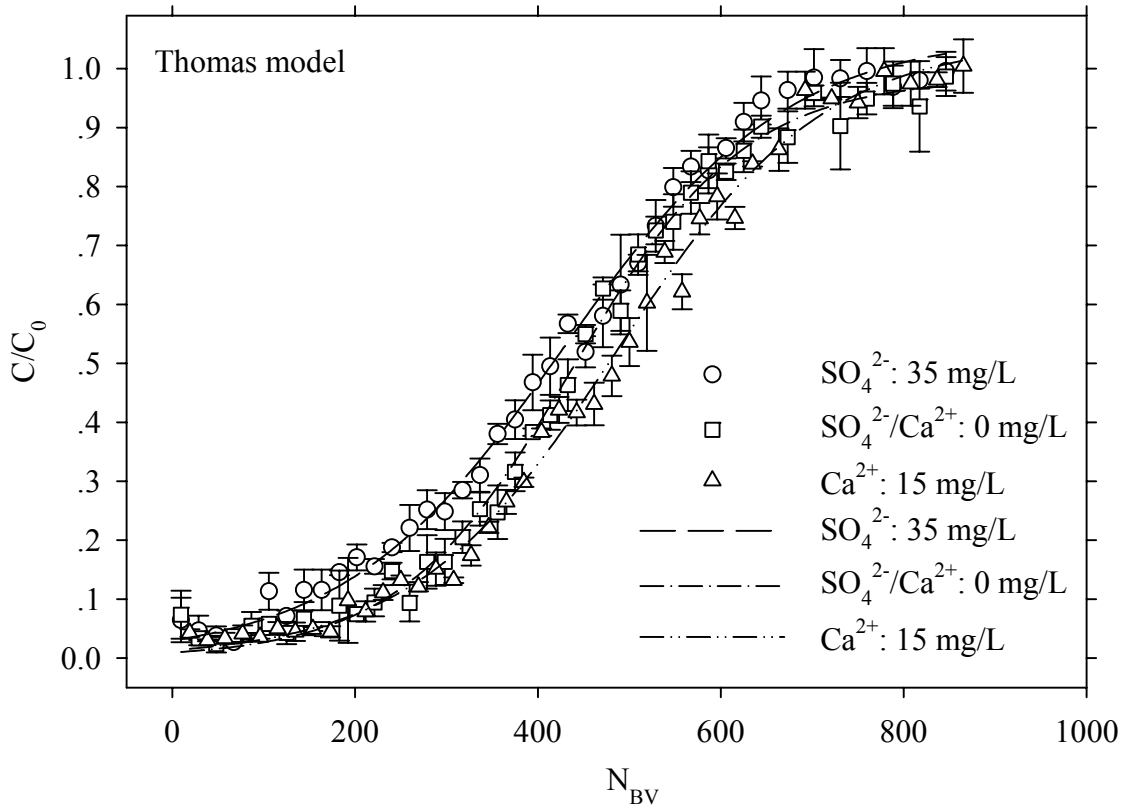

Figure 6-9. Foreign ions effect on BTC of P adsorption on AOCM fitted by Thomas model. Experiments were carried out: influent P 0.5 mg/L with presence of Sulfate 35 mg/L, influent P 0.5 mg/L only, influent P 0.5 mg/L with presence of Calcium 15 mg/L; pH7; ionic strength 0.01M KCl; AOCM size 2 ~ 4. 75 mm; surface loading 40 L/(m^2-min). The parameters corresponding to the model were shown in Table 6-2.

The numbers of bed volume of breakthrough were 124, 221 and 228, the numbers of bed volume of exhaustion were 625, 673 and 681, and the adsorption capacities from BTC were mg/g 0.3278, 0.3588 and 0.3779 mg/g for influent P 0.5 mg/L with presence of Sulfate 35 mg/L, influent P 0.5 mg/L only, influent P 0.5 mg/L with presence of Calcium 15 mg/L respectively. Apparently, Sulfate inhibited and Calcium promoted P adsorption on AOCM. However both effects were indicated to be limited under typical urban rainfall runoff conditions due to the low interacting concentration levels. In addition, the competition effect by Sulfate could be

compensated by enhancing effect by Calcium. Therefore it is suggested effects of coexisting ions of urban rainfall runoff P adsorption on AOCM are insignificant.

APPLICABILITY OF BTC MODELS

The BTC data of P adsorption on AOCM constructed under different conditions were fitted with Thomas model (Figure 6-5, Figure 6-6, Figure 6-7, Figure 6-8 and Figure 6-9), mechanistic Freundlich model (Figure 6-10, Figure 6-11, Figure 6-12, Figure 6-13and Figure 6-14)and mechanistic Langmuir model (Figure 6-15, Figure 6-16, Figure 6-17, Figure 6-18 and Figure 6-19), with all the corresponding parameters were shown in Table 6-2, Table 6-3 and Table 6-4 respectively.

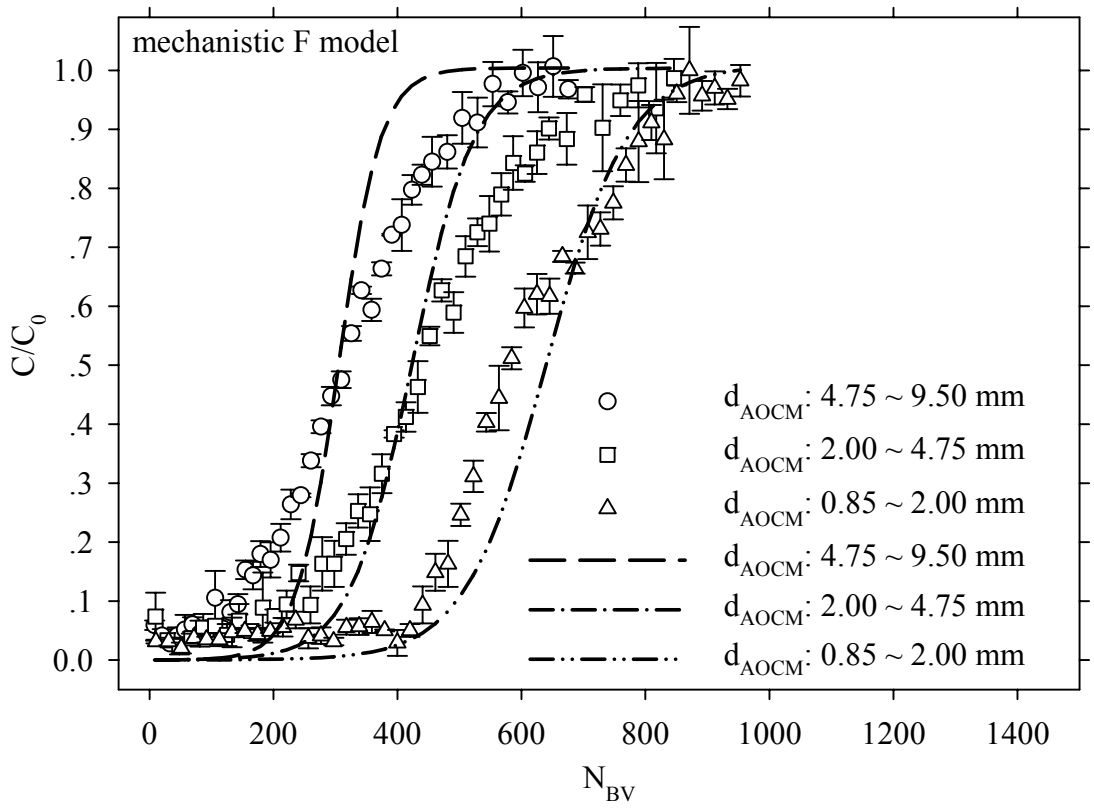

Figure 6-10. Size effect on BTC of P adsorption on AOCM fitted by mechanistic Freundlich model. Parameters related were shown in Table 6-3.

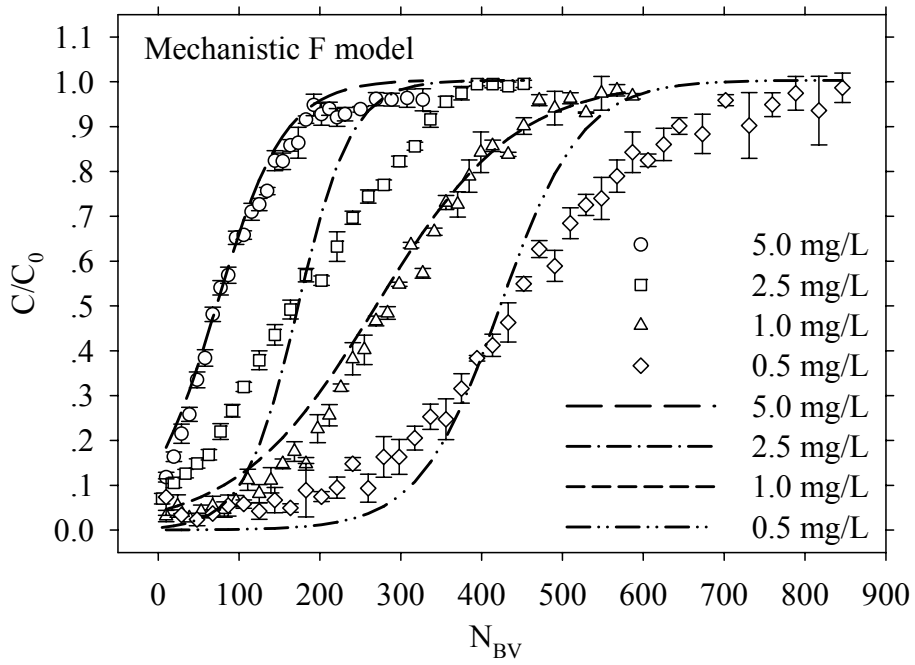

Figure 6-11. Influent P concentration effect on BTC of P adsorption on AOCM fitted by mechanistic Freundlich model. The parameters were shown in Table 6-3.

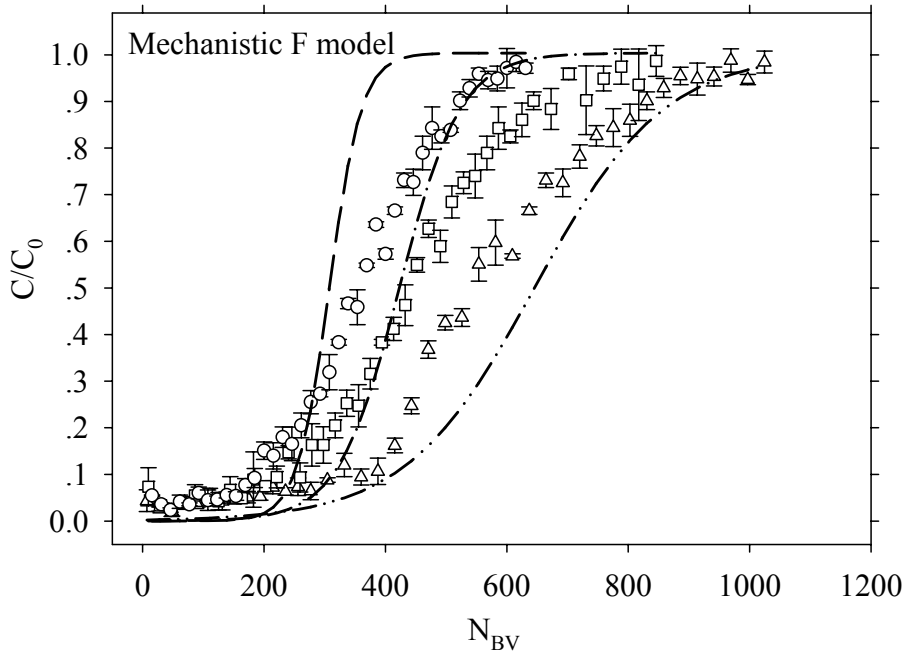

Figure 6-12. Surface loading rate effect on BTC of P adsorption on AOCM fitted by mechanistic Freundlich model. The parameters were shown in Table 6-3.

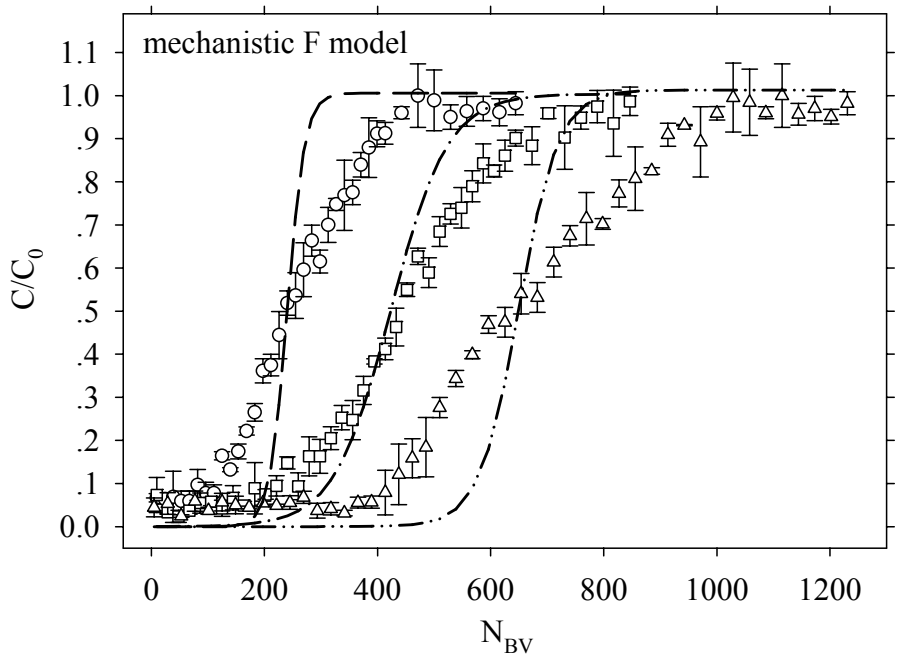

Figure 6-13. pH effect on BTC of P adsorption on AOCM fitted by mechanistic Freundlich model. The parameters related were shown in Table 6-3.

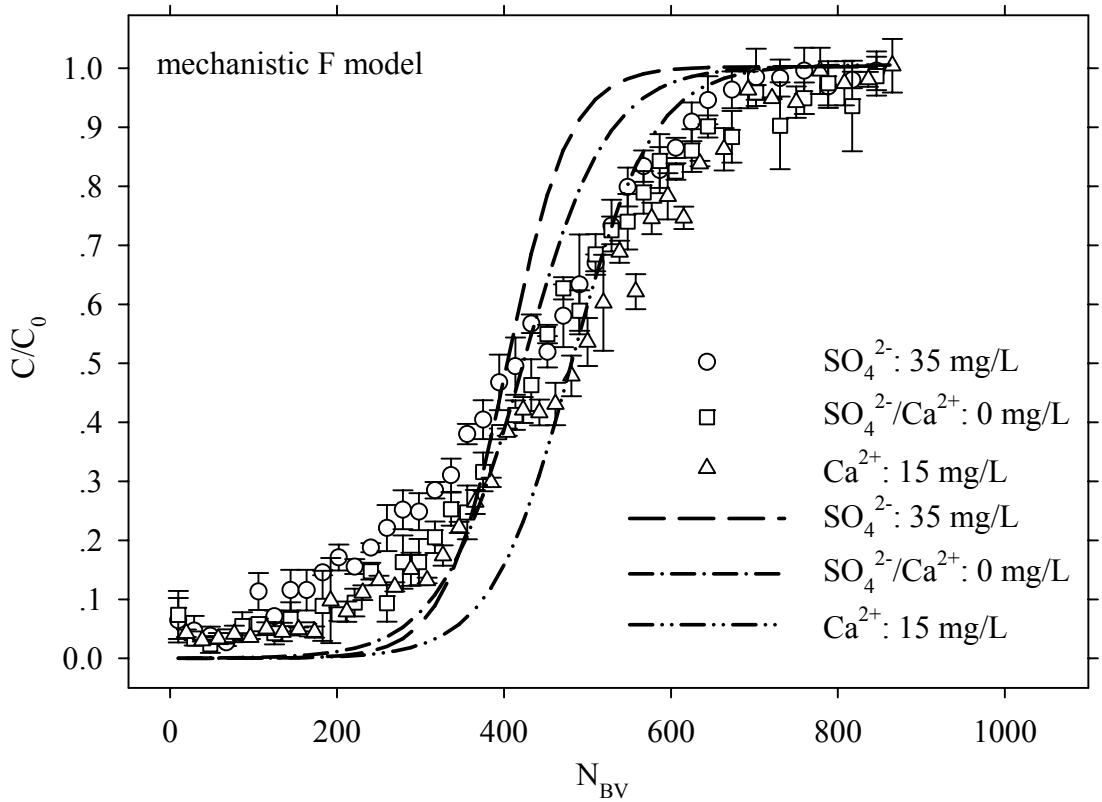

Figure 6-14. Foreign ions effect on BTC of P adsorption on AOCM fitted by mechanistic Freundlich model. The parameters corresponding to the model were shown in Table 6-3.

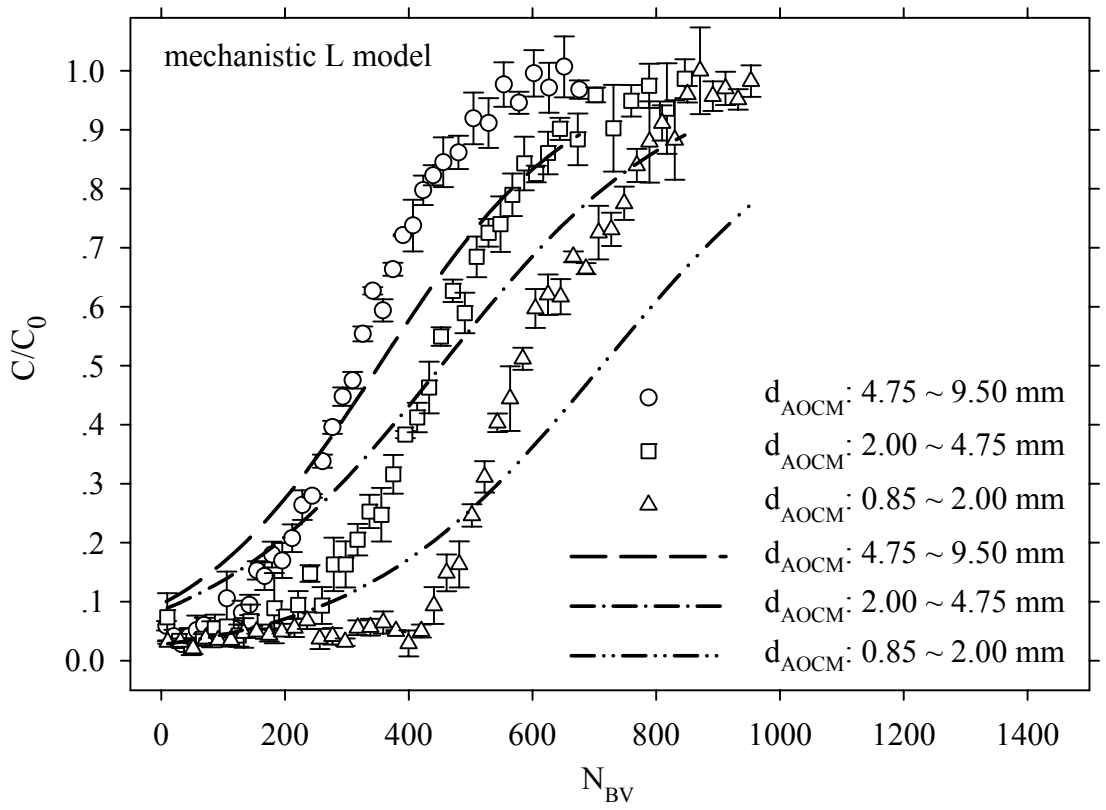

Figure 6-15. Size effect on BTC of P adsorption on AOCM fitted by mechanistic Langmuir model. Parameters related were shown in Table 6-4.

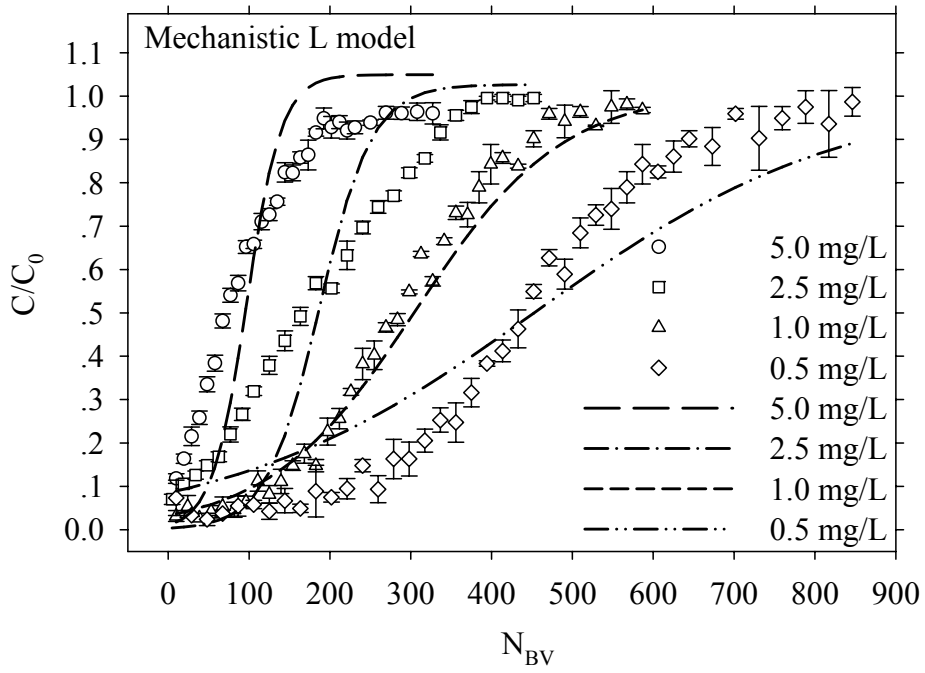

Figure 6-16. Influent P concentration effect on BTC of P adsorption on AOCM fitted by mechanistic Langmuir model. The parameters of the model were shown in Table 6-4.

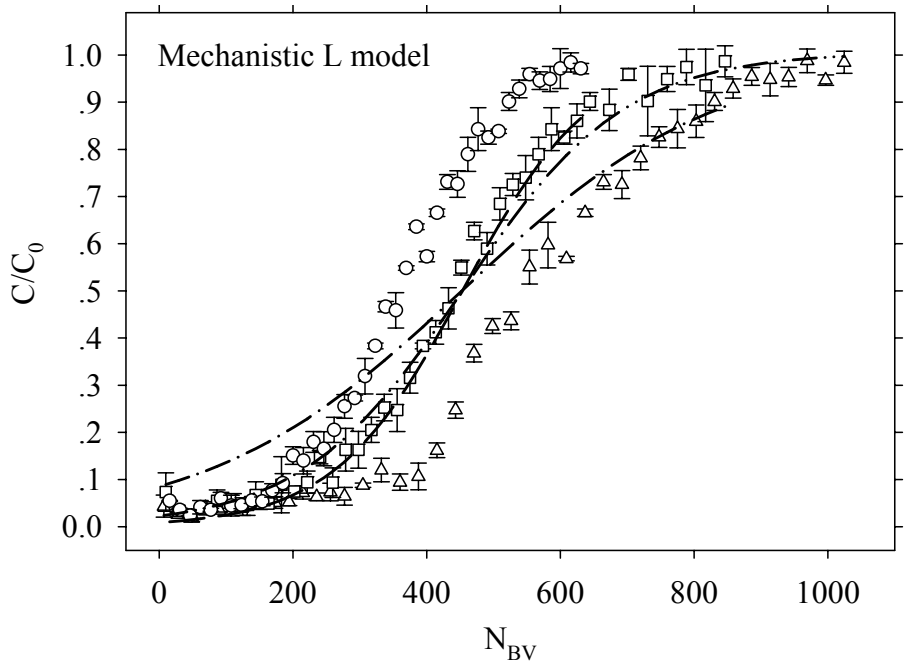

Figure 6-17. Surface loading rate effect on BTC of P adsorption on AOCM fitted by mechanistic Langmuir model. The parameters corresponding to the model were shown in Table 6-4.

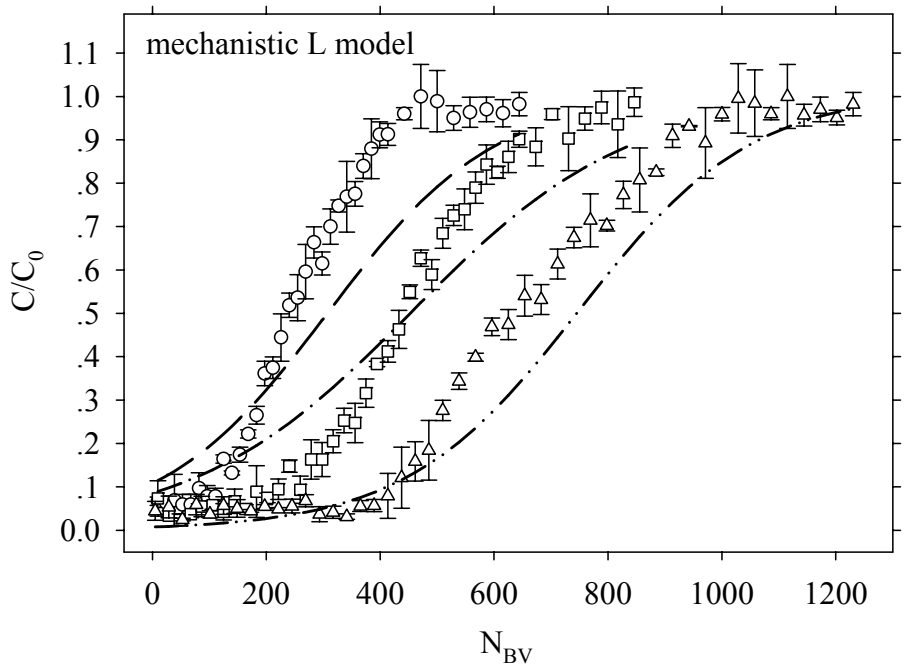

Figure 6-18. pH effect on BTC of P adsorption on AOCM fitted by mechanistic Langmuir model. The parameters related to the model were shown in Table 6-4.

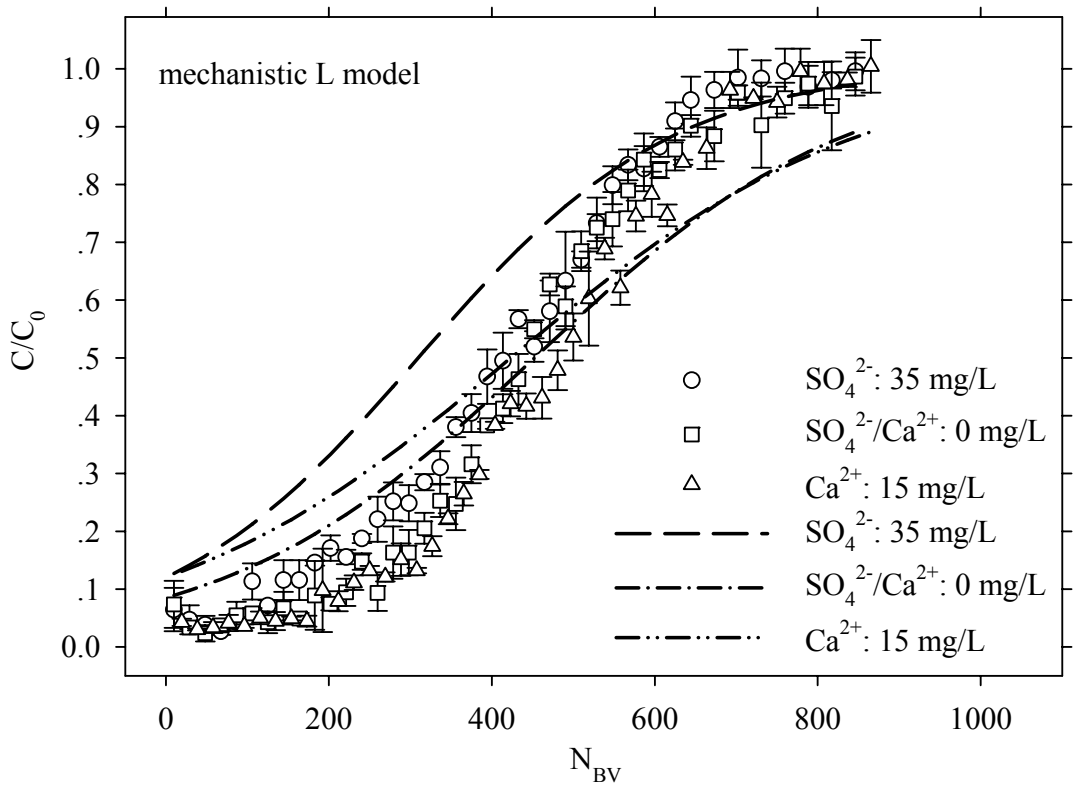

Figure 6-19. Foreign ions effect on BTC of P adsorption on AOCM fitted by mechanistic Langmuir model. The parameters corresponding to the model were shown in Table 6-4.

It is not surprising to find that Thomas model showed the best representation of data with all the correlation coefficients higher than 0.98. As an empirical model, Thomas model was obtained by least square fitting of experimental data. It is very satisfying to see that mechanistic Freundlich model not only obtained high value of correlation coefficients (0.85 ~ 0.98) for most of the experimental conditions but also followed the data trend very well. It is acceptable to find the majority of correlation coefficients mechanistic Langmuir model were more than 0.8. Two possible reasons could explain the better of mechanistic Freundlich model over the mechanistic Langmuir model. The primary reason is that Freundlich is better than Langmuir from isotherm result. The secondary is that non dimensional numbers were used in mechanistic Langmuir model. Nonetheless, it is concluded that both mechanistic models are applicable for BTC data

modeling. Besides, the superiority of mechanistic model over the empirical model is that data are less needed, if any.

IMPLICATIONS AND DISCUSSION

Urban rainfall runoff is a very complicated system, therefore actual performance of adsorptive filtration AOCM column would be affected by multi-factors such as concentration and size distribution of particulate matter, partitioning of particulate and dissolved P, solution pH, P concentration range, hydrological flow rate and pattern of a special event, concentration range of coexisting ions such as Calcium and Sulfate. It is nearly impossible to evaluate adsorption performance of AOCM by real rainfall runoff as influent. Therefore this study highlighted effects of a few primary factors based on the previous isotherms and kinetics results. Though further studies are needed, these experimental results of BTC of P adsorption on AOCM using synthetic rainfall runoff already provide critical information on strategy of scale up and the two mechanistic models proved the good applicability in terms of prediction.

CONCLUSIONS

The simulated urban rainfall-runoff phosphorus (P) removal by innovative upflow adsorption column filled with highly porous Aluminum Oxide Coated Media (AOCM) was studied for its breakthrough curve (BTC) characteristics and feasibility as a subsequent adsorptive filtration process for hydrodynamic separator effluents containing low concentrations in both P and particulate matter. This study provides insights on conditions pertinent to the design of engineered in-situ P treatment, such as how adsorption equilibrium and kinetics, bulk and intraparticle mass transfer, solution pH, P loading concentration, hydraulic retention time, surface loading and coexisting ions affect the P transport and BTC on porous AOCM.

This research presents two mechanistic and two empirical BTC models respectively for adsorbate of simulated urban rainfall-runoff dissolved P transport and adsorption in heterogeneous AOCM column. The modeling could facilitate efforts to design full-scale systems and predict their performance. The mechanistic Langmuir model and mechanistic Freundlich model incorporates convective/dispersion transport, mass balance on adsorption column, intraparticle mass transfer Linear Driving Fore (LDF) model, nonlinear equilibrium adsorption models and corresponding initial and boundary conditions. The physical parameters of mechanistic models have been determined on the basis of independent results of a suite of experiments of equilibrium and kinetics of P adsorption on AOCM studied or formulated correlations. The reliability of the mechanistic models has been verified in its capability to simulate a set of BTC data of P adsorption AOCM. Empirical Thomas model and empirical Bed-depth-service-time model have reached same simulation result after mathematical derivation. The good applicability of the empirical models was confirmed by high values of correlation coefficients.

Breakthrough curve of P adsorption on AOCM demonstrated typical S shape. The numbers of bed volume (N_{BV}) for breakthrough are in terms of a couple of hundreds and numbers of bed volume (N_{BV}) for exhaustion are of double or triple value. Smaller AOCM size leads to better BTC due to higher contacting area. Good BTC favors with slightly acidic pH, low P concentration and low surface loading. Enhancement effect from Ca addition and inhibition effect from Sulfate presence were not very significant because interacting concentrations were low. The maximum adsorption capacities calculated from BTC are generally smaller than values from adsorption isotherm, indicating the presence of mass-transfer limitations and limited contact time in the flow through systems.

In brief, results of BTC of P adsorption on AOCM column indicate that AOCM are capable of efficient and effective treatment for urban rainfall runoff. BTC models, especially mechanistic models, would provide valuable and cost effective information in guiding design and operation of full-scale adsorption columns.

REFERENCES

APHA- American Public Health Association. (1998). Standard Methods for the Examination of Water and Wastewater, (20th Ed.) A.D. Eaton, L.S. Clesceri, A.E. Greenberg (Eds.), American Public Health Association, American Water Works Association and Water Environmental Federation, Washington, D.C.

Badruzzaman, M., Westerhoff, P. and Knappe, D.R.U. 2004. Intraparticle diffusion and adsorption of arsenate onto granular ferric hydroxide (GFH). Water Research, 38, 4002-4012.

Bai, M., Roegiers, J.C. and Inyang, H.I., 1996. Contaminant Transport in Nonisothermal Fractured Porous Media. Journal of Environmental Engineering, 122(5). 416-423.

Brosillon, S., Manero, M.H. and Foussard, J.N., 2001. Mass Transfer in VOC Adsorption on Zeolite: Experimental and Theoretical Breakthrough Curves. Environmental Science & Technology, 35(17), 3571-3575.

Bubba, M.D., Arias, C.A. and Brix, H., 2003. Phosphorus Adsorption Maximum of Sands for Use as Media in Subsurface Flow Constructed Reed Beds as Measured by the Langmuir Isotherm. Water Research, 37, 3390-3400.

Burris, D.R., Hatfield, K. and Wolfe, N.L., 1996. Laboratory Experiments with Heterogeneous Reactions in Mixed Porous Media. Journal of Environmental Engineering, 122(8), 685-691.

Chellam, S., and Wiesner M.R. (1993). Slip flow through porous media with permeable boundaries: implications for the dimensional scaling of packed beds. Water Environmental Research, 65, 744-749.

Chern, J.M. and Chien, Y.W. 2001. Adsorption isotherms of benzoic acid onto activated Carbon and breakthrough curves in fixed-bed columns. Ind. Eng. Chem. Res. 40, 3775-3780.

Cookson, J.T. Jr., 1969. Design of Activated Carbon Adsorption Beds. 42nd Annual Conference of the Water Pollution Control Federation, 2124-2134.

Edwards, O.W. and Huffman, E.O. 1959. J. Phys. Chem. 63, 1830-1833.

Fu, Y. and Viraraghavan, T., 2003. Column Studies for Biosorption of Dyes from Aqueous Solutions on Immobilized Aspergillus niger fungal biomass. Water SA, 29(4), 465-472.

Hatfield, K., Burris, D.R. and Wolfe, N.L., 1996. Analytical model for heterogeneous reactions in mixed porous media. Journal of Environmental Engineering. 676-684.

Hutchins, R.A. 1973. New simplified design of activated carbon system. J. Am. Chem. Engrg. 80, 133-138.

Jusoh, A.B, Noor, M.J.M.M. and Piow, S.B., 2002. Model Studies on Granular Activated Carbon Adsorption in Fixed Bed Filtration. Water Science and Technology, 46(9), 127-135.

Ko, D.C.K., Porter, J.F. and Mckay, G., 2001. Determination of Solid-Phase Loading for the Removal of Metal Ion from Effluents Using Fixed-Bed Adsorbers. Environmental Science & Technology, 35(13), 2797-2803.

Lee, V.K.C., Porter, J.F. and McKay G., 2003. Fixed Bed Modeling for Acid Dye Adsorption onto Activated Carbon. Journal of Chemical Technology and Biotechnology, 78, 1281-1289.

Lee, V.K.C., Porter, J.F. and McKay, G., 2000. Development of Fixed-Bed Adsorber Correlation Models. Ind. Eng. Chem. Res., 39(7), 2427-2433.

Lin, S.H. and Huang, C.Y., 2000. Modeling of Aqueous BTEX Adsorption in Column and Multistage Adsorbers. Journal of Environmental Engineering, 126(9), 802-806.

Liu, D.F., Sansalone, J.J. and Cartledge, F.K. 2005. Comparison of sorptive filter media for treatment of metals in runoff. Journal of Environmental Engineering. 1178-1186.

Metcal & Eddy, 2003. Wastewater engineering: treatment and reuse, McGraw Hill.

Reed, B. E., Jamil, M., and Thomas, B. (1996). “Effect of pH, empty bed contact time and hydraulic loading rate on lead removal by granular activated carbon columns.” Water Environment Research, 68(5), 877-882.

Reynolds, T. M. And Richards, P. A., 1996. Unit Operations and Processes in Environmental Engineering, PWS Publishing Company, Boston, pp 798.

Sakakibara, Y. and Nakajima, H., 2002. Phosphate Removal and Recovery by a Novel Electrolytic Process. Water Science and Technology, 46(11), 147-152.

Sansalone, J.J. and Buchberger, S.G., 1997. Partitioning and First Flush of Metals in Urban Roadway Storm Water. Journal of Environmental Engineering, American Society of Civil Engineers, Vol. 123. No. 2, February, pp 134-143.

Sperlich, A., Werner, A., Benz, A., Amy, G., Worch, E. and Jekel, M., 2005. Breakthrough Behavior of Granular Ferric Hydroxide (GFH) Fixed-Bed Adsorption Filters: Modeling and Experimental Approaches. Water Research, 39, 1190-1198.

Srivastava, S.K., Gupta, V.K. and Mohan, D. 1997. Removal of lead and Chromium by activated slag-a blast-furnace waste. Journal of Environmental Engineering, 461-468.

Thirunavukkarasu, O.S., Viraraghavan, T. and Subramanian, K.S., 2003. Arsenic Removal from Drinking Water Using Iron Oxide-Coated Sand. Water, Air, and Soil Pollution, 142, 95-111.

Tien, C. 1994. Adsorption calculations and modeling; Butterworth-Heinemann: Washington.

Visvanathan, C., Werellagama, D.R.I.B and Aim, R.B., 1996. Surface Water Pretreatment Using Floating Media Filter. Journal of Environmental Engineering, 122(1), 25-33.

Yoshida, H., Jitsukawa, H. and Galinada, W.A., 2004. Breakthrough and Elution Curves for Adsorption of Phosphates on an OH-Type Strongly Basic Ion Exchanger. Ind. Eng. Chem. Res., 43, 3394-3402.

CHAPTER 7 GLOBAL SUMMARY AND CONCLUSION

This research examined the influence of hydrology on urban runoff phosphorus partitioning, distribution of particulate phosphorus among sediment, settleable and suspended particles fractions, and dissolved phosphorus speciation from a research site in Baton Rouge, Louisiana. A number of rainfall-runoff events were examined from 1088-m^2 urban source area watershed. The hydrologic characteristics of these events ranged from flow-limited to mass-limited events for TP and particulate transport. The equilibrium phosphorus distribution across a wide gradation of particles captured by hydrodynamic separation were examined and quantified based on TP mass and concentration. This study is unique in that rainfall-runoff sampling strategy and phosphorus analysis methodology were addressed for the entire gradation of particulate matter transported, not just the suspended and dissolved fractions. Results indicate that depending on the hydrologic transport and antecedent dry period that a significant fraction of TP can be associated with the sediment size fraction. Measured EMCs of TP from the site significantly exceeds common water quality standards (EPA 1986). Speciation results for the dissolved fraction indicate that phosphate is dominant with the forms of HPO_4^{2-} and $H_2PO_4^{1-}$ and therefore these two species would dominate the bioavailability of dissolved phosphorus. Understanding partitioning and speciation of phosphorus as a function of hydrologic transport and time is crucial for designing unit operations and processes for source area watersheds. The dissolved fraction tends to be inversely related to hydrologic transport - lower dissolved fractions at higher flow rates and vice versa. While there were variations in hydrology during each individual event, the mean partition dissolved fractions ranged from 0.11 to 0.45. Distribution of particulate phosphorus between sediment, settleable and suspended particles was dependent on hydrology, which functioned as driving force for the transport of particles. At higher runoff flow

rates, greater particulate phosphorus was entrained and mobilized. Equilibrium granulometric distribution showed that particulate-bound phosphorus association capacity ranging from 0.82 to 3.4 [mg/g], increased with deceasing particle size, as would be expected by definition of solid phase concentration. Smaller particles normally have larger specific surface area but relatively lower total surface area with respect to the entire gradation. Results from this study indicate that effective control of rainfall-runoff phosphorus from source area watersheds requires unit operations and processes that account for particulate-bound species, hydrologic transport and speciation of phosphorus.

On the basis of representative manual sampling and appropriate particulate bound P measurement in terms of sediment bound fraction, settleable bound fraction and suspended fraction, this study investigated pollutant transport modeling of particulate-bound phosphorus in urban rainfall-runoff at the upper end of a small Portland cement concrete (PCC) watershed and in-situ removal mechanism and efficiency by a hydrodynamic separator. Such a study would help understanding how particulate bound fraction of phosphorus, which is a predominant over dissolved fraction, was transported in the urban rainfall-runoff events, evaluating phosphorus potential fate and bioavailability, and shedding sight on effective in-situ control of P which was considered a major cause of eutrophication.

Developed from regression model, P pollutant model based on power law equation was triggered by the finding that the transient loadings of particulate matter and P associated with followed the same characteristics of mass limited or flow limited. In addition, temporal P association capacities on particulate matters were also found in the limited range. The high values for coefficients of determination found when applying the model indicate that the simple power law equation could correlate temporal mass loads of particulate matter and particulate

bound P. Such a manner makes it possible to economically predict P loading through measuring the more assessable particulate matter and also facilitates better unit operation and process (UOP) selection.

The P removal mechanisms by hydrodynamic separator are a combination of dynamic screening and quiescent settling. Removal efficiencies of particulate bound phosphorus are pronouncedly dependent of size of particulate matter and distribution of particulate mass and hydrological parameters of the specific events. Generally, removal efficiency for overall particulate bound P was in the range of 10~50%, with highest removal efficiency for sediment bound P (normally more than 60%), medium removal efficiency for settleable bound P (mostly 30~60%) and lowest removal efficiency for suspended bound P (around 10%).

Results from this study indicate that P pollution model could be successfully applied for intra-event P transport in urban rainfall-runoff. Besides, hydrodynamic separation could effectively remove particulate-bound phosphorus. Nevertheless, runoff P treatment is needed because stringent discharge limit for P are promulgated and dissolved fraction of P is still of concern.

Obtaining reliable adsorption equilibrium is crucial since the isotherms so derived generally were utilized as the corner stone for further adsorption design and engineering application. The adsorption of phosphate on aluminum oxide coated media (AOCM) has been found to be strongly dependent on pH and maximum removal efficiencies have been obtained at slightly acidic conditions. Phosphorus adsorption was shown to increase with decreasing AOCM adsorbent size. While calcium enhanced P adsorption by forming ternary complexes, Sulfate inhibited P adsorption by competing for the common active sites. Ionic strength and Nitrate has little effect on P adsorption. Low desorbability, which likely resulted from strong bonding

between P and AOCM, was also obtained under experimental conditions. The use of AOCM for adsorption of phosphorus from aqueous solution has a prominent advantage because very porous substrate facilitates fully contact between phosphorus and AOCM. Good adsorption capacities were obtained for the typical conditions of urban rainfall runoff. Thus it is concluded that AOCM is a low-cost while effective adsorbent for phosphorus adsorption. Easy availability and high adsorption capacity make AOCM superior to the other adsorbents for phosphate removal. It is also found Freundlich isotherm could successfully represent data of P adsorption on AOCM. Upon treatments by AOCM, phosphorus concentrations could be reduced to a suitable level for discharge into natural surface waters, which suggests the promising application of AOCM.

Both of the reaction kinetics and the diffusion mechanism were applied to adequately describe the data of P adsorption kinetics by AOCM. It is found that pseudo second order reaction model fitted the data best under all experimental conditions and intraparticle diffusion model could be successfully applied for the first hour P adsorption kinetics.

The kinetics of P adsorption on AOCM was fast for the typical urban rainfall runoff conditions, with the reactions completed within the first few hours, sometimes even within minutes. Finer size of AOCM showed quicker P kinetics. The higher initial P concentration, the longer reaction time and vice versa. The high surface loading rate and the higher sorbent solution ratio, the better kinetics could be obtained. Lower pH not only promotes faster adsorption but also ensure higher adsorption capacity. Ionic strength and nitrate have little effect on P adsorption kinetics. While calcium accelerates noticeable P adsorption kinetics by forming ternary complexes, Sulfate inhibited appreciable P adsorption kinetics by competition for common sites. Adsorption capacities obtained from recirculating kinetics agree with the batch adsorption isotherm findings. Pore diffusion was suggested as rate limiting step for P adsorption

kinetics on AOCM by comparison of film diffusion, effective intra particle diffusion and pore diffusion through half time method, parallel pore method and Boyd's method.

The simulated urban rainfall-runoff phosphorus (P) removal by innovative upflow adsorption column filled with highly porous Aluminum Oxide Coated Media (AOCM) was studied for its breakthrough curve (BTC) characteristics and feasibility as a subsequent adsorptive filtration process for hydrodynamic separator effluents containing low concentrations in both P and particulate matter. This study provides insights on conditions pertinent to the design of engineered in-situ P treatment, such as how adsorption equilibrium and kinetics, bulk and intraparticle mass transfer, solution pH, P loading concentration, hydraulic retention time and surface loading affect the transport and BTC on porous AOCM.

This research presents two mechanistic and two empirical BTC models respectively for adsorbate of simulated urban rainfall-runoff dissolved P transport and adsorption in heterogeneous AOCM columns. The modeling could facilitate efforts to design full-scale systems and predict their performance. The mechanistic Langmuir model and mechanistic Freundlich model incorporates convective/dispersion transport, mass balance on adsorption column, intraparticle mass transfer Linear Driving Force (LDF) model, nonlinear equilibrium adsorption models and corresponding initial and boundary conditions. The physical parameters of mechanistic models have been determined on the basis of independent results of a suite of experiments of equilibrium and kinetics of P adsorption on AOCM studied or formulated correlations. The reliability of the mechanistic models has been verified in its capability to simulate a set of BTC data of P adsorption AOCM. Empirical Thomas model and empirical Bed-depth-service-time model have reached same simulation result after mathematical derivation. Potential applicability of the empirical models was confirmed by high values of R^2.

Breakthrough curve of P adsorption on AOCM demonstrated typical S shape. The numbers of bed volume (N_{BV}) for breakthrough are in terms of a couple of hundreds and numbers of bed volume (N_{BV}) for exhaustion are of double or triple value. Smaller AOCM size leads to better BTC due to higher contacting area. Good BTC favors with slightly acidic pH, low P concentration and low surface loading. Enhancement effect from Ca addition and inhibition effect from sulfate presence were not very significant because interacting concentrations were low. The maximum adsorption capacities calculated from BTC are generally smaller than values from adsorption isotherm, indicating the presence of mass-transfer limitations and limited contact time in the flow through systems. Results of BTC of P adsorption on AOCM column indicate that AOCM are capable of efficient and effective treatment for urban rainfall runoff. BTC models, especially mechanistic models, would provide valuable and cost effective information in guiding design and operation of full-scale adsorption columns.

VITA

Jia Ma received his Bachelor of Science degree in chemical engineering from Tianjin University, People's Republic of China, in July, 1995. He got his master's degree in chemical engineering from Beijing University of Chemical Technology, People's Republic of China, in July, 2000. He came to United States to pursue advanced study in August, 2000. He got his master's degree in chemical engineering at Louisiana State University in December, 2003. He started his Doctoral degree in the department of civil and environmental engineering at Louisiana State University in August, 2003. His graduate research was focused on the speciation, equilibrium and kinetics of rainfall-runoff phosphorus in adsorptive-filtration unit operations and processes. He worked under the guidance of Dr. John J. Sansalone. Jia Ma will receive the degree of Doctor of Philosophy from Louisiana State University in December, 2005.